E.T.S. de Ingeniería Industrial,
Informática y de Telecomunicación

Design, Optimization and Manufacture Modelling of Reflector-Based High-Performance Antenna Systems

Máster Universitario en
Ingeniería de Telecomunicación

Trabajo Fin de Máster

Daniel Valcázar Berdofe

Jorge Teniente Vallinas

Pamplona, 29 de Junio de 2017

upna Universidad Pública de Navarra
Nafarroako Unibertsitate Publikoa

Acknowledgments

With this work comes not only the end of a Master's Degree, but of a lifetime of studying. Studying to become someone, which in my case turned out to be a professional in the field of engineering (I would have settled for Rockstar, though). And while I'm putting the (sometimes agonizing) hours spent in classrooms behind me, I truly feel like I still have everything to learn. A new phase begins in my life, with different environments, different responsibilities and different pressures ahead.

Throughout all the defining moments, both good and bad, the support of my friends and family has been a constant in aiding me during all these years. Be it through music, a helping hand or even a few encouraging words, these people have helped me thrive academically, become a better person and, most importantly, to make the most of my time and enjoy this life I'm living.

Thanks in particular to Aitor, Gonzalo and everyone at Anteral, Jorge Teniente and every other amazing teacher and classmate at UPNA, IES Comercio and CP Caballero de la Rosa over the years, the extended Arnie family, all my family and every friend I've made overseas, the ever-expanding TovH community… I'm sure to be forgetting people, but you're in my heart as well.

Most importantly, I need to give a special Thank You to the people whose unconditional love have made all this worth it. Lucky, thanks boy. Gab, thanks for being there and making music and memories. Papá, gracias por los madrugones de Lunes para ir a la estación. Mom, thanks for the endless cookies and cakes. Gatinha, obrigado por ser voçê e me dar forças para continuar.

Here in this moment
You never needed much more
Than this
To satisfy your only wish
To feel your heart forever growing
While forgiving those who know the way

Abstract

This work deals with the creation of two parabolic reflector systems, one single offset reflector centered at 275 GHz and one dual Cassegrain reflector at 340 GHz. Based on a set of initial specifications, both systems are electrically designed using a combination of specialized software programs (including *HFSS*, *µWave Wizard* and *GRASP*), after which the manufacturing models are created taking the pertinent precautions into account. Once the manufactured models are received (machined by a third party), they are measured in Near-Field to verify their correct operation, using transformation techniques (with custom *MATLAB* scripts) to compute their Far-Field performances and compare them to the simulated design results. To understand the operation of these types of systems, a theoretical overview of parabolic reflector antennas is presented, as well as conclusions about the finished systems and possible investigative lines and advancements to pursue in the future.

Index Terms

Parabolic Antenna, Cassegrain Reflector, Offset Reflector, Terahertz Band, Antenna Design

Index

Table of Illustrations

Chapter 1

Introduction

Parabolic antenna systems aren't a recent discovery [1], but are still being used for a variety of applications due to their particular advantages. Because of the parabola's properties, parabolic reflectors offer narrower beamwidths than most other types of antennas, which is to say they are antennas with some of the highest available gain [2]. The main drawback to this is that the reflector dishes need to be comparatively much, much larger than their operating frequency's wavelength, which realistically limits the use of these types of antennas to frequencies above and including the microwave range (between 0.3 and 300 GHz).

Aside from their more traditional use in radio telescopes, RADAR systems and satellite communications transmitters and receivers [1][3], parabolic antennas are being used increasingly in recent years for wireless transmissions [4], such as for data link communications of television/telephone signals or Local Area Network/backup copy links between a corporation's buildings, for instance.

At the same time, the number of applications at the high end of the millimeter band (30 to 300 GHz) and beginning of the submillimeter band (300 GHz to 3 THz) is continuously increasing, including real-time non-ionizing imaging [5] (in a plethora of fields including medicine, security, quality control, biochemistry…) and ultra-high-rate wireless data transmission over short distances [6][7]. Because these bands present very high frequencies, reflector antennas are easier to manufacture for these applications than other types of antennas with smaller size-to-wavelength ratios.

This work deals with the creation of two different parabolic reflector antennas from the ground up: one single offset reflector at 220 GHz and one dual Cassegrain reflector at 340 GHz. These systems were requested by two different clients, and have been created as custom solutions tailored to very particular needs and requirements. The design of both systems has been carried out using different software programs for each part of the process:

1. Reflector System design (with an ideal/non-real feed) using TICRA's *GRASP*.
2. Pyramidal Feedhorn design using ANSOFT's *HFSS* and Mician's *μWave Wizard*.
3. Combination of the previous two in *GRASP*, using *MATLAB* to process the radiation data exported from *HFSS* and format it to import into *GRASP*.
4. Full System simulation (as well as any dimensional fine-tuning) in *GRASP*.
5. 3D Mechanical Model design in *HFSS*, based on the *GRASP* model.
6. Post-manufacturing verification measurements, using *MATLAB* to treat the resulting data.

The most relevant steps of each design are detailed in this document, as well as the pertinent results for each carried-out simulation. A more detailed account of select results is available in this work's annex section.

The structuring of the remaining chapters is as follows:

- Chapter 2 presents an overview of parabolic reflector antennas, how they operate and their different types and applications.
- Chapter 3 deals with the design, manufacture and measurement of a 275 GHz Offset Reflector Antenna.
- Chapter 4 deals with the design, manufacture and measurement of a 340 GHz Cassegrain Reflector Antenna.
- Chapter 5 is a conclusion of the obtained results, as well as an overview of possible advances to be made in the future.

References

[1] Y. Rahmat-Samii and R. L. Haupt, “Reflector Antenna Developments: A Perspective on the Past, Present and Future,” *IEEE Antennas Propag. Mag.*, vol. 57, no. 2, pp. 85–95, 2015.

[2] W. L. Stutzman and G. A. Thiele, *Antenna Theory and Design*, 3rd ed. USA: Wiley, 2012.

[3] S. Makino, “Historical Review of Refrector Antenna Systems Developed By,” *Int. Symp. Antennas Propag.*, no. 2, p. 8196, 2006.

[4] H.-J. Song *et al.*, “Terahertz wireless communication link at 300 GHz,” *Proc. - 2010 IEEE Int. Top. Meet. Microw. Photonics, MWP 2010*, pp. 42–45, 2010.

[5] E. N. Grossman, J. Gordon, D. Novotny, and R. Chamberlin, “Terahertz active and passive imaging,” *8th Eur. Conf. Antennas Propag. (EuCAP 2014)*, pp. 2221–2225, Apr. 2014.

[6] K. Ishigaki, M. Shiraishi, S. Suzuki, M. Asada, N. Nishiyama, and S. Arai, “Direct intensity modulation and wireless data transmission characteristics of terahertz-oscillating resonant tunnelling diodes,” *Electron. Lett.*, vol. 48, no. 10, p. 582, 2012.

[7] L. Lopacinski, S. Buechner, and R. Kraemer, “Improved Turbo Product Coding dedicated for 100 Gbps Wireless Terahertz Communication,” 2016.

Chapter 2

Parabolic Reflector Systems

Parabolic Reflectors

Properties and Behavior

A parabola is a conic curve defined as the line whose points are equidistant from a line, directrix, and a point, focus (see Fig. 2.1).

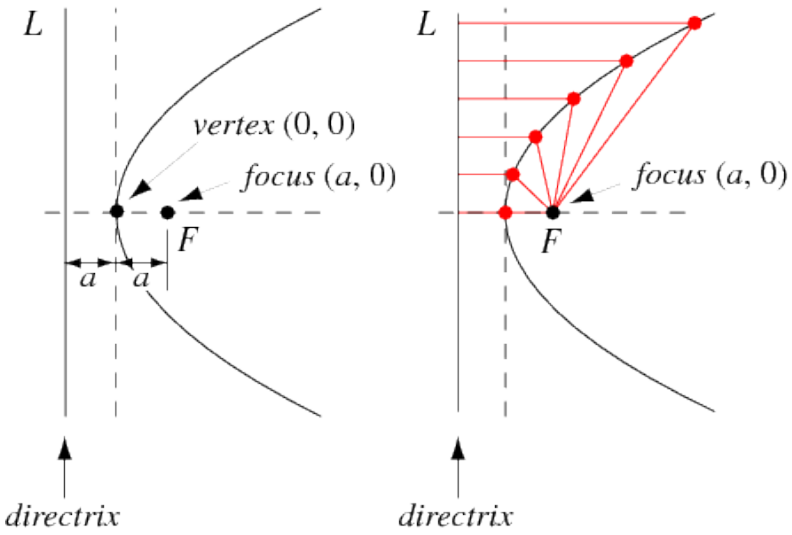

Fig. 2.1: Parabola Properties Diagram [1]

The parabola's point closest to the focus and directrix is known as the vertex, and the distance between the vertex and the focus (or the directrix) is known as the focal length, the defining parameter of a parabola. The shorter the focal length, the wider the parabola will be, according to the following equation [1]:

$$z(x) = \frac{x^2}{4f}$$

A crucial property of the parabolic surface is that rays emitted from its focus reflect on its surface and bounce outward perpendicular to its directrix, as can be seen in Fig. 2.2. More importantly, the reflected rays within a flat wavefront are in phase with each other in a frequency independent (optical) manner, which creates non-destructive interferences and provides the reflector's gain. This gain will be higher the higher the operating frequency is, due to the fact that a fixed-size reflector is electrically "bigger" as the waves' wavelength decreases (more waves "fit" within a same-sized reflector dish).

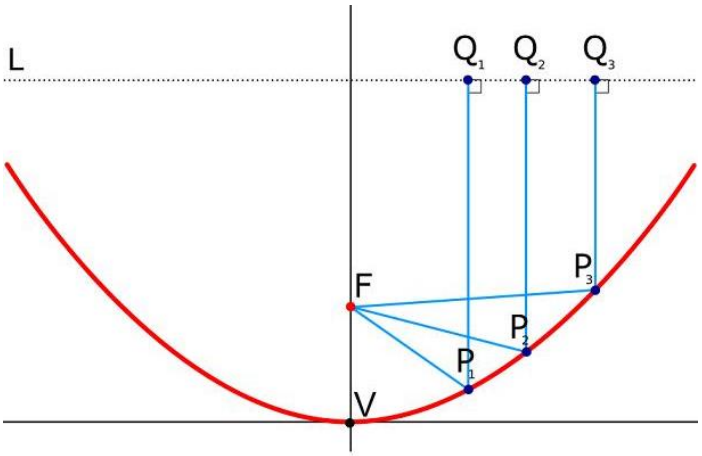

Fig. 2.2: Parabola Radiation Property

The reverse radiation property is also true: rays that are incident on the reflector perpendicular to its directrix will be received at the focus in phase.

Types and Applications

There are several different configurations for parabolic reflector antennas depending on the use they are to be given [2]. A common method of classifying these configurations is with regards to how the waves are fed from the feedhorn to the reflector dish [3]:

- Axial or front-fed: the feed is placed at the same spot as the parabola's focus facing the reflector dish, employing a wide beam to cover it completely.
- Offset: the feed is still positioned at the focus, but angled and off to a side of the dish, which is an asymmetric segment of a parabola (as opposed to a symmetric reflector). Antennas for home satellite television receivers and antennas aboard communications satellites are usually offset reflector parabolic reflectors.
- Cassegrain: the feed is no longer positioned at the focus, but instead behind the reflector facing outward. The feed illuminates a hyperbolic or parabolic convex secondary reflector (smaller than the main one), which in turn illuminates the main dish. It is mainly used in radio telescopes and satellite ground stations.
- Gregorian: same configuration as the Cassegrain reflector, but using a concave secondary reflector instead of a convex one. It was first used by James Gregory to design the very first astronomical telescope in the 17th century.

Single Offset Parabolic Reflector

In a basic front-fed parabolic reflector antenna configuration (Fig. 2.3), the feed is placed at the parabolic dish's focus aimed directly at its vertex (that is, the feed is aligned with the reflector's axis). However, this configuration has one main drawback: the feed and its support struts (which are usually metallic) are directly in the path of incoming and outcoming waves, which directly reduces its aperture efficiency [4].

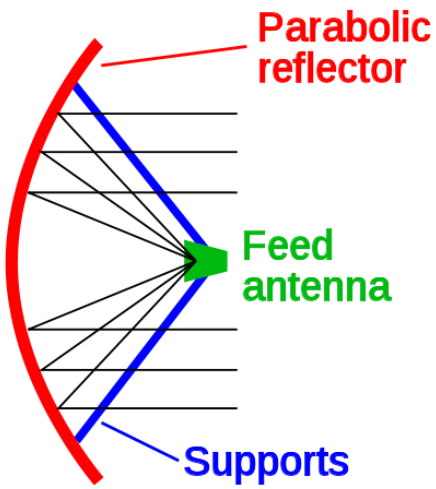

Fig. 2.3: Front-fed Parabolic Reflector Antenna Profile

In the case of aperture antennas (which includes parabolic reflectors), the aperture efficiency (e_a) is the ratio between an antenna's effective aperture in terms of radiation (A_{eff}) and the area of its physical aperture (A_{phy}). In the case of parabolic reflectors, the physical area can be expressed like so (where *r* is the reflector's radius and *d* its diameter) [5]:

$$A_{phy} = \pi r^2 = \pi \frac{d^2}{4}$$

In other words, the effective aperture area can be expressed as:

$$A_{eff} = A_{phy} e_a = \pi \frac{d^2}{4} e_a$$

And therefore, a parabolic reflector's gain can be expressed as:

$$G = \frac{4\pi A_{eff}}{\lambda^2} = \left(\frac{\pi d}{\lambda}\right)^2 e_a$$

As can be appreciated, for a fixed wavelength (frequency), a reflector dish's gain is directly dependent on its diameter and aperture efficiency. For applications where the feed and its

support structure are large enough when compared to the reflector dish to block a significant amount of power from being received or transmitted, such as for home satellite television receivers, the aperture efficiency can be affected to the point where there is a very noticeable reduction in the overall gain.

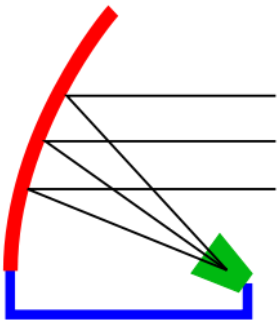

Fig. 2.4: Single Offset Parabolic Reflector Antenna Profile

An offset reflector configuration (Fig. 2.4) reduces or avoids this problem altogether [5], by using an asymmetric segment of a parabola instead of a "complete" one. A diagram illustrating this is shown in Figure 2.5, where the offset reflector (dark blue) is seen as a part of a larger parabolic reflector (green) with the focus (orange) for reference. In this configuration, the feed needs to be tilted and more directive in order to cover the smaller angle subtended from the focus to the edges of the reflector.

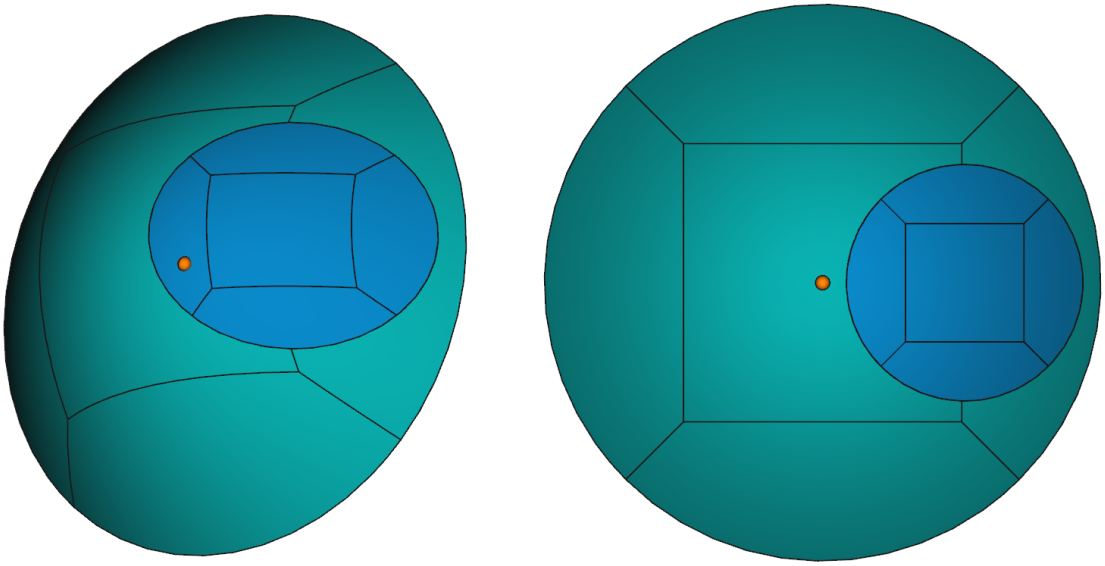

Fig. 2.5: Offset Reflector as a Segment of a Full Parabolic Reflector

When simulating with Ticra's *GRASP* software, the intervening parameters to configure an offset reflector are the operating frequency, the diameter of the aperture projected on boresight (which is circular), the focal length and the offset, which is the distance from the parabola's axis to the center of the aperture's circular projection [6].

An additional application where offset reflectors are useful is aboard communications satellites. Because of the very limited power available to them in outer space (which mainly comes through solar cells that transform the Sun's energy into electrical power), it is essential that the antenna systems are as efficient as possible, and as has been previously mentioned, parabolic reflectors in an offset configuration offer the best aperture efficiency (and lose less power when transmitting and receiving).

Dual Cassegrain Reflector

A Cassegrain Reflector Antenna is a type of parabolic antenna comprised of two reflective surfaces: a parabolic dish (referred to here as the main reflector) and a smaller, convex hyperbolic reflector (referred to as the subreflector). The subreflector is centered above the main reflector, and the feed is on or behind the main reflector (aimed at the subreflector). In this configuration, the waves emitted from the feed bounce once off of the subreflector and again off the main reflector, preserving their phase the same way as in a single front-fed parabolic reflector (as can be seen in Fig. 2.6).

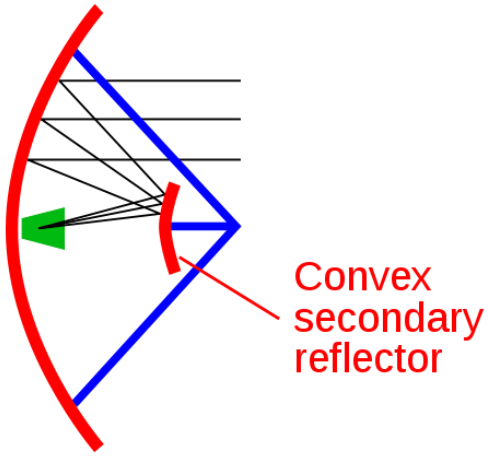

Fig. 2.6: Double Cassegrain Reflector Antenna Profile

For this configuration to operate properly, each of the three elements must be positioned precisely with regards to each other. To understand this properly, we must first study the reflective properties of the hyperbola.

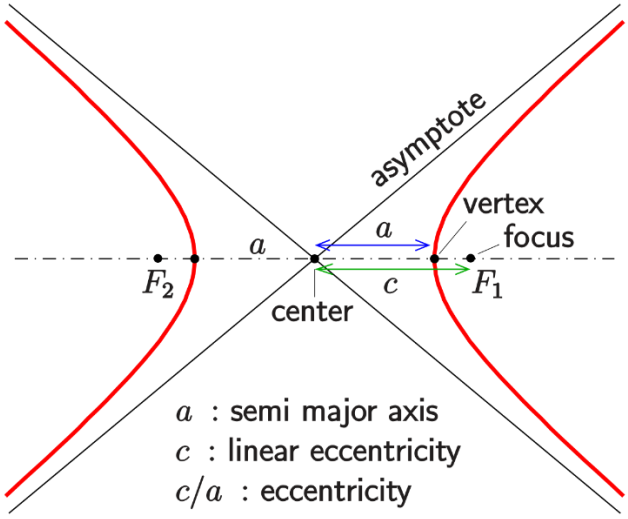

Fig. 2.7: Hyperbola Properties Diagram

A hyperbola is a set of two identical curves, which are symmetrical around a center (Fig. 2.7). Each of the curves has a focus and a vertex, both aligned with the center: both focuses are at a distance *c* from the center, and both vertexes are at a distance *a* from the center (with *c* always being larger than *a*). The hyperbola curves are defined as the curves whose points satisfy the following equation:

$$|D_1 - D_2| = 2a$$

Where D_1 is the distance from any point of the curve to one focus and D_2 is the distance to the other focus. Through this property we find the correct way to position both reflectors and the feed within the Cassegrain configuration [7]: the subreflector (whose profile is one side of the hyperbola curve) needs its focus to be in the same spot as the main reflector's, while the feed must be positioned with its phase center at the subreflector's opposite focus. If aligned correctly, this means that the rays emitted from the feed will bounce off the subreflector towards the main reflector in phase as if they were being emitted from its own focus (see Fig. 2.8).

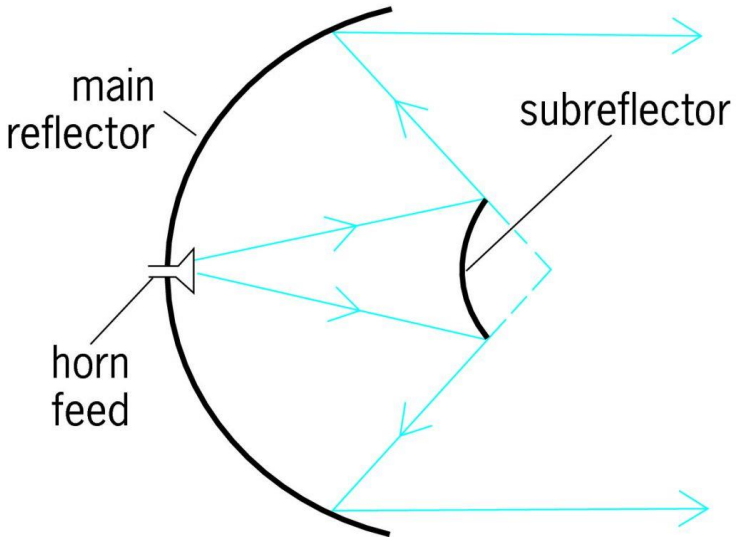

Fig. 2.8: Cassegrain Reflector Ray Reflection [8]

When simulating with Ticra's *GRASP* software, the intervening parameters to configure a Cassegrain reflector are: the operating frequency, the main reflector's diameter, its focal distance (to position the subreflector's focus in the same place), the distance between the hyperbola's focuses (twice the subreflector's focal length, to position the feed relative to the subreflector) and the subreflector's eccentricity (the relationship between the subreflector's focal length *c* and the vertex distance *a*, to modify the size of the subreflector by changing *a* for a fixed *c*) [9].

As for the hyperbolic relfector's equation, it can be written as:

$$\frac{z^2}{a^2} - \frac{x^2}{b^2} = 1$$

Where it is assumed that all the focuses are aligned along the Z-axis and the main reflector radiates in its same direction. Knowing that $b^2 = c^2 - a^2$ and expressing it as a function of x:

$$z(x) = a\sqrt{\left(1 + \frac{x^2}{b^2}\right)} = a\sqrt{\left(1 + \frac{x^2}{c^2 - a^2}\right)}$$

The added complexity to be able to design (and later manufacture) this kind of system is done for several reasons. In the case of radio telescopes and satellite communication ground antennas, the feeds and assorted RF front-end electronic components (waveguides, filters, junctions, etc.) would cause a very considerable amount of blockage to the radiation if configured in a standard front-fed configuration [5]; in a Cassegrain configuration, all these necessary assemblies can be placed behind the main reflector.

An additional advantage in the case of receiving satellite ground antennas is the lower antenna noise temperature, due to the fact that the spillover radiation (the energy from the feed that misses the reflector) is directed at the sky instead of at the ground, which would introduce additional thermal noise due to its warm temperature. Because of this, Cassegrain antennas offer a higher sensitivity, signal-to-noise ratio and dynamic range than traditional front-fed antennas.

References

[1] Eric W. Weisstein, “Parabola,” *MathWorld--A Wolfram Web Resource*. [Online]. Available: http://mathworld.wolfram.com/Parabola.html.

[2] Y. Rahmat-Samii and R. L. Haupt, “Reflector Antenna Developments: A Perspective on the Past, Present and Future,” *IEEE Antennas Propag. Mag.*, vol. 57, no. 2, pp. 85–95, 2015.

[3] H. Lehpamer, *Microwave Transmission Networks: Planning, Design and Deployment*, 2nd ed. USA: McGraw-Hill, 2010.

[4] C. A. Balanis, “Front-Fed Parabolic Reflector,” in *Antenna Theory*, 3rd ed., USA: Wiley, 2005, pp. 896–926.

[5] A. Cardama, L. Jofre, J. M. Rius, J. Romeu, S. Blanch, and M. Ferrando, “Reflectores Parabólicos,” in *Antenas*, 2nd ed., Spain: Ediciones UPC, 2002, pp. 276–299.

[6] K. Pontoppidan, Ed., “Useful Geometrical Relations: Single Reflector Design,” in *GRASP Technical Description*, TICRA, 2008, pp. 368–369.

[7] C. A. Balanis, “Cassegrain Reflectors,” in *Antenna Theory*, 3rd ed., USA: Wiley, 2005, pp. 926–934.

[8] *McGraw-Hill Concise Encyclopedia of Engineering*. McGraw-Hill, 2002.

[9] K. Pontoppidan, Ed., “Useful Geometrical Relations: Dual Reflector Design,” in *GRASP Technical Description*, TICRA, 2008, pp. 370–379.

Chapter 3

340 GHz Dual-Cassegrain Reflector System

Initial Design Requirements and Considerations

The design and manufacture of a 340GHz Cassegrain-configuration reflector system has been undertaken, with the aim of it being used for proof-of-concept feasibility measurements in the context of an outdoor communication environment.

The system's requirements, as initially agreed upon with the client, can be seen here:

Parameter	Value
Qty.	2 units
Antenna Type	Dual-Cassegrain Reflector Antenna
Central Frequency	340 GHz
Bandwidth	10 GHz
Gain	> 45 dBi
Input waveguide	Standard WR2.8
Feed Type	Pyramidal Smooth Wall Horn
VSWR	< 1.3 (S_{11} < -17.6 dB)
Radome	Required
Radome type	Gore-Tex Fabric Radome

Fig. 3.1: Cassegrain Reflector System Initial Requirements

In short, the reflector system must operate with a gain of at least 45 dBi and a Return Loss below -17.6 dB between 335 and 345 GHz. The system has two main components:

- A Dual Reflector Cassegrain Antenna, comprised of a parabolic main reflector dish and a hyperbolic subreflector dish (as well as a support structure to maintain both these elements in place with regards to each other).
- A Pyramidal Smooth-walled Feedhorn, fed using a standard WR2.8 waveguide interface, with an appropriate radiation pattern so as to maximize the total gain after being amplified by the reflector dishes arranged in the Cassegrain configuration, so that the complete antenna reaches the minimum required 45 dBi gain.

Using a WR2.8 waveguide means that the most significant difficulty in manufacturing the system will come from creating said waveguide's input slot, which measures a mere 0.71 x 0.36 mm.

The system will be operating in an outdoor environment, so it will possibly be subject to rain, snow and various other sources of erosion and damage. To avoid such effects, a radome made from water-resistant Gore-Tex fabric will be put over the system and screwed in place to seal its edges and prevent leakage to the inside.

Initial Design

After some tests, the first design for the system was created using a 100mm diameter and 30mm focal length for the main reflector dish, as well as a distance between the hyperbolic subreflector's focii of 21mm (or c = 10.5mm) and an eccentricity (e) of 1.5 [1][2]. This can be appreciated in Figure 4.2.

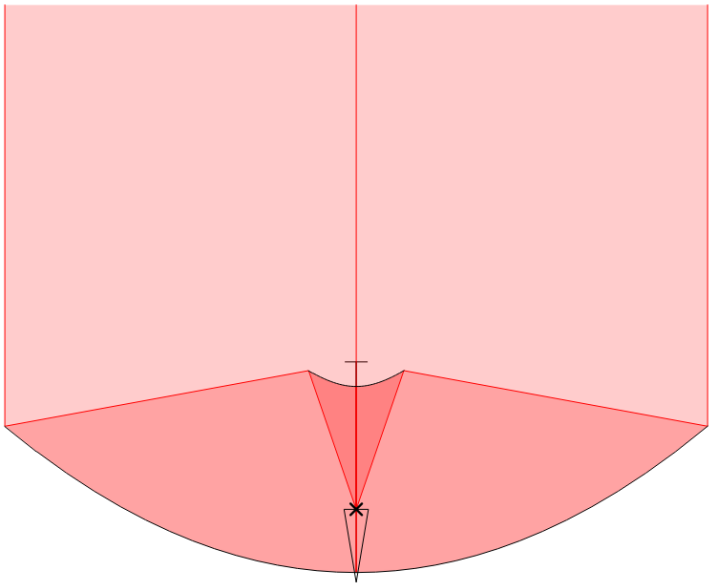

Fig. 3.2: Cassegrain Reflector Initial Design Profile and Relative Positioning

The specific equations for the reflective surfaces in this case are (with X and Z in millimeters) [3]:

- Main Reflector: $z(x) = \frac{x^2}{120}$
- Subreflector: $z(x) = 7\sqrt{1 + \left(\frac{x}{7.83}\right)^2}$

The feedhorn included by default is an ideal one, with an emitted Gaussian beam to cover a subtended angle of 18.92º from the feed's aperture to the rim of the subreflector.

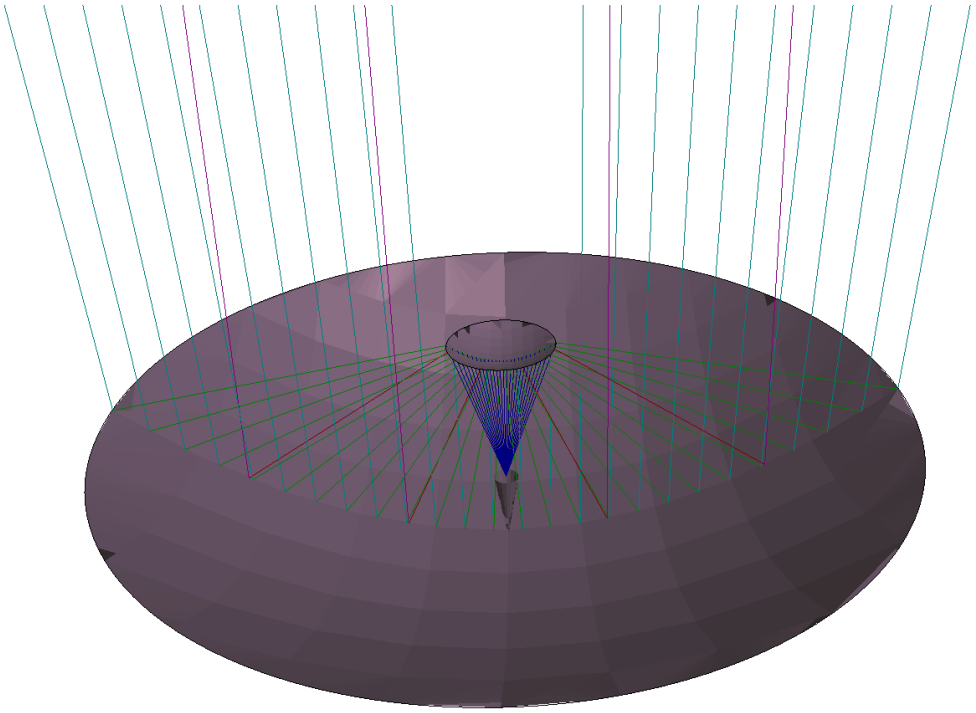

Fig. 3.3: Cassegrain Reflector Initial Model GRASP Design, including Ray Plot

When the feedhorn radiates power, the rays hit the subreflector, which directs them toward the main reflector, from where they are reflected parallel to the Z axis (the radiation direction). However, in order to accurately simulate the radiation pattern the system produces, the amount of power that hits the subreflector for a second time must be taken into account; this is because these twice-reflected rays (the ones that initially hit the main reflector directly under the subreflector, shown in Fig. 4.3 in red and magenta) now have different phases and reflection angles, and can negatively affect the shape and gain of the total radiation pattern [4].

With all this in mind, the resulting radiation patterns are shown below in Figures 4.4 to 4.6:

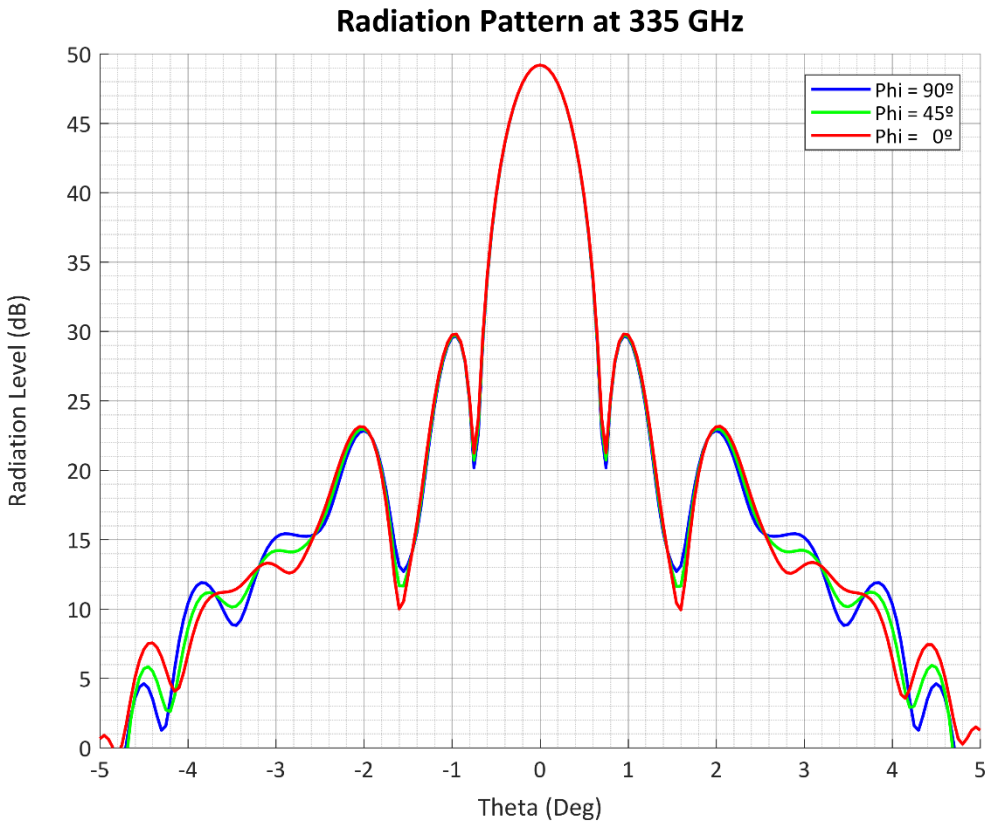

Fig. 3.4: Cassegrain Reflector Initial Model Far-Field Radiation Pattern at 335 GHz

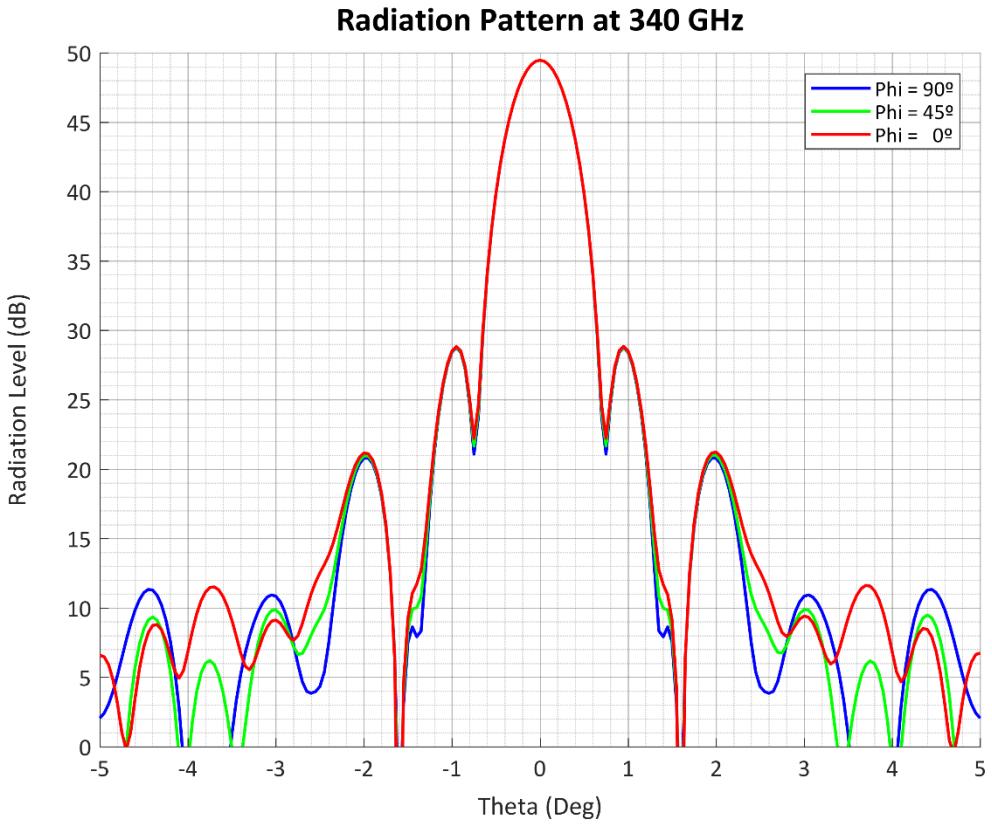

Fig. 3.5: Cassegrain Reflector Initial Model Far-Field Radiation Pattern at 340 GHz

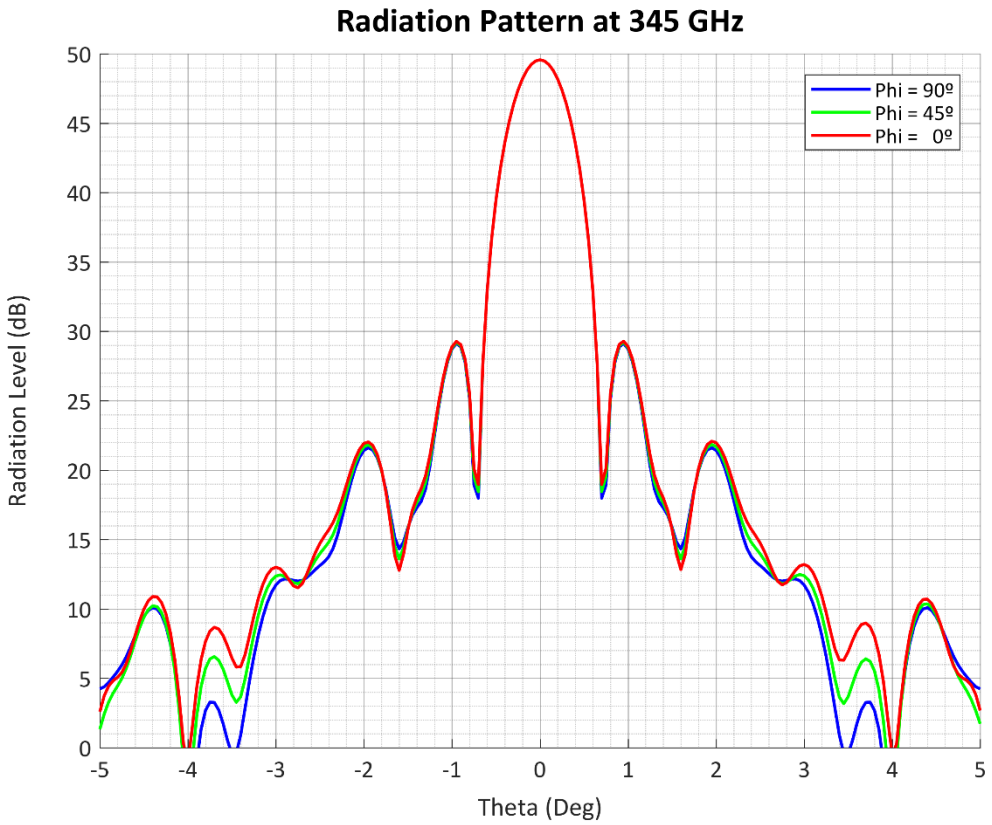

Fig. 3.6: Cassegrain Reflector Initial Model Far-Field Radiation Pattern at 345 GHz

Second Version (Including Pyramidal Feedhorn)

After verifying that the design produces enough gain using an ideal feedhorn, it is replaced in *GRASP* with a 15mm long, 19dBi WR2.8 pyramidal horn. Said horn was previously designed in *HFSS* to approximate the Gaussian beam as closely as possible, with an inner aperture measuring 3mm by 2.25mm optimized to obtain highly symmetrical phi radiation planes. Fig. 4.7 shows the horn's radiation pattern at 330GHz.

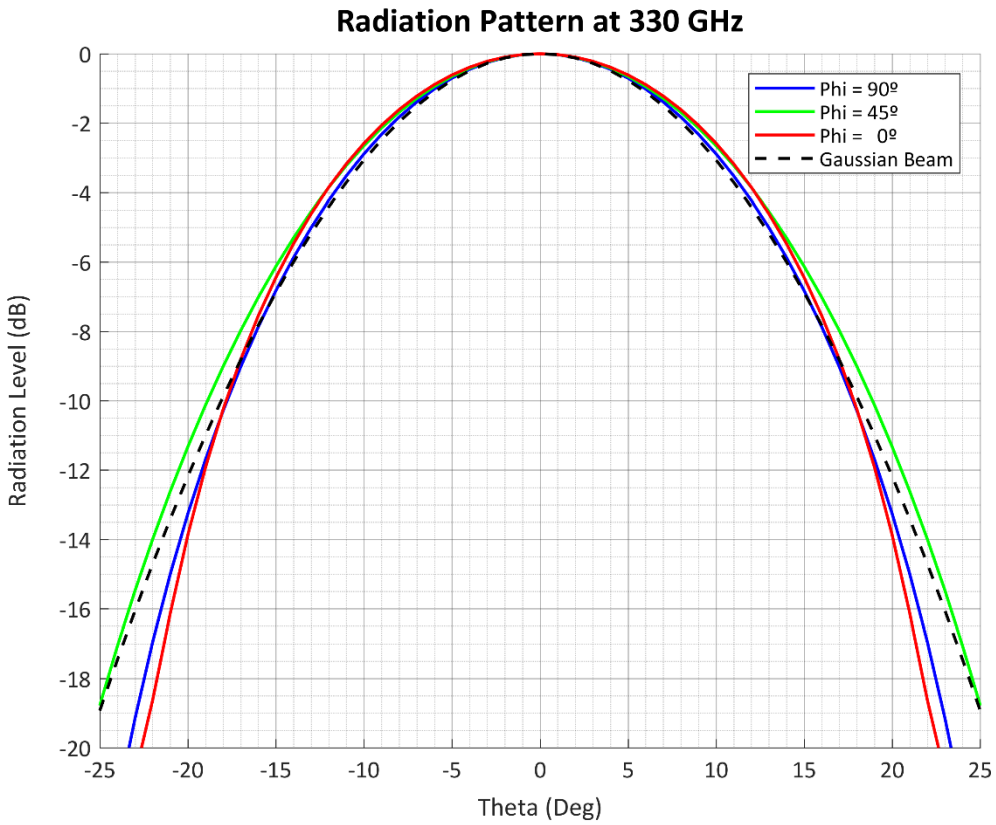

Fig. 3.7: Cassegrain Reflector Pyramidal Feedhorn Radiation Pattern at 330 GHz

The horn's patterns for each frequency point are imported into *GRASP*, which then computes the radiation patterns for the full system, seen here in Figures 4.8 to 4.10:

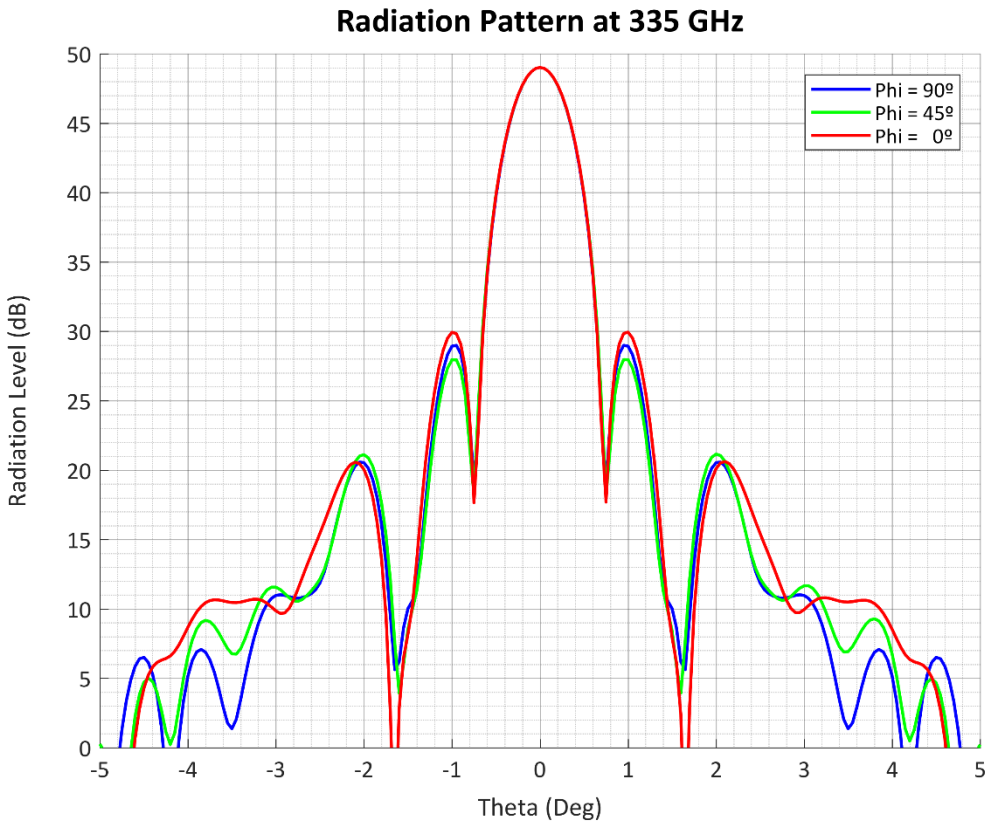

Fig. 3.8: Cassegrain Reflector Second Model Far-Field Radiation Pattern at 335 GHz

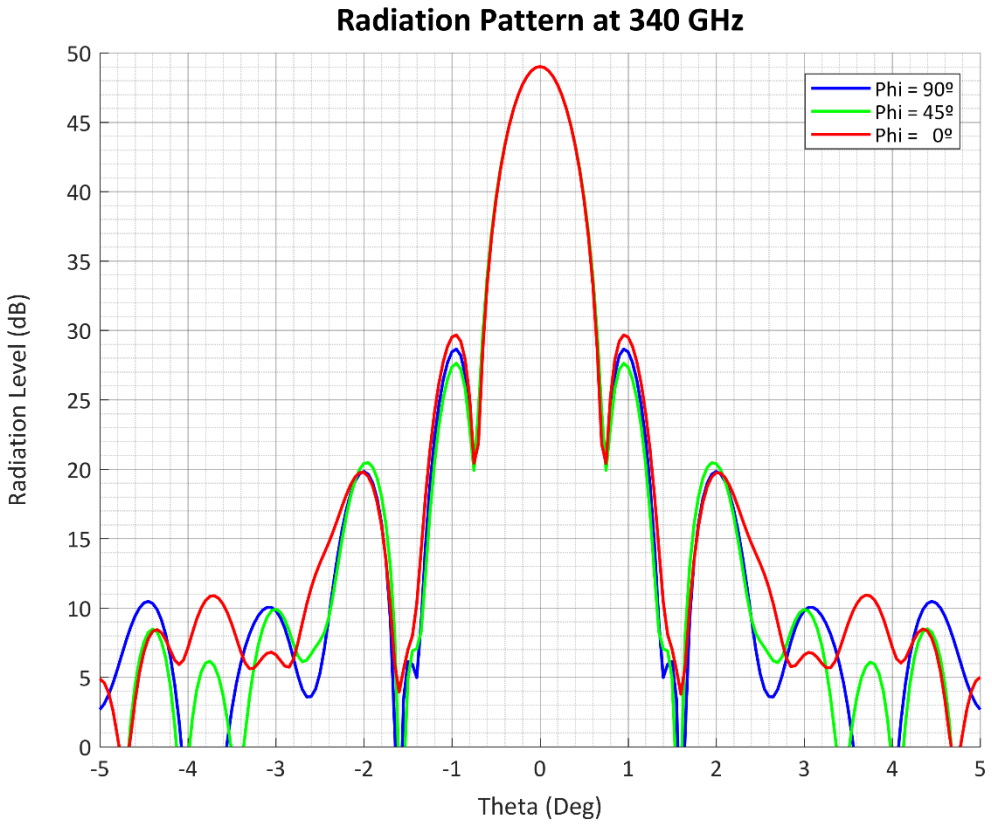

Fig. 3.9: Cassegrain Reflector Second Model Far-Field Radiation Pattern at 340 GHz

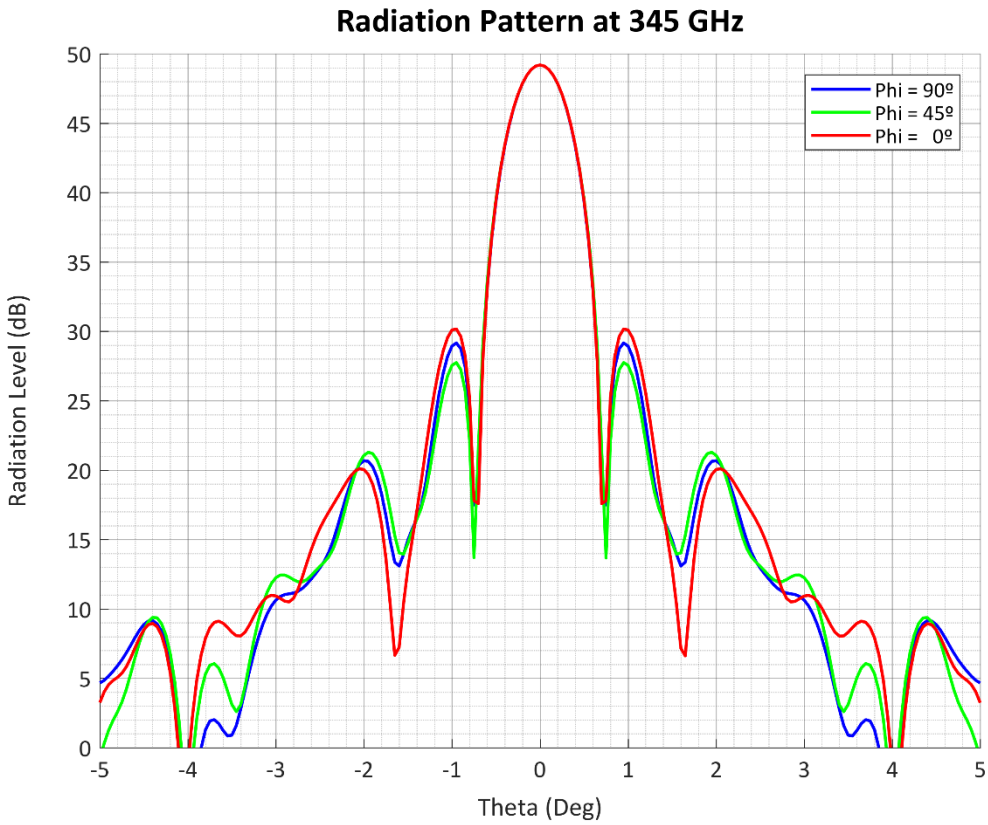

Fig. 3.10: Cassegrain Reflector Second Model Far-Field Radiation Pattern at 345 GHz

Third Version (Including Support Struts)

By default, *GRASP* only creates the appropriate reflective surfaces, but when creating a simulation model in *GRASP* it is important to be able to accurately reproduce the mechanical model, which may include a variety of support struts that can introduce additional scattering effects and affect the radiation.

GRASP allows for the creation of rectangular scatterers, so four of these were created to replicate the strut support structure to be used to hold the subreflector in place above the main reflector dish (as can be seen in Fig. 4.11).

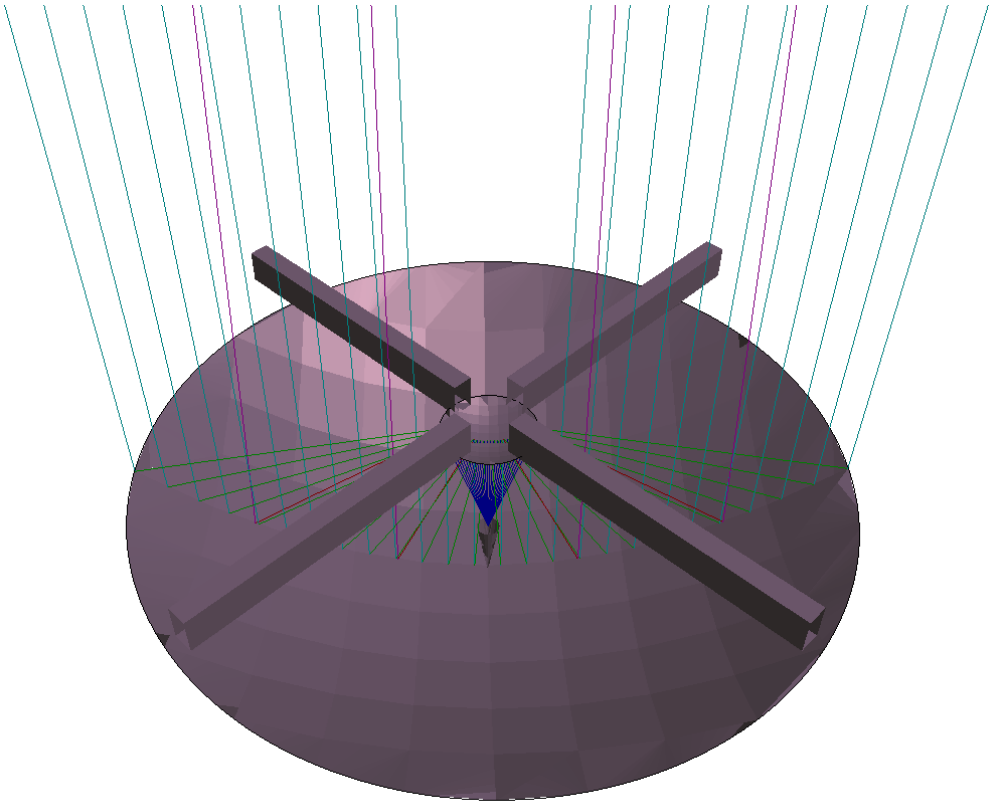

Fig. 3.11: GRASP Cassegrain Reflector Design, including Metallic Support Struts

Struts of different widths were simulated and their results compared to the radiation with no struts. Figures 4.12 to 4.14 show the radiation pattern at 340 GHz with struts 1mm and 3mm in width for 0º, 45º and 90º respectively.

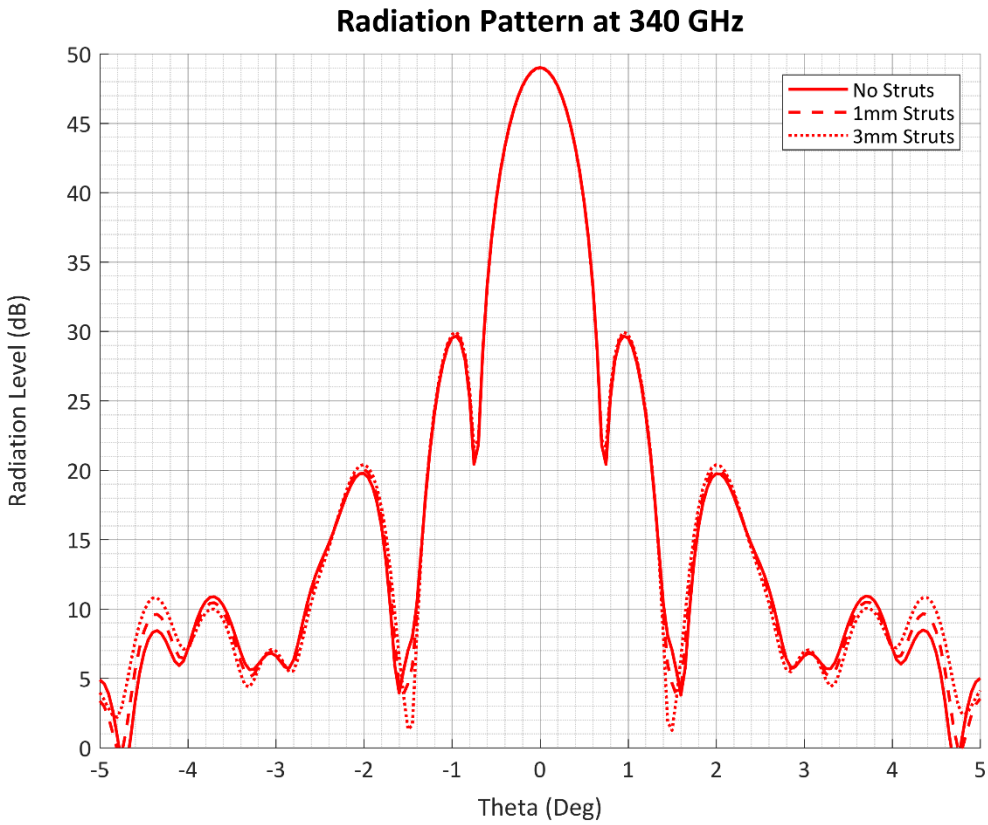

Fig. 3.12: Cassegrain Reflector including Support Struts Far-Field Radiation Pattern, Phi = 0º

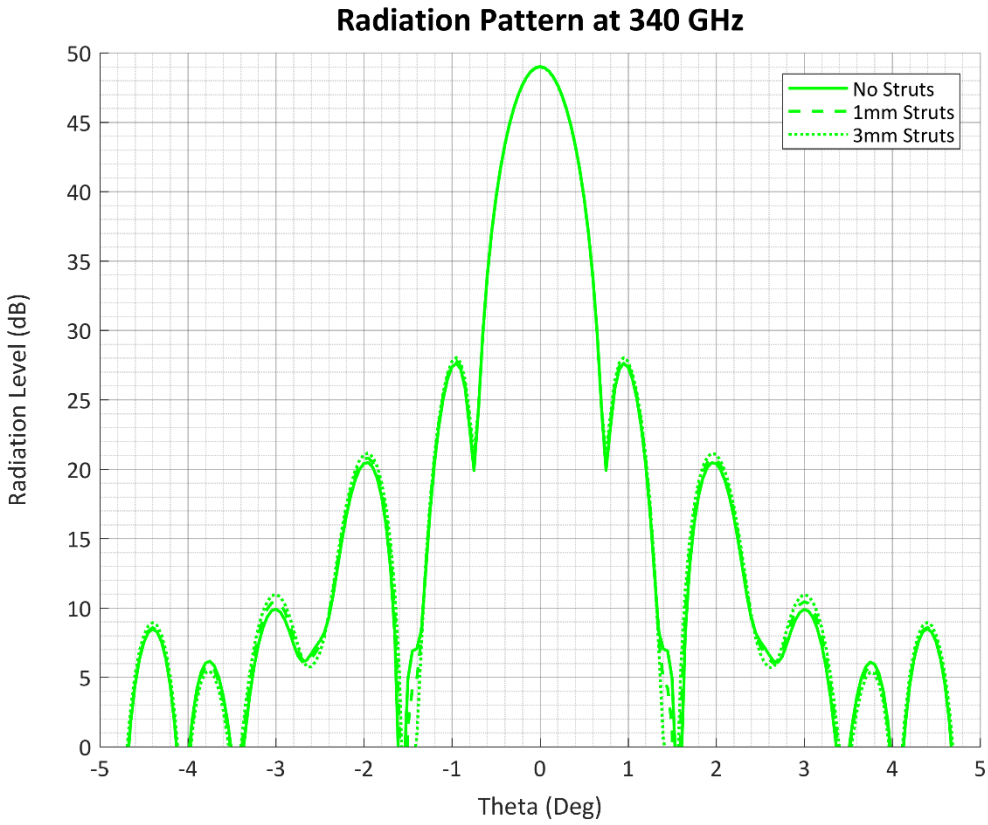

Fig. 3.13: Cassegrain Reflector including Support Struts Far-Field Radiation Pattern, Phi = 45º

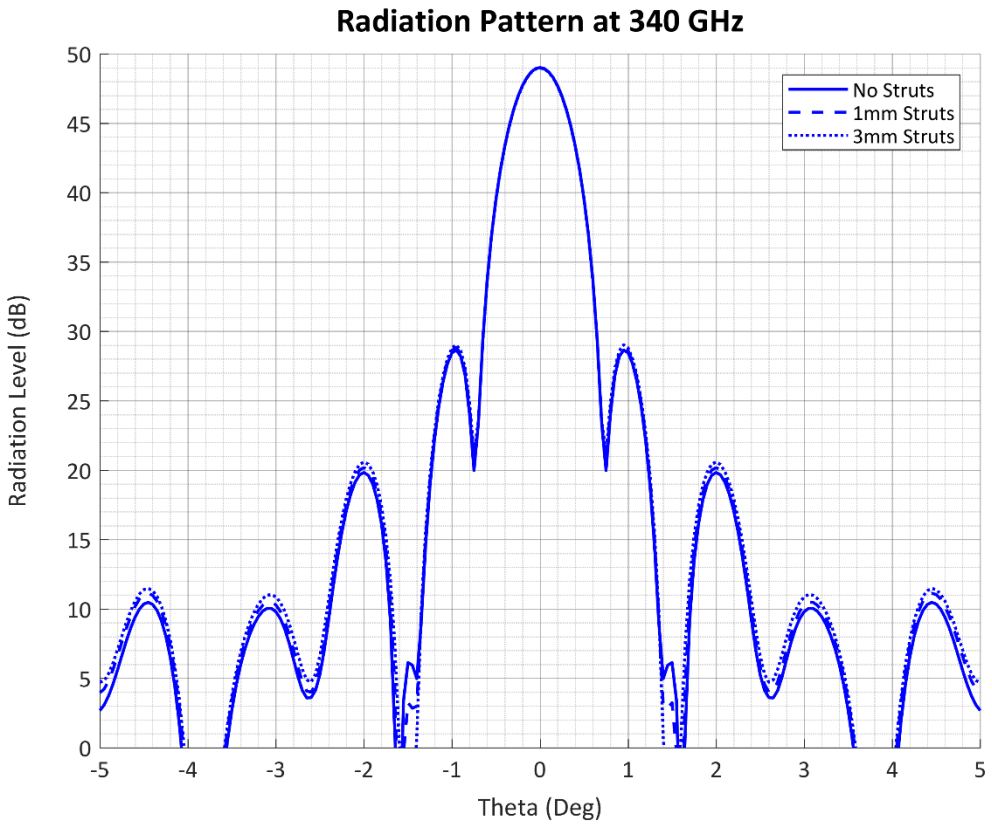

Fig. 3.14: Cassegrain Reflector including Support Struts Far-Field Radiation Pattern, Phi = 90º

As can be extracted from these results, the variation in the radiation pattern generated by the introduction of the support struts is extremely minimal, with variations of no more than 1.5 dB in the side lobes and no discernable variation in the main lobe. With this in mind, the 3mm struts were chosen for the final model because of their ease of fabricability when compared to the thinner alternatives.

Final Design

During the creation of the 3D model for manufacturing (design images and more details under “Mechanical Model” later in this document), it was discovered that the original design had problems.

Namely, two main concerns arose: for one, the support structure needed to be elevated above the edge of the reflector, which made the system higher around the reflector and more difficult to manufacture; also, the feedhorn needed to be introduced inside the base of the reflector almost its full length, which added another challenge with regards to physically being able to screw the feed to the main reflector.

With that in mind, the final design was carried out using the same diameter (100mm) and eccentricity (e = 1.5), but with the main reflector focal length *and* distance between the hyperbolic subreflector’s focii of 25mm (which means f = 25mm and c = 12.5mm).

In this configuration, the subreflector’s rim is at the same height (distance along the Z axis) as the main reflector’s, and the feed’s aperture is positioned at the reflector’s base. Both these facts make for simpler alignment and manufacturing (Figure 4.15).

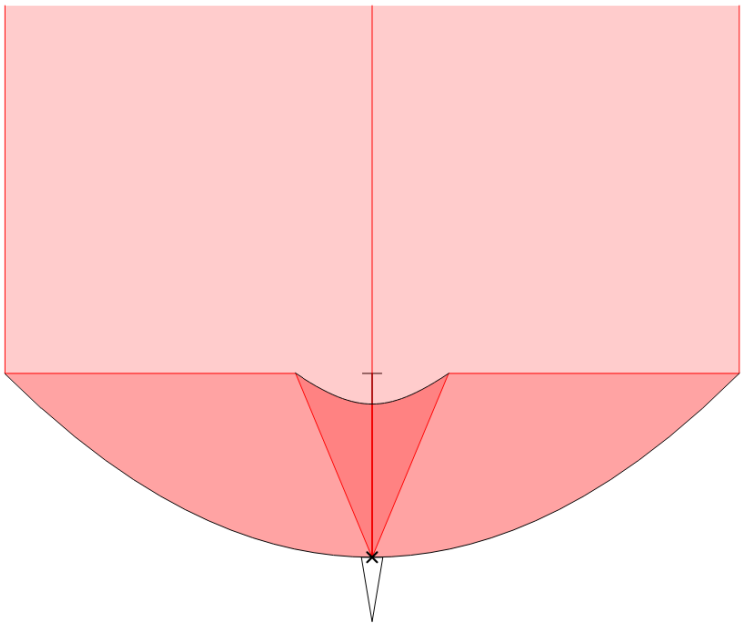

Fig. 3.15: Cassegrain Reflector Final Design Profile and Relative Positioning

The specific equations for the reflective surfaces in this case are (with X and Z in millimeters):

- Main Reflector: $z(x) = \frac{x^2}{100}$
- Subreflector: $z(x) = 8.33\sqrt{1 + \left(\frac{x}{9.32}\right)^2}$

For this configuration, the half-angle subtended from the feed to the subreflector's edge is 22.62º. This means that the necessary ideal Gaussian beam would be less directive (wider), so the pyramidal horn designed for the original, slightly more directive beam will suffice in this case.

Additionally, at this time the client relayed an update informing that the system had to function over a 20 GHz bandwidth (from 330 to 350 GHz). It was fortunately confirmed that the system could operate at these frequencies with the same capabilities without the need for any sort of modification.

The simulated results for the definitive version of the system, including a pyramidal WR2.8 feedhorn and four rectangular support struts, are as follows:

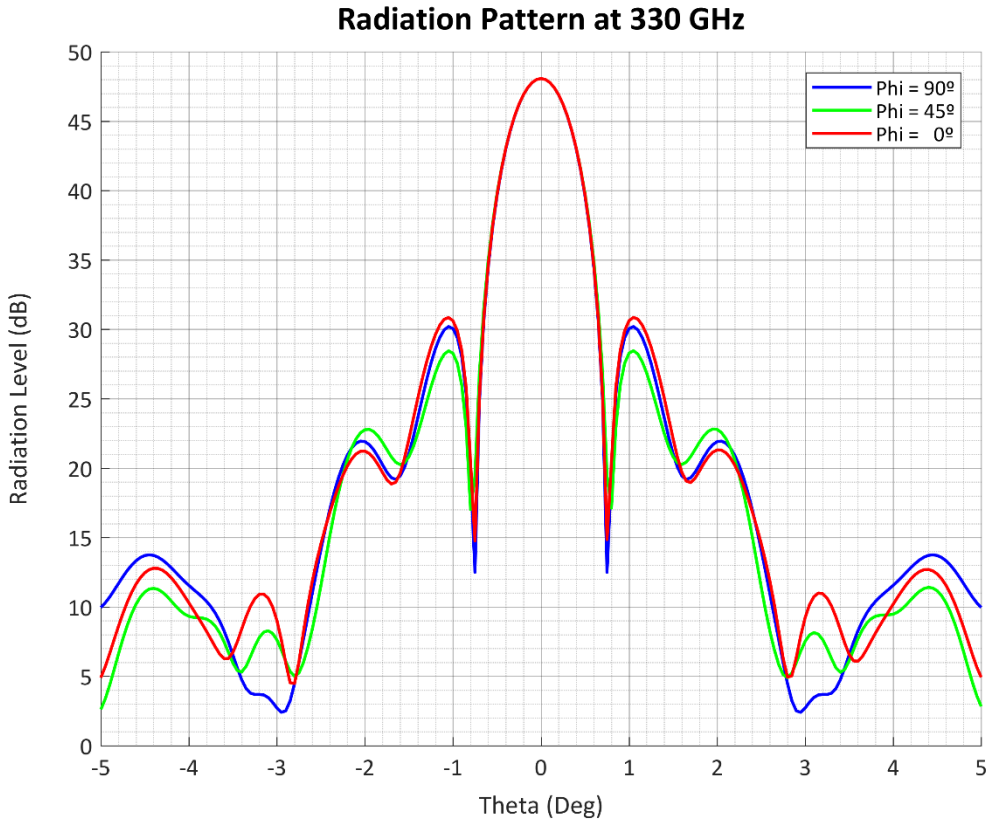

Fig. 3.16: Cassegrain Reflector Final Model Far-Field Radiation Pattern at 330 GHz

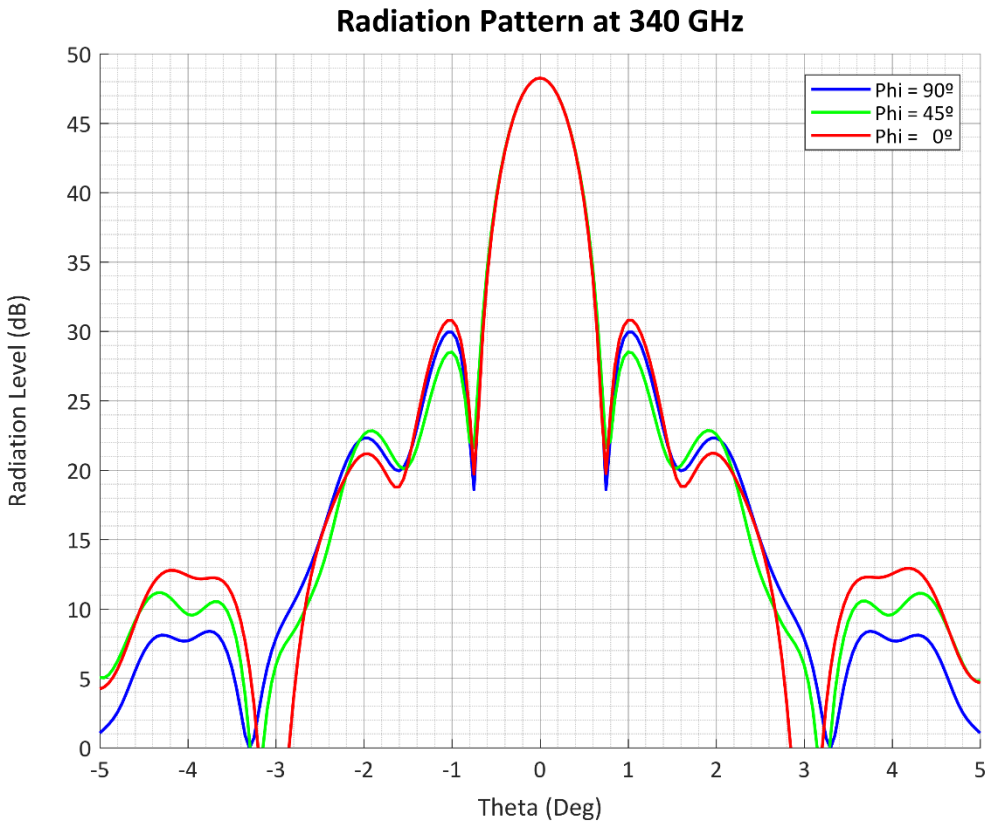

Fig. 3.17: Cassegrain Reflector Final Model Far-Field Radiation Pattern at 340 GHz

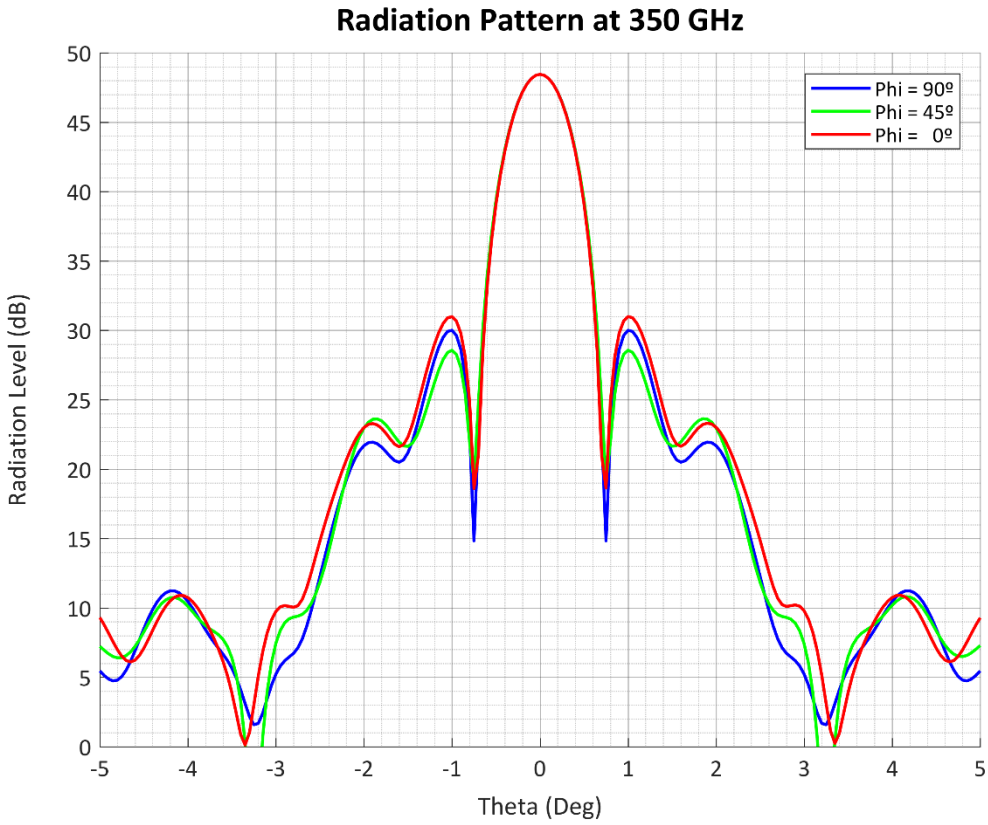

Fig. 3.18: Cassegrain Reflector Final Model Far-Field Radiation Pattern at 350 GHz

Displacement Simulations

When carrying out simulations in *GRASP*, it is assumed that every one of the elements intervening in the radiation is in its precise position with regards to the rest. Because operating at 340GHz implies having a wavelength of 0.88mm, a 200µm displacement in the positioning of one of these components would mean moving almost λ/4, and a 500µm displacement would mean moving more than λ/2.

Since these small displacements can occur and have the potential to not be trivial [5], simulations have been done displacing both the subreflector dish and the feedhorn 200 and 500µm to see how the radiation pattern would be affected.

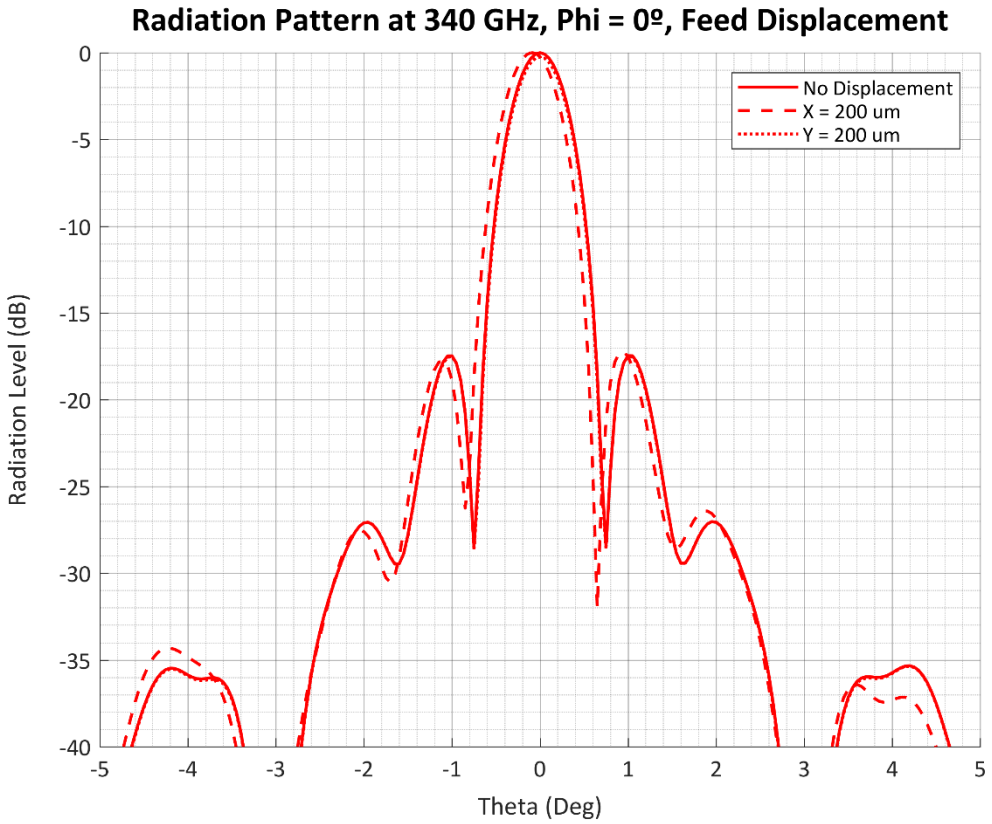

Fig. 3.19: Cassegrain Reflector Final Model Feedhorn X and Y-axis Displacement Test (200 µm)

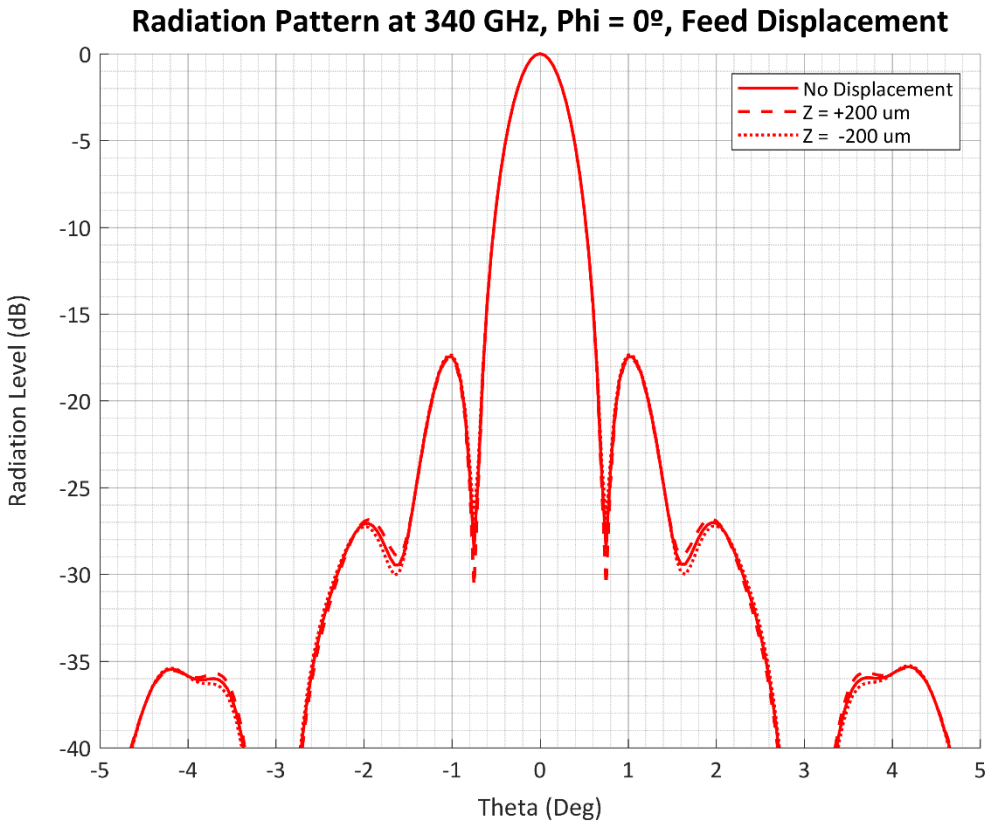

Fig. 3.20: Cassegrain Reflector Final Model Feedhorn Z-axis Displacement Test (200 µm)

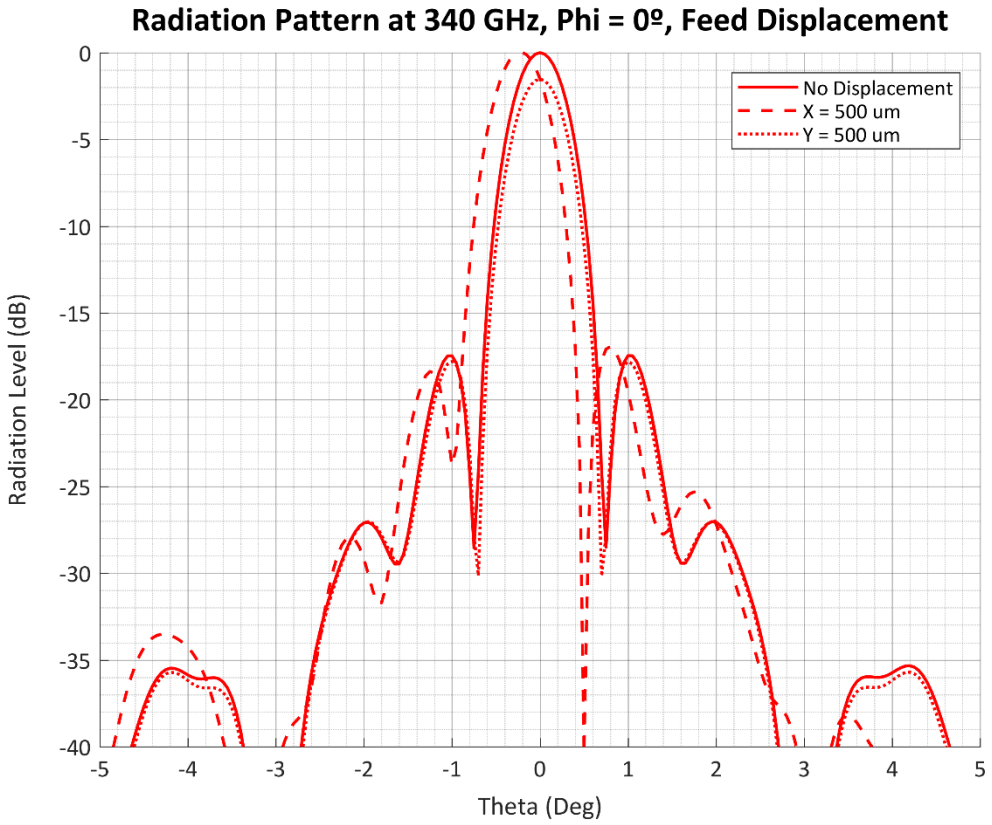

Fig. 3.21: Cassegrain Reflector Final Model Feedhorn X and Y-axis Displacement Test (500 µm)

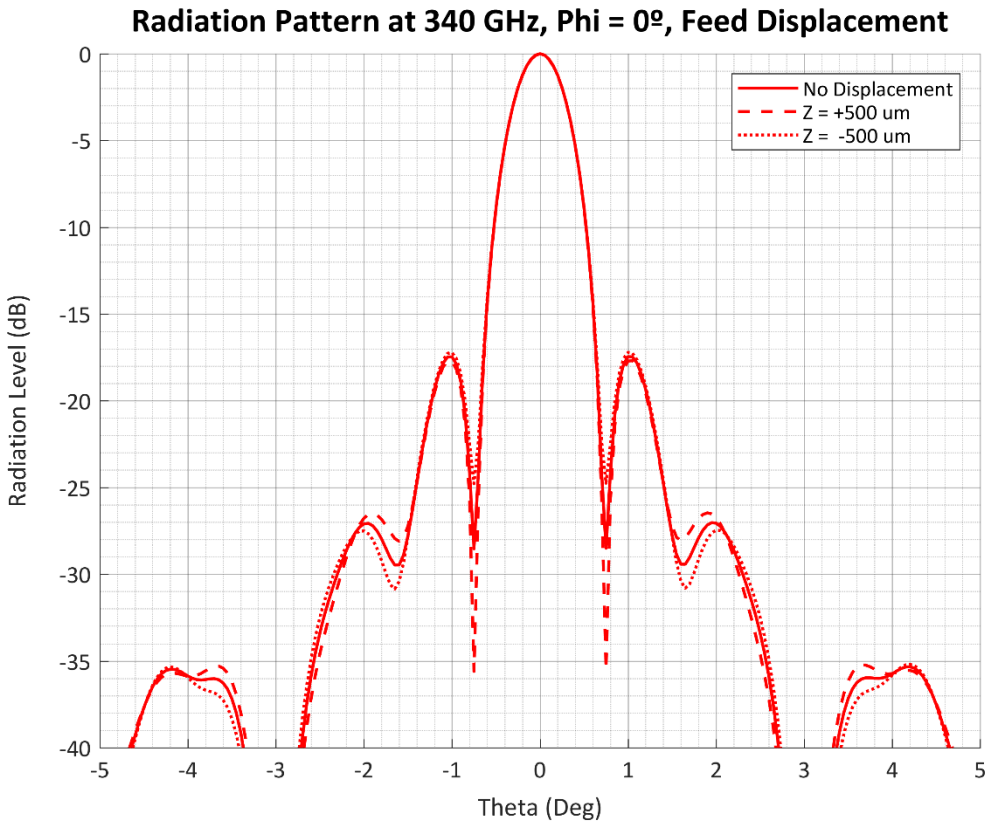

Fig. 3.22: Cassegrain Reflector Final Model Feedhorn Z-axis Displacement Test (500 µm)

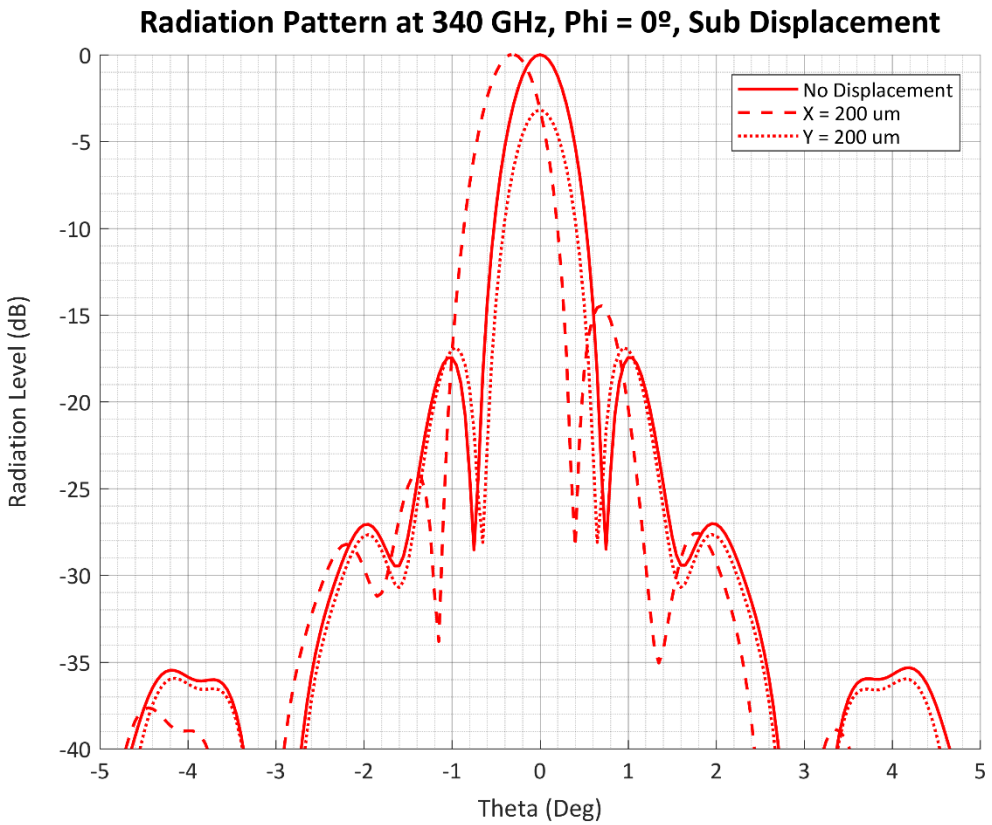

Fig. 3.23: Cassegrain Reflector Final Model Subreflector X and Y-axis Displacement Test (200 µm)

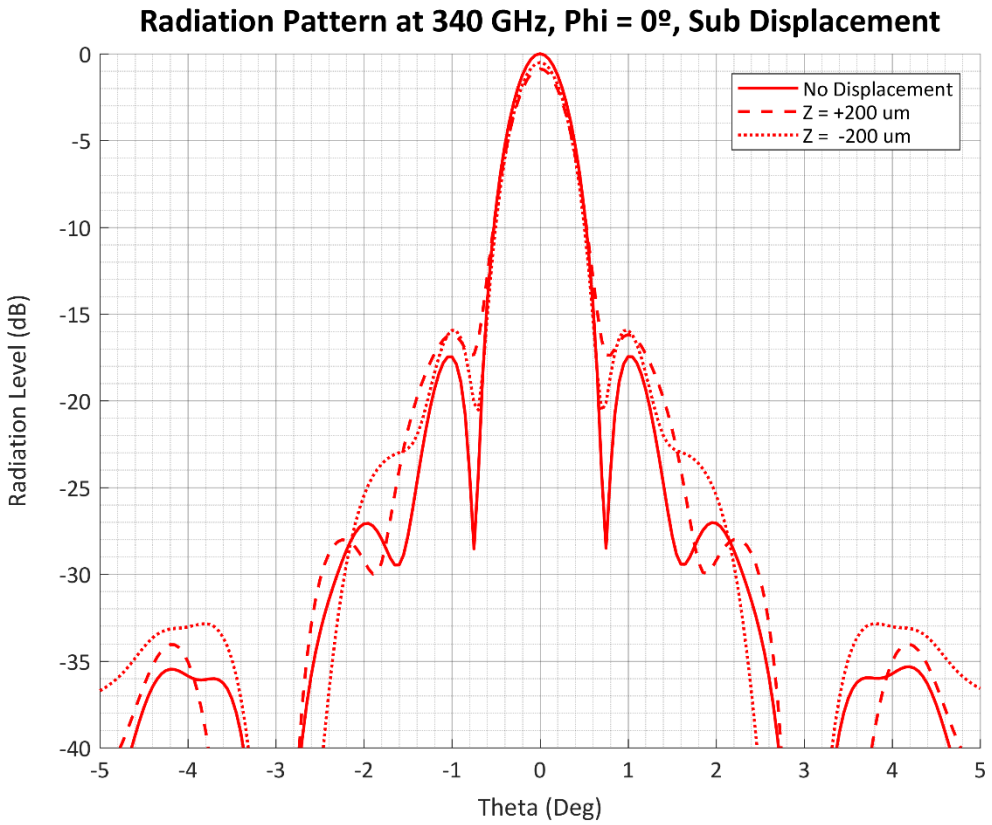

Fig. 3.24: Cassegrain Reflector Final Model Subreflector Z-axis Displacement Test (200 μm)

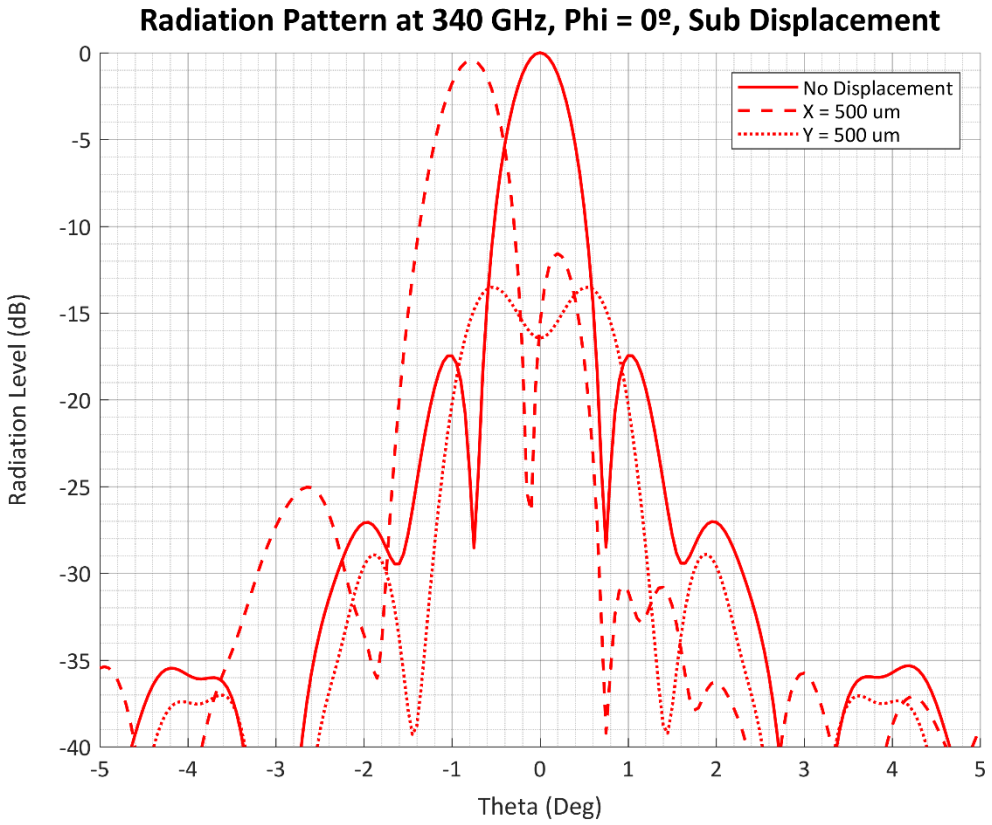

Fig. 3.25: Cassegrain Reflector Final Model Subreflector X and Y-axis Displacement Test (500 μm)

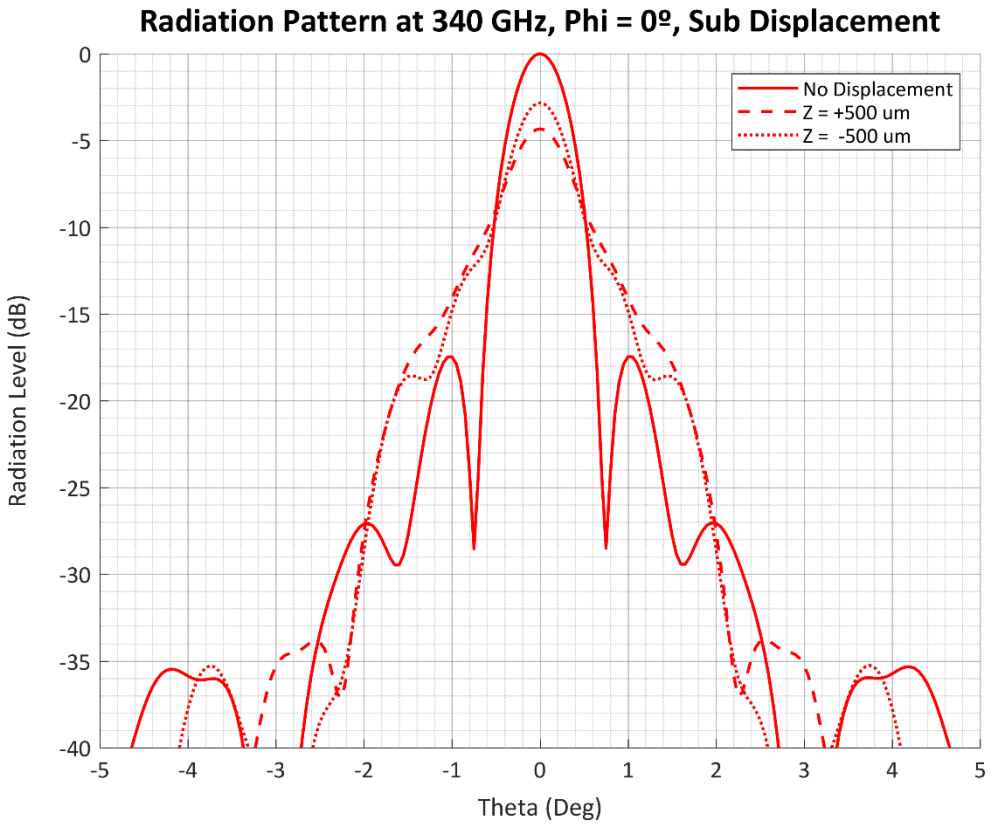

Fig. 3.26: Cassegrain Reflector Final Model Subreflector Z-axis Displacement Test (500 µm)

It is important to know the extent of these variations in order to determine the manufacturing tolerances of each component and the precision of their assembly in order to be measured accurately.

The comparison graphs show that displacing the feedhorn barely has any noticeable effects, especially when moving it along the Z axis. With 500 µm, the X and Y axis displacements imply a 0.3º shift of the main lobe at most, which translates to a 2 dB loss at 0º.

As for the subreflector, these results prove that (as could be expected) its relative positioning is the most crucial. Moving it along the Z axis incurs in a worst-case 0º gain loss of 4.5 dB (for Z = +500 µm) due to destructive phase interference. Displacing the X and Y axes is much worse, creating a loss of 17 dB for a 500 µm variation due to a 0.9º shift in the main lobe's position.

Mechanical Model

Once the simulated model was deemed valid, the feedhorn, subreflector and main reflector were imported into *HFSS* to create the mechanical model around them.

The original design for the 3D model had the two problems listed above: having the subreflector above the main reflector caused the structure outside it to significantly increase in height (and therefore possibly introduce additional scattering and/or reflections), and the feedhorn's length prevented its proper fixed positioning with regards to the reflector dishes. Both these issues were solved for the final design, although both are included for clarity and comparison purposes.

Initial Design

The first design had an outer diameter of 144mm and a total height of 50mm.

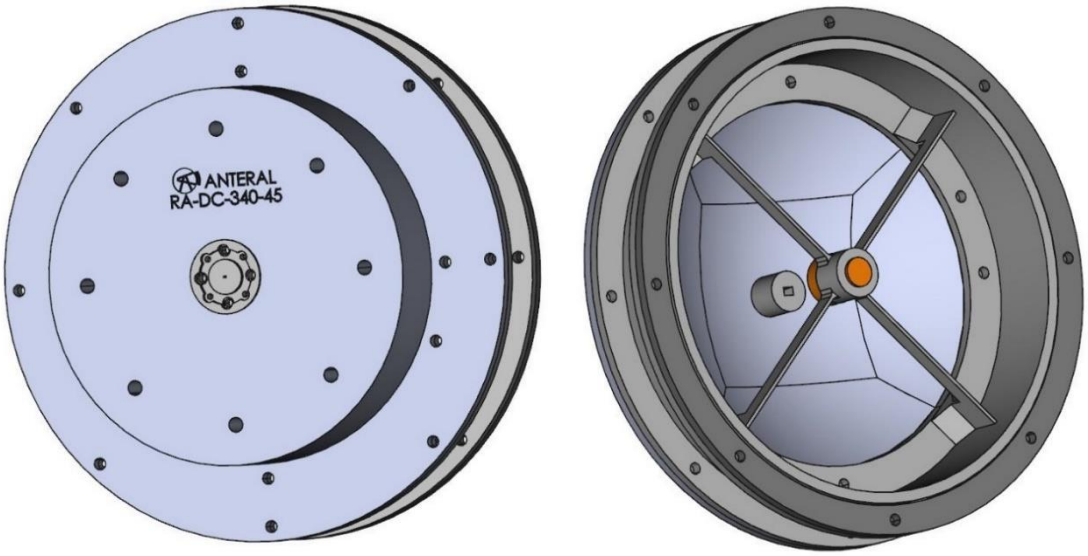

Fig. 3.27: Bottom and Top View of the Original 3D Mechanical Model

Final Design

The definitive design has an outer diameter of 140mm and a total height of 41.8mm (plus the feedhorn's base).

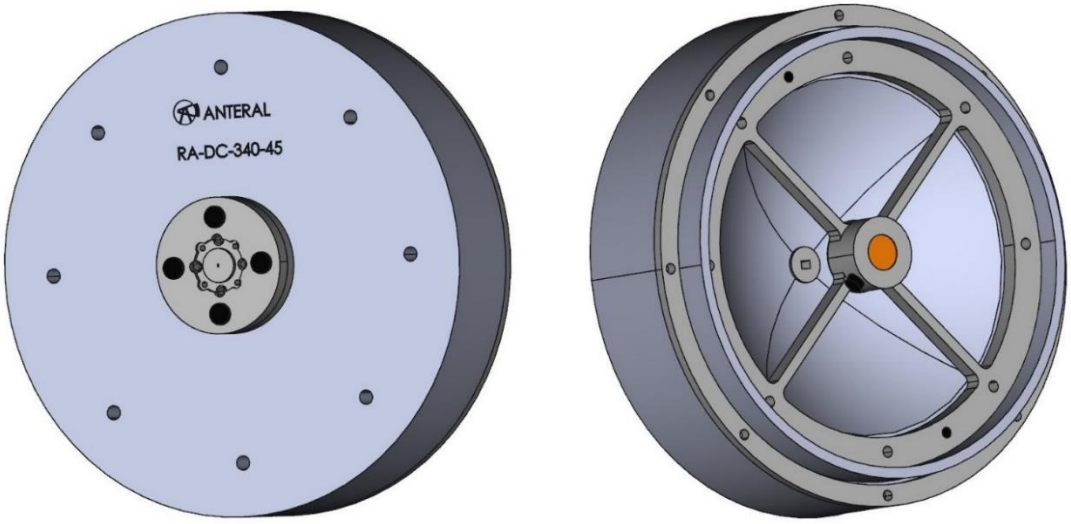

Fig. 3.28: Bottom and Top View of the Final 3D Mechanical Model

Manufactured System

After completing the design, the system was manufactured and received for measuring and testing. Figures 4.29 to 4.33 show images of the completed system.

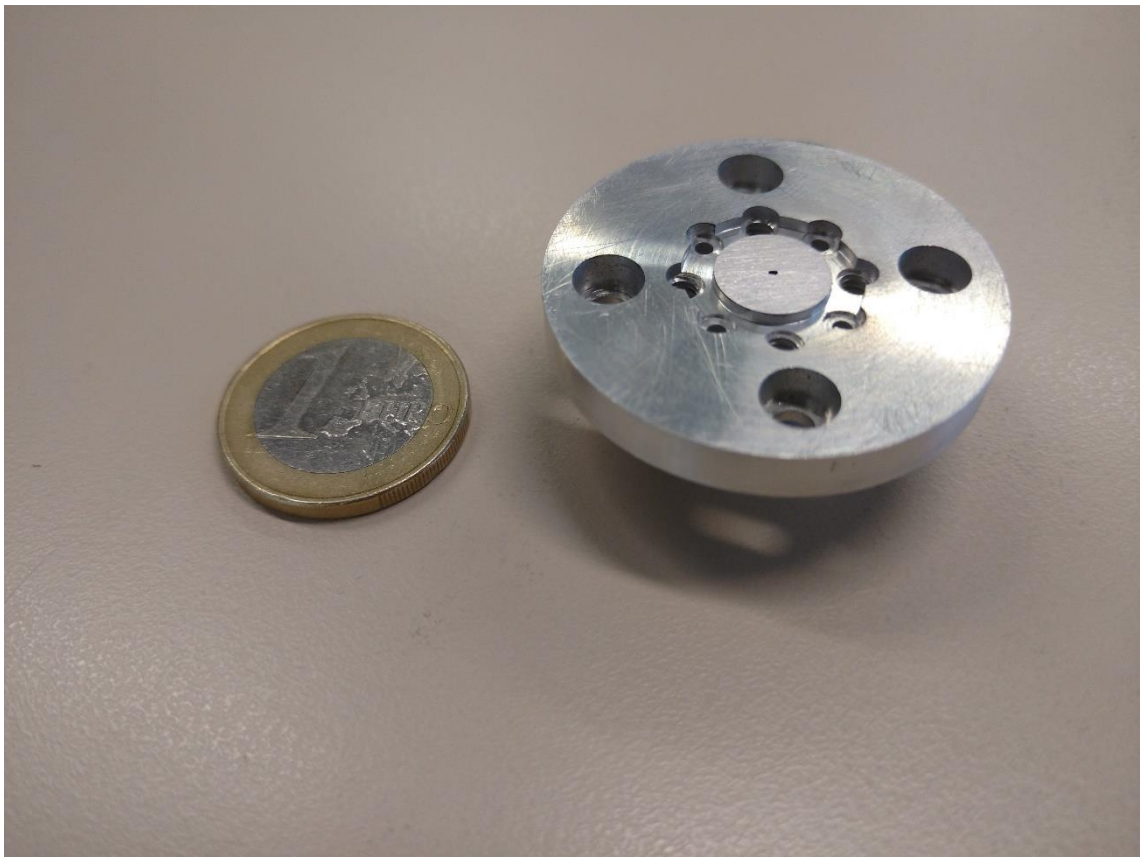

Fig. 3.29: RA-DC-45-340 Manufactured Model (a)

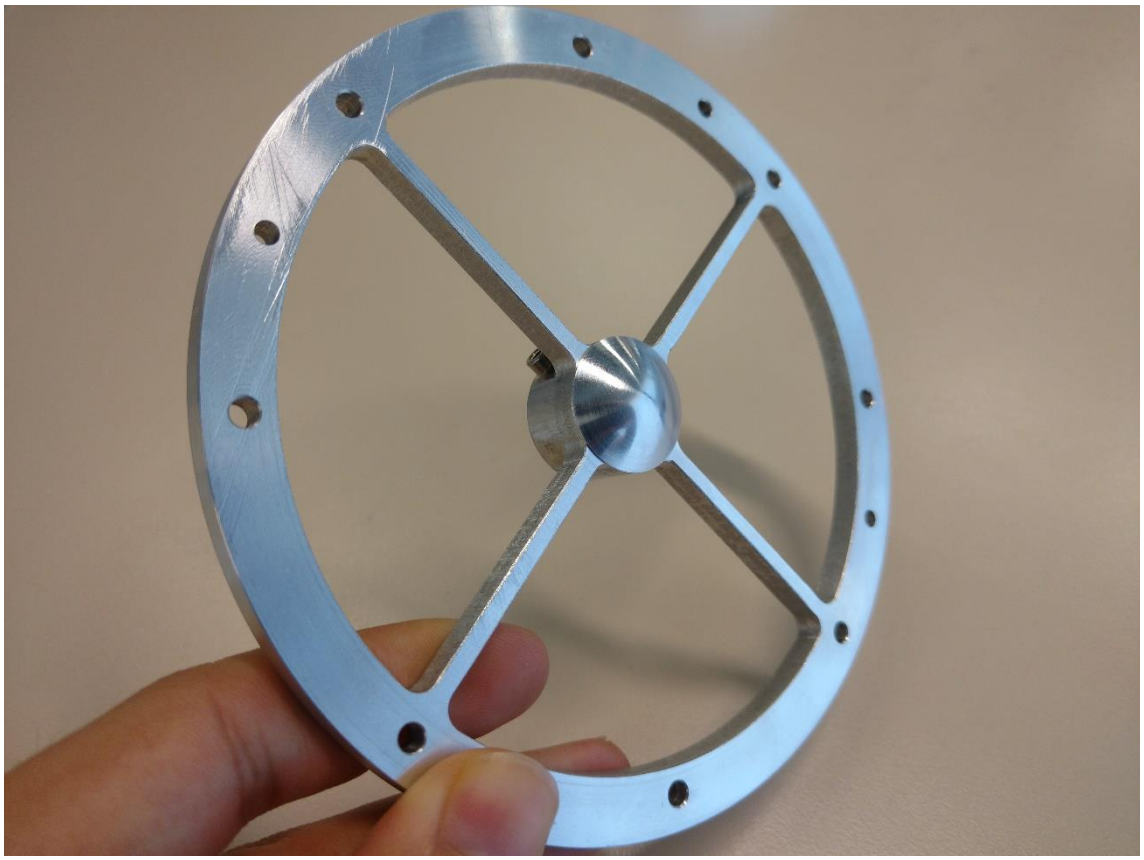

Fig. 3.30: RA-DC-45-340 Manufactured Model (b)

Fig. 3.31: RA-DC-45-340 Manufactured Model (c)

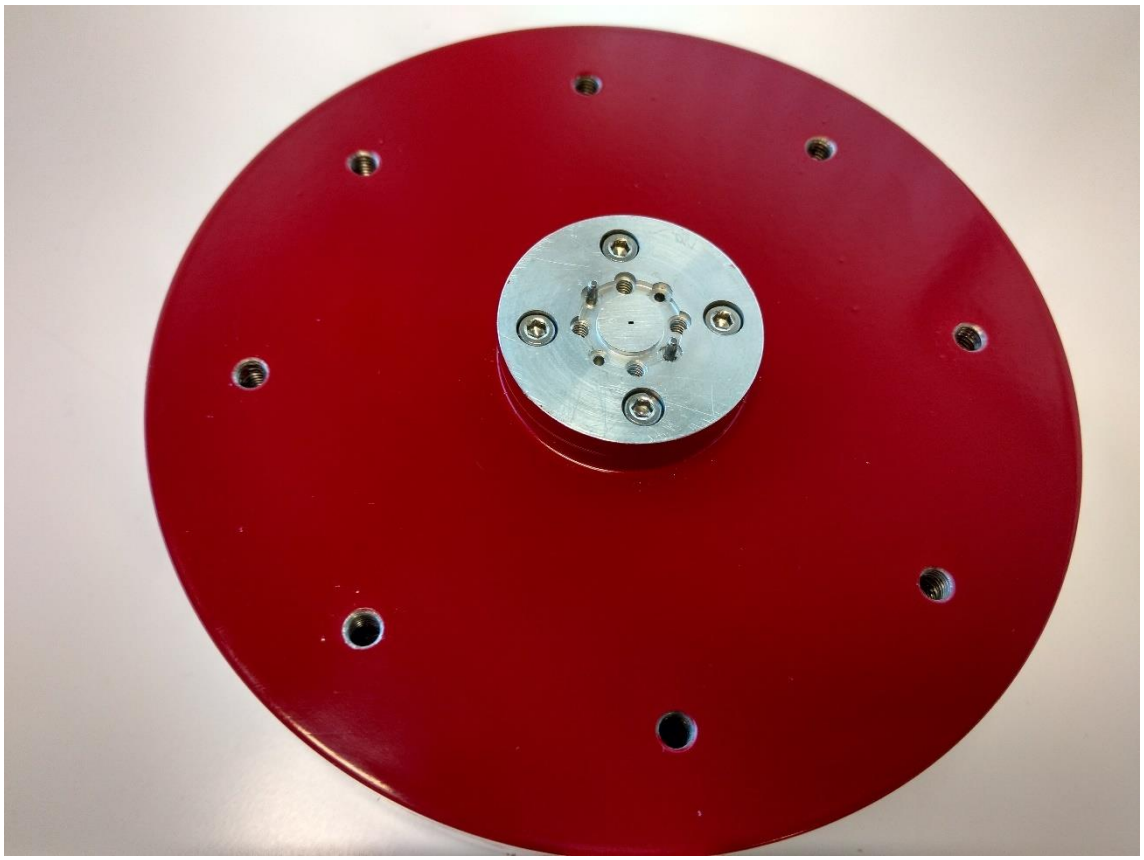

Fig. 3.32: RA-DC-45-340 Manufactured Model (d)

Fig. 3.33: RA-DC-45-340 Manufactured Model (e)

Measurements

The system was measured in Near-Field, using two 325-500 GHz sources in the configuration shown below.

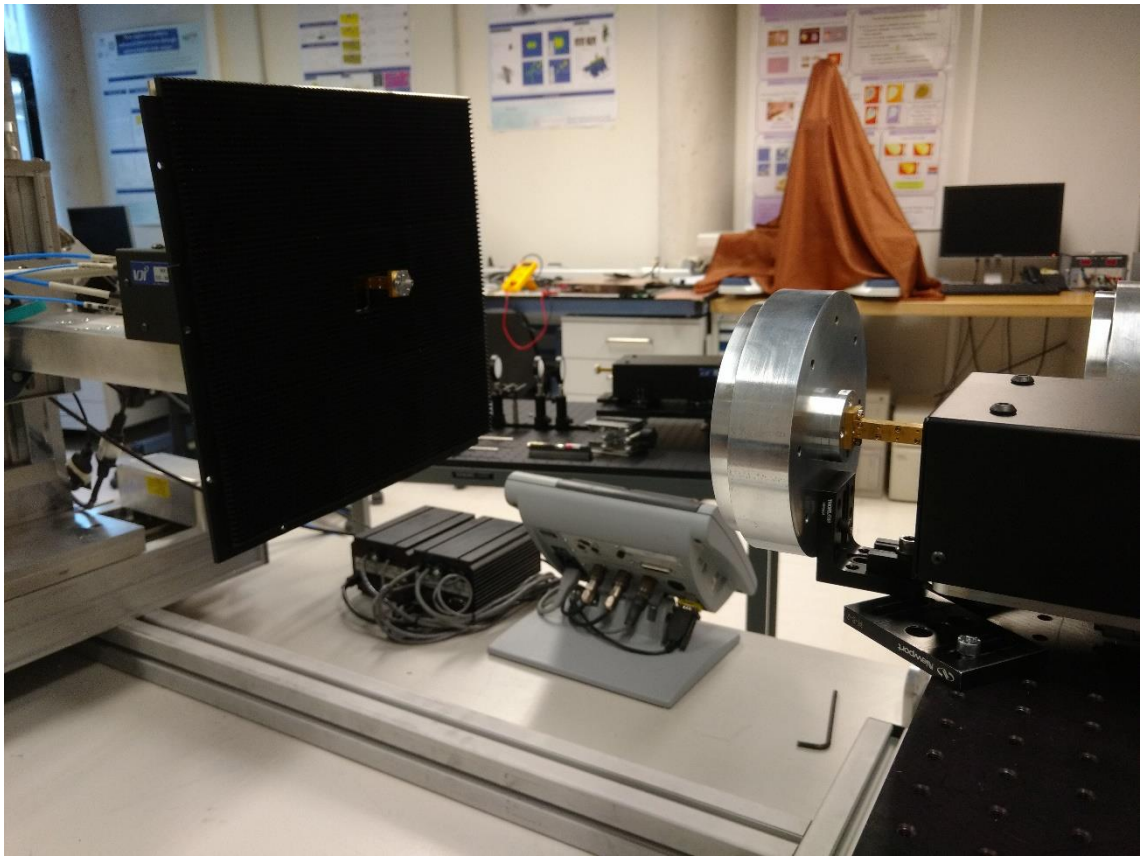

Fig. 3.34: RA-DC-45-340 Measurement Setup (a)

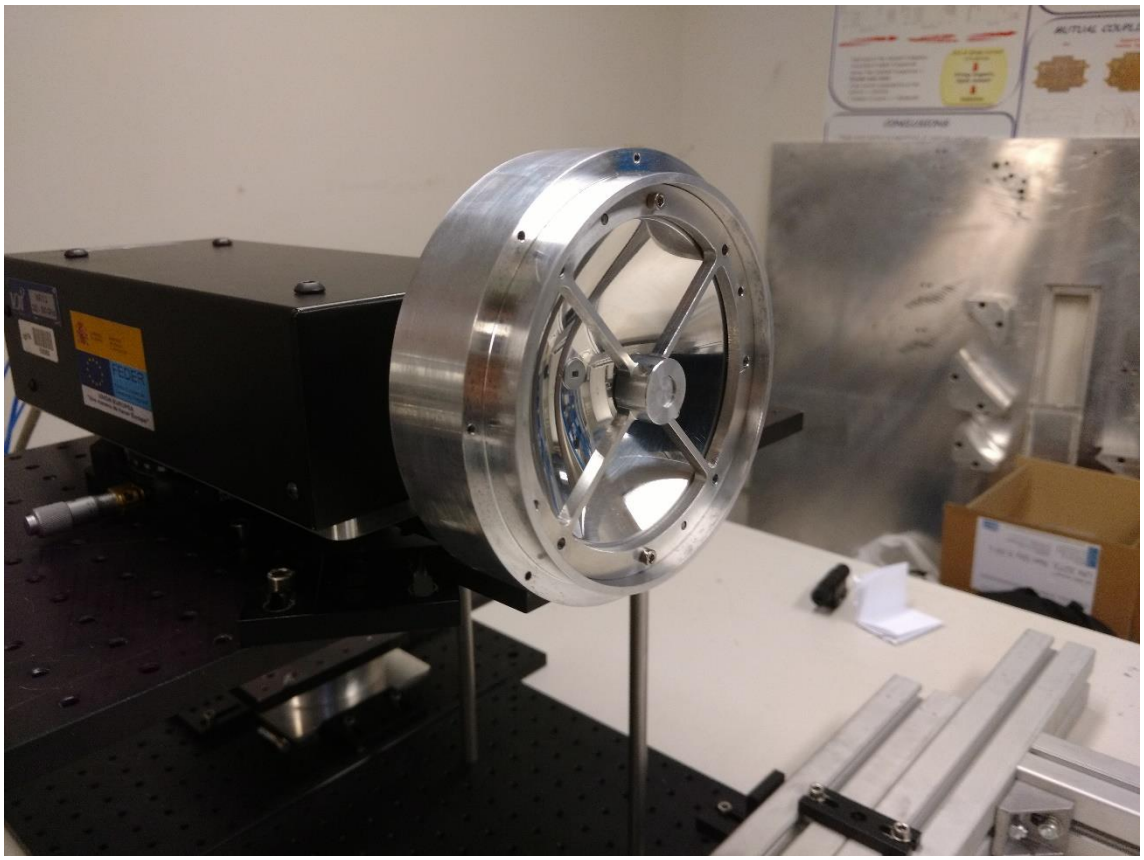

Fig. 3.35: RA-DC-45-340 Measurement Setup (b)

Figures 4.36 to 4.41 show the measured near-field radiation results, figure 4.42 shows the measured directivity and figures 4.43 to 4.47 show the measured far-field radiation results for the manufactured system. The solid lines are the measured values, while the dashed lines are the simulated values included for comparison's sake (the values have been normalized to a 0dB maximum).

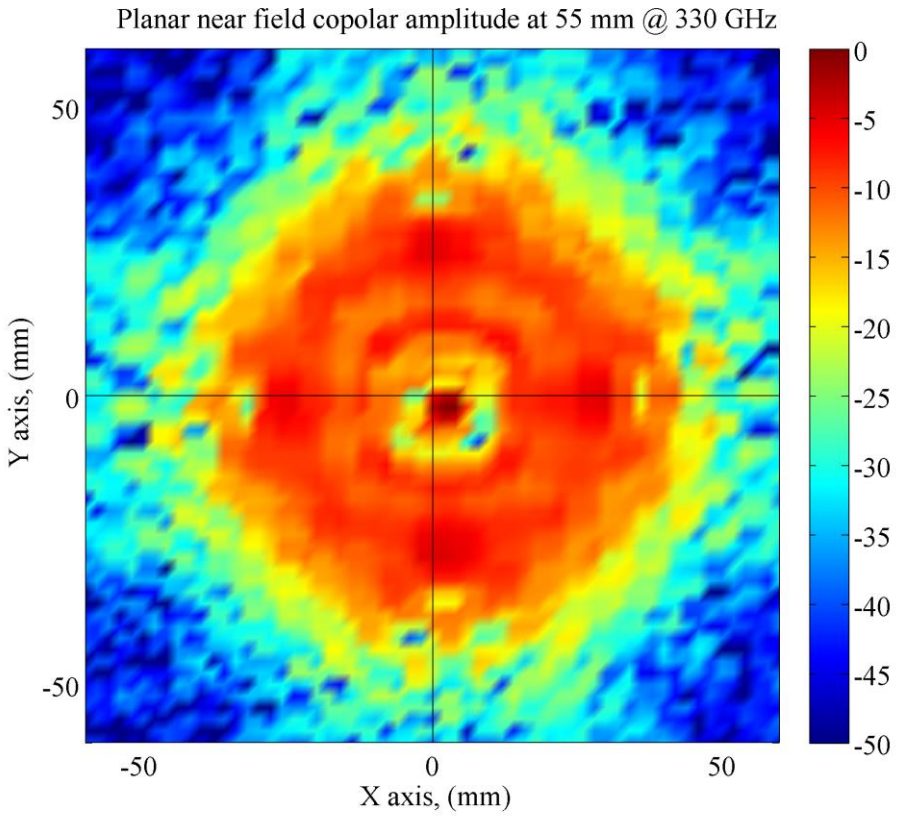

Fig. 3.36: RA-DC-45-340 Measured Near-Field Radiation Pattern Amplitude at 330 GHz

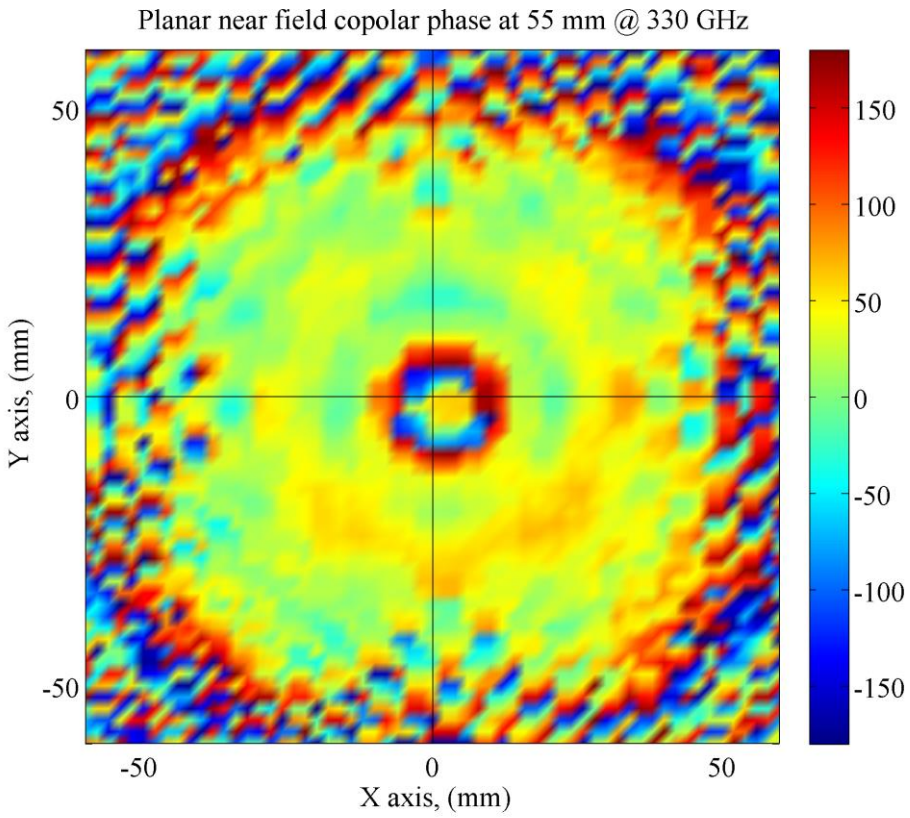

Fig. 3.37: RA-DC-45-340 Measured Near-Field Radiation Pattern Phase at 330 GHz

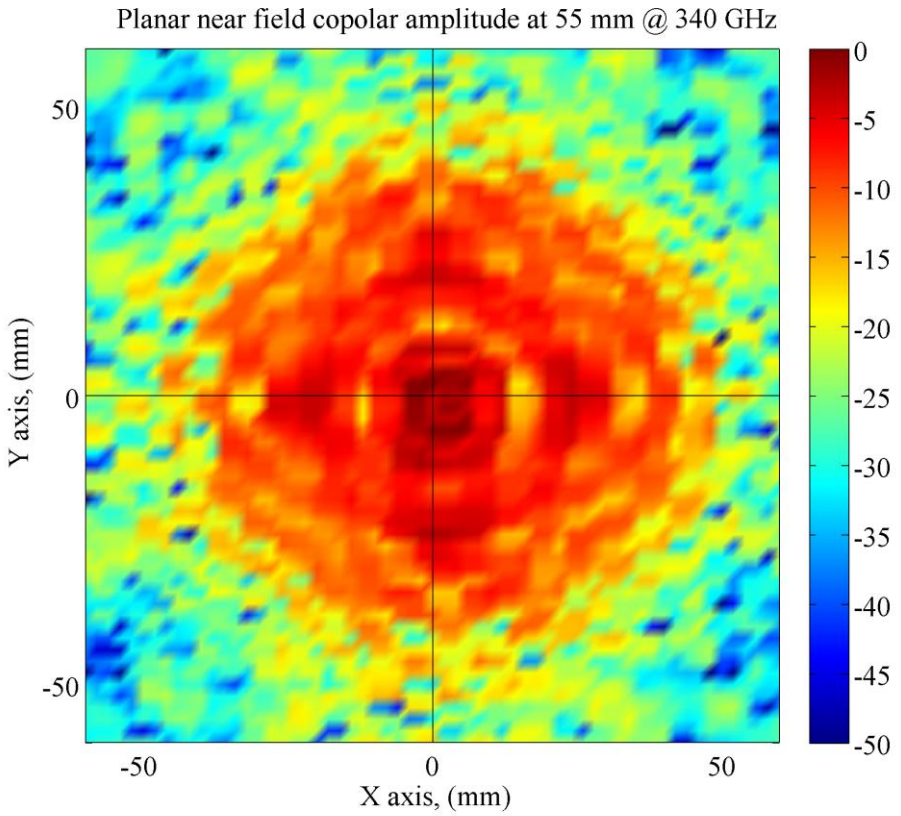

Fig. 3.38: RA-DC-45-340 Measured Near-Field Radiation Pattern Amplitude at 340 GHz

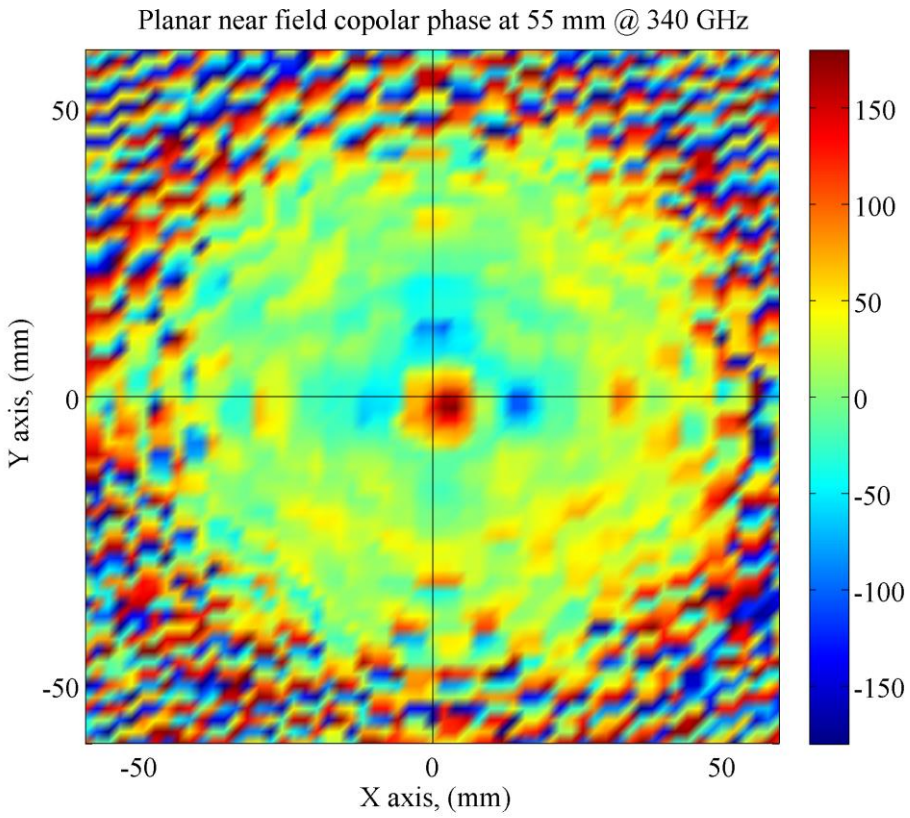

Fig. 3.39: RA-DC-45-340 Measured Near-Field Radiation Pattern Phase at 340 GHz

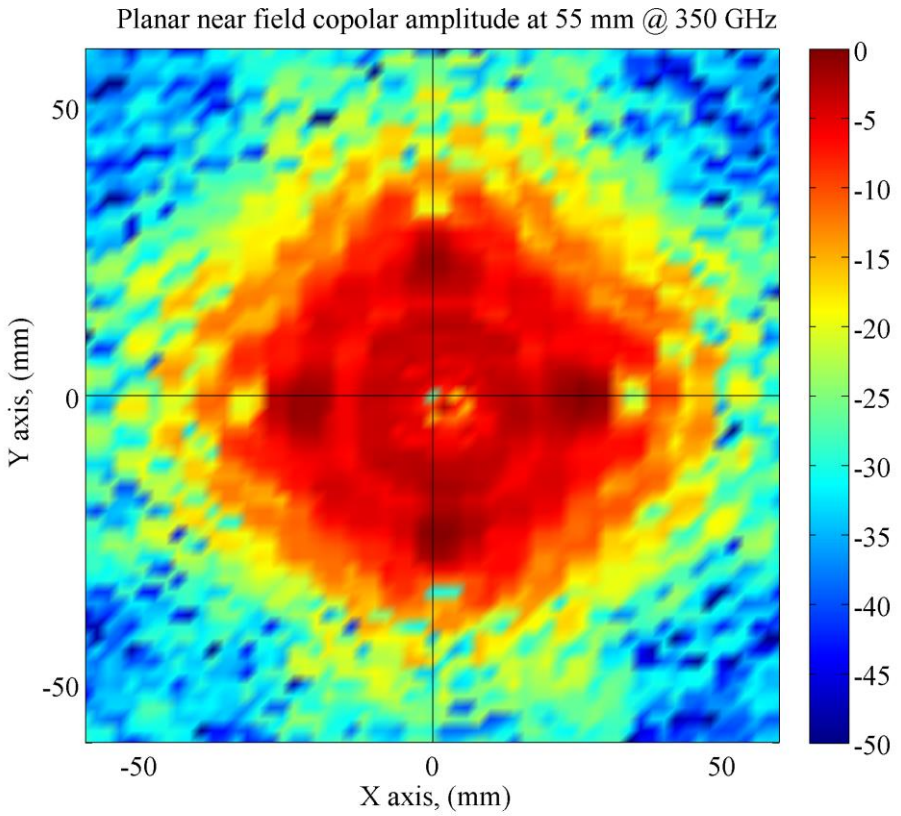

Fig. 3.40: RA-DC-45-340 Measured Near-Field Radiation Pattern Amplitude at 350 GHz

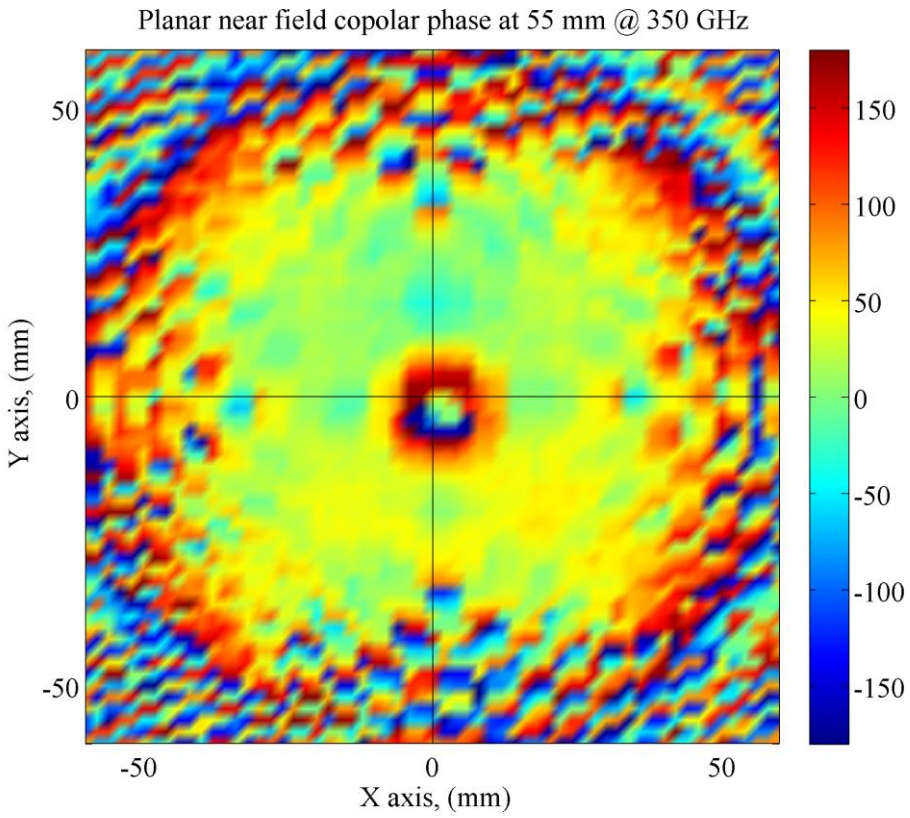

Fig. 3.41: RA-DC-45-340 Measured Near-Field Radiation Pattern Phase at 350 GHz

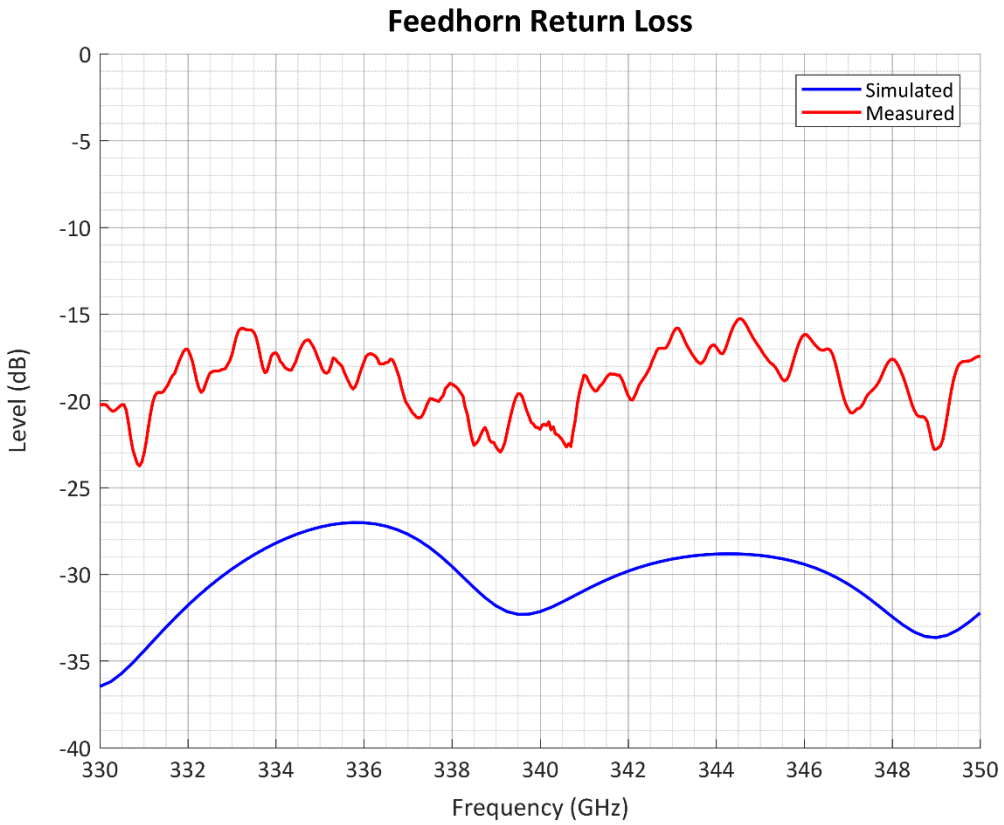

Fig. 3.42: RA-DC-45-340 Measured and Simulated Return Loss Across the Frequency Band

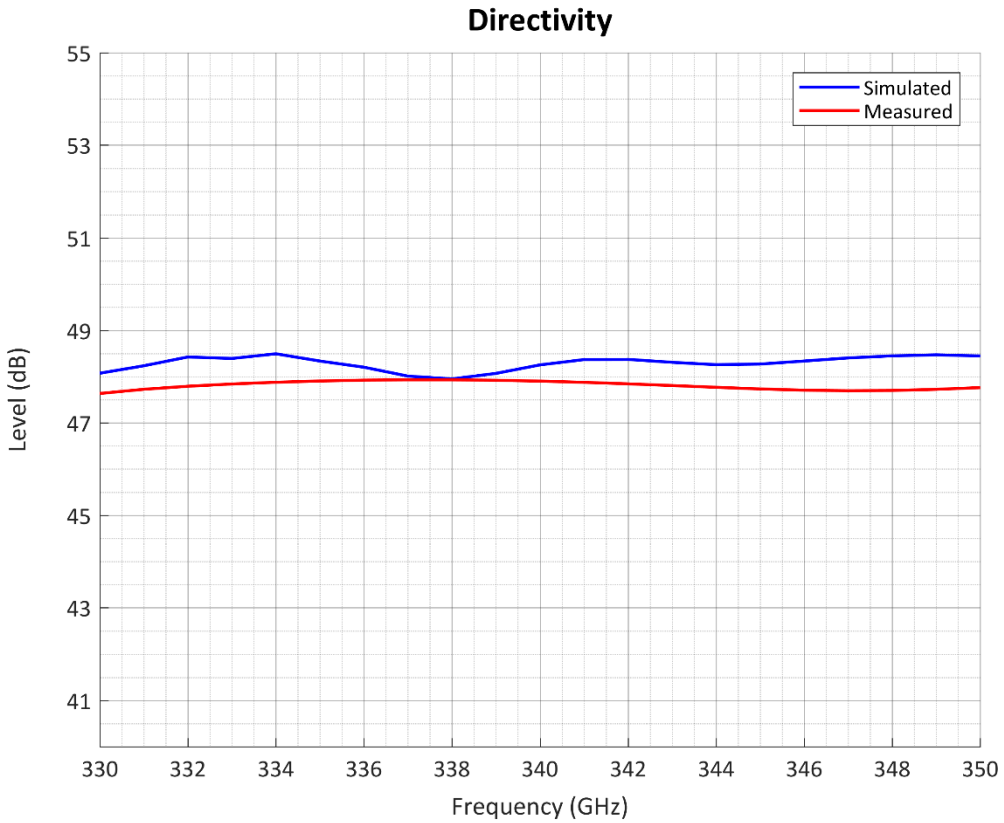

Fig. 3.43: RA-DC-45-340 Measured and Simulated Directivity Across the Frequency Band

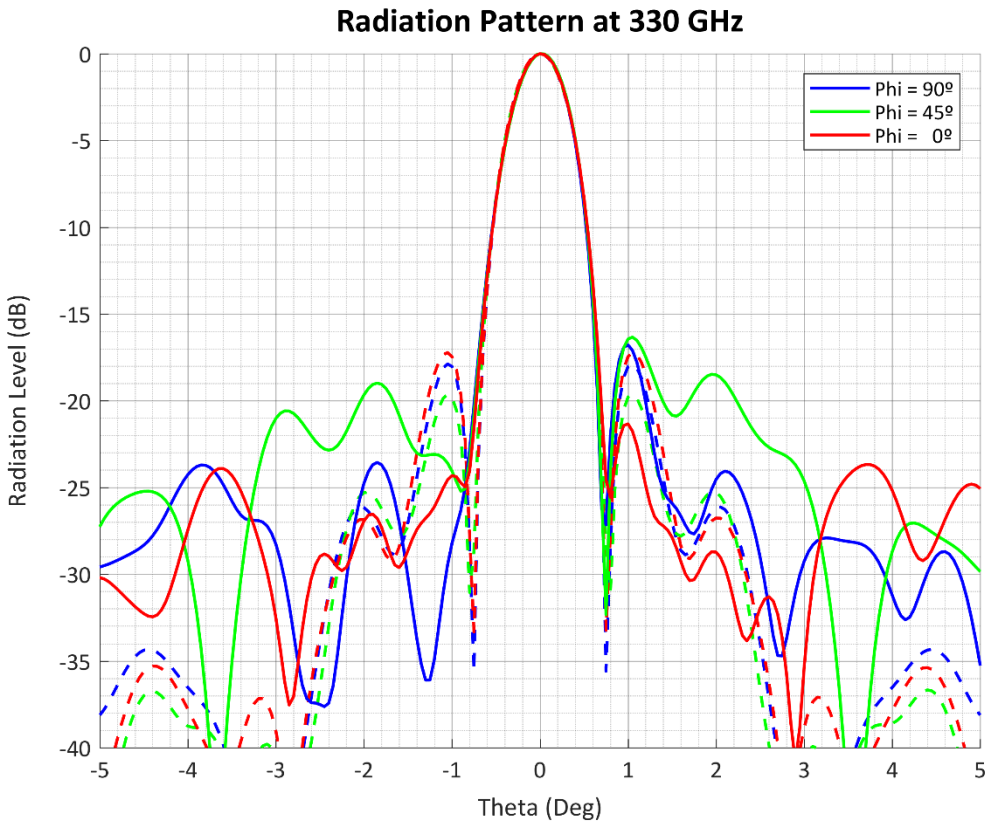

Fig. 3.44: RA-DC-45-340 Measured and Simulated Far-Field Radiation Pattern at 330 GHz

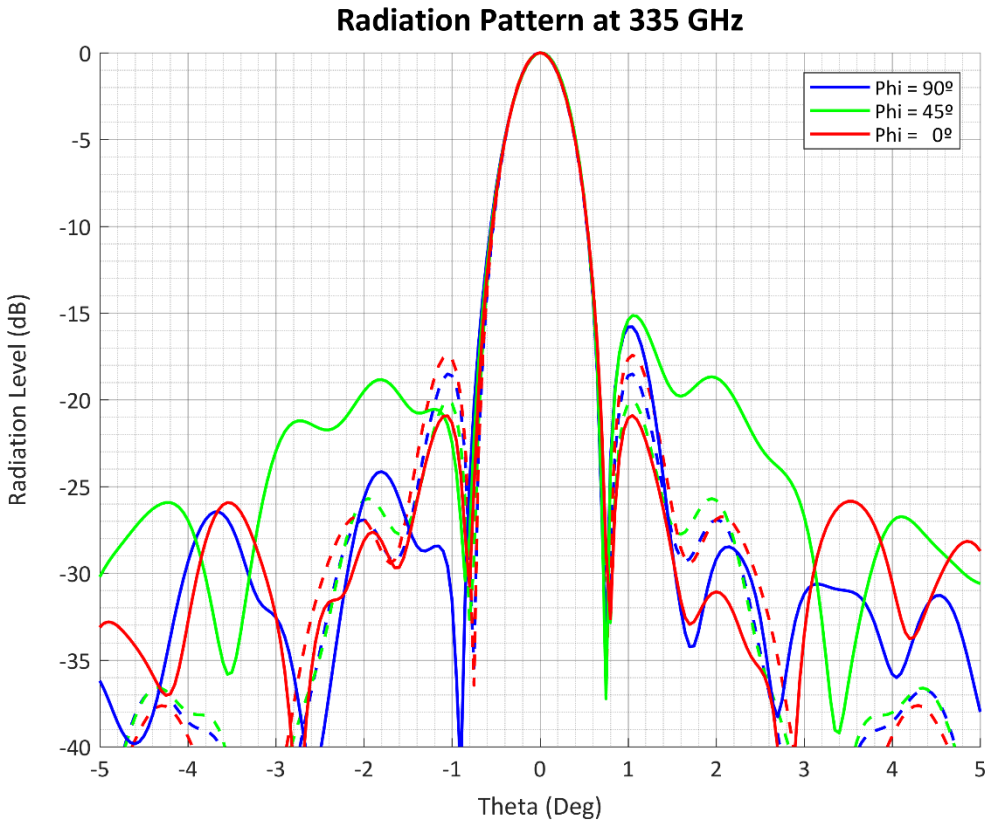

Fig. 3.45: RA-DC-45-340 Measured and Simulated Far-Field Radiation Pattern at 335 GHz

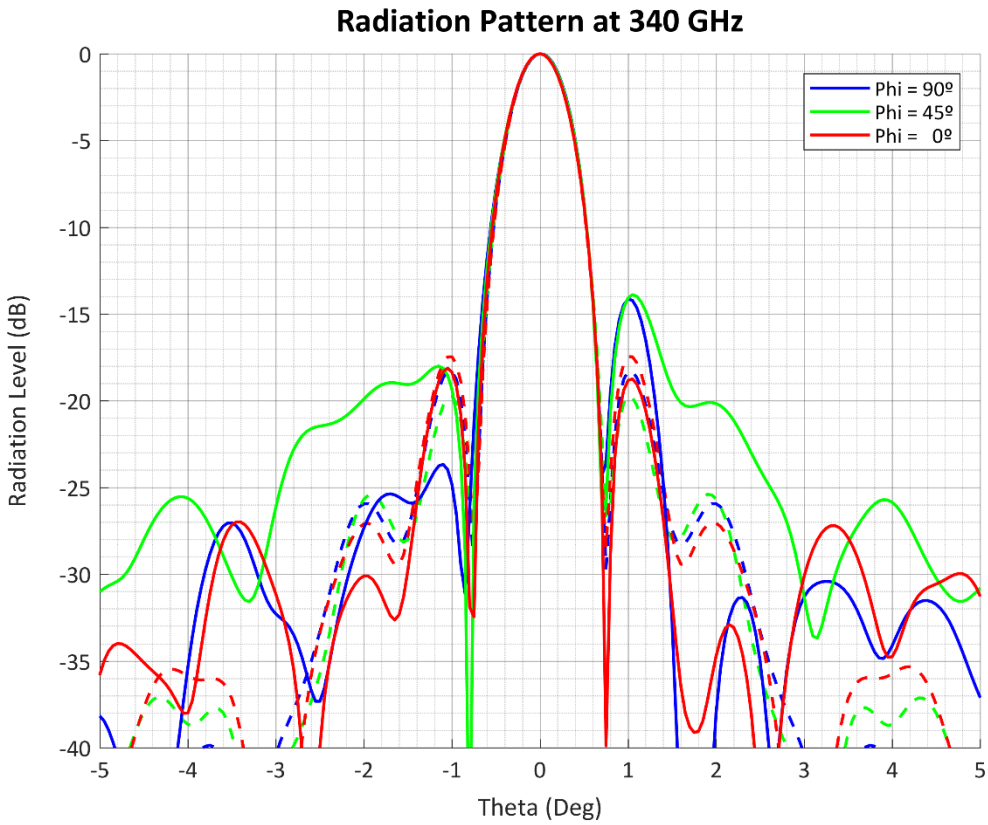

Fig. 3.46: RA-DC-45-340 Measured and Simulated Far-Field Radiation Pattern at 340 GHz

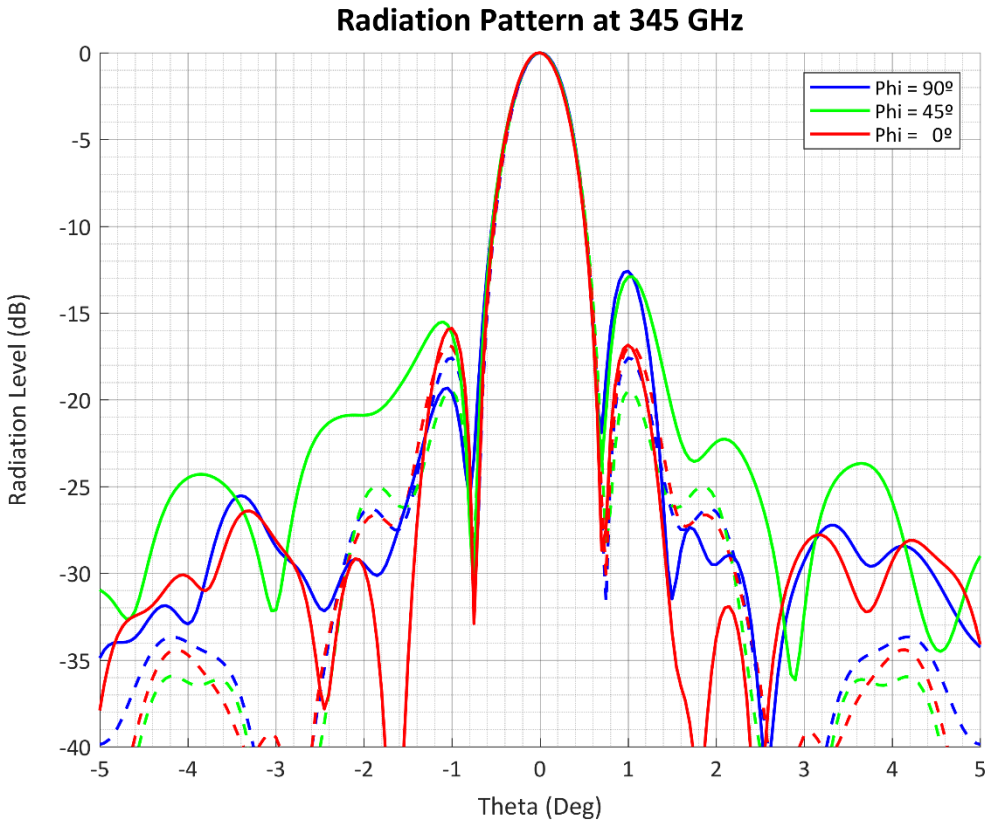

Fig. 3.47: RA-DC-45-340 Measured and Simulated Far-Field Radiation Pattern at 345 GHz

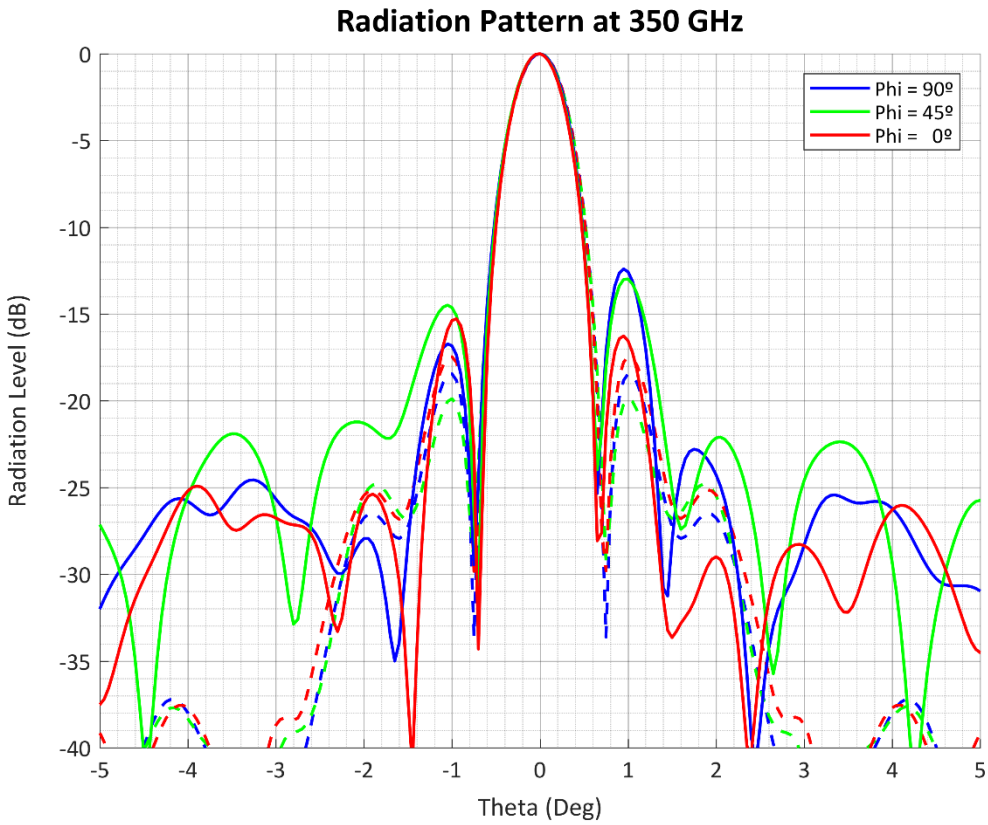

Fig. 3.48: RA-DC-45-340 Measured and Simulated Far-Field Radiation Pattern at 350 GHz

References

[1] K. Pontoppidan, Ed., “Useful Geometrical Relations: Hyperboloids,” in *GRASP Technical Description*, TICRA, 2008, pp. 360–363.

[2] K. Pontoppidan, Ed., “Useful Geometrical Relations: Paraboloids,” in *GRASP Technical Description*, Denmark: TICRA, 2008, pp. 357–360.

[3] K. Pontoppidan, Ed., “Useful Geometrical Relations: Dual Reflector Design,” in *GRASP Technical Description*, TICRA, 2008, pp. 370–379.

[4] A. Tadjalli and J. Rashed-mohassel, “Blockage Minimization in Cassegrain and Gregorian Reflectors with Increased Flexibility’,” 2002.

[5] M.-H. Chung, D.-Y. Byun, and V. B. Khaikin, “Alignment tolerances of antenna optics for KVN 21-m shaped cassegrain antenna,” pp. 186–187, 2007.

Chapter 4

275 GHz Single-Offset Reflector System

Initial Design Requirements and Considerations

The design and manufacture of a 275 GHz reflector system has been undertaken, with the aim of it being used for rain attenuation measurements in the Terahertz (submillimeter) wave range.

The system's requirements, as agreed upon with the client, are as follows:

Parameter	Value
Qty.	2 units
Antenna Type	Single-Offset Reflector Antenna
Central Frequency	275 GHz
Bandwidth	110 GHz
Gain	> 50 dBi
Input Waveguide	Standard WR3.4
Feed Type	Pyramidal Smooth Wall Horn
S11	< -10 dB

Fig. 4.1: Offset Reflctor System Initial Requirements

The reflector system must work between 220 and 330 GHz with at least 50 dBi of gain and a Return Loss below -10 dB. The system is comprised of two main elements:

- An Offset Parabolic Reflector, which is a sub-section of a larger symmetrical parabolic dish.
- A Pyramidal Smooth-walled Feedhorn, fed using a standard WR3.4 waveguide interface, with an appropriate radiation pattern so as to maximize the total gain after being amplified by the reflector, so that the complete antenna reaches the minimum required 50 dBi gain.

Having a WR3.4 waveguide means that the most complex and critical step in creating the system will come from manufacturing the waveguide's input aperture, which measures only 0.86 x 0.43 mm.

Initial Design

After some tests, the first design for the ellipsoidal system [1][2] was created using a 200mm diameter and 85mm focal length for the reflector dish, as can be appreciated in Figure 3.2.

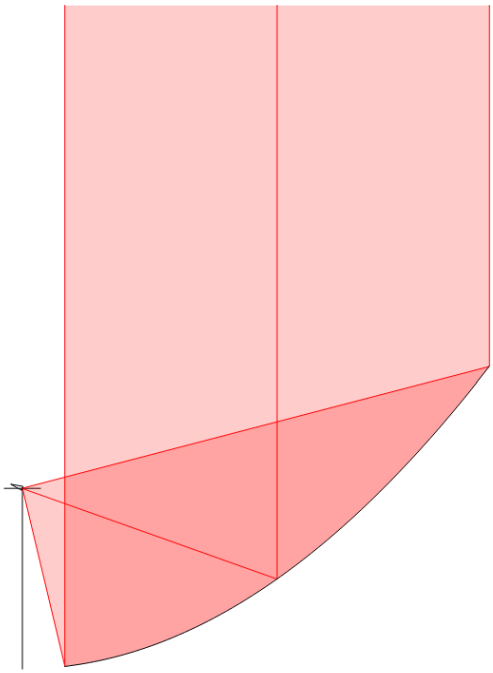

Fig. 4.2: Offset Reflector Final Design Profile and Relative Positioning

The specific equation for the complete parabolic surface in this case is (with X and Z in millimeters) [3]:

$$z(x) = \frac{x^2}{340}$$

The offset reflector surface is the intersection of said parabolic reflector with a 200mm diameter cylinder placed with its base on the XY plane (and its sides parallel to the Z axis) centered at X = 120mm. This means that the offset reflector ranges between 20 and 220mm on the X axis and between -100 and 100mm on the Y axis.

The feedhorn included by default in this design is an ideal one, which emits a Gaussian beam to cover the surface of the subreflector dish with the highest efficiency possible at a certain half-angle (in this case, 45.6º measured from the feed's aperture to the rim of the subreflector).

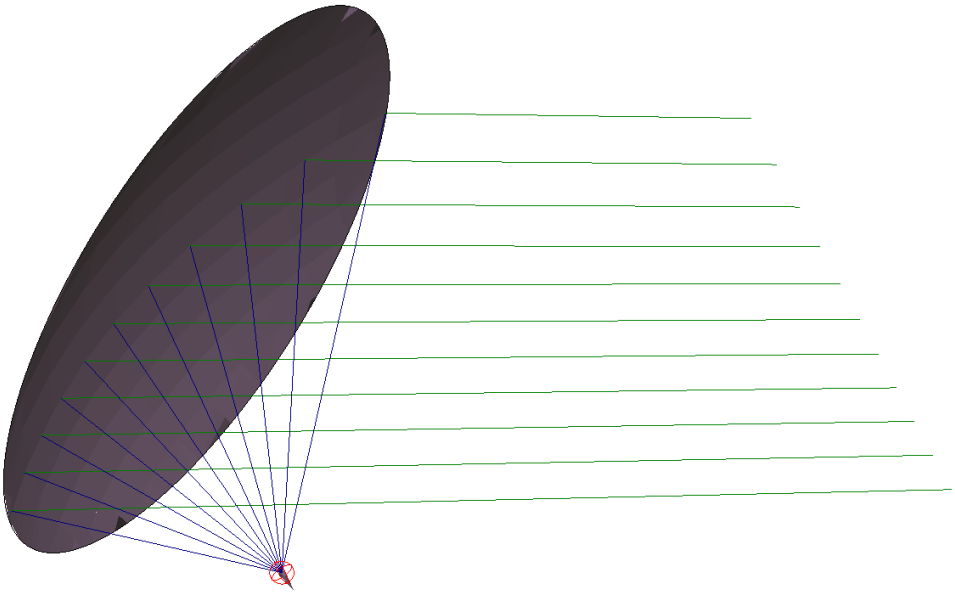

Fig. 4.3: Offset Reflector GRASP Design, including Ray Plot

The simulated results for the system, employing a gaussian beam-emitting ideal feedhorn, are as follows:

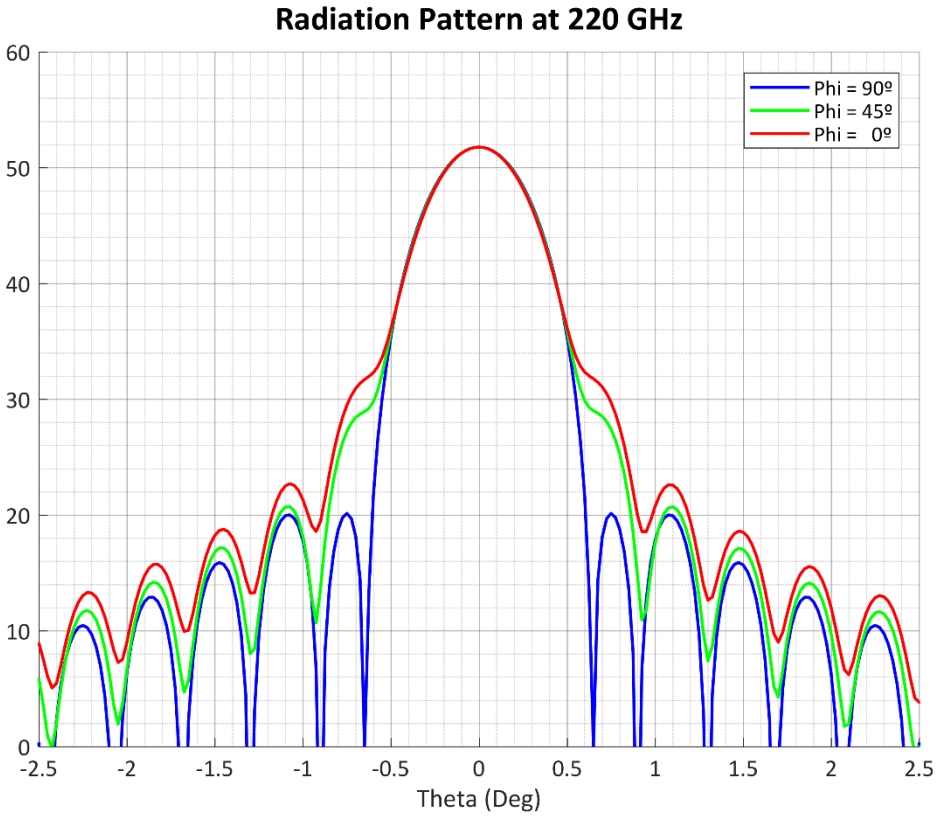

Fig. 4.4: Offset Reflector Initial Model Far-Field Radiation Pattern at 220 GHz

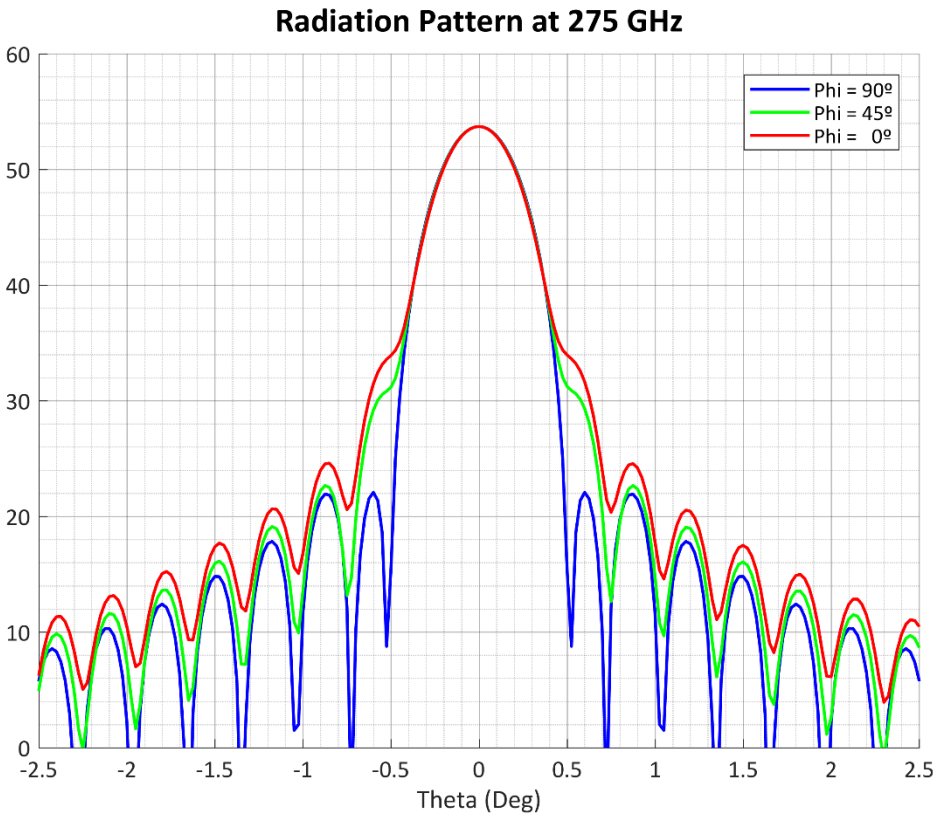

Fig. 4.5: Offset Reflector Initial Model Far-Field Radiation Pattern at 275 GHz

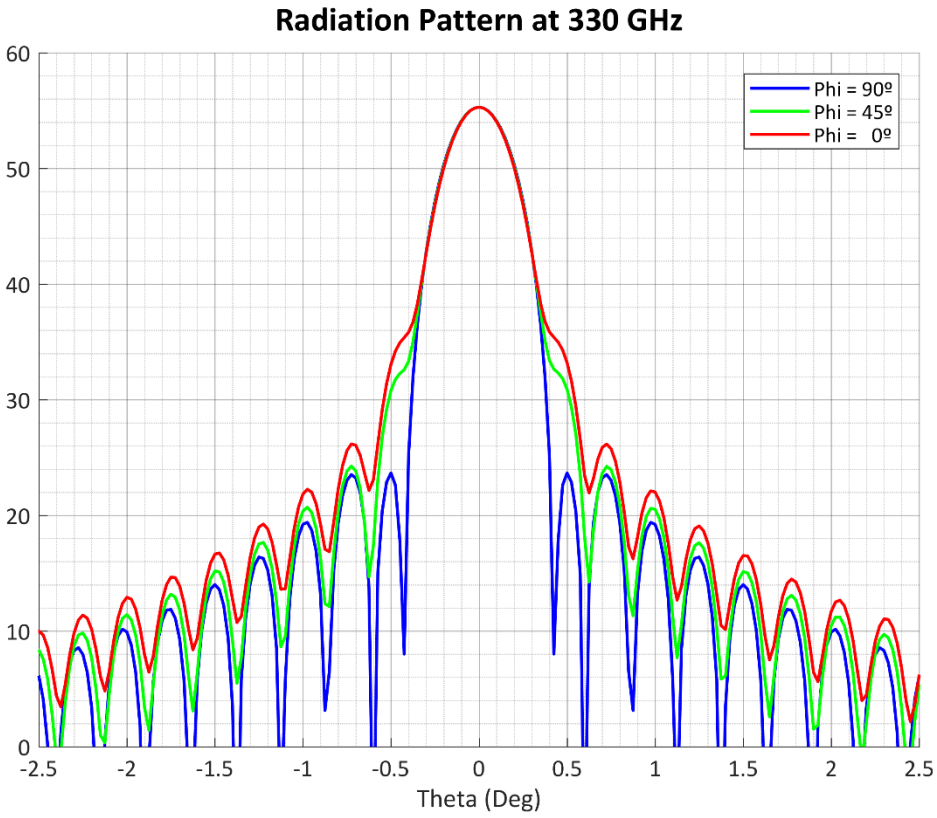

Fig. 4.6: Offset Reflector Initial Model Far-Field Radiation Pattern at 330 GHz

Final Design

When the initial design is deemed satisfactory in terms of gain using an ideal feedhorn, it is replaced in *GRASP* with a 10mm long, 19dBi WR3.4 pyramidal horn. Said horn was previously designed in *HFSS* to approximate the particular Gaussian beam as closely as possible, with an inner output aperture measuring 2mm by 1.5mm optimized to obtain highly symmetrical phi radiation planes. Fig. 3.7 shows its radiation pattern at 220GHz.

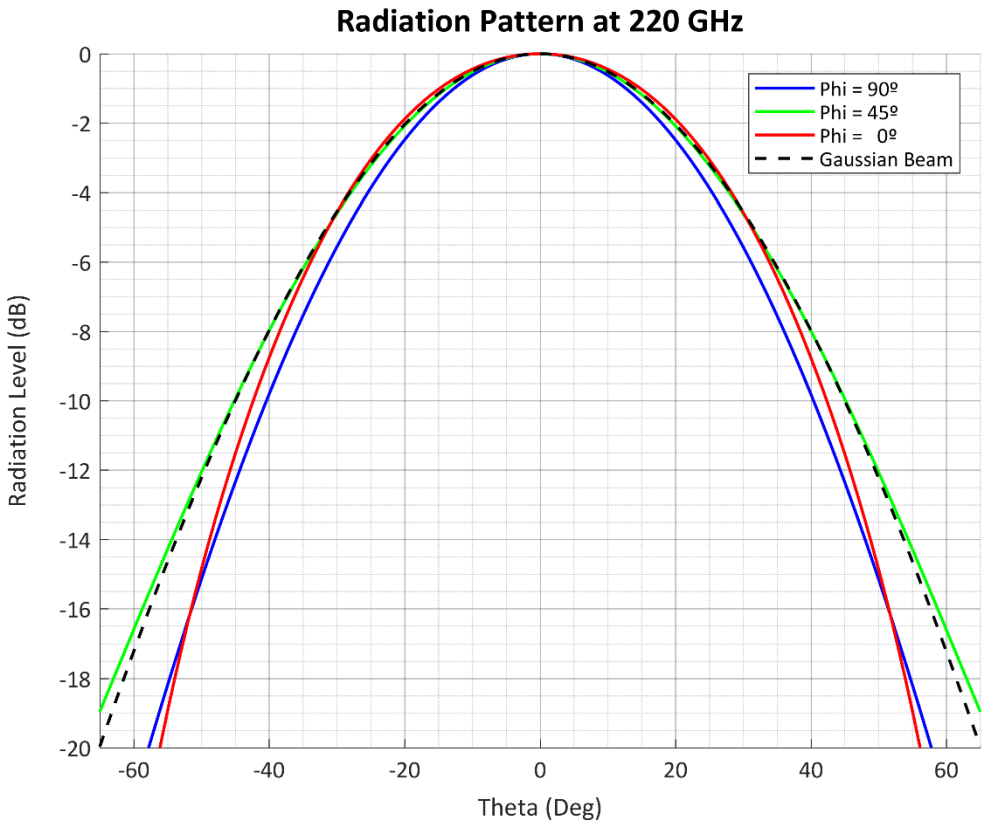

Fig. 4.7: Offset Reflector Pyramidal Feedhorn Radiation Pattern at 220 GHz

The horn's patterns for each frequency point are imported into *GRASP*, which then calculates the radiation patterns for the full system:

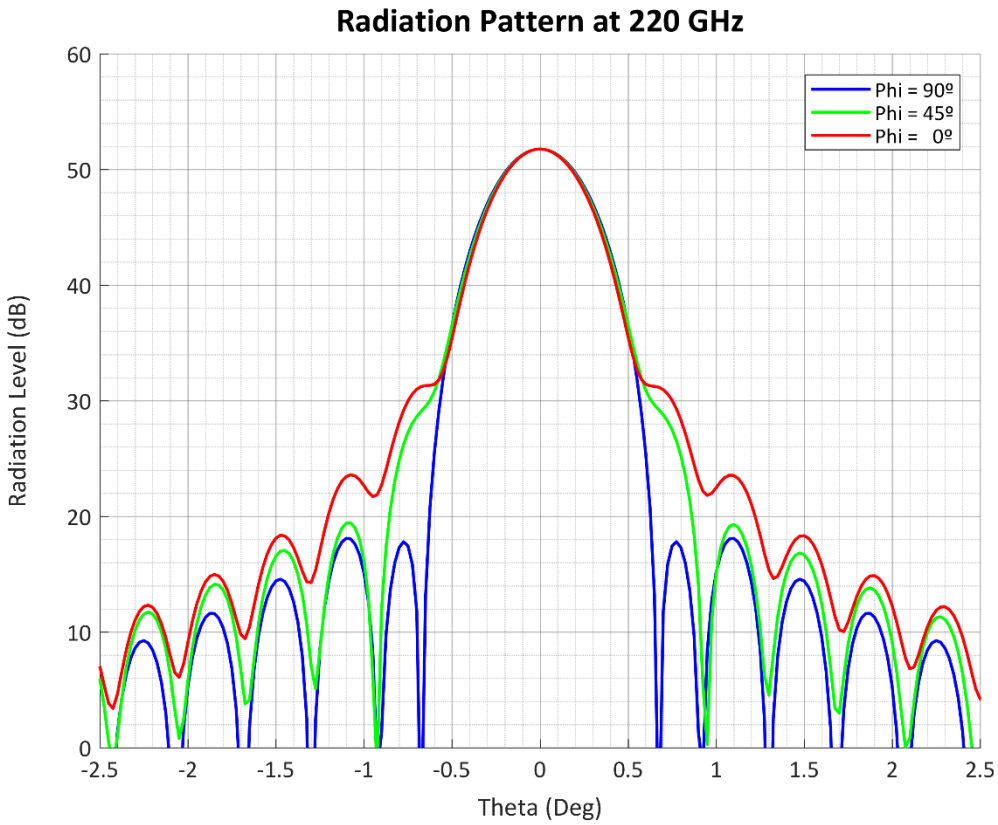

Fig. 4.8: Offset Reflector Final Model Far-Field Radiation Pattern at 220 GHz

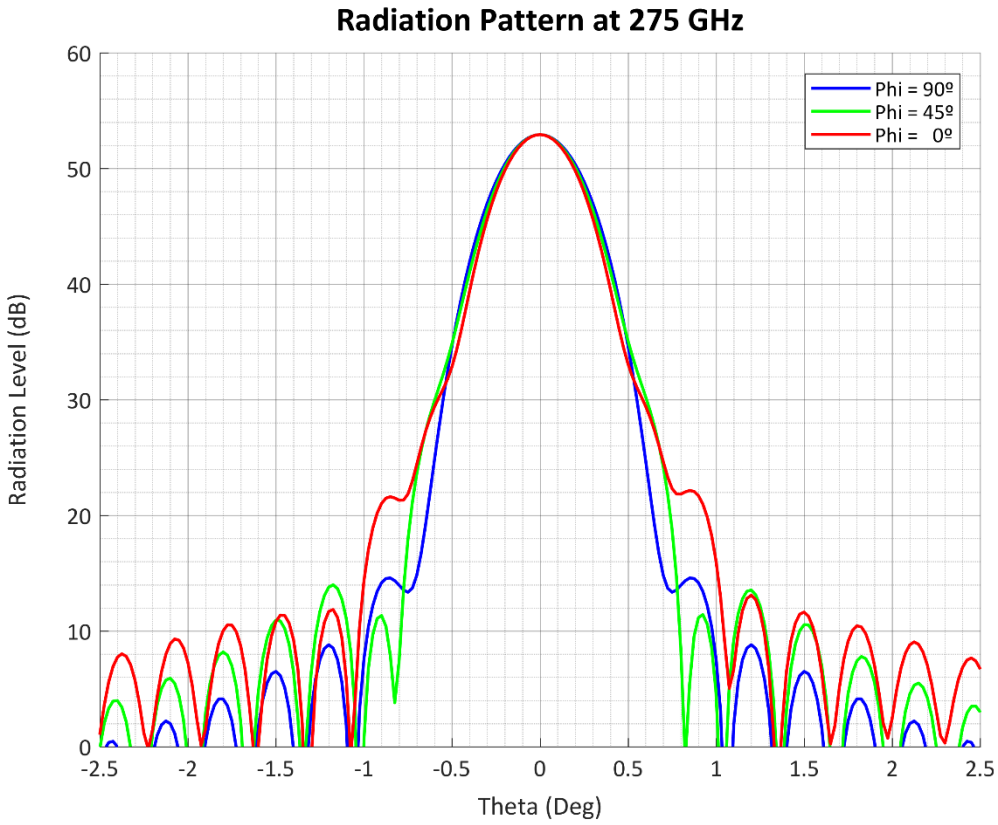

Fig. 4.9: Offset Reflector Final Model Far-Field Radiation Pattern at 275 GHz

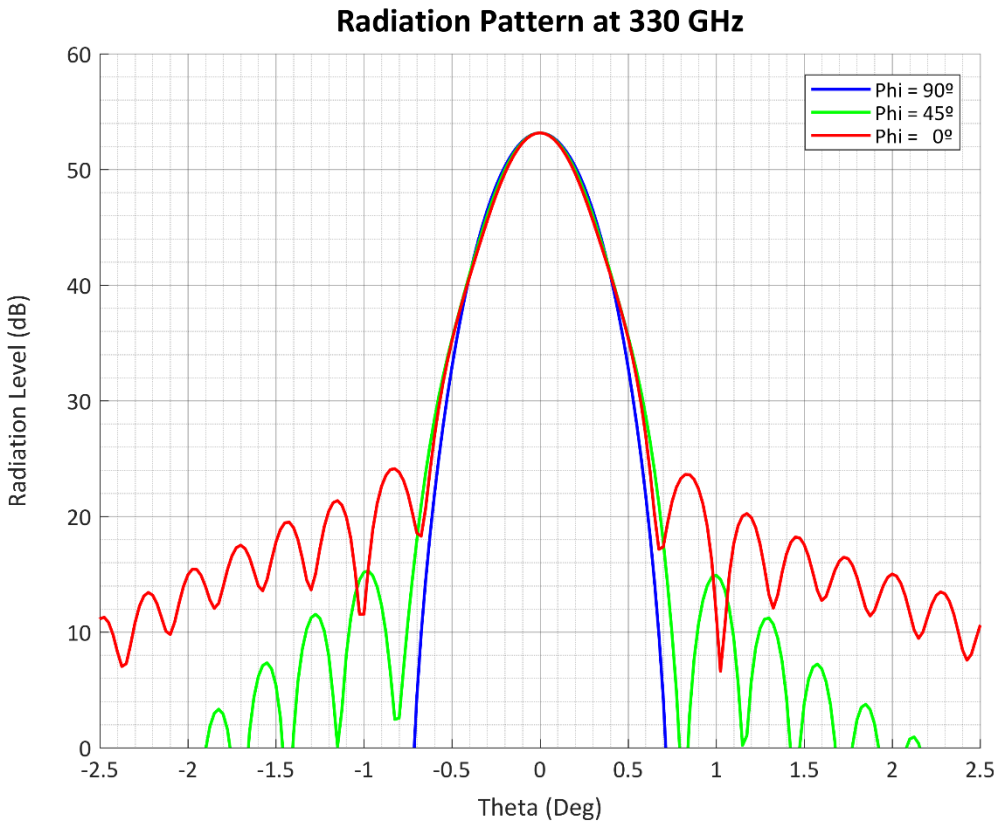

Fig. 4.10: Offset Reflector Final Model Far-Field Radiation Pattern at 330 GHz

Displacement Simulations

When carrying out simulations in *GRASP*, it is assumed that every one of the elements intervening in the radiation is in its precise position with regards to the rest. Operating at 275GHz implies having a wavelength of 1.09mm, which means a 200µm displacement in the positioning of one of these components would mean moving almost λ/4, and a 500µm displacement would mean moving almost λ/2.

Since these small displacements can occur and could be non-trivial, simulations have been done displacing the feedhorn 200 and 500µm to see how the radiation pattern would be affected.

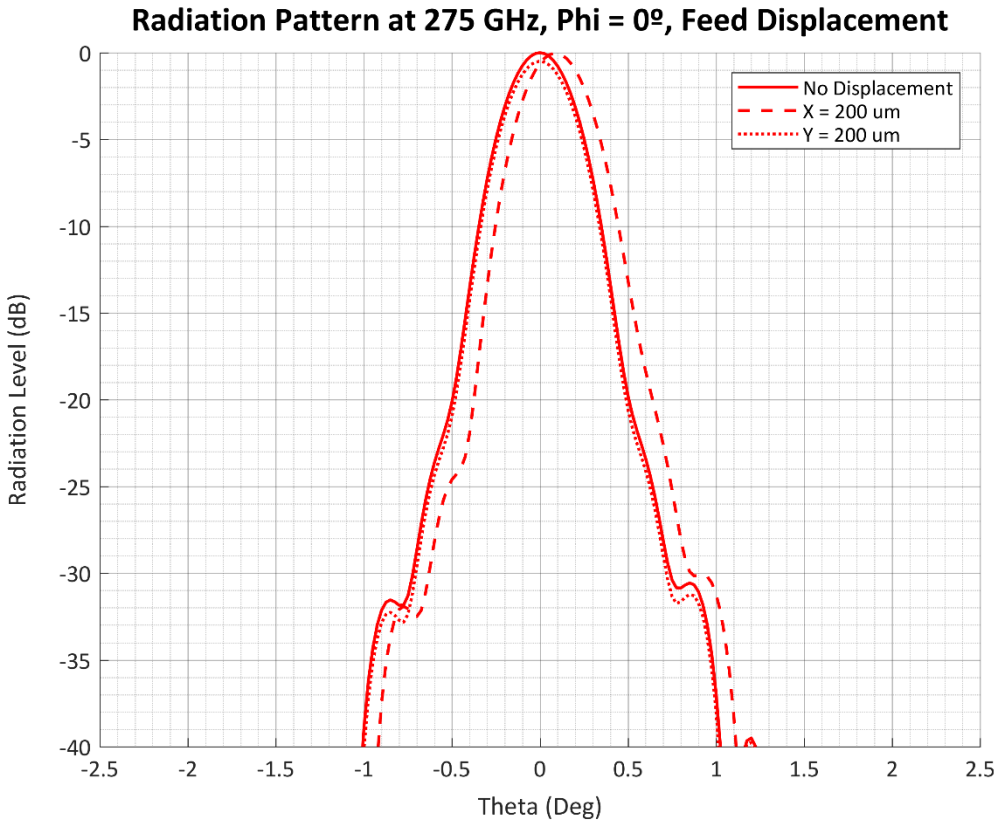

Fig. 4.11: Offset Reflector Final Model Feedhorn X and Y-axis Displacement Test (200 µm)

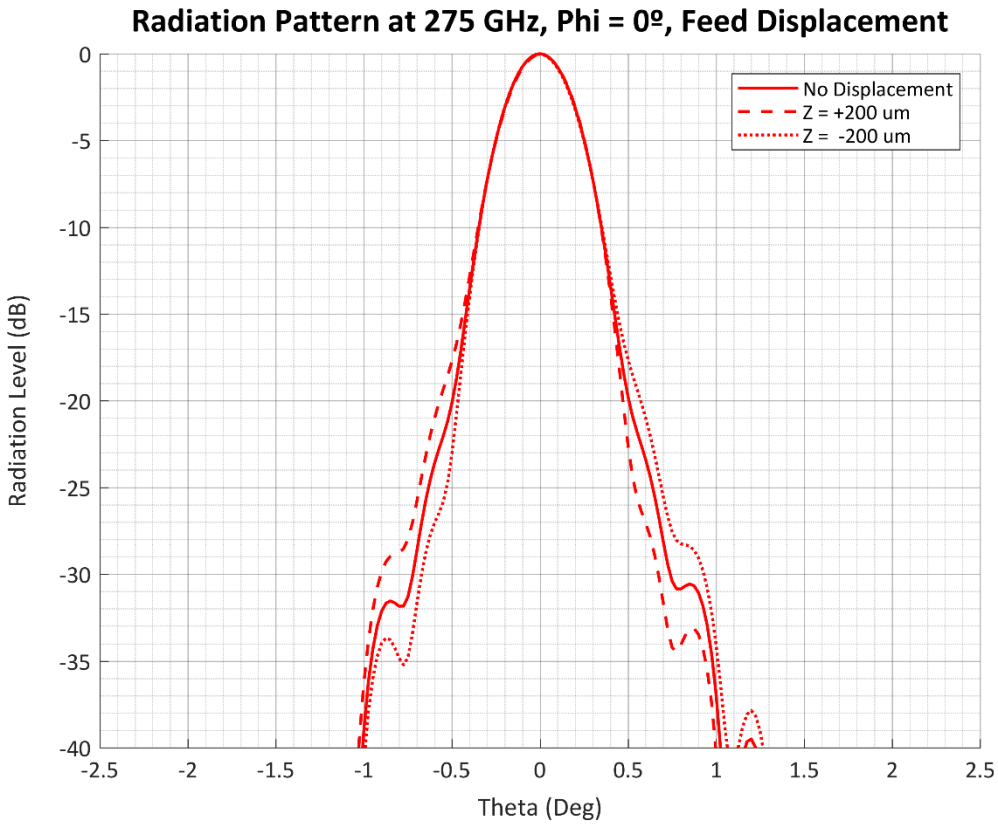

Fig. 4.12: Offset Reflector Final Model Feedhorn Z-axis Displacement Test (200 µm)

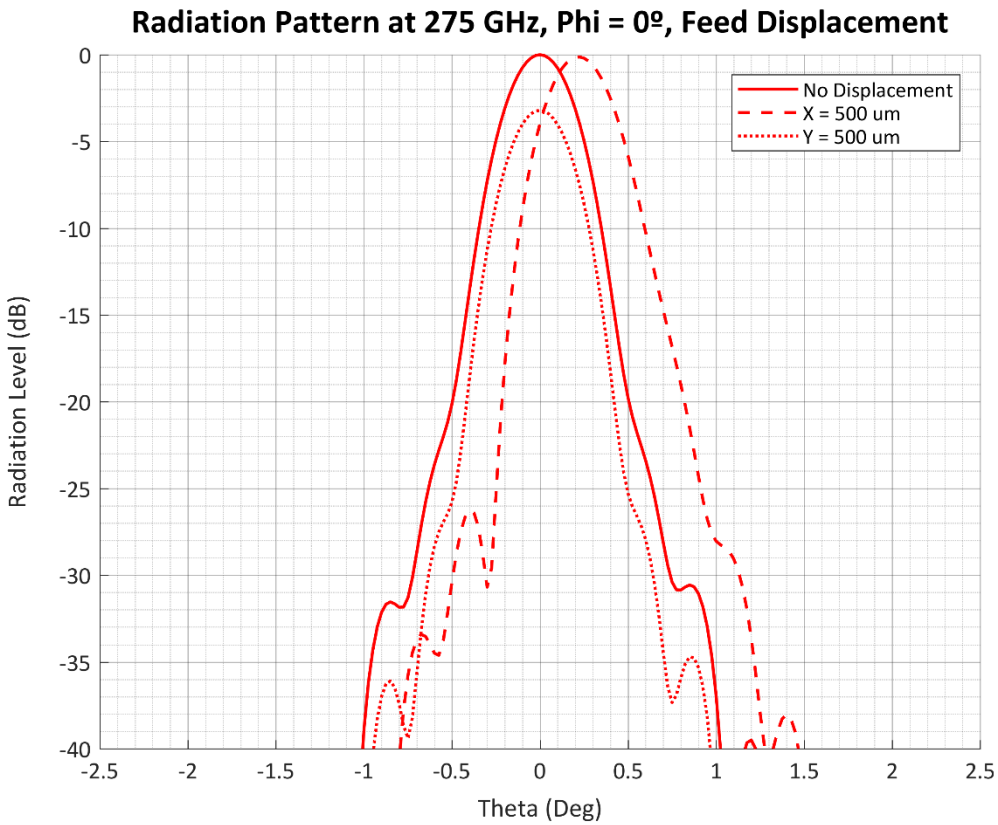

Fig. 4.13: Offset Reflector Final Model Feedhorn X and Y-axis Displacement Test (500 µm)

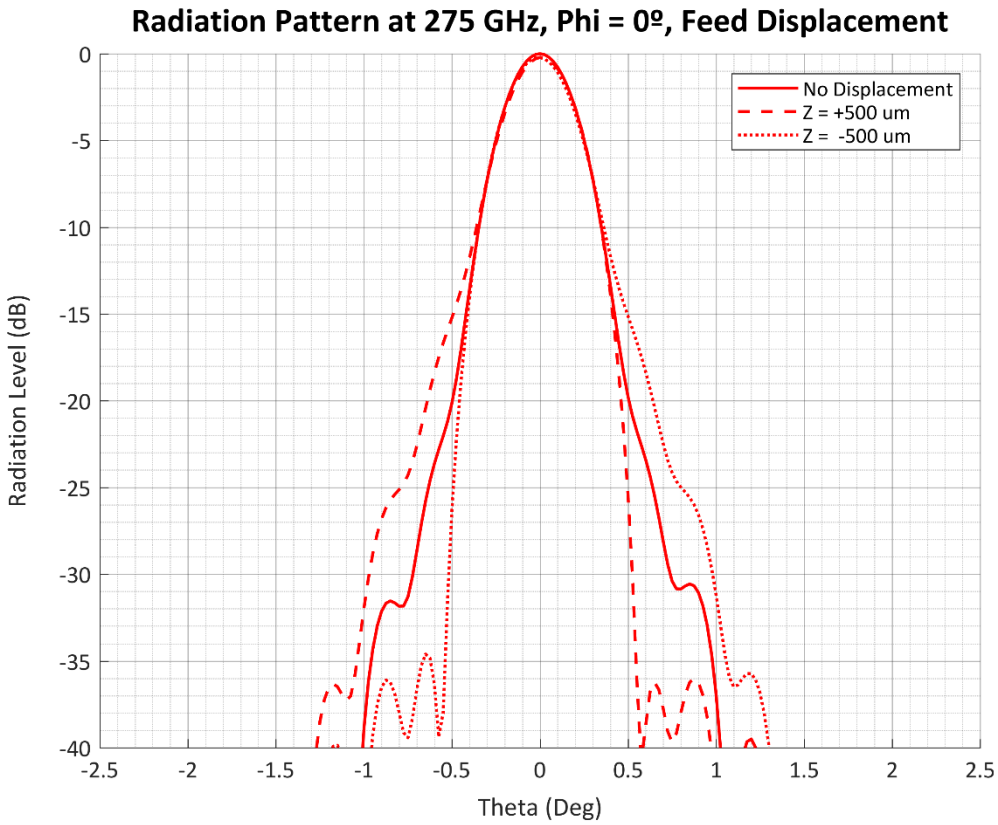

Fig. 4.14: Offset Reflector Final Model Feedhorn Z-axis Displacement Test (500 µm)

It is important to know the extent of these variations in order to determine the manufacturing tolerances of each component and the precision of their assembly in order to be measured accurately.

The comparison graphs show that displacing the feedhorn barely has any noticeable effects, especially when moving it along the Z axis. With 500 µm, the X and Y axis displacements imply a 0.25º shift of the main lobe at most, which translates to a 3.5 dB loss at 0º.

Mechanical Model

Once the simulated model was deemed valid, the feedhorn and reflector surface were imported into *HFSS* to create the mechanical model around them.

The original design for the 3D model was slightly modified before manufacturing, to be able to provide sufficient support for the reflector disc. The final disc is thicker and its enclosure more symmetrical, with its back a flat surface to ease the mounting to the base plate. Both designs are included for comparison purposes.

Initial Design

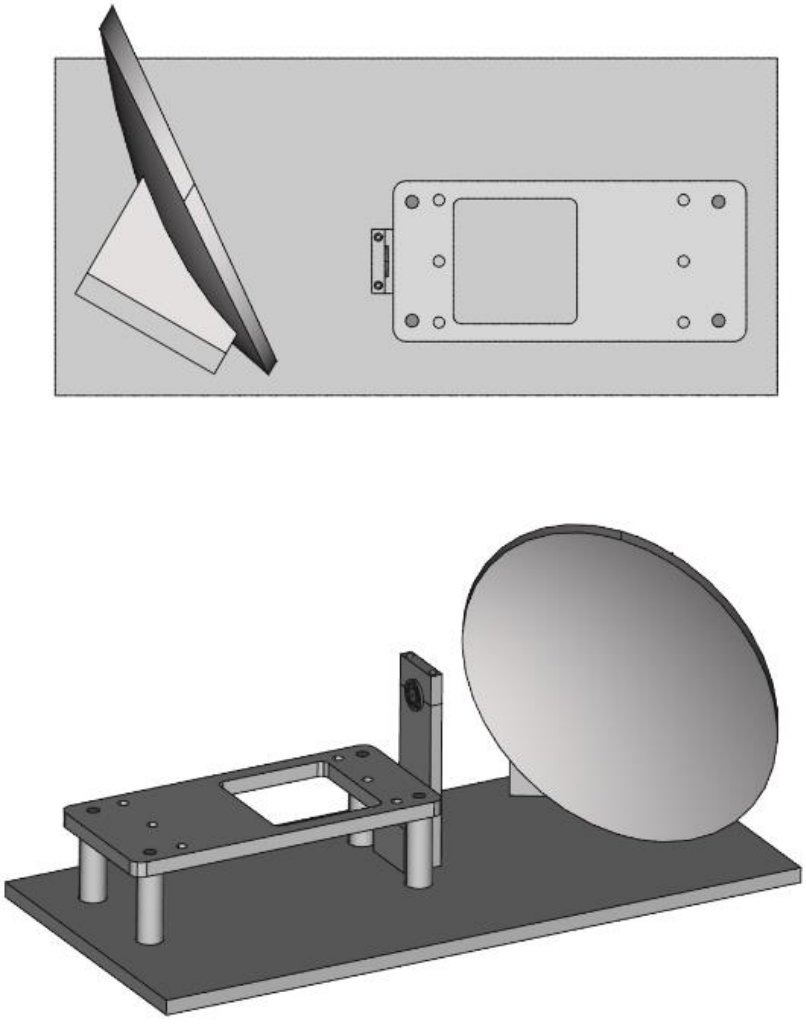

Fig. 4.15: Top and Side View of the Initial 3D Mechanical Model of the Offset Reflector

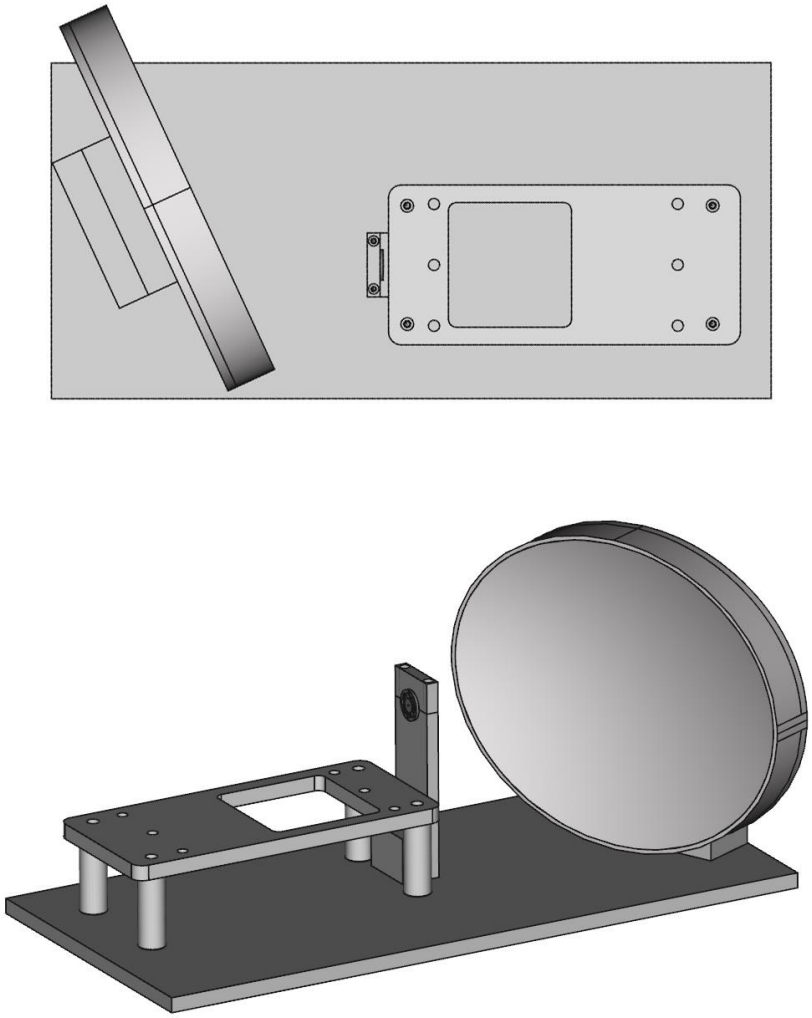

Fig. 4.16: Top and Side View of the Final 3D Mechanical Model of the Offset Reflector

Manufactured System

After completing the design, the system was created and received for verification purposes. Figures 3.17 to 3.19 show images of the completed system.

Fig. 4.17: RA-SO-WR3.4-50 Manufactured Model (a)

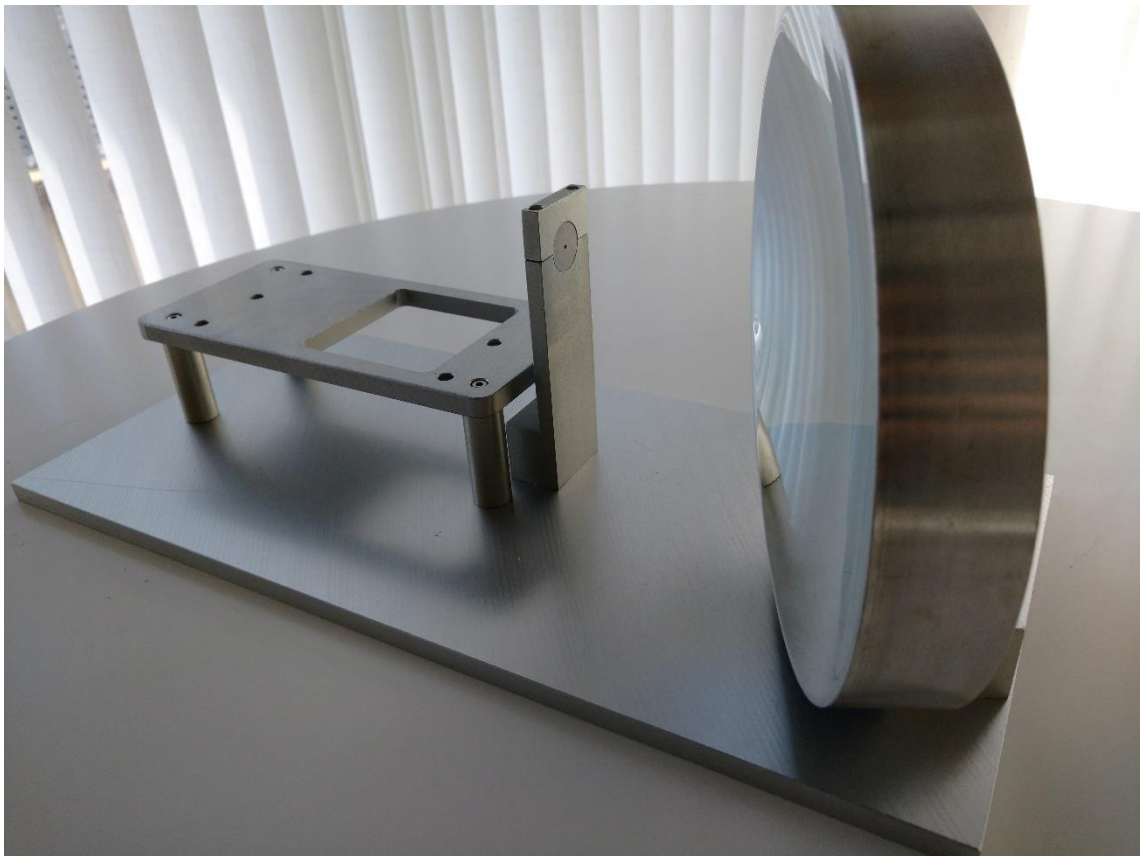

Fig. 4.18: RA-SO-WR3.4-50 Manufactured Model (b)

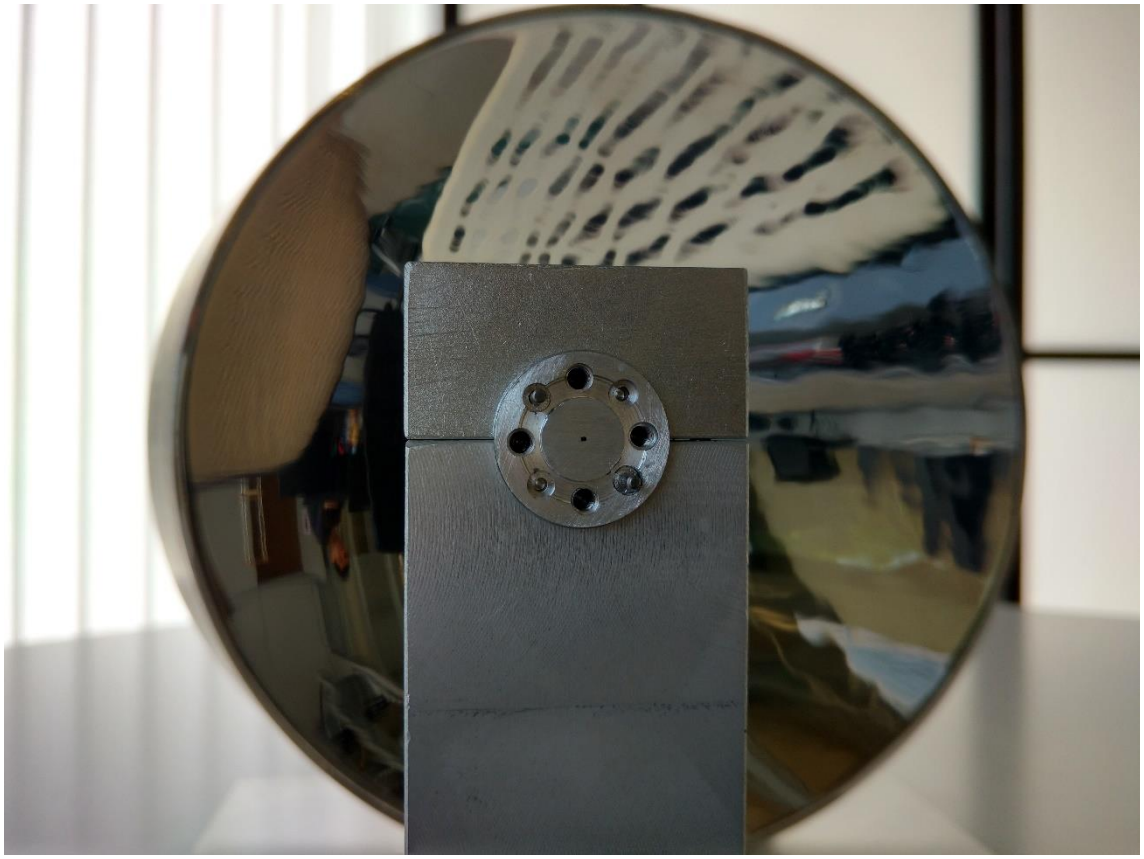

Fig. 4.19: RA-SO-WR3.4-50 Manufactured Model (c)

Measurements

The system was measured in Near-Field, using two 220-330 GHz sources in the configuration shown below in Figures 3.20 and 3.21.

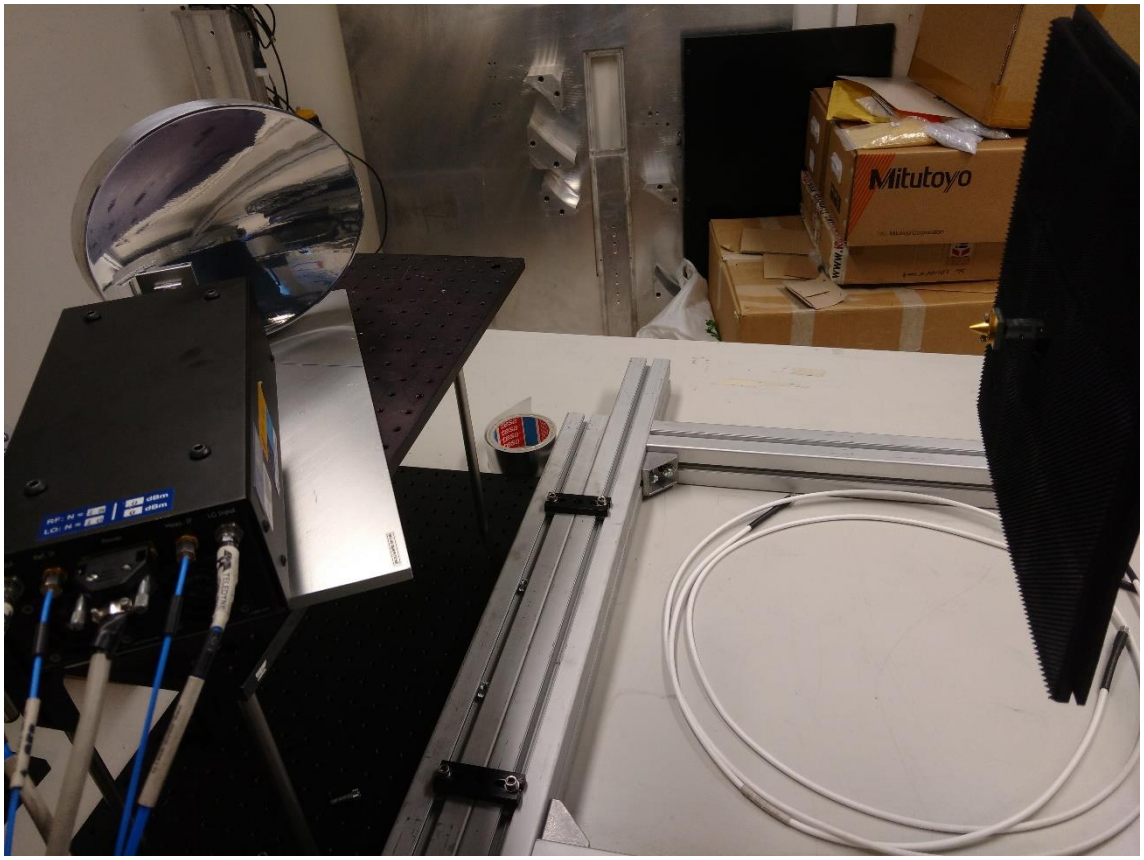

Fig. 4.20: RA-SO-WR3.4-50 Measurement Setup (a)

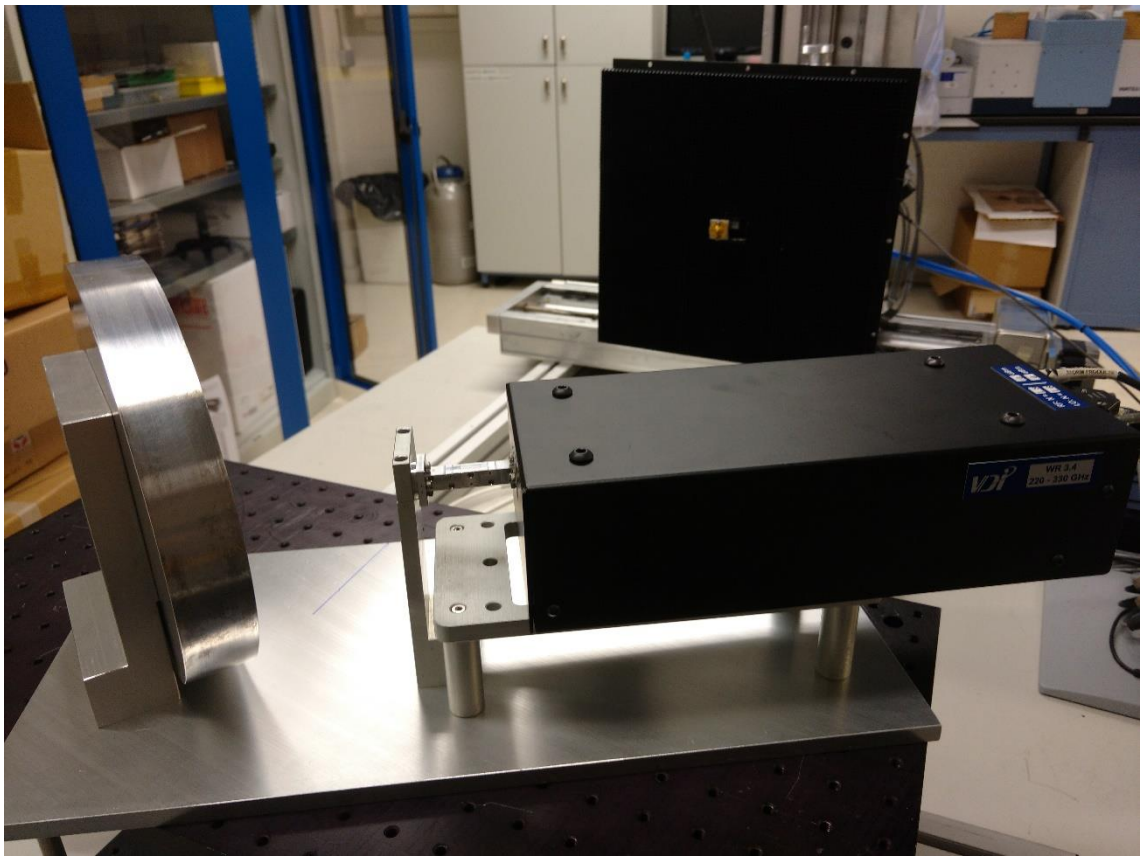

Fig. 4.21: RA-SO-WR3.4-50 Measurement Setup (b)

Figures 3.22 to 3.27 show the near-filed radiation results, figure 3.28 shows the measured directivity and figures 3.29 to 3.33 show the measured far-field radiation results for the manufactured system. The solid lines are the measured values, while the dashed lines are the simulated values included for comparison's sake (the values have been normalized to a 0dB maximum).

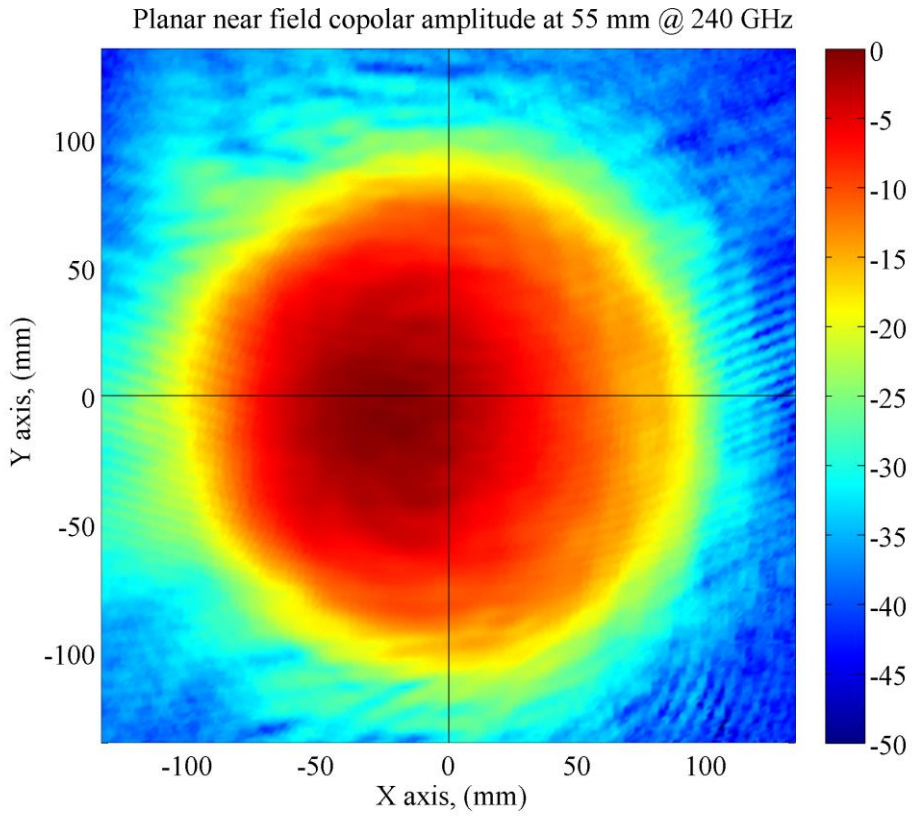

Fig. 4.22: RA-SO-WR3.4-50 Measured Near-Field Radiation Pattern Amplitude at 240 GHz

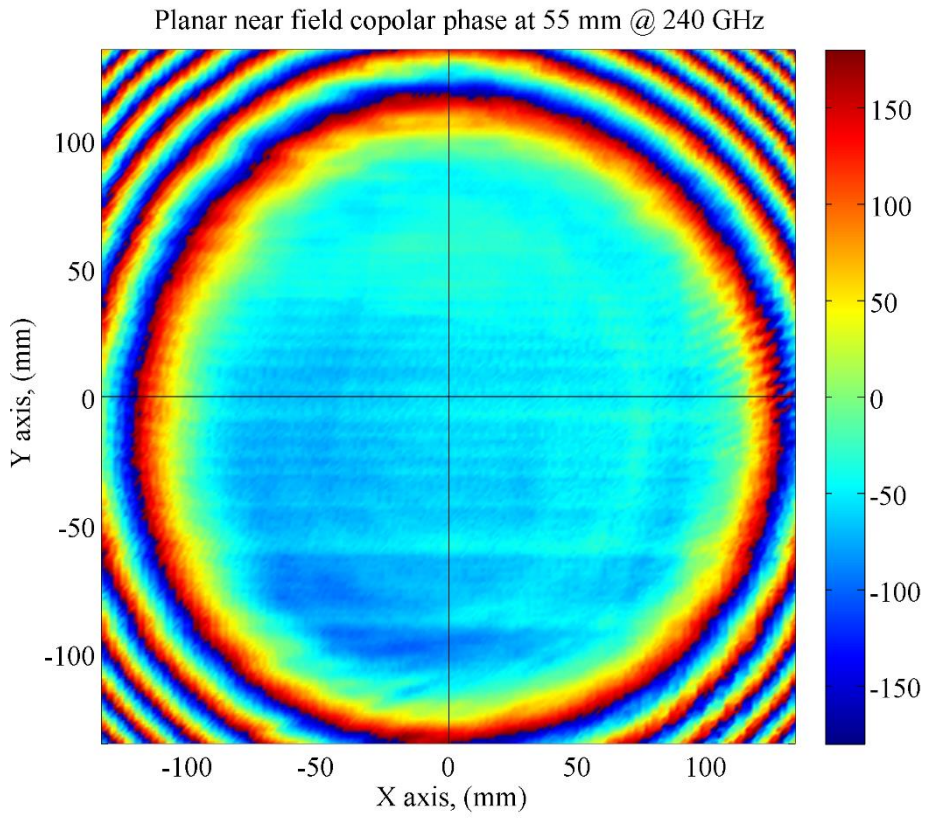

Fig. 4.23: RA-SO-WR3.4-50 Measured Near-Field Radiation Pattern Phase at 240 GHz

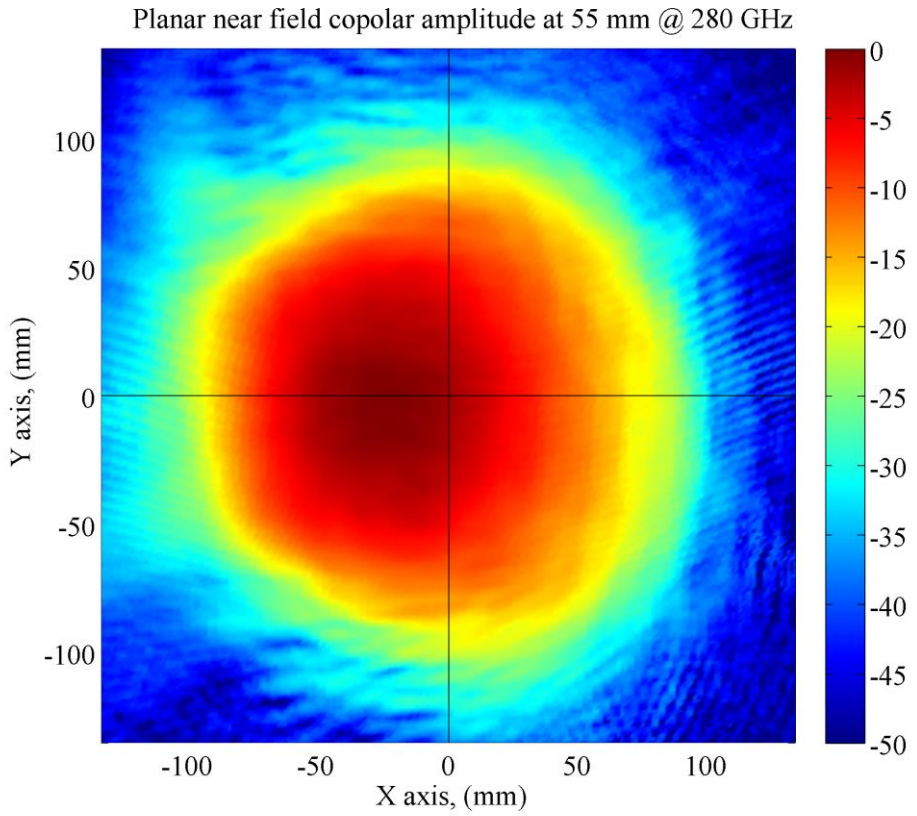

Fig. 4.24: RA-SO-WR3.4-50 Measured Near-Field Radiation Pattern Amplitude at 280 GHz

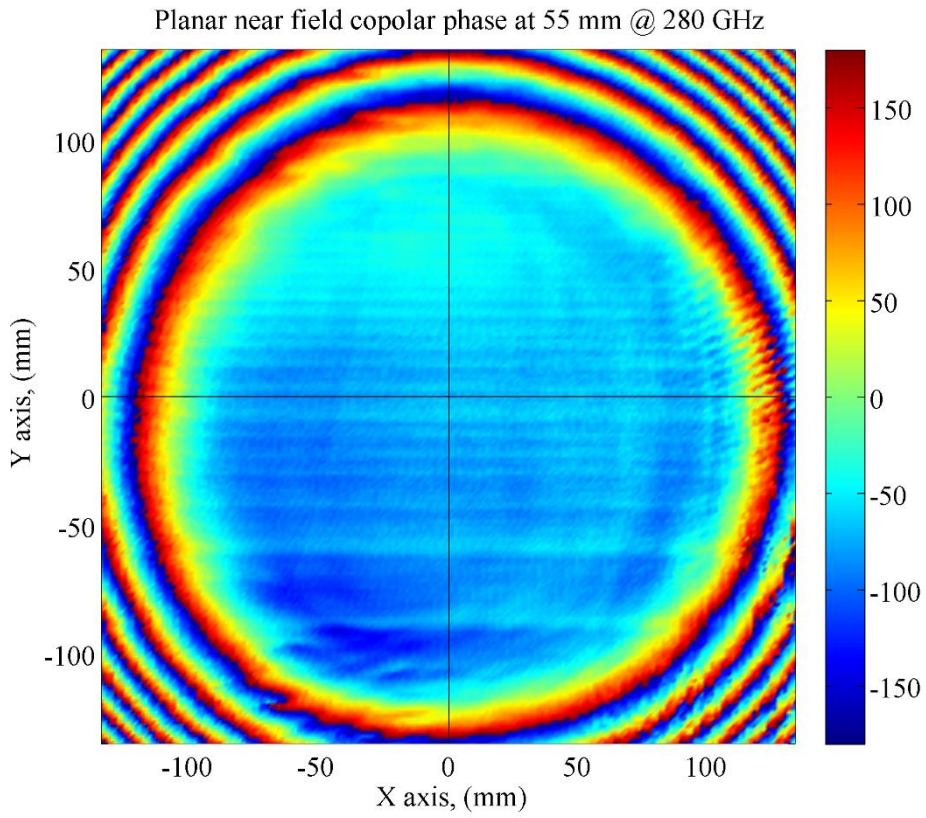

Fig. 4.25: RA-SO-WR3.4-50 Measured Near-Field Radiation Pattern Phase at 280 GHz

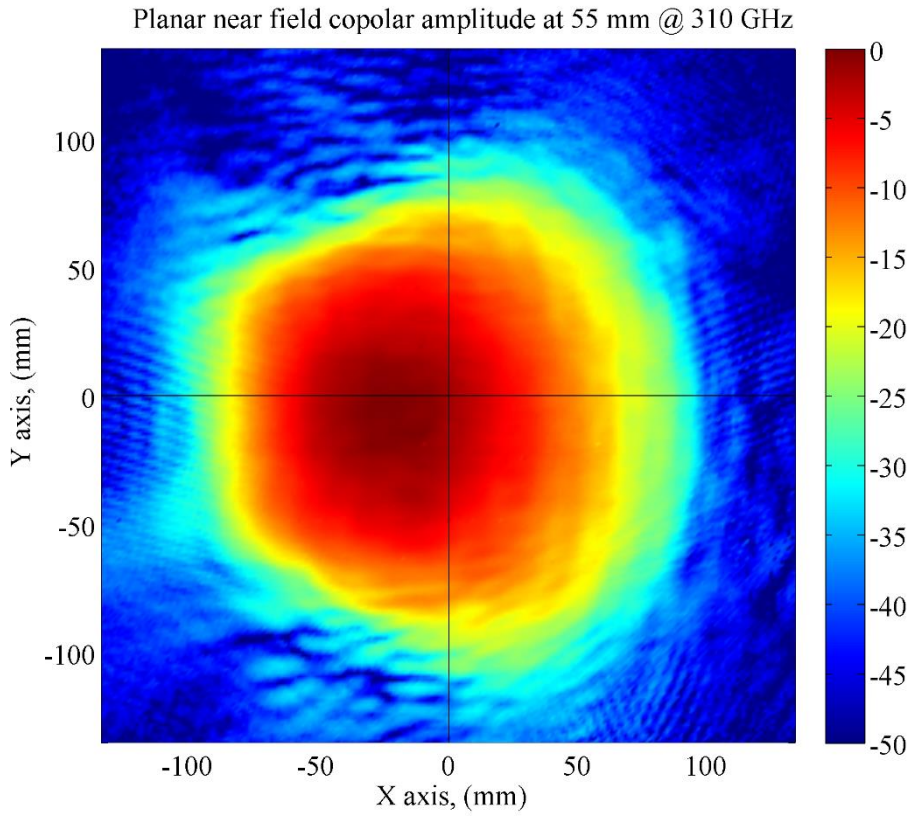

Fig. 4.26: RA-SO-WR3.4-50 Measured Near-Field Radiation Pattern Amplitude at 310 GHz

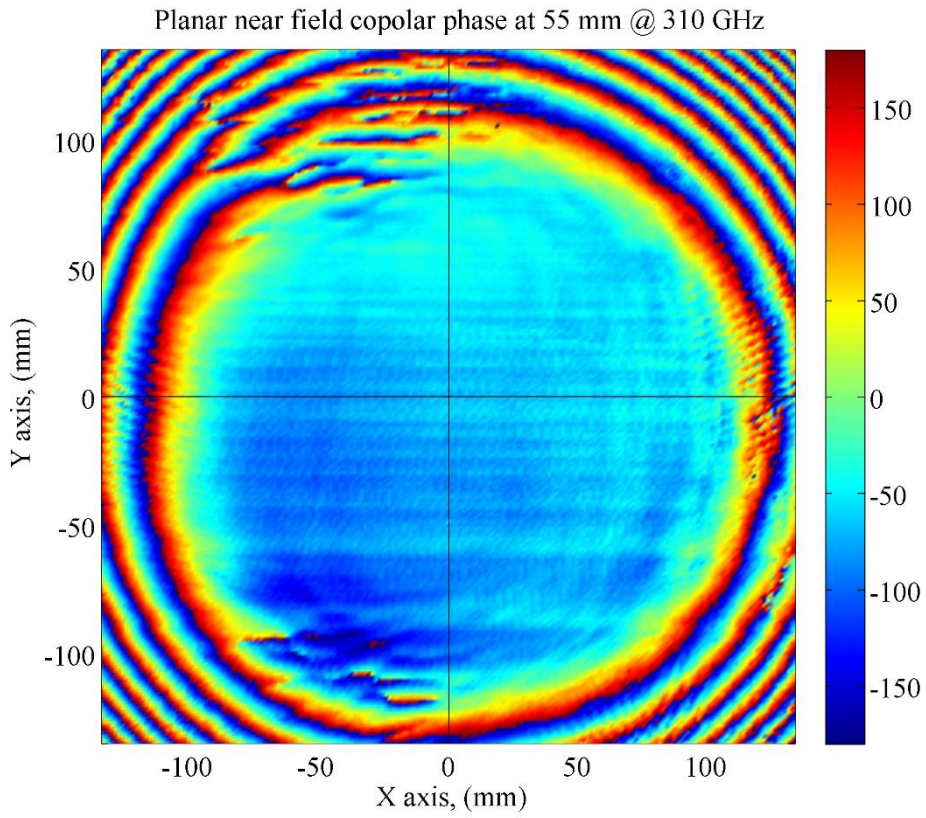

Fig. 4.27; RA-SO-WR3.4-50 Measured Near-Field Radiation Pattern Phase at 310 GHz

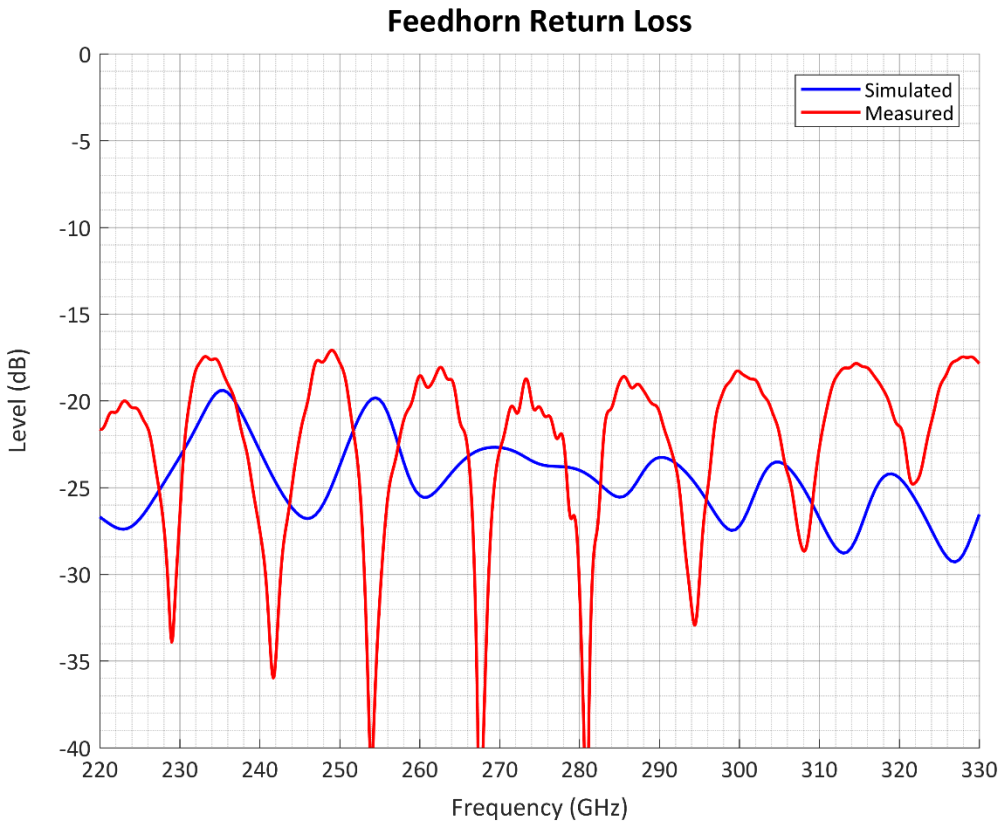

Fig. 4.28: RA-SO-WR3.4-50 Measured and Simulated Return Loss Across the Frequency Band

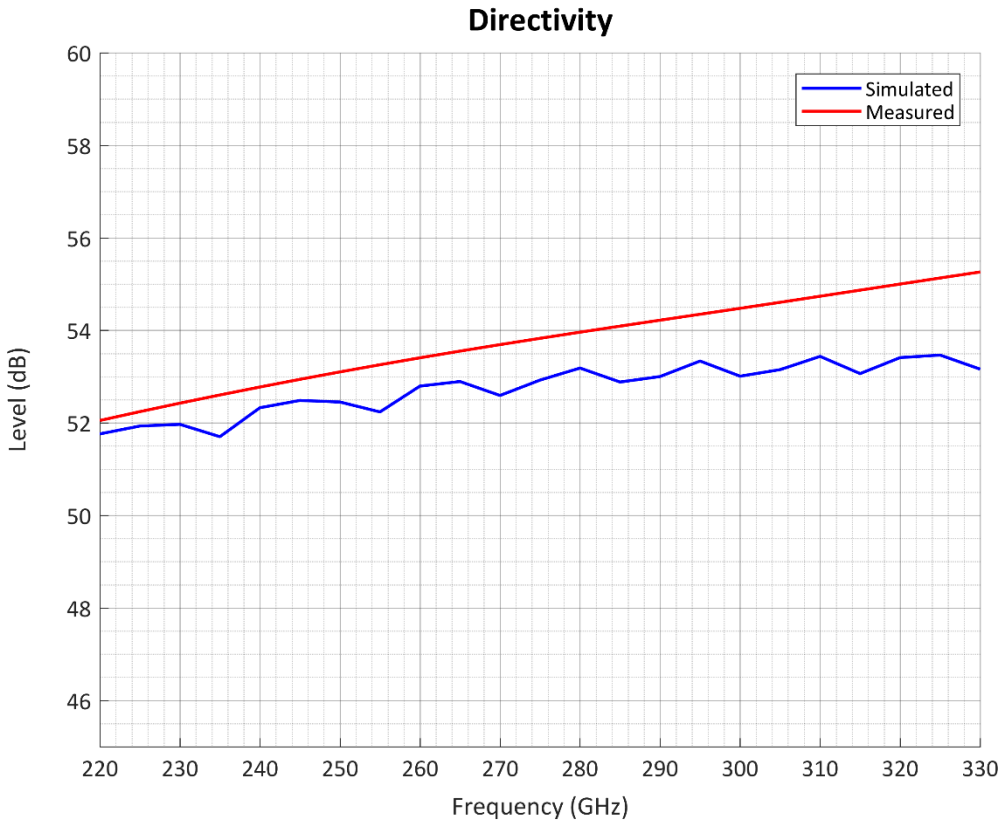

Fig. 4.29: RA-SO-WR3.4-50 Measured and Simulated Directivity Across the Frequency Band

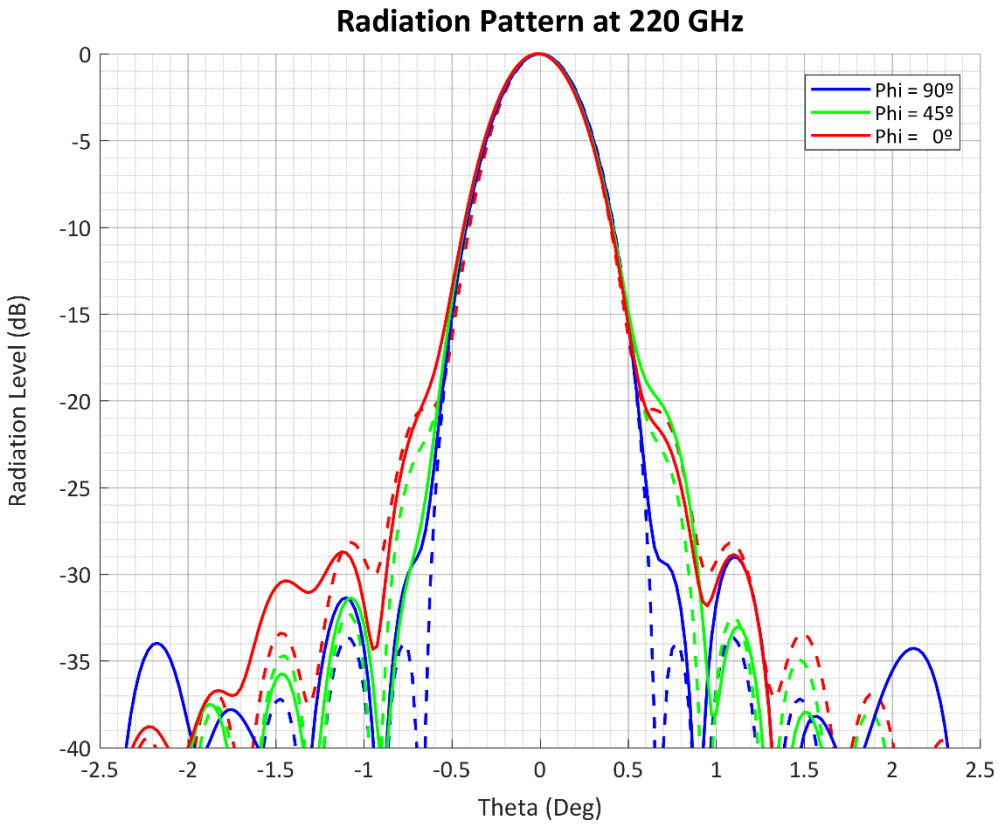

Fig. 4.30: RA-SO-WR3.4-50 Measured and Simulated Far-Field Radiation Pattern at 220 GHz

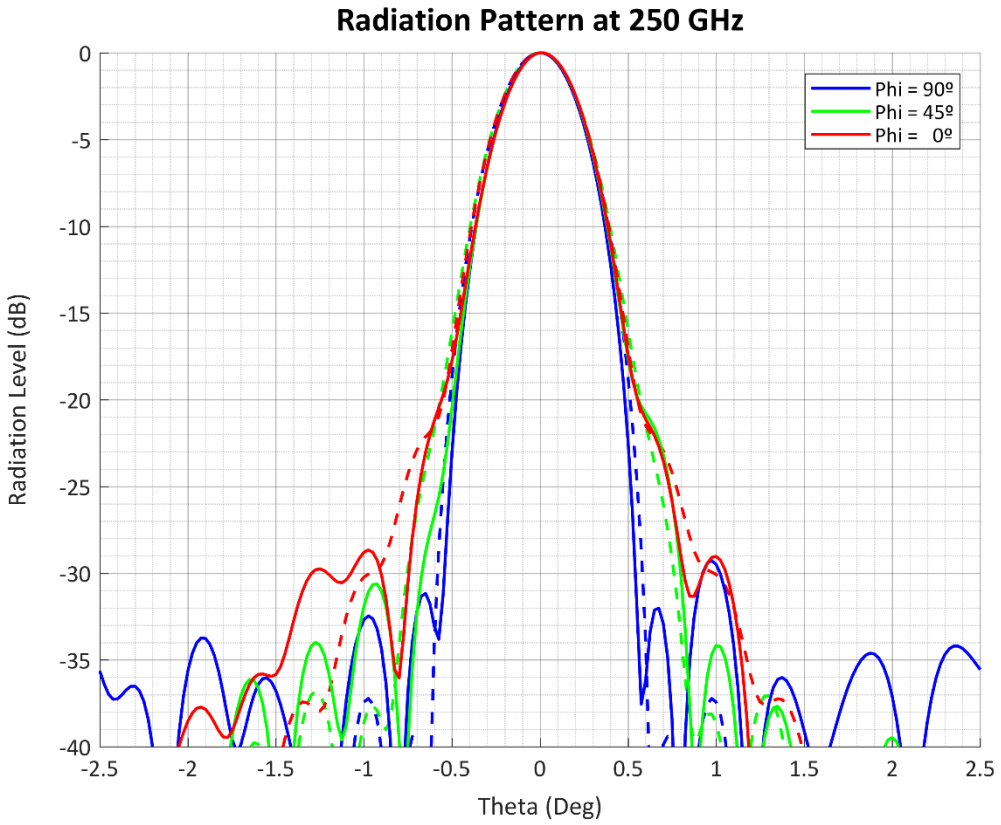

Fig. 4.31: RA-SO-WR3.4-50 Measured and Simulated Far-Field Radiation Pattern at 250 GHz

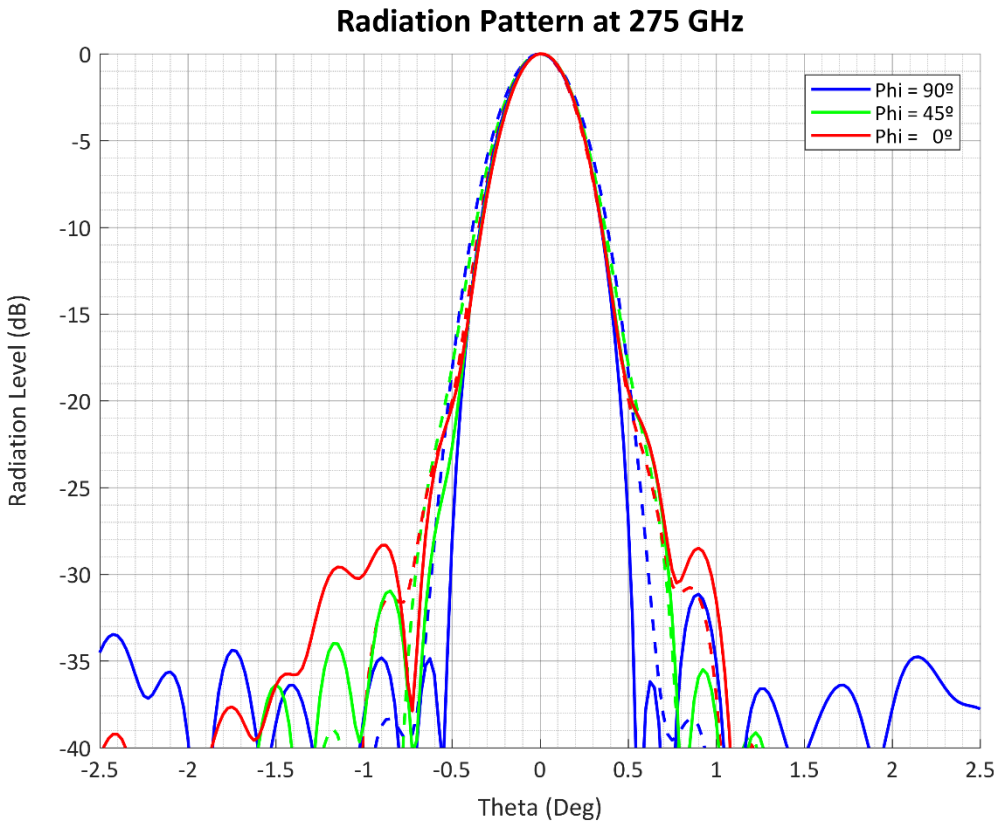

Fig. 4.32: RA-SO-WR3.4-50 Measured and Simulated Far-Field Radiation Pattern at 275 GHz

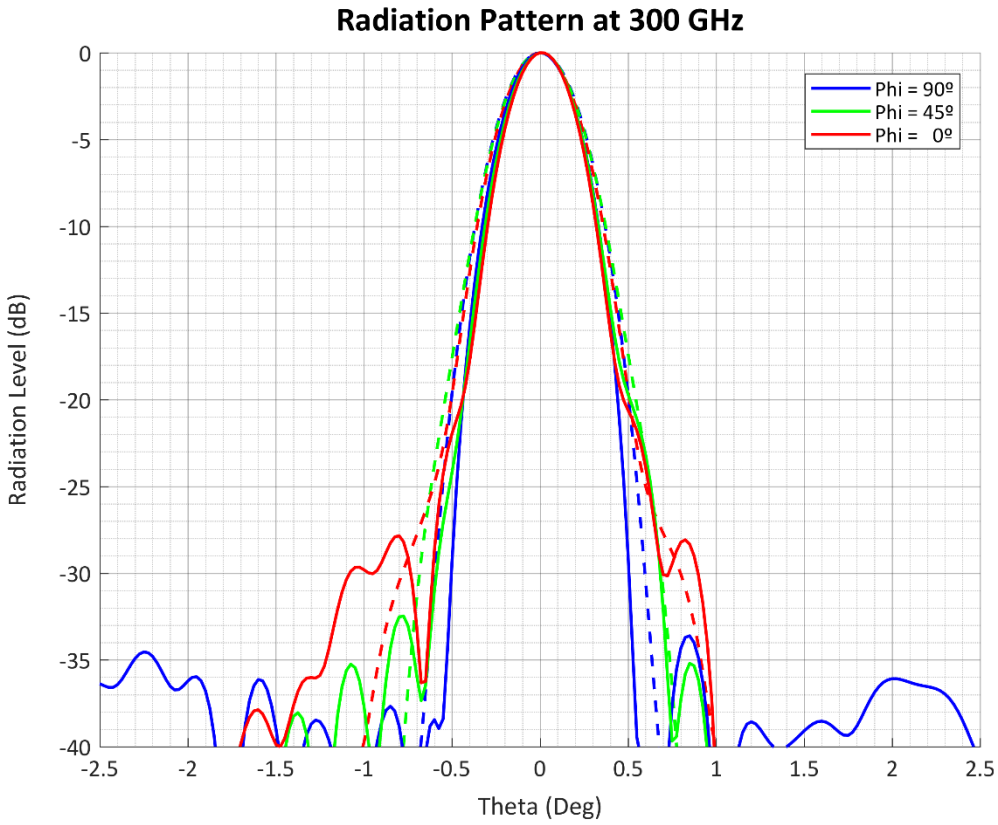

Fig. 4.33: RA-SO-WR3.4-50 Measured and Simulated Far-Field Radiation Pattern at 300 GHz

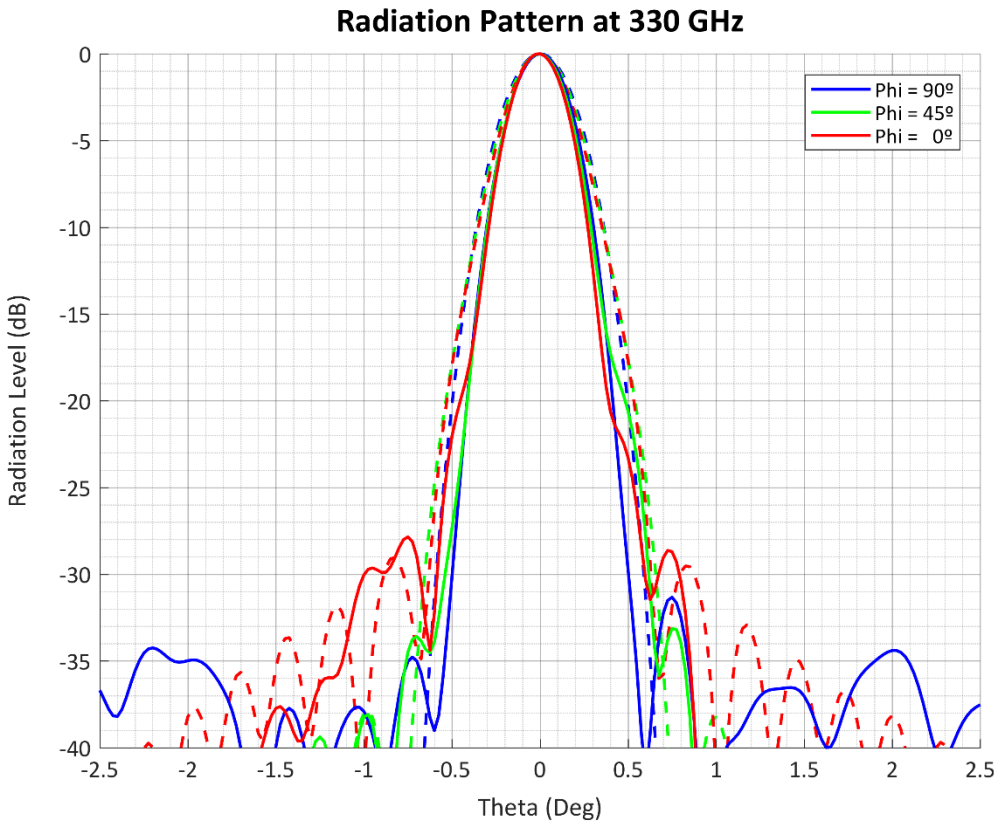

Fig. 4.34: RA-SO-WR3.4-50 Measured and Simulated Far-Field Radiation Pattern at 330 GHz

References

[1] K. Pontoppidan, Ed., “Reflectors: Ellipsoid,” in *GRASP Technical Description*, Denmark: TICRA, 2008, p. 16.

[2] K. Pontoppidan, Ed., “Useful Geometrical Relations: Ellipsoids,” in *GRASP Technical Description*, TICRA, 2008, pp. 363–365.

[3] K. Pontoppidan, Ed., “Useful Geometrical Relations: Single Reflector Design,” in *GRASP Technical Description*, TICRA, 2008, pp. 368–369.

Chapter 5

Conclusions and Future Developments

Conclusions

The goal of this work was to create two similar, yet different, types of reflector-based antenna systems from the ground up, using only the clients' requirements as starting points.

This includes simulating with software programs *GRASP*, *μWave Wizard* and *HFSS* (sometimes sequentially and sometimes in parallel), creating the definitive 3D model around the final simulated designs and measuring the finished product using a PNA-X N5242A network analyzer and several different heads.

Additionally, *MATLAB* scripts were programmed for various purposes:

- Loading different types of files, both simulated (input and output Radiation files from *HFSS* and *GRASP*) and measured (S11 and Radiation files from the Network Analyzer).
- Converting the format of different datasets for use in various programs.
- Calculating the Directivity of an antenna from its Radiation Pattern theta cuts.
- Centering of measured Near-Field data.
- Transforming of Near-Field measurements into Far-Field Radiation Patterns.
- Plotting simulated and measured results (Radiation Patterns, Directivities, etc.).

Each of the aforementioned phases of the process was carried out ensuring that appropriate precautions were taken during each step, especially when importing results generated with one software program into a different one. These precautions include verifying the input and output format and unit, making sure the simulated system works somewhat better than desired and testing the displacement of its elements, all to ensure that misalignments during manufacturing and/or assembly affect the final outcome as little as possible.

The end result is satisfactory as both manufactured systems were confirmed to work as expected within reasonable margins, meaning that the measures taken during software simulation to compensate non-ideal effects were adequate.

It is also worth noting that, as of this writing, both clients have received their respective systems and are content with the result. Therefore, both projects can be considered a success.

Future Developments

With the results from both systems laid out, there are several options worth exploring with regards to their advancement within *Anteral SL*. The first would be to normalize one or several different models to be sold as standard (non-custom) products, to be used for a variety of applications.

Creating several models of each type of reflector would be relatively simple: the bigger the size, the higher the gain that can be achieved. Following this directive, different models can be crafted for various amounts of gain, each with its own fixed reflector size. So, for instance, there could be three cassegrain reflector models, for example 30 dBi, 45 dBi and 60 dBi. The feedhorns to be used with these systems do not need to be fixed though, which could open up a very wide array of possibilities and combinations.

By using various types of feedhorn with the same reflector, we can fine-tune its gain to be more or less than its ideal design value, reduce its side lobes and Return Loss and even broaden its bandwidth. Unfortunately, in this case the limit isn't set by computing power or know-how in terms of the design phase, but by the physical limitations of antenna manufacturing.

As was mentioned in previous chapters, because of the wavelength at which these systems operate, manufacturing of the feedhorns is a very delicate and complex process. In the case of the feedhorns for both systems presented in this work, manufacturing was done employing a technique known as electroerosion. The tools that intervene in this process have a certain size, which determines the precision that they can sculpt and erode with.

This means that, to be able to make a corrugated horn at 300 GHz, each corrugation would be around 50 µm thick, which is less than some usual manufacturing tolerances. This, as of this writing, renders the process unfeasible in terms of manufacturing costs, if not purely because of physical constraints.

As the technologies and techniques to manufacture high-frequency components progress, the viability of producing feedhorns with higher capabilities than pyramidal horns (such as corrugated or spline-profiled feeds) will hopefully increase.

Annex

Complete Simulation and Measurement Results

275 GHz Offset Reflector System

Initial Model

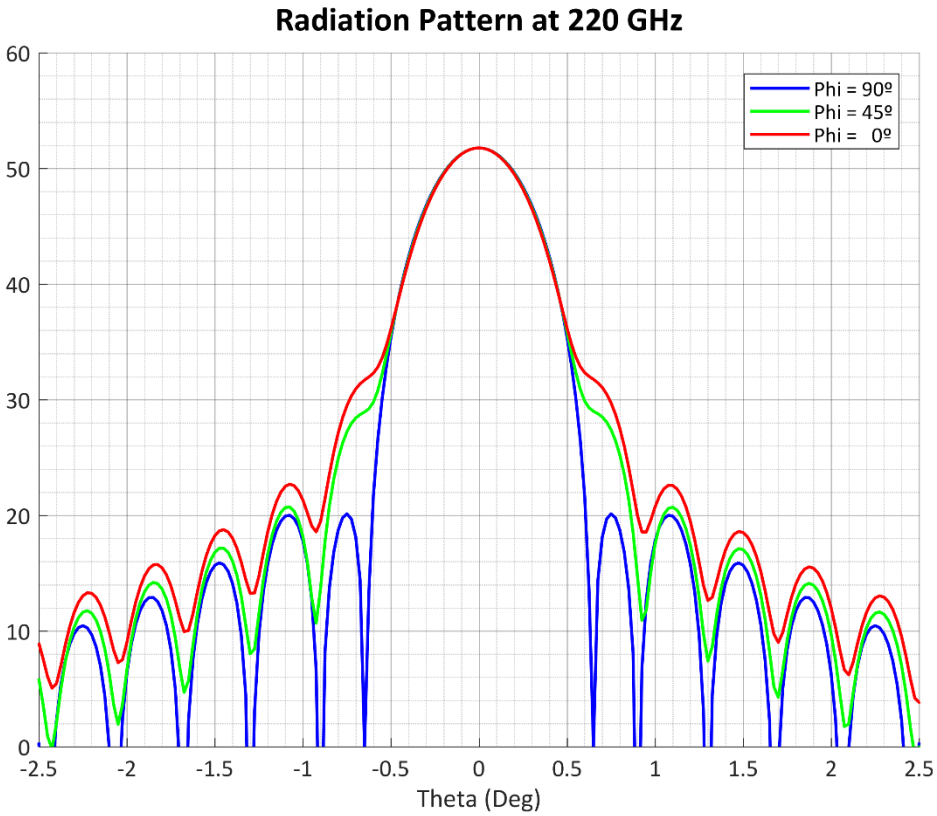

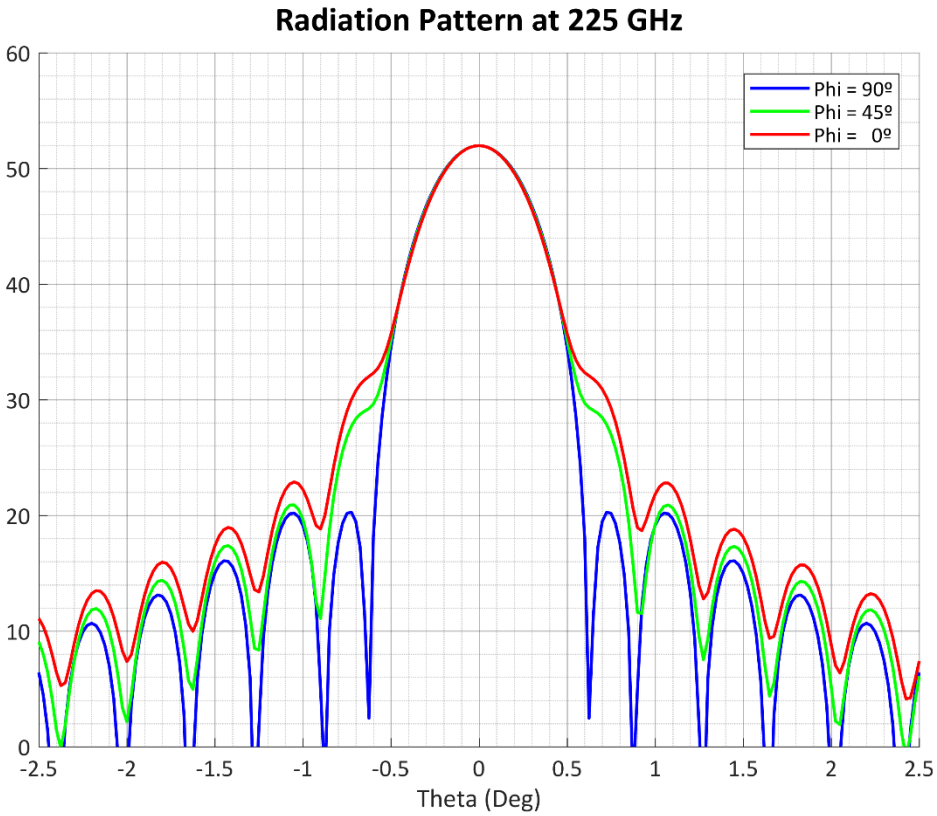

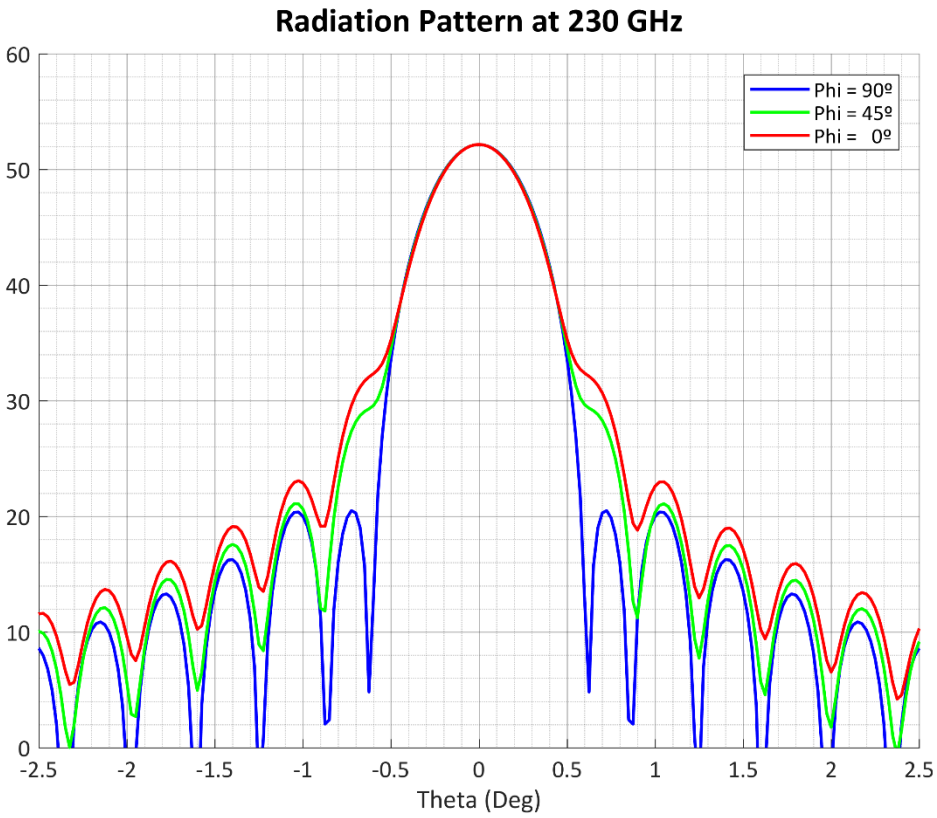
Radiation Pattern at 230 GHz
Phi = 90º
Phi = 45º
Phi = 0º
60
50
40
30
20
10
0
-2.5
-2
-1.5
-1
-0.5
0
0.5
1
1.5
2
2.5
Theta (Deg)

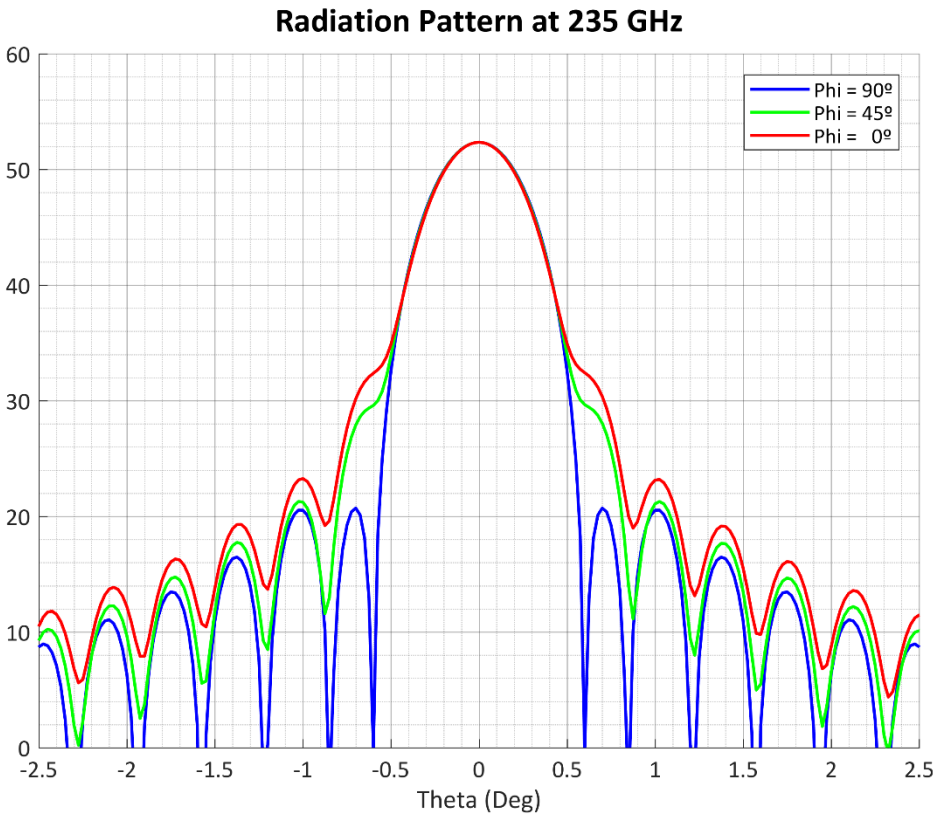
Radiation Pattern at 235 GHz
Phi = 90º
Phi = 45º
Phi = 0º
60
50
40
30
20
10
0
-2.5
-2
-1.5
-1
-0.5
0
0.5
1
1.5
2
2.5
Theta (Deg)

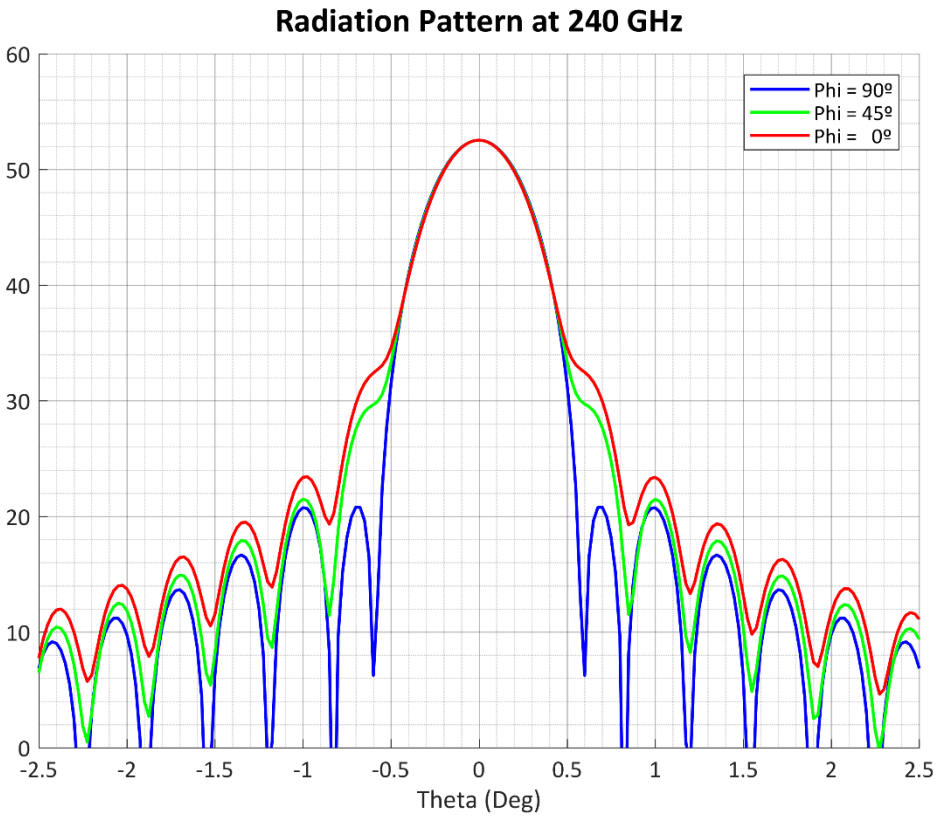
Radiation Pattern at 240 GHz
Phi = 90º
Phi = 45º
Phi = 0º
60
50
40
30
20
10
0
-2.5
-2
-1.5
-1
-0.5
0
0.5
1
1.5
2
2.5
Theta (Deg)

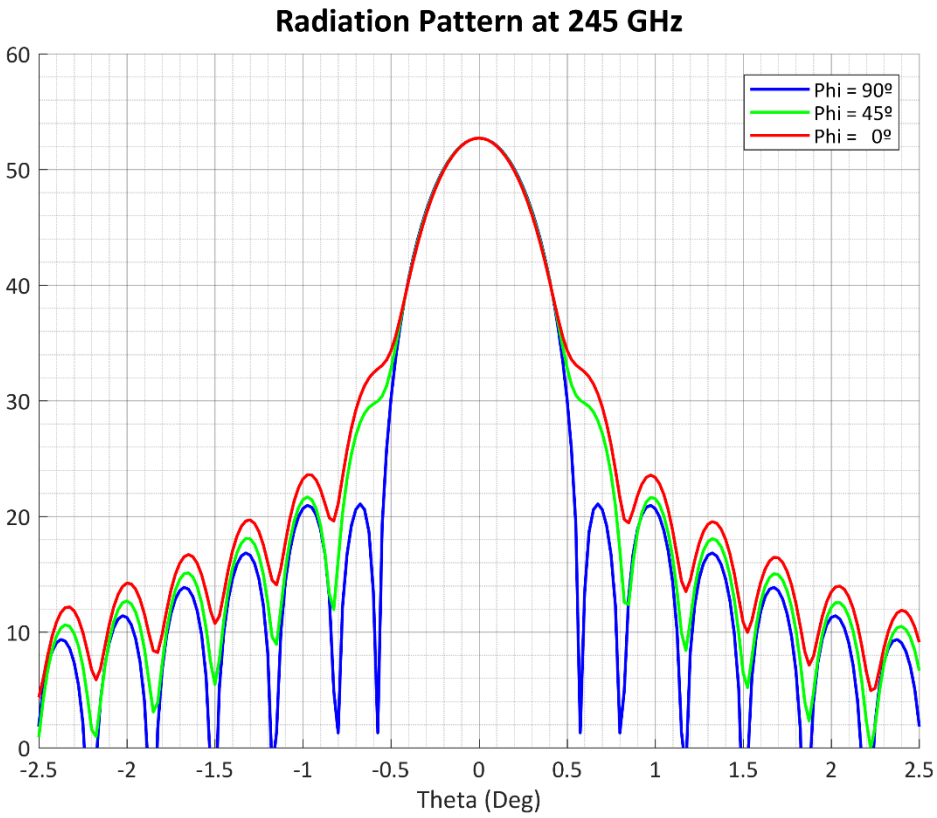
Radiation Pattern at 245 GHz
Phi = 90º
Phi = 45º
Phi = 0º
60
50
40
30
20
10
0
-2.5
-2
-1.5
-1
-0.5
0
0.5
1
1.5
2
2.5
Theta (Deg)

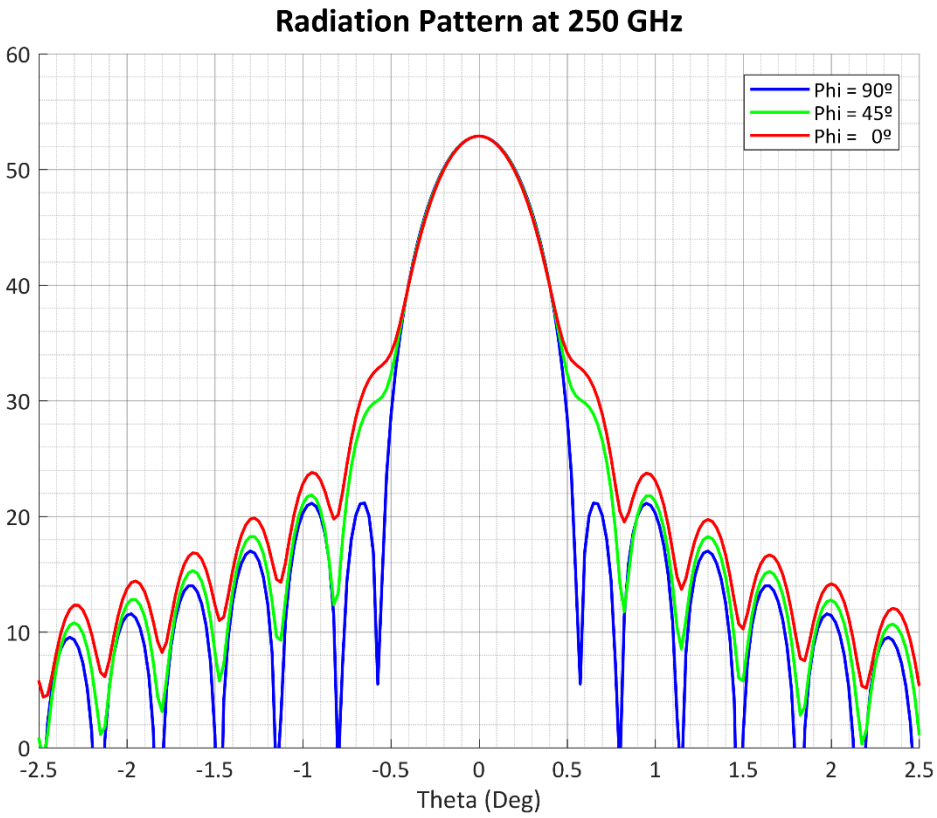
Radiation Pattern at 250 GHz
Phi = 90º
Phi = 45º
Phi = 0º
60
50
40
30
20
10
0
-2.5
-2
-1.5
-1
-0.5
0
0.5
1
1.5
2
2.5
Theta (Deg)

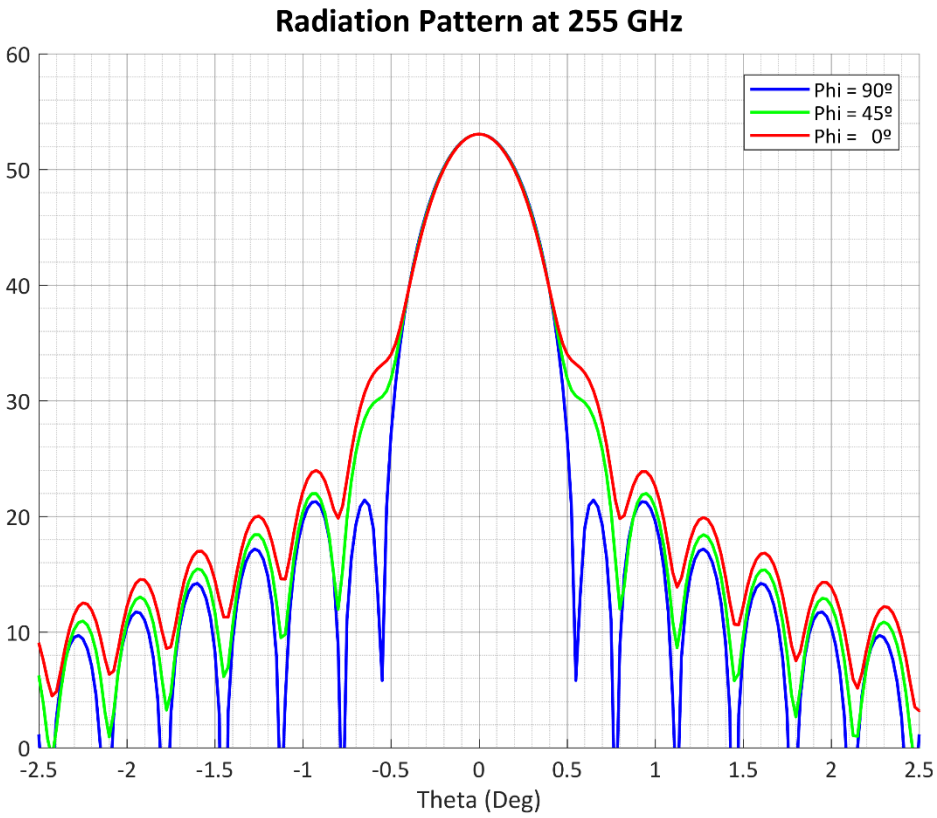
Radiation Pattern at 255 GHz
Phi = 90º
Phi = 45º
Phi = 0º
60
50
40
30
20
10
0
-2.5
-2
-1.5
-1
-0.5
0
0.5
1
1.5
2
2.5
Theta (Deg)

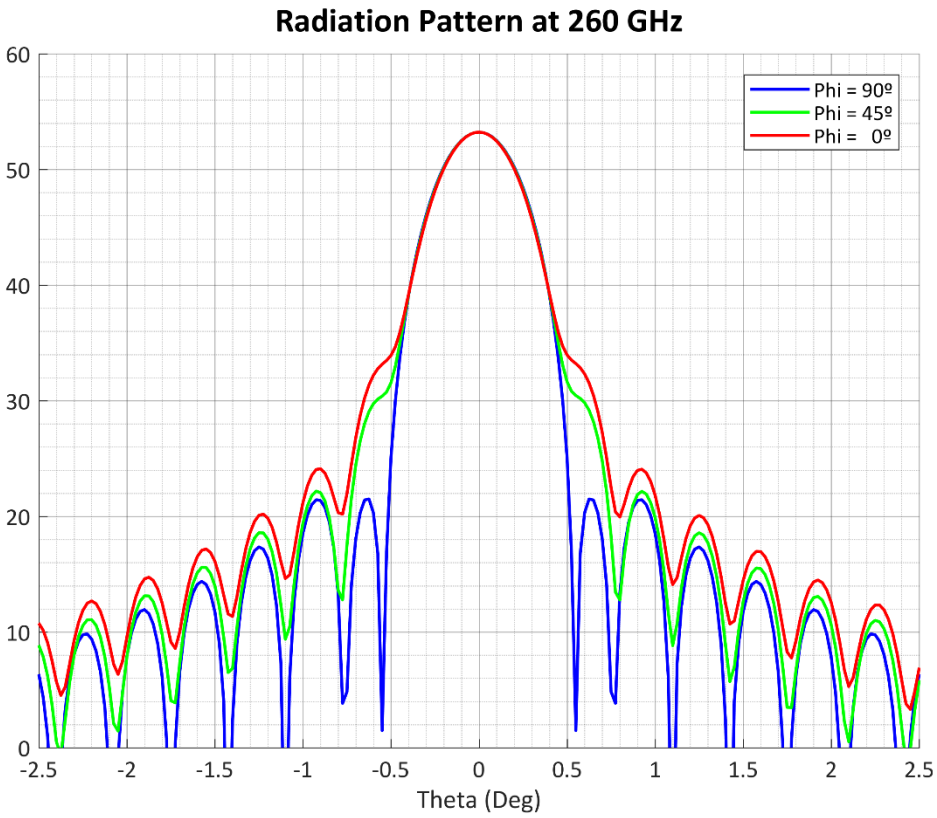
Radiation Pattern at 260 GHz
Phi = 90º
Phi = 45º
Phi = 0º
60
50
40
30
20
10
0
-2.5
-2
-1.5
-1
-0.5
0
0.5
1
1.5
2
2.5
Theta (Deg)

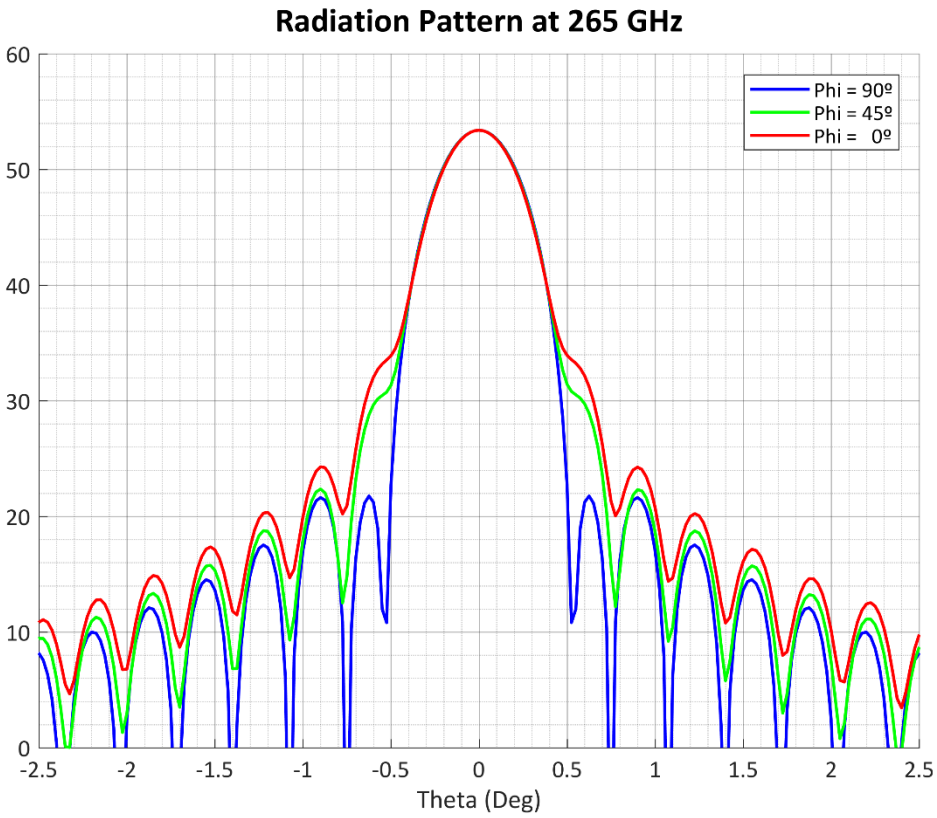
Radiation Pattern at 265 GHz
Phi = 90º
Phi = 45º
Phi = 0º
60
50
40
30
20
10
0
-2.5
-2
-1.5
-1
-0.5
0
0.5
1
1.5
2
2.5
Theta (Deg)

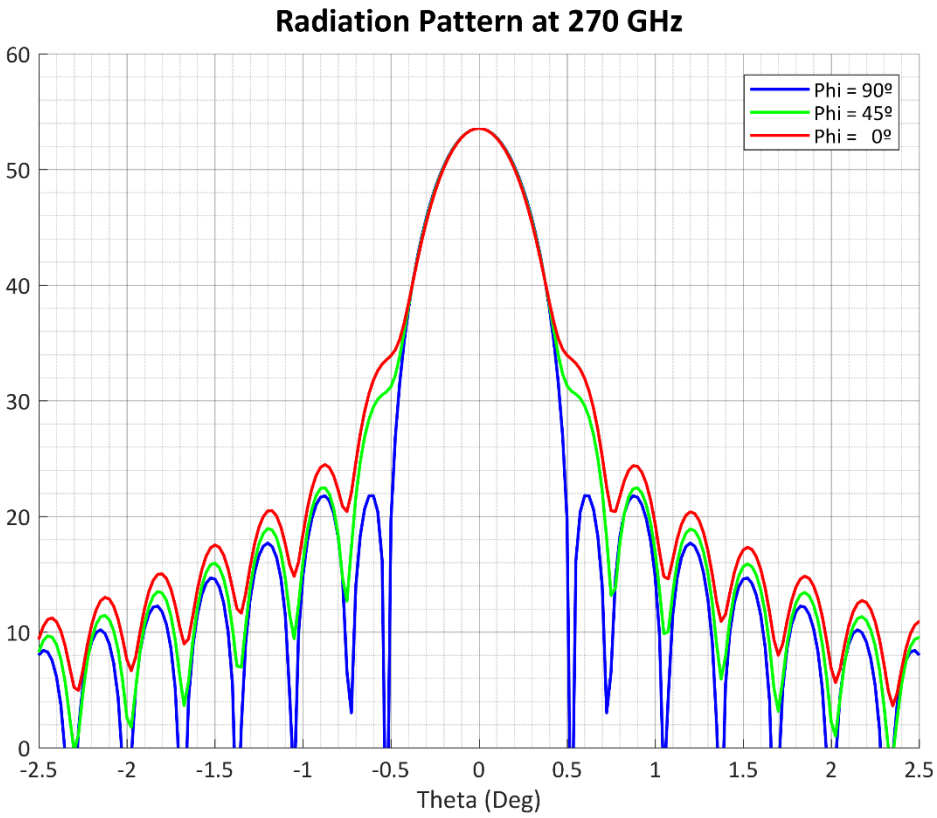
Radiation Pattern at 270 GHz
Phi = 90º
Phi = 45º
Phi = 0º
60
50
40
30
20
10
0
-2.5
-2
-1.5
-1
-0.5
0
0.5
1
1.5
2
2.5
Theta (Deg)

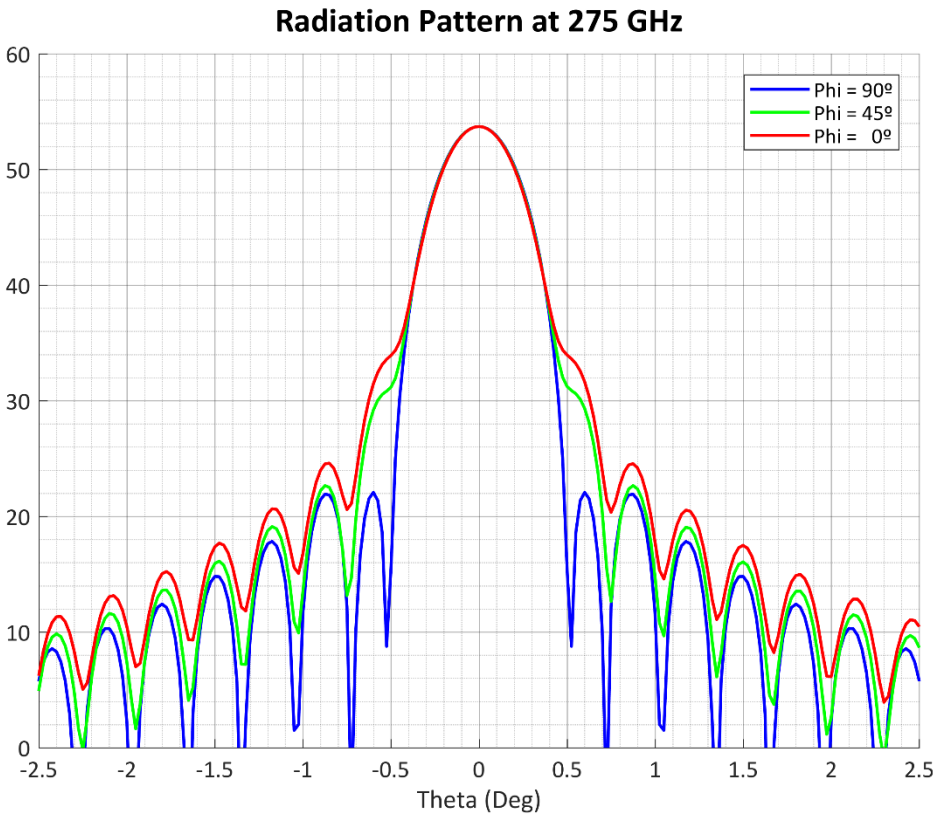
Radiation Pattern at 275 GHz
Phi = 90º
Phi = 45º
Phi = 0º
60
50
40
30
20
10
0
-2.5
-2
-1.5
-1
-0.5
0
0.5
1
1.5
2
2.5
Theta (Deg)

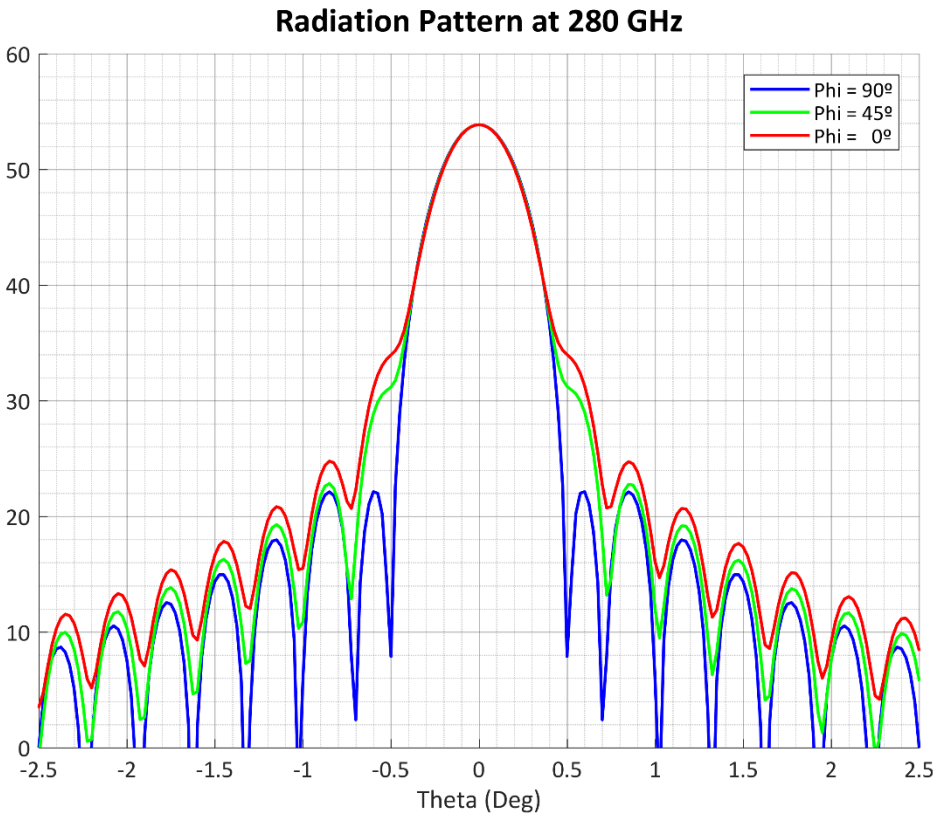
Radiation Pattern at 280 GHz
Phi = 90º
Phi = 45º
Phi = 0º
60
50
40
30
20
10
0
-2.5
-2
-1.5
-1
-0.5
0
0.5
1
1.5
2
2.5
Theta (Deg)

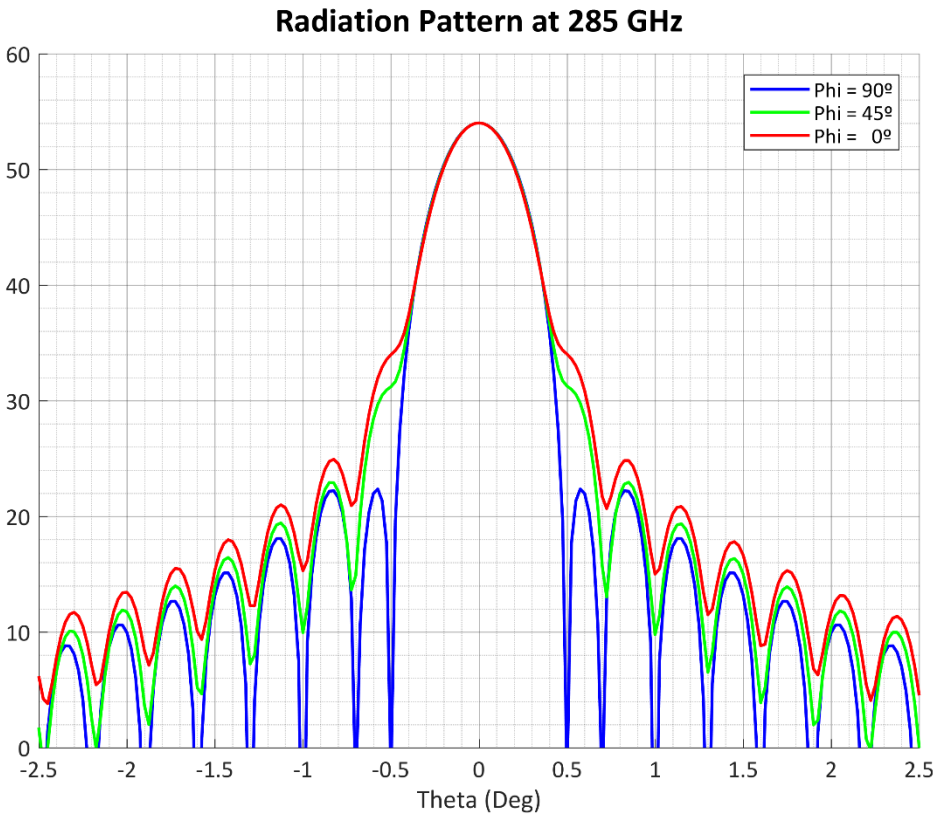
Radiation Pattern at 285 GHz
Phi = 90º
Phi = 45º
Phi = 0º
60
50
40
30
20
10
0
-2.5
-2
-1.5
-1
-0.5
0
0.5
1
1.5
2
2.5
Theta (Deg)

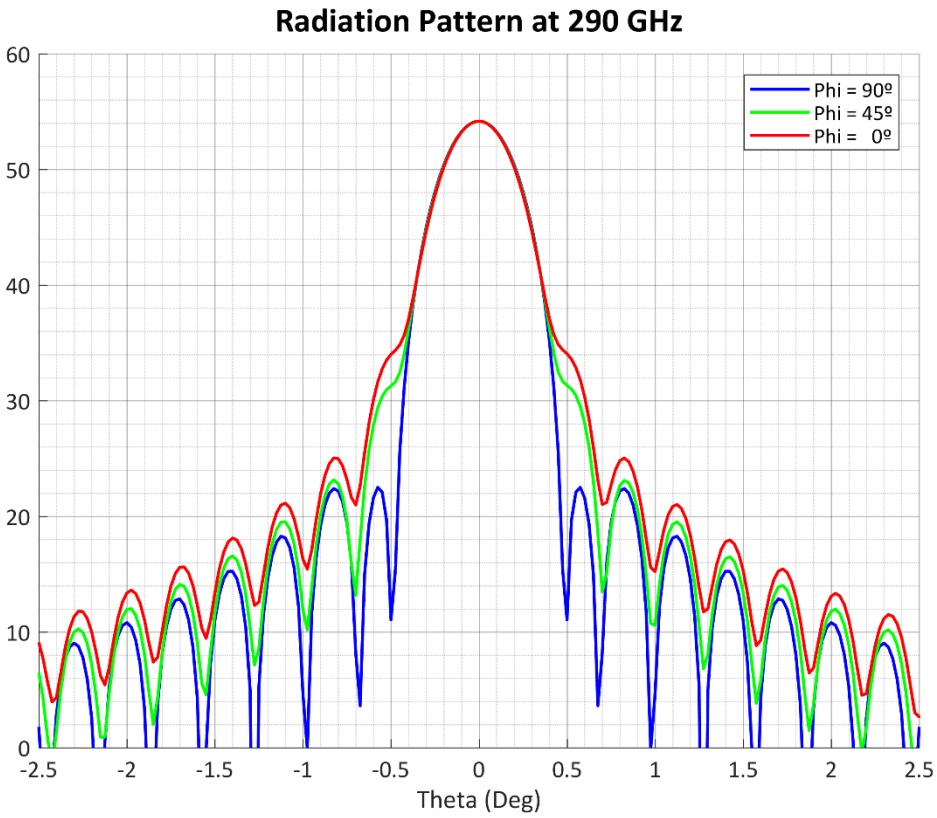
Radiation Pattern at 290 GHz
Phi = 90º
Phi = 45º
Phi = 0º
60
50
40
30
20
10
0
-2.5
-2
-1.5
-1
-0.5
0
0.5
1
1.5
2
2.5
Theta (Deg)

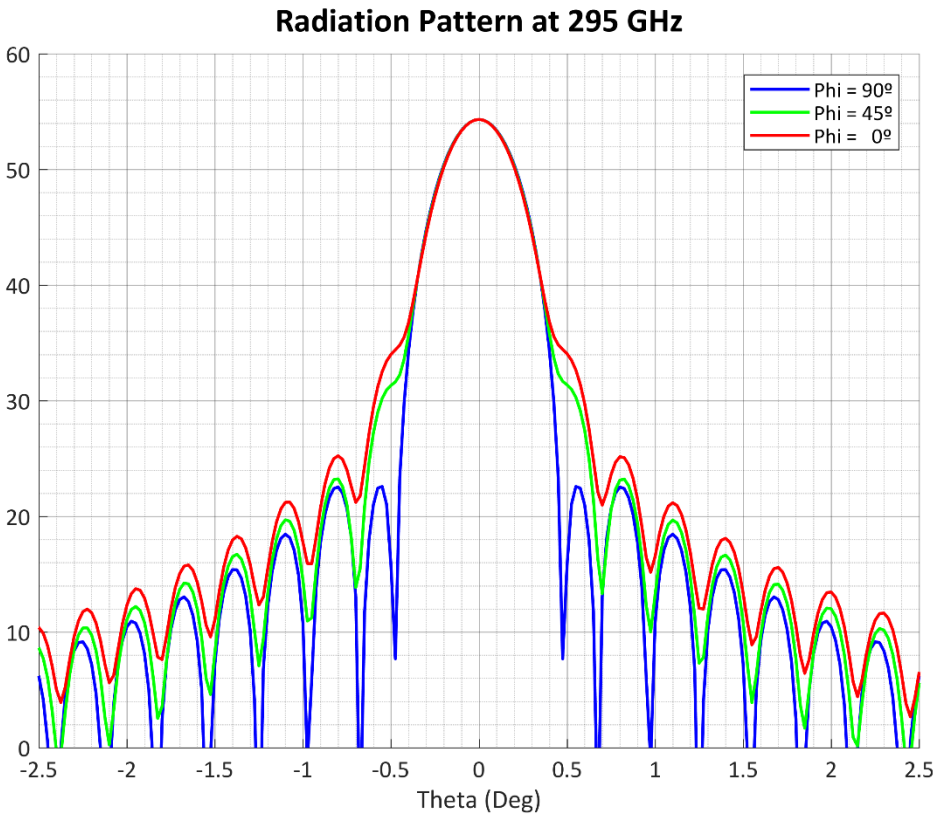
Radiation Pattern at 295 GHz
Phi = 90º
Phi = 45º
Phi = 0º
60
50
40
30
20
10
0
-2.5
-2
-1.5
-1
-0.5
0
0.5
1
1.5
2
2.5
Theta (Deg)

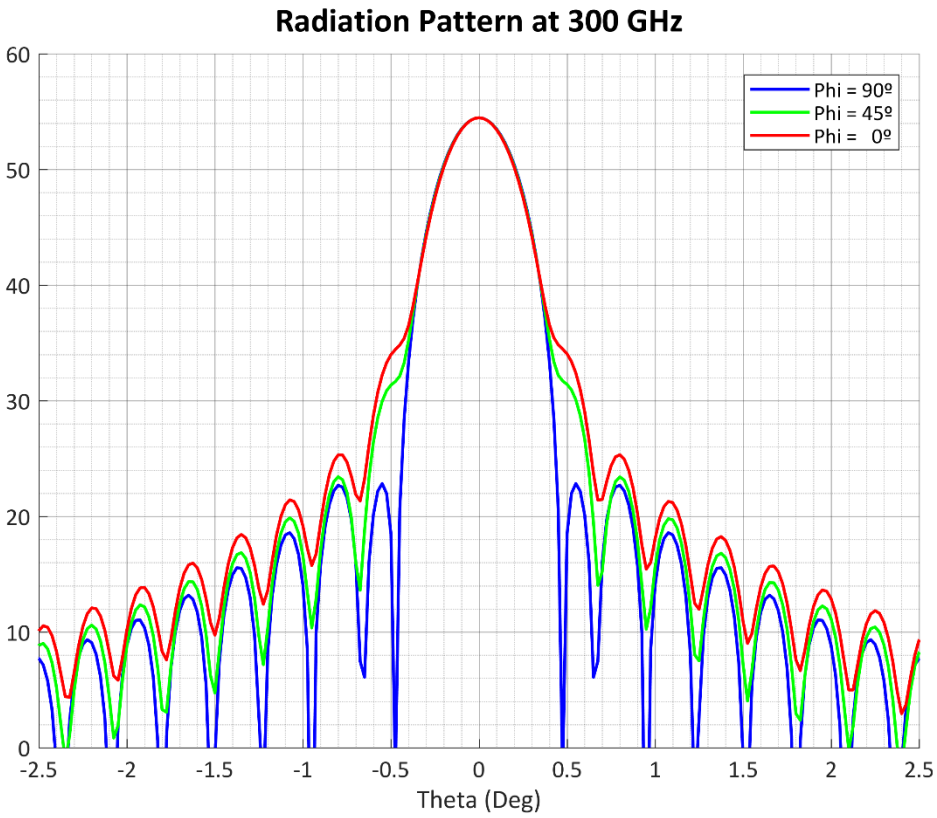
Radiation Pattern at 300 GHz
Phi = 90º
Phi = 45º
Phi = 0º
60
50
40
30
20
10
0
-2.5
-2
-1.5
-1
-0.5
0
0.5
1
1.5
2
2.5
Theta (Deg)

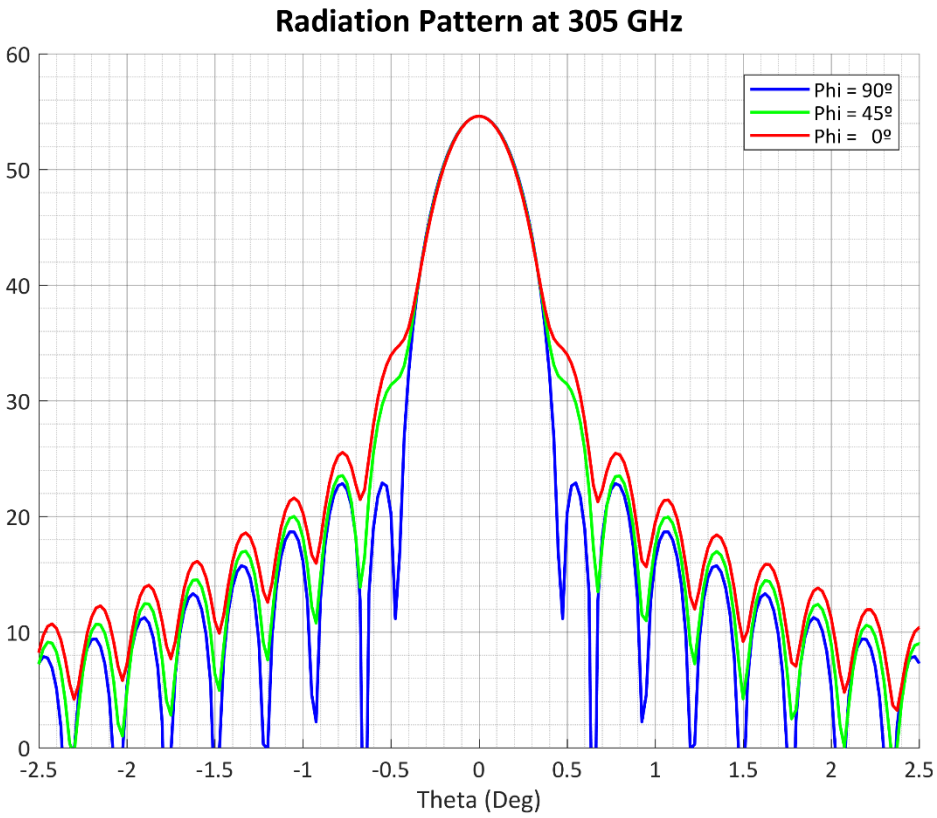
Radiation Pattern at 305 GHz
Phi = 90º
Phi = 45º
Phi = 0º
60
50
40
30
20
10
0
-2.5
-2
-1.5
-1
-0.5
0
0.5
1
1.5
2
2.5
Theta (Deg)

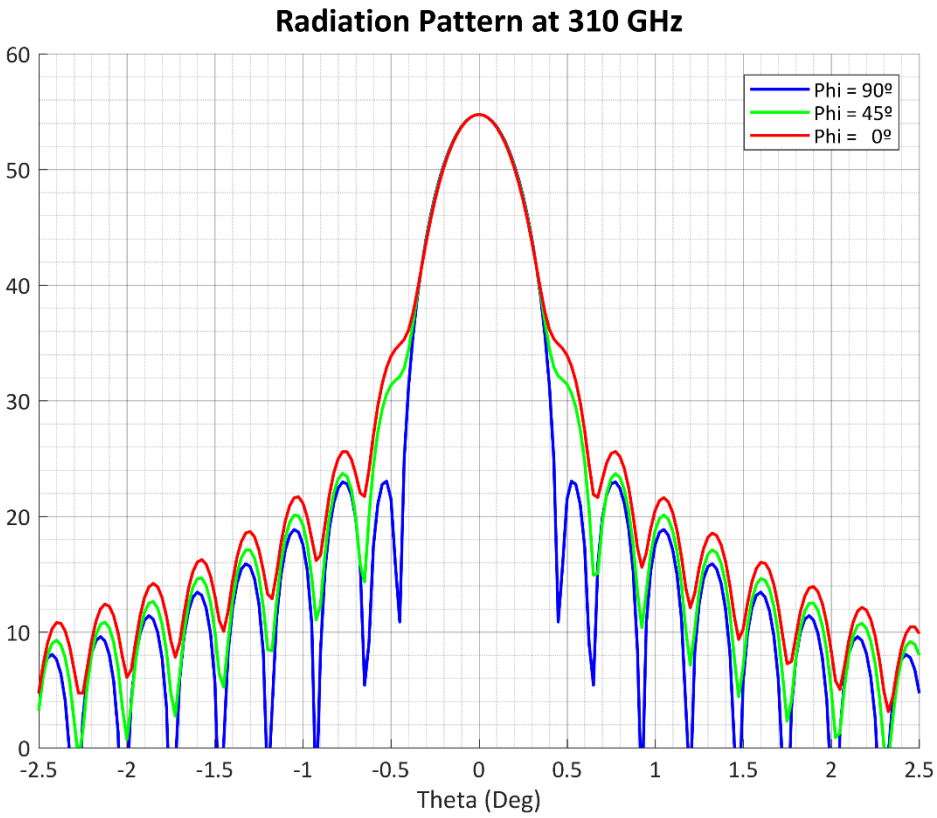
Radiation Pattern at 310 GHz
Phi = 90º
Phi = 45º
Phi = 0º
60
50
40
30
20
10
0
-2.5
-2
-1.5
-1
-0.5
0
0.5
1
1.5
2
2.5
Theta (Deg)

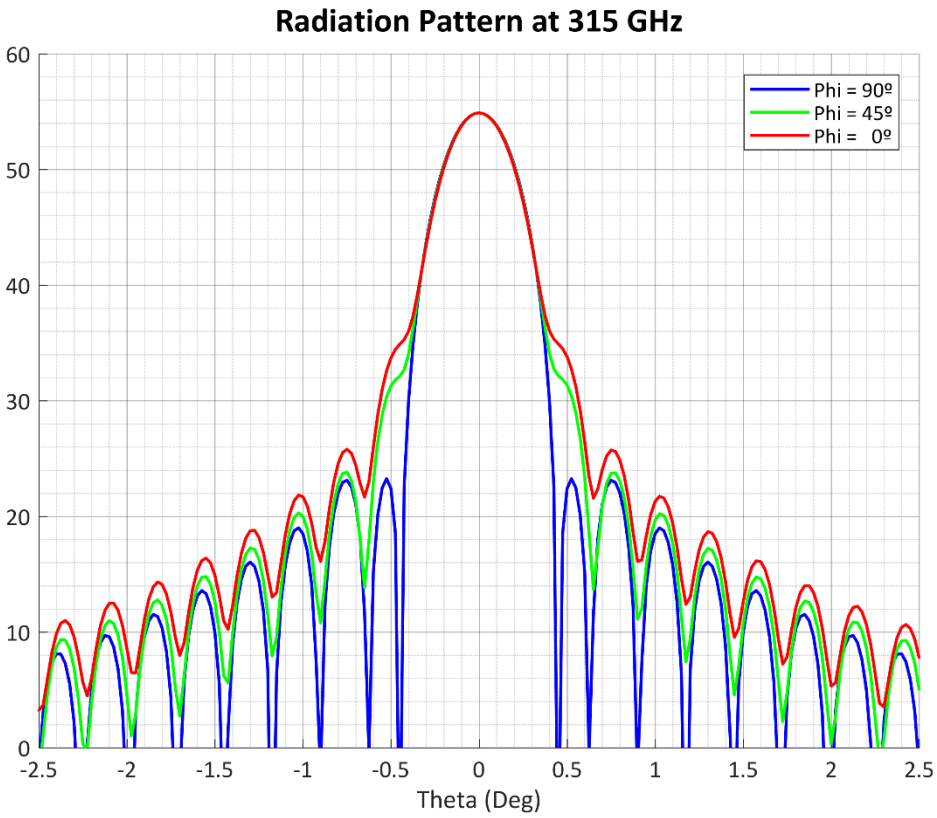
Radiation Pattern at 315 GHz
Phi = 90º
Phi = 45º
Phi = 0º
60
50
40
30
20
10
0
-2.5
-2
-1.5
-1
-0.5
0
0.5
1
1.5
2
2.5
Theta (Deg)

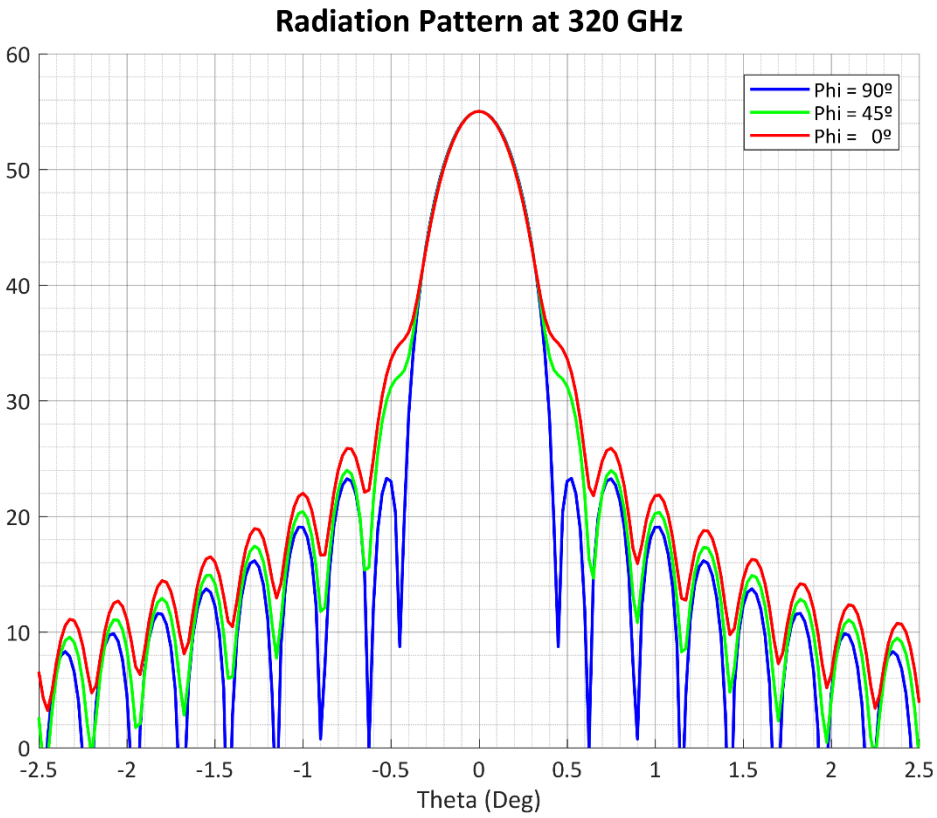
Radiation Pattern at 320 GHz
Phi = 90º
Phi = 45º
Phi = 0º
60
50
40
30
20
10
0
-2.5
-2
-1.5
-1
-0.5
0
0.5
1
1.5
2
2.5
Theta (Deg)

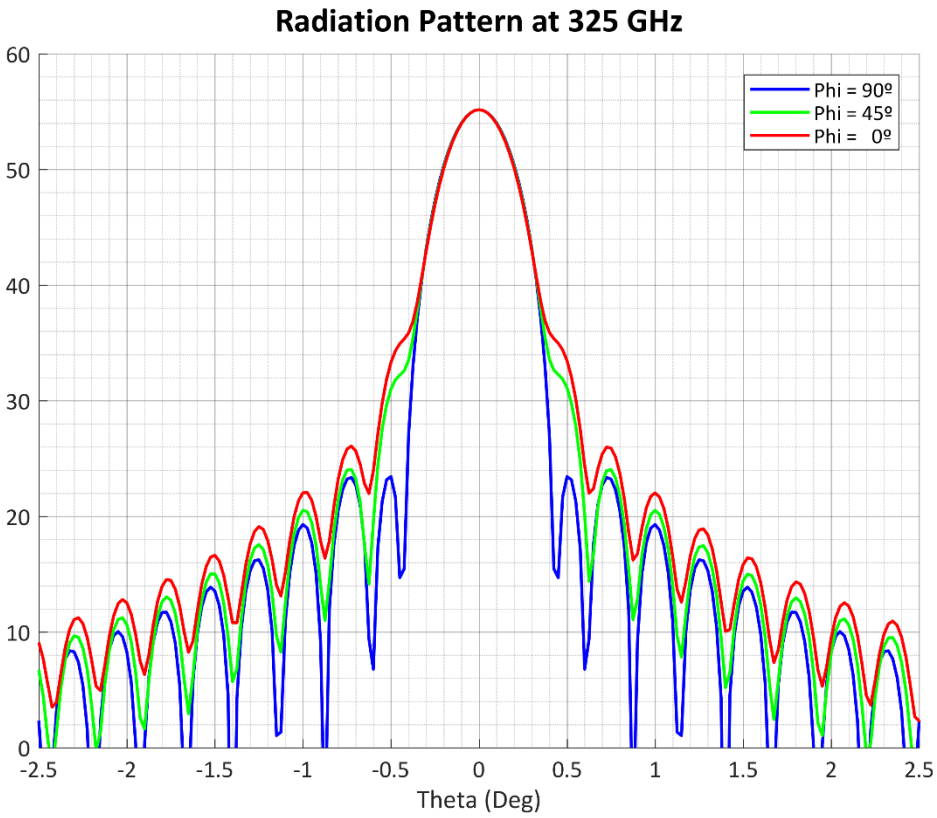
Radiation Pattern at 325 GHz
Phi = 90º
Phi = 45º
Phi = 0º
60
50
40
30
20
10
0
-2.5
-2
-1.5
-1
-0.5
0
0.5
1
1.5
2
2.5
Theta (Deg)

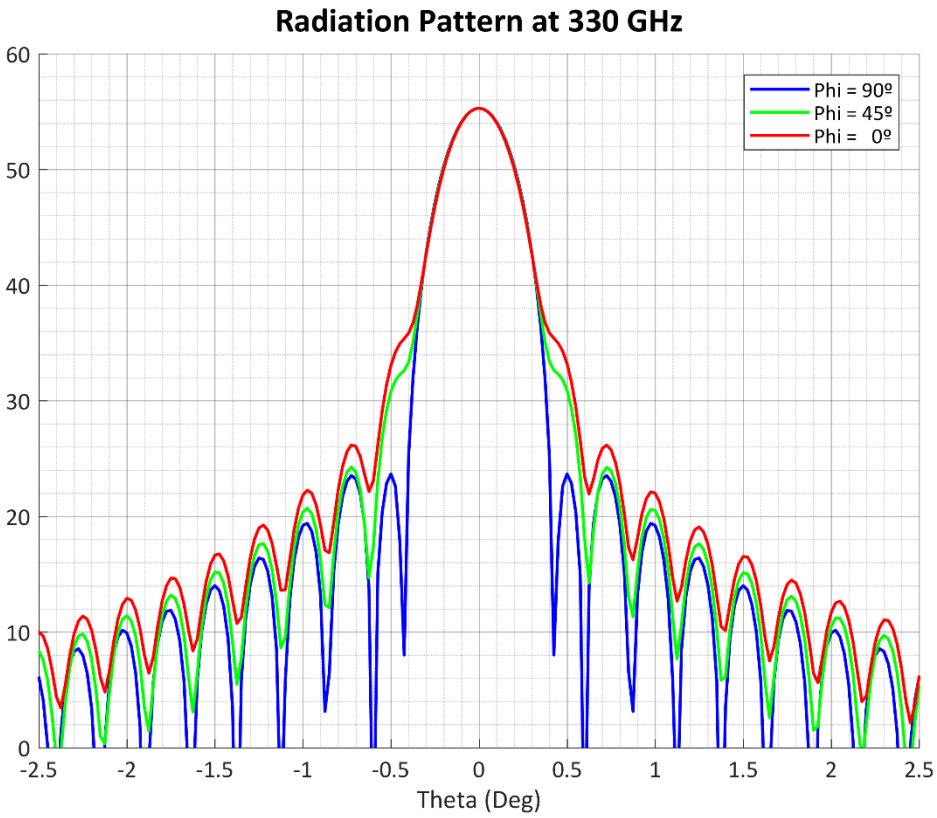
Radiation Pattern at 330 GHz
Phi = 90º
Phi = 45º
Phi = 0º
60
50
40
30
20
10
0
-2.5
-2
-1.5
-1
-0.5
0
0.5
1
1.5
2
2.5
Theta (Deg)

Final Model

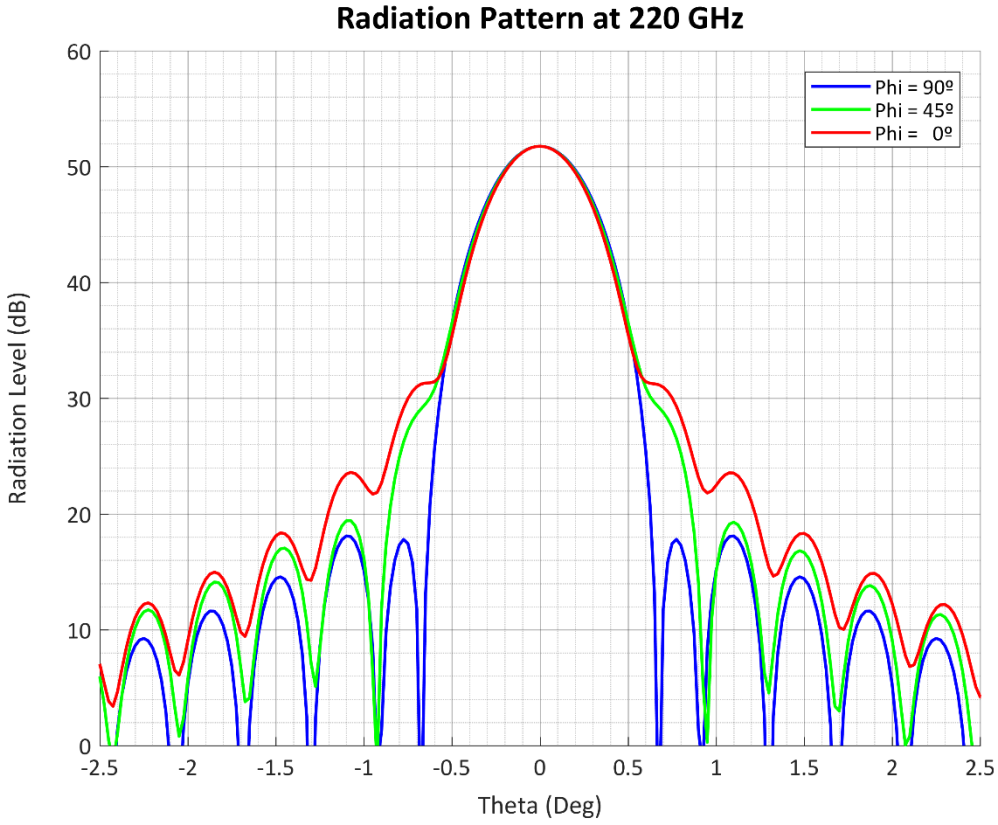
Radiation Pattern at 220 GHz
Phi = 90º
Phi = 45º
Phi = 0º
Radiation Level (dB)
Theta (Deg)
60
50
40
30
20
10
0
-2.5
-2
-1.5
-1
-0.5
0
0.5
1
1.5
2
2.5

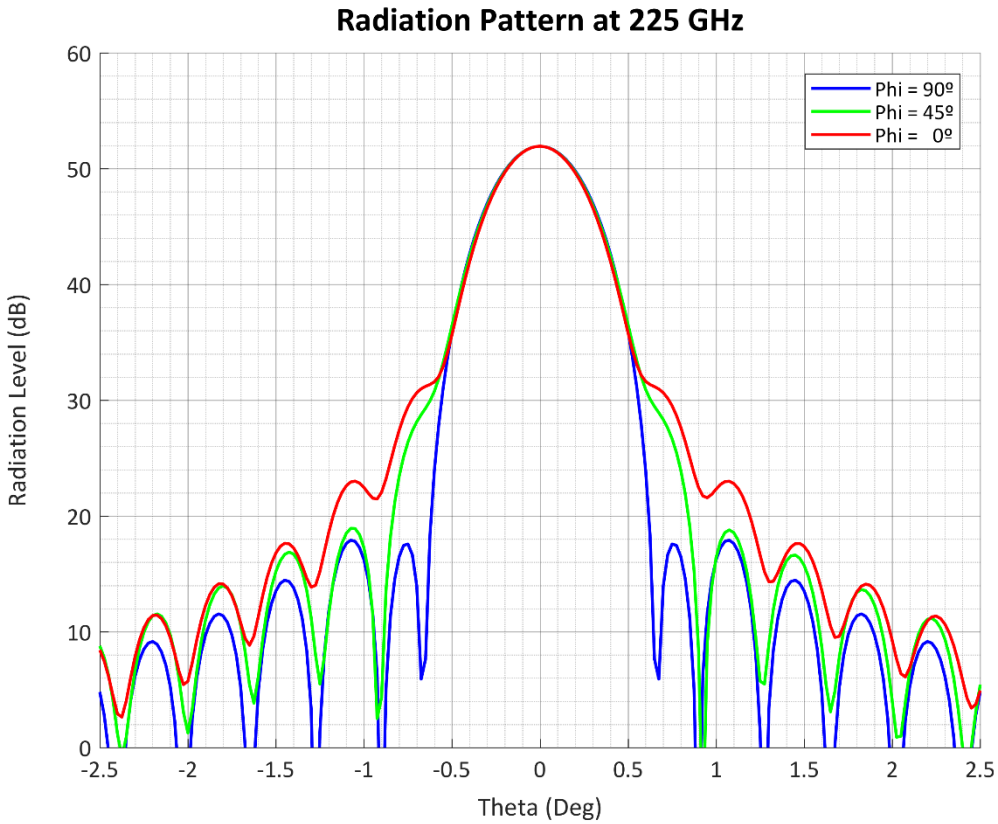
Radiation Pattern at 225 GHz
Phi = 90º
Phi = 45º
Phi = 0º
Radiation Level (dB)
Theta (Deg)
60
50
40
30
20
10
0
-2.5
-2
-1.5
-1
-0.5
0
0.5
1
1.5
2
2.5

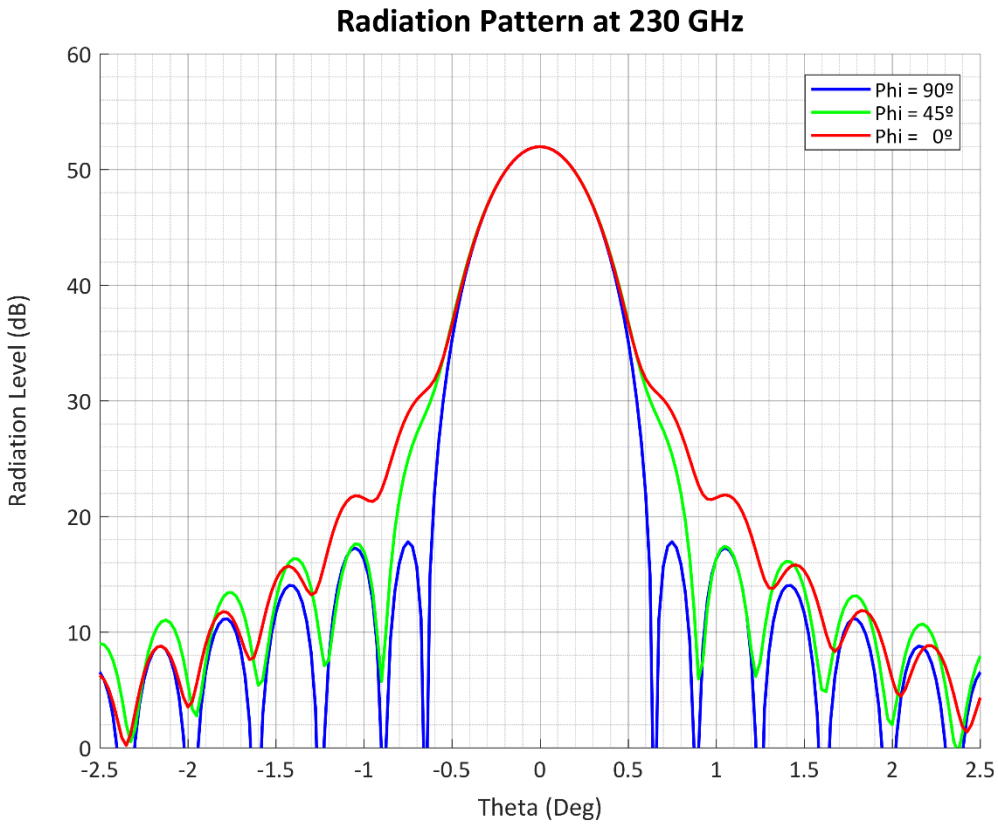
Radiation Pattern at 230 GHz
Phi = 90º
Phi = 45º
Phi = 0º
Radiation Level (dB)
Theta (Deg)
60
50
40
30
20
10
0
-2.5
-2
-1.5
-1
-0.5
0
0.5
1
1.5
2
2.5

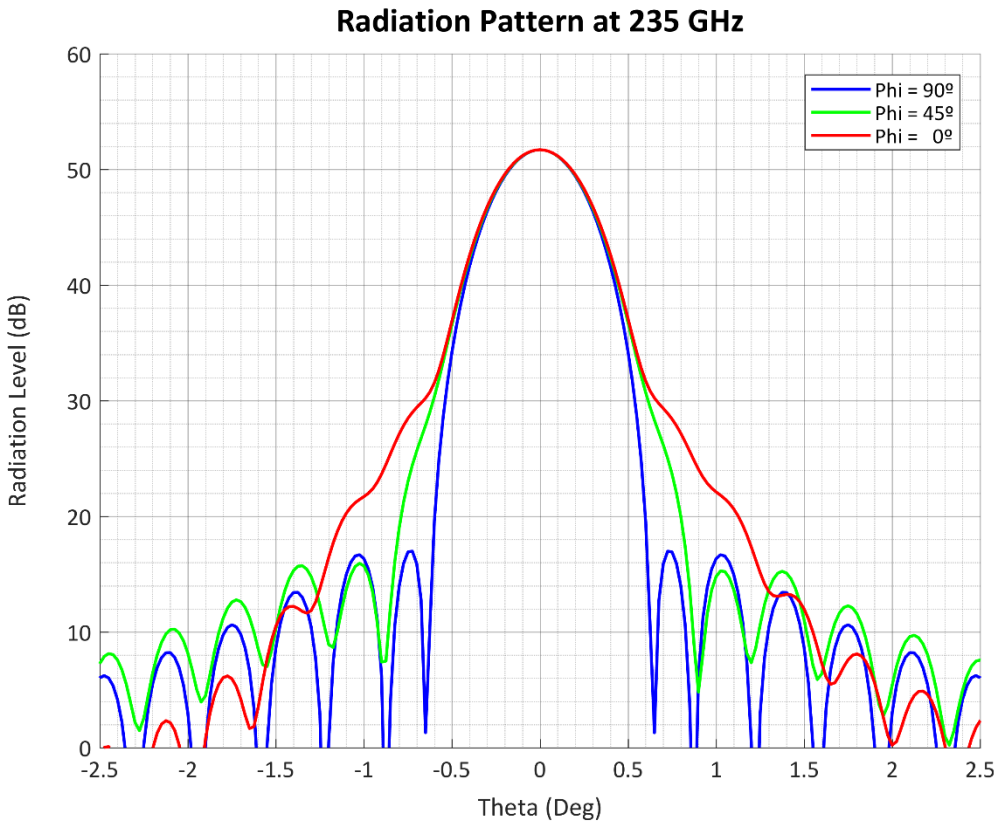
Radiation Pattern at 235 GHz
Phi = 90º
Phi = 45º
Phi = 0º
Radiation Level (dB)
Theta (Deg)
60
50
40
30
20
10
0
-2.5
-2
-1.5
-1
-0.5
0
0.5
1
1.5
2
2.5

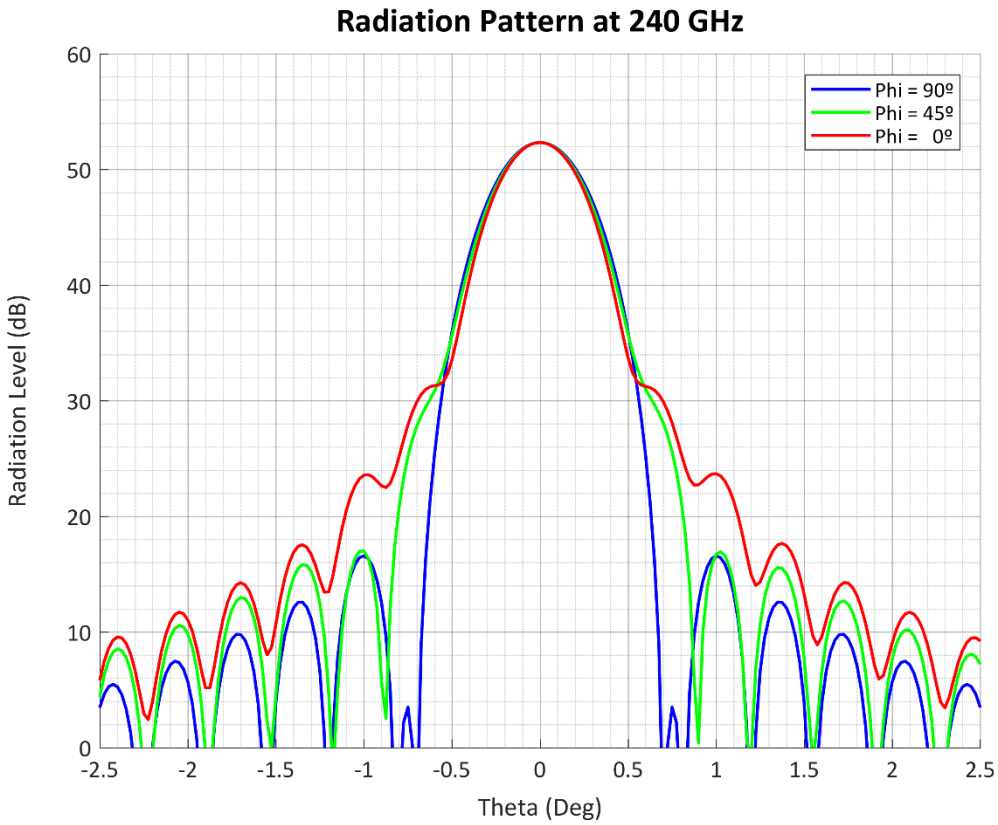
Radiation Pattern at 240 GHz
Phi = 90º
Phi = 45º
Phi = 0º
Radiation Level (dB)
Theta (Deg)
60
50
40
30
20
10
0
-2.5
-2
-1.5
-1
-0.5
0
0.5
1
1.5
2
2.5

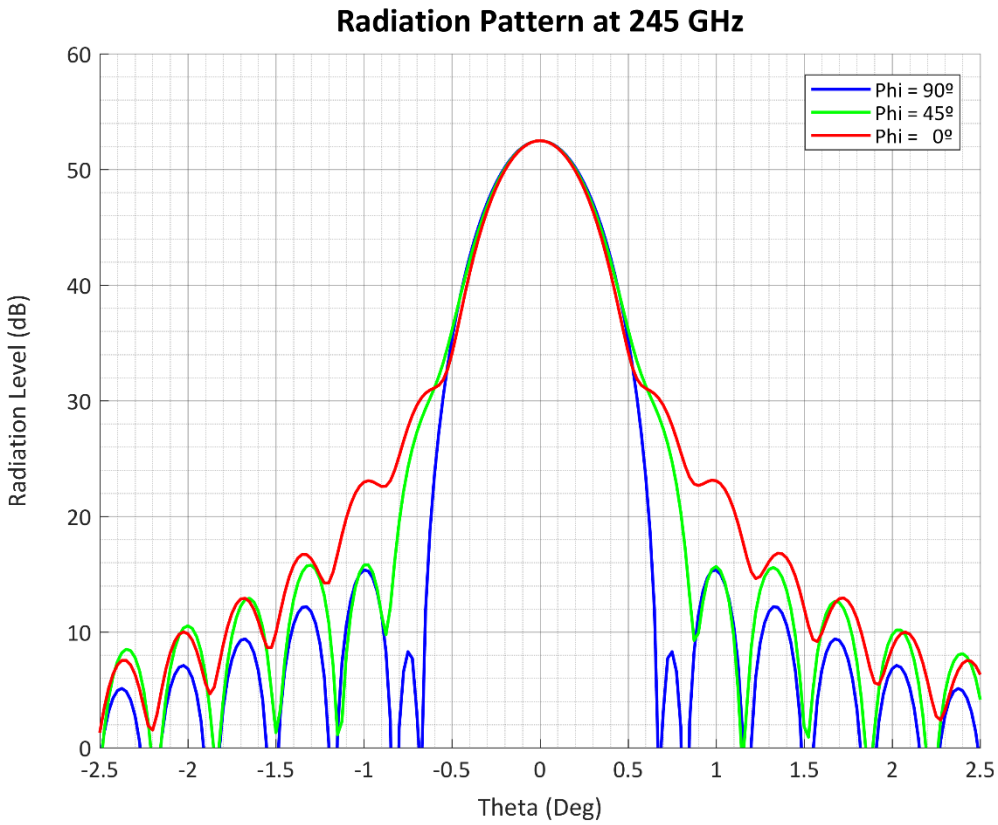
Radiation Pattern at 245 GHz
Phi = 90º
Phi = 45º
Phi = 0º
Radiation Level (dB)
Theta (Deg)
60
50
40
30
20
10
0
-2.5
-2
-1.5
-1
-0.5
0
0.5
1
1.5
2
2.5

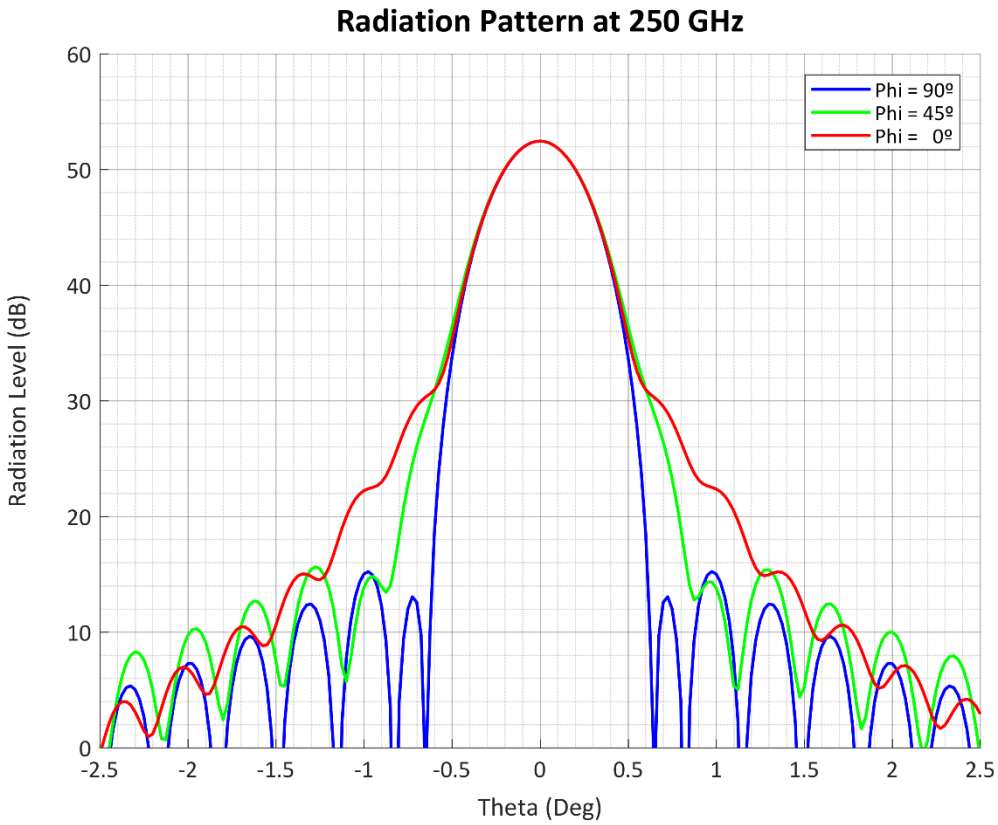
Radiation Pattern at 250 GHz
Phi = 90º
Phi = 45º
Phi = 0º
Radiation Level (dB)
Theta (Deg)
60
50
40
30
20
10
0
-2.5
-2
-1.5
-1
-0.5
0
0.5
1
1.5
2
2.5

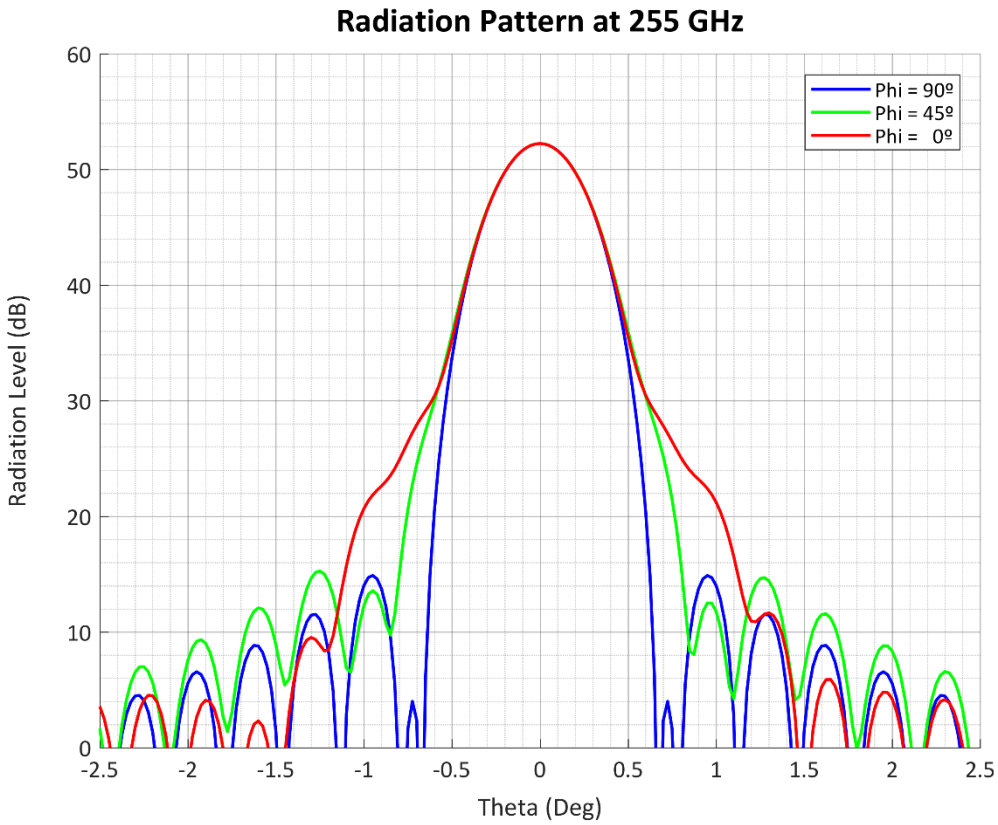
Radiation Pattern at 255 GHz
Phi = 90º
Phi = 45º
Phi = 0º
Radiation Level (dB)
Theta (Deg)
60
50
40
30
20
10
0
-2.5
-2
-1.5
-1
-0.5
0
0.5
1
1.5
2
2.5

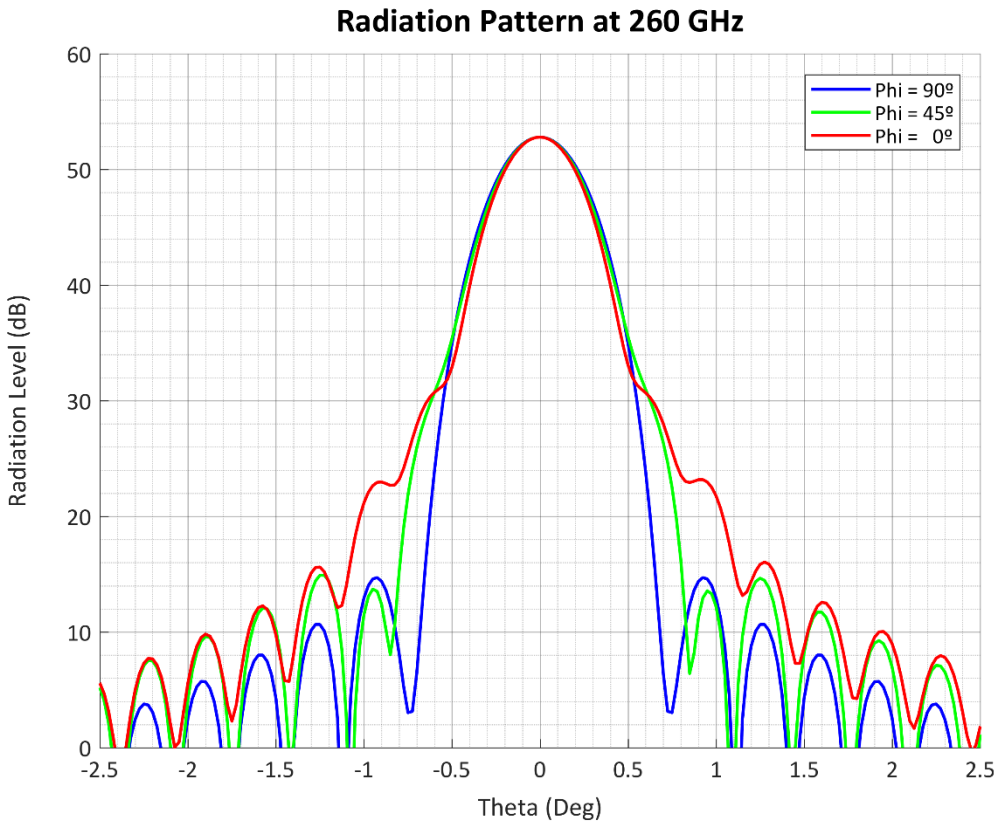
Radiation Pattern at 260 GHz
Phi = 90º
Phi = 45º
Phi = 0º
Radiation Level (dB)
Theta (Deg)
60
50
40
30
20
10
0
-2.5
-2
-1.5
-1
-0.5
0
0.5
1
1.5
2
2.5

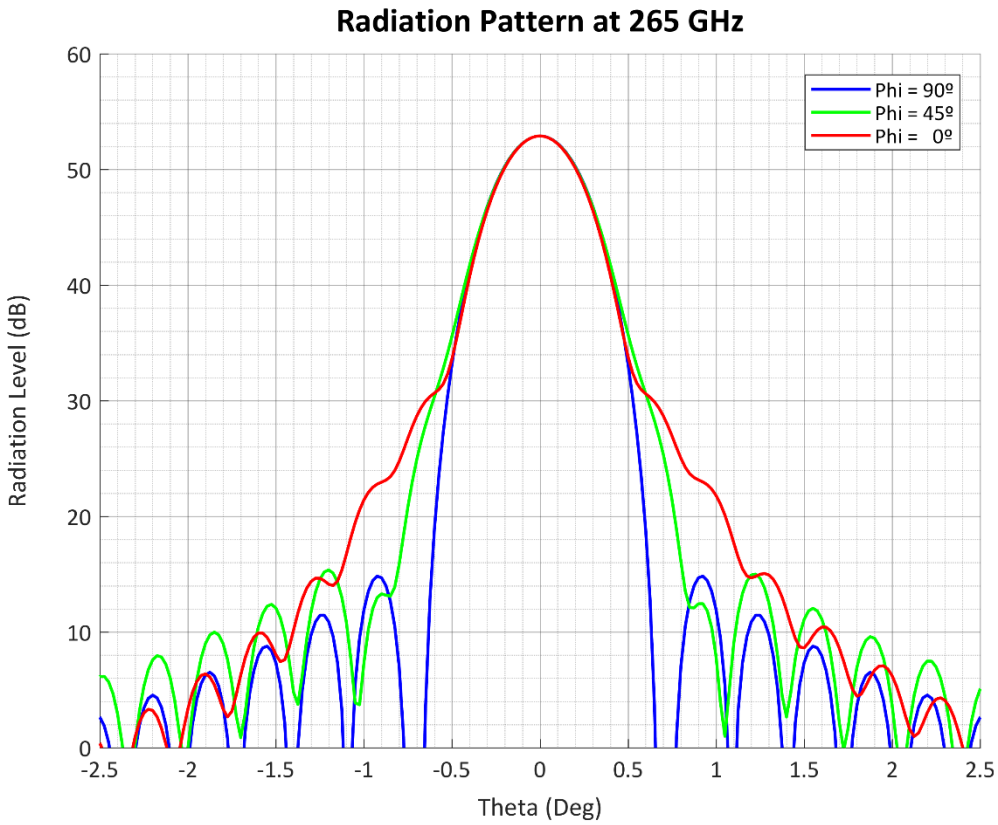
Radiation Pattern at 265 GHz
Phi = 90º
Phi = 45º
Phi = 0º
Radiation Level (dB)
Theta (Deg)
60
50
40
30
20
10
0
-2.5
-2
-1.5
-1
-0.5
0
0.5
1
1.5
2
2.5

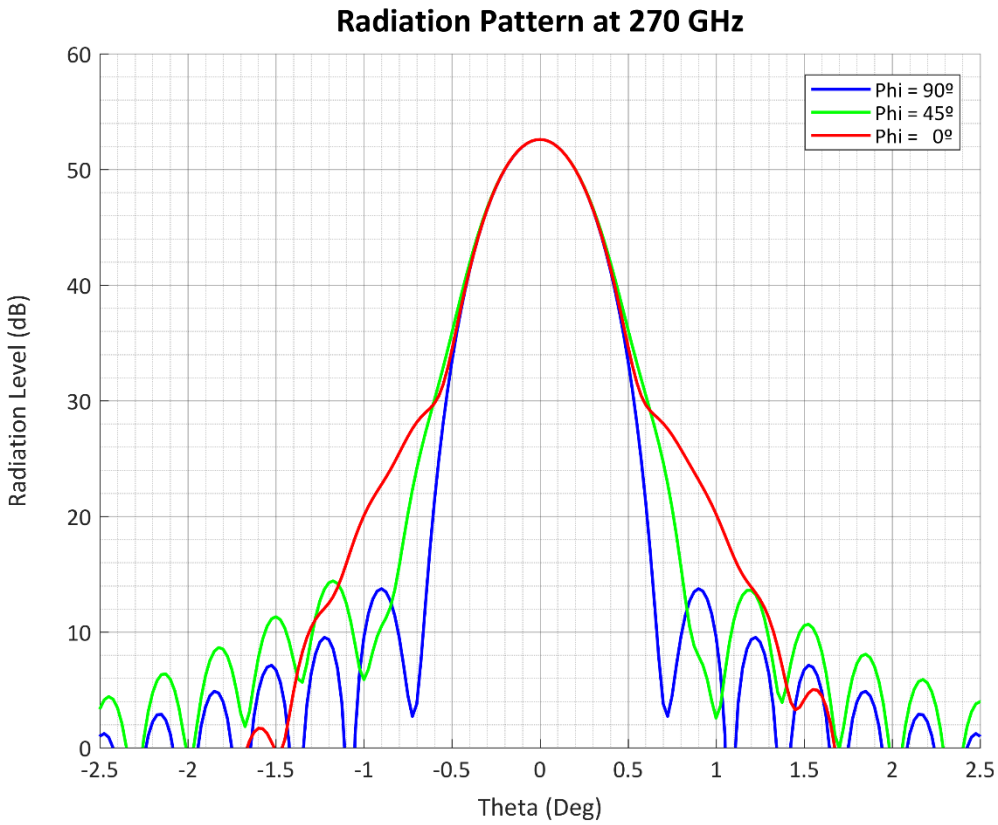
Radiation Pattern at 270 GHz
Phi = 90º
Phi = 45º
Phi = 0º
Radiation Level (dB)
Theta (Deg)
60
50
40
30
20
10
0
-2.5
-2
-1.5
-1
-0.5
0
0.5
1
1.5
2
2.5

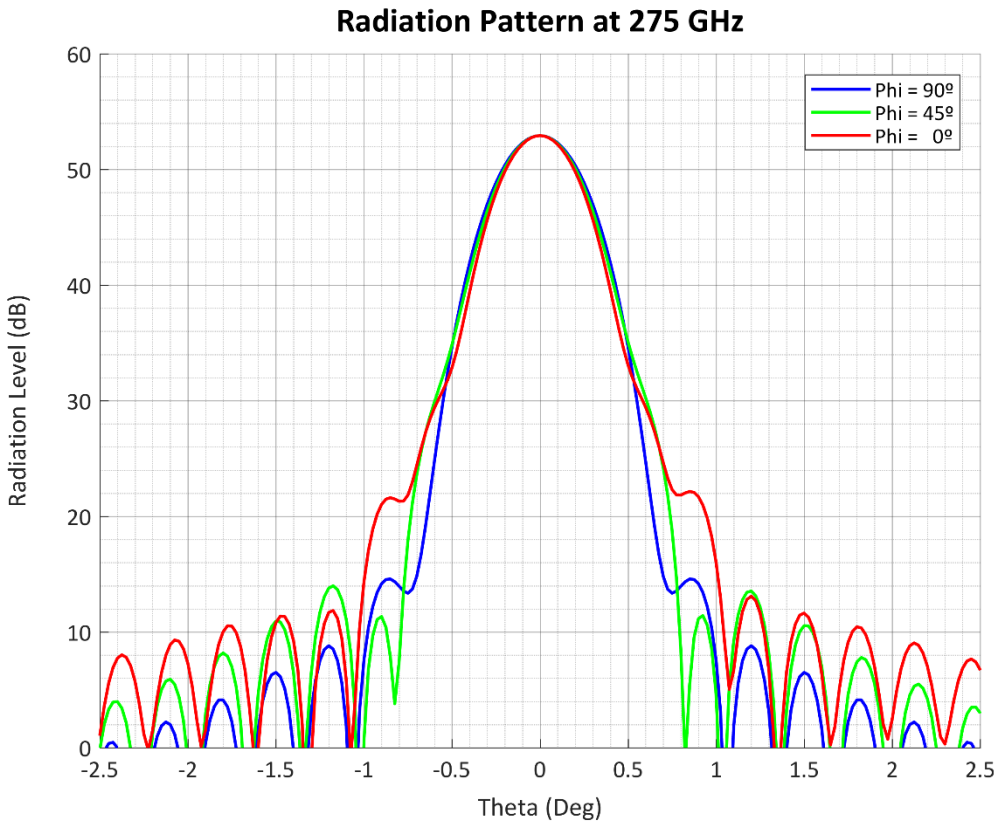
Radiation Pattern at 275 GHz
Phi = 90º
Phi = 45º
Phi = 0º
Radiation Level (dB)
Theta (Deg)
60
50
40
30
20
10
0
-2.5
-2
-1.5
-1
-0.5
0
0.5
1
1.5
2
2.5

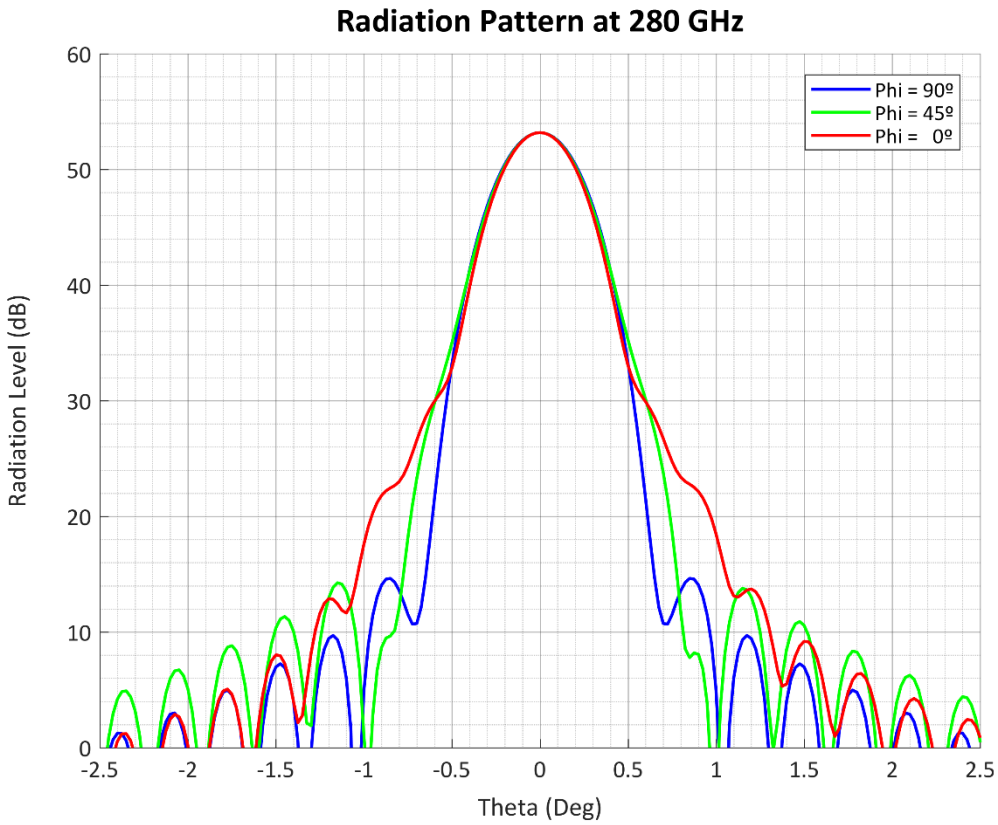
Radiation Pattern at 280 GHz
Phi = 90º
Phi = 45º
Phi = 0º
Radiation Level (dB)
Theta (Deg)
60
50
40
30
20
10
0
-2.5
-2
-1.5
-1
-0.5
0
0.5
1
1.5
2
2.5

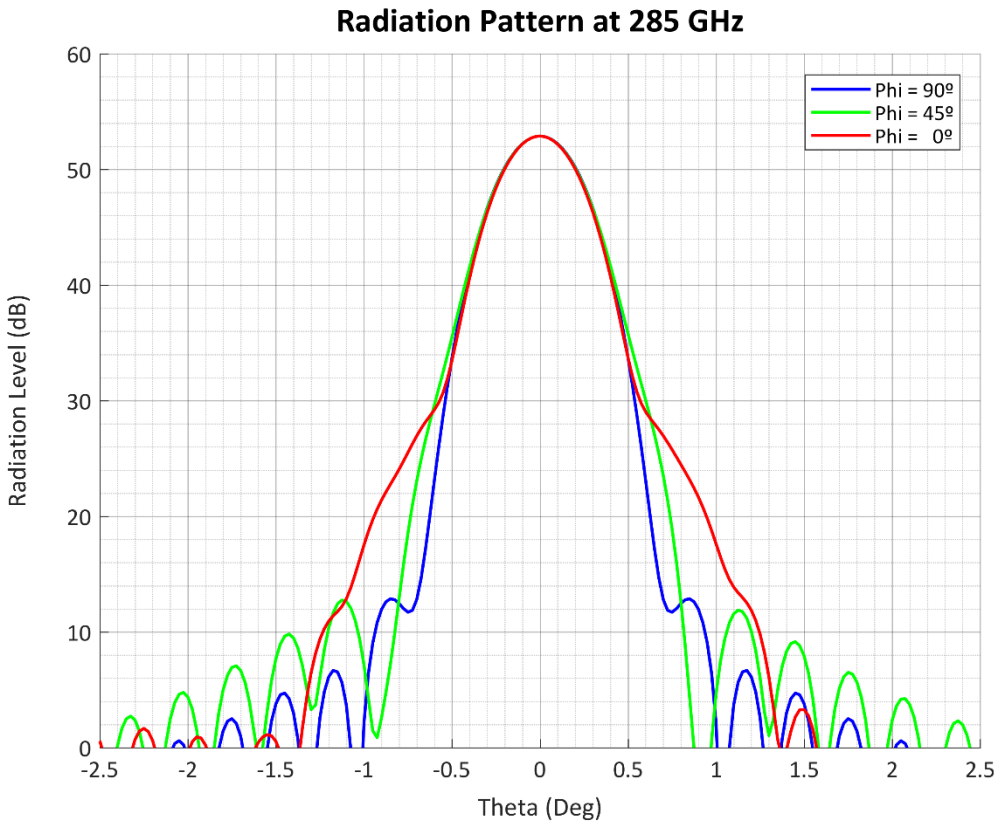
Radiation Pattern at 285 GHz
Phi = 90º
Phi = 45º
Phi = 0º
Radiation Level (dB)
Theta (Deg)
60
50
40
30
20
10
0
-2.5
-2
-1.5
-1
-0.5
0
0.5
1
1.5
2
2.5

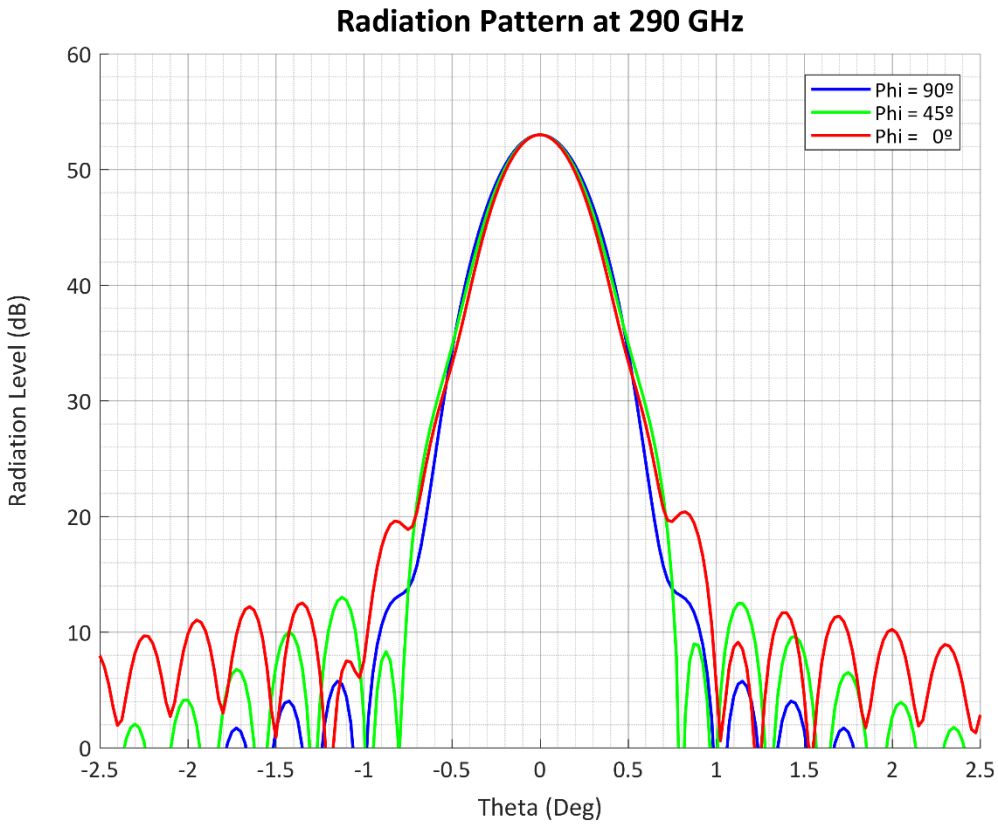
Radiation Pattern at 290 GHz
Phi = 90º
Phi = 45º
Phi = 0º
Radiation Level (dB)
Theta (Deg)
60
50
40
30
20
10
0
-2.5
-2
-1.5
-1
-0.5
0
0.5
1
1.5
2
2.5

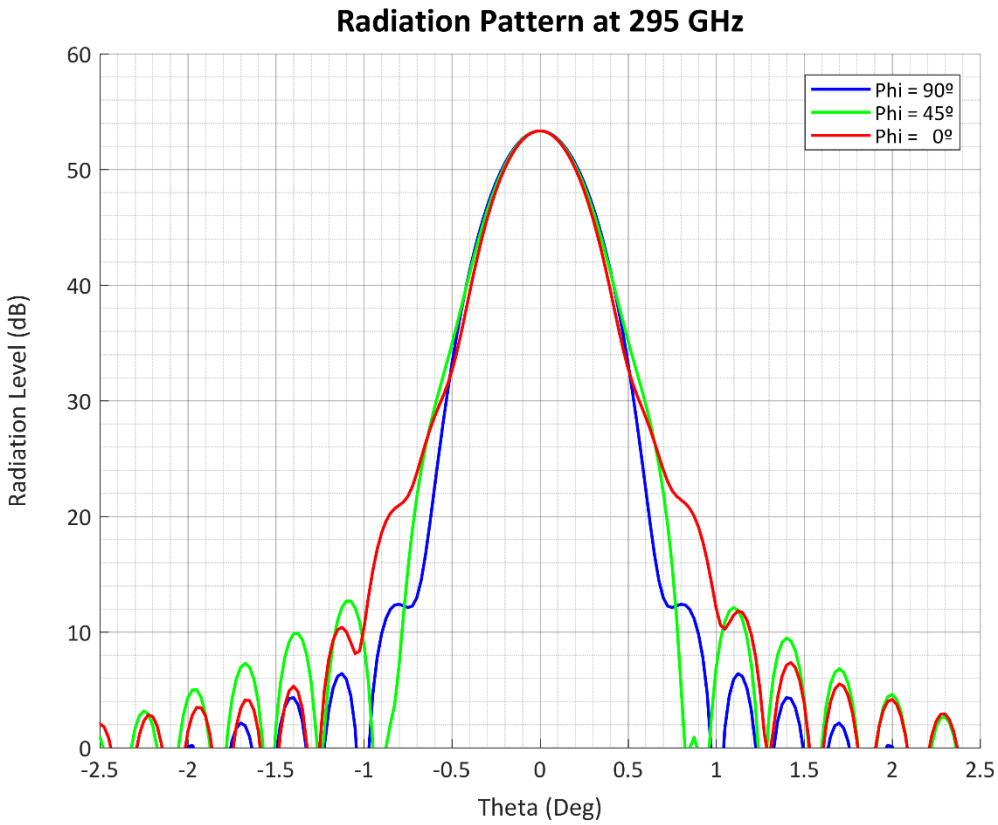
Radiation Pattern at 295 GHz
Phi = 90º
Phi = 45º
Phi = 0º
Radiation Level (dB)
Theta (Deg)
60
50
40
30
20
10
0
-2.5
-2
-1.5
-1
-0.5
0
0.5
1
1.5
2
2.5

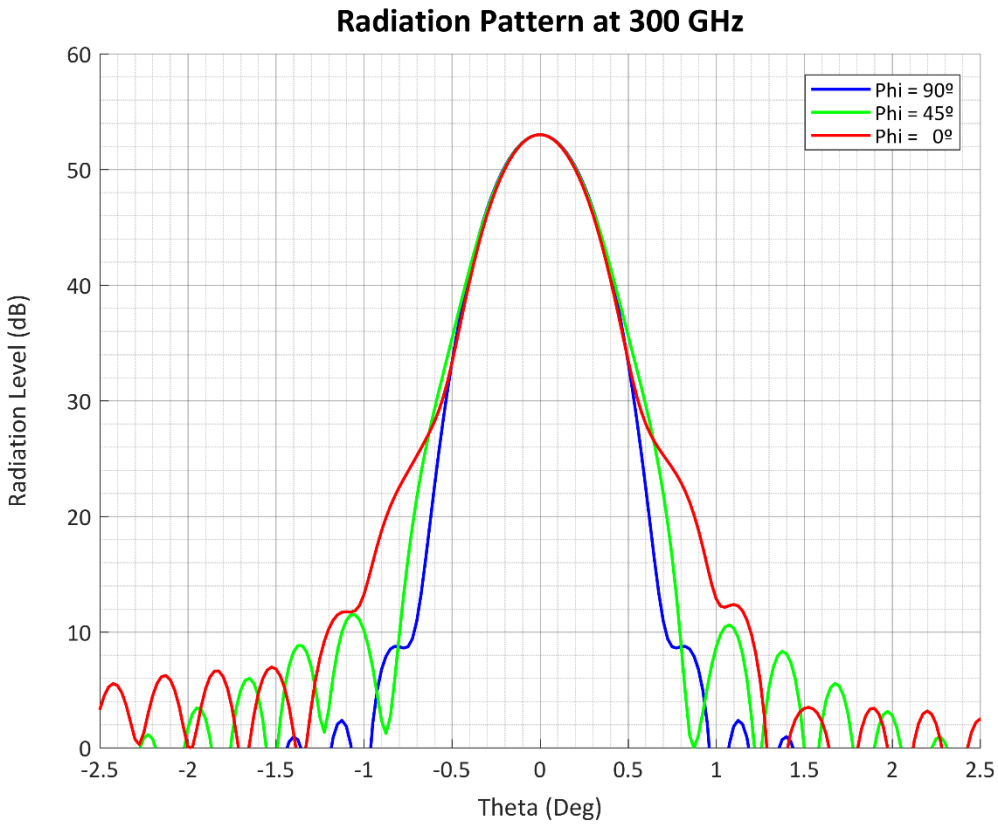
Radiation Pattern at 300 GHz
Phi = 90º
Phi = 45º
Phi = 0º
Radiation Level (dB)
Theta (Deg)
60
50
40
30
20
10
0
-2.5
-2
-1.5
-1
-0.5
0
0.5
1
1.5
2
2.5

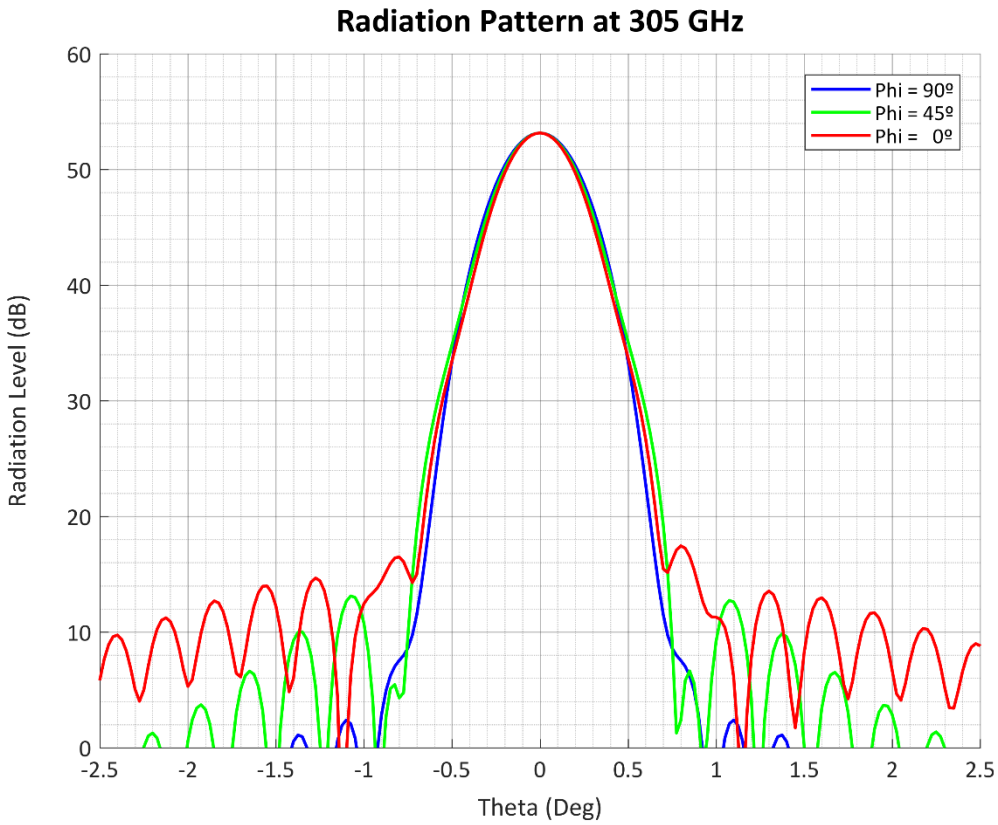
Radiation Pattern at 305 GHz
Phi = 90º
Phi = 45º
Phi = 0º
Radiation Level (dB)
Theta (Deg)
60
50
40
30
20
10
0
-2.5
-2
-1.5
-1
-0.5
0
0.5
1
1.5
2
2.5

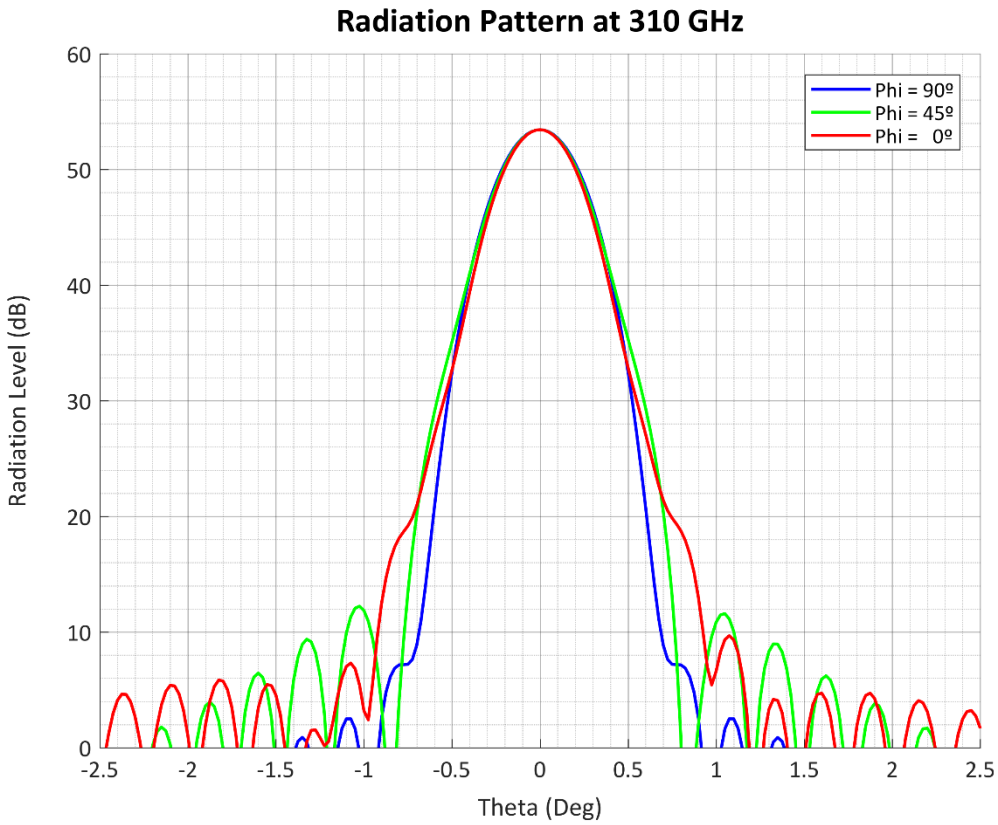
Radiation Pattern at 310 GHz
Phi = 90º
Phi = 45º
Phi = 0º
Radiation Level (dB)
Theta (Deg)
60
50
40
30
20
10
0
-2.5
-2
-1.5
-1
-0.5
0
0.5
1
1.5
2
2.5

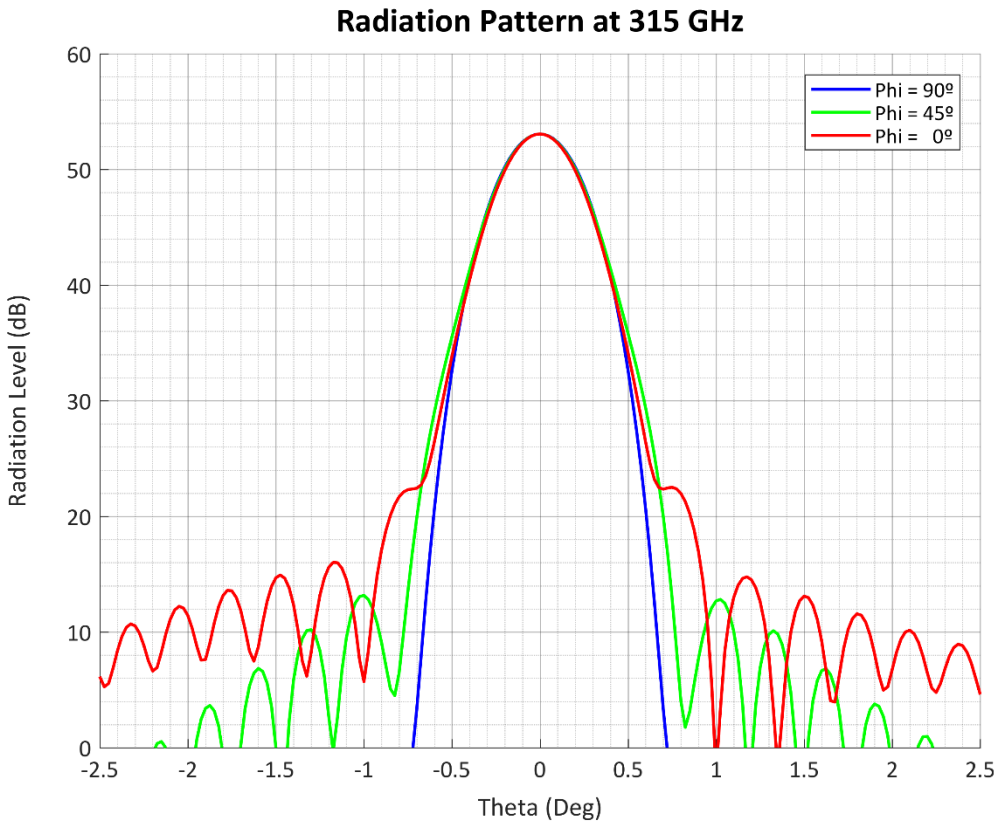
Radiation Pattern at 315 GHz
Phi = 90º
Phi = 45º
Phi = 0º
Radiation Level (dB)
Theta (Deg)
60
50
40
30
20
10
0
-2.5
-2
-1.5
-1
-0.5
0
0.5
1
1.5
2
2.5

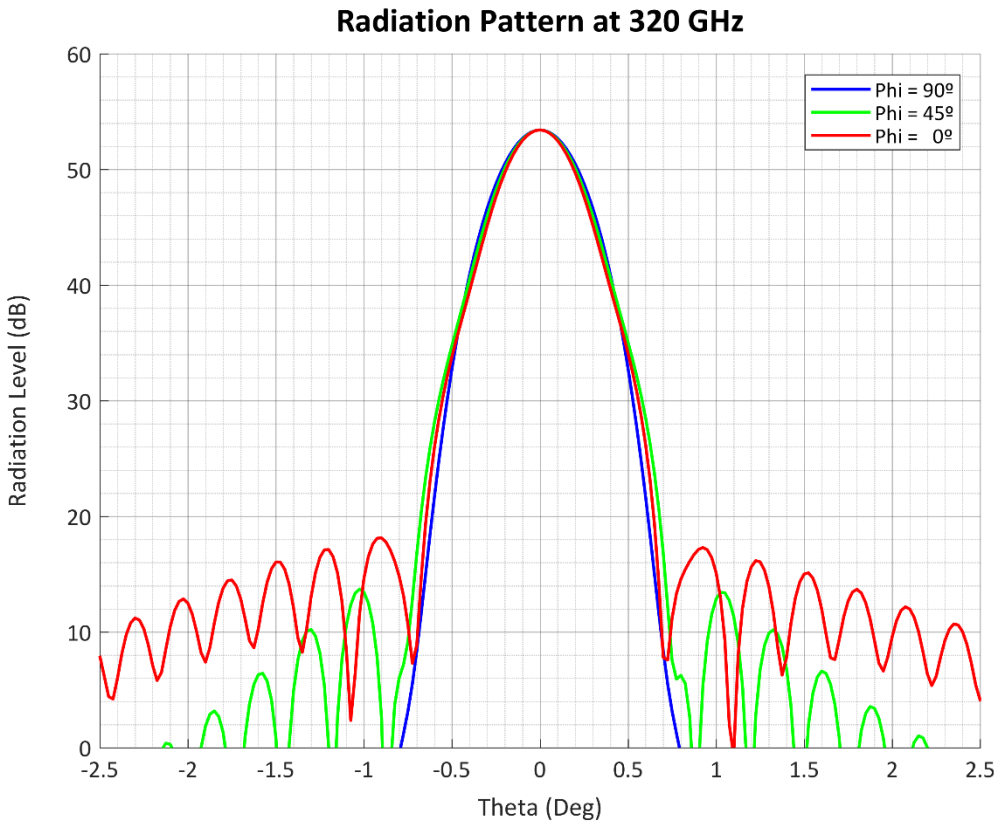
Radiation Pattern at 320 GHz
Phi = 90º
Phi = 45º
Phi = 0º
Radiation Level (dB)
Theta (Deg)
60
50
40
30
20
10
0
-2.5
-2
-1.5
-1
-0.5
0
0.5
1
1.5
2
2.5

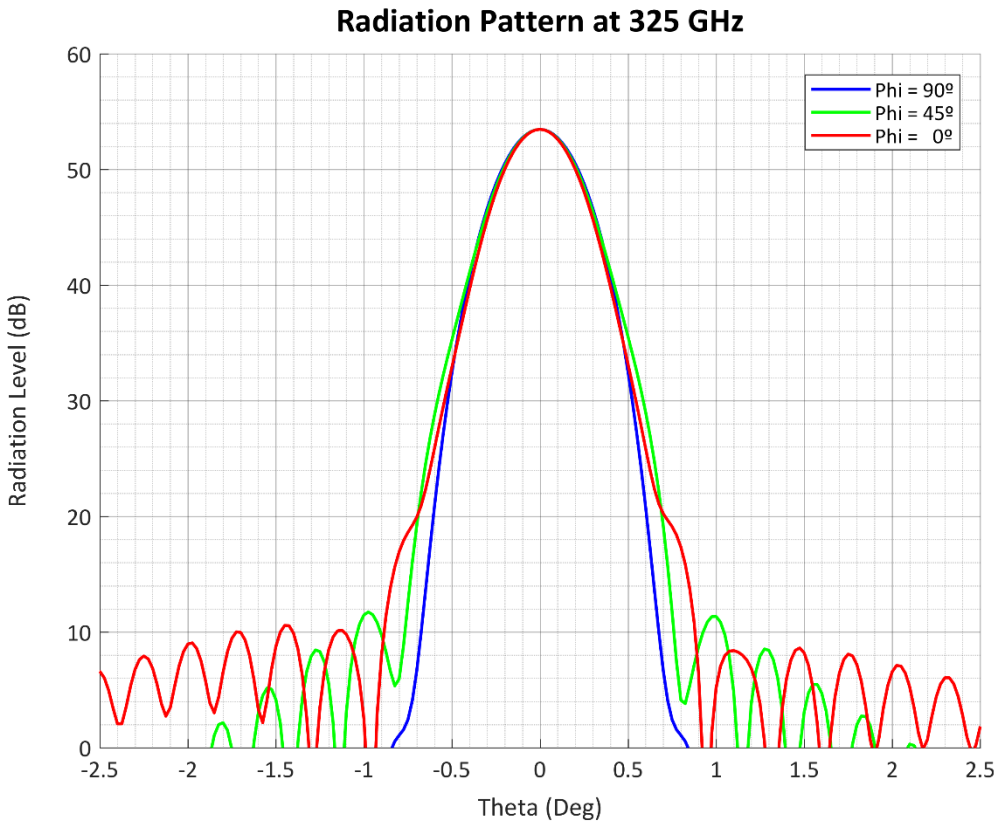
Radiation Pattern at 325 GHz
Phi = 90º
Phi = 45º
Phi = 0º
Radiation Level (dB)
Theta (Deg)
60
50
40
30
20
10
0
-2.5
-2
-1.5
-1
-0.5
0
0.5
1
1.5
2
2.5

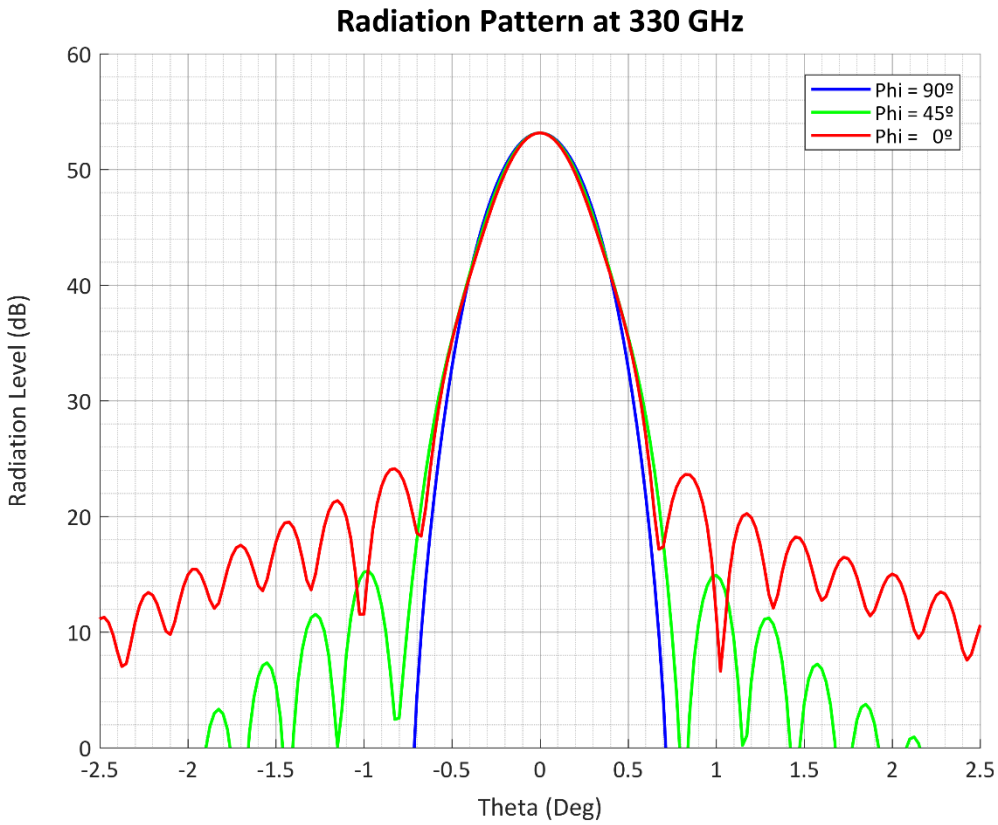
Radiation Pattern at 330 GHz
Phi = 90º
Phi = 45º
Phi = 0º
Radiation Level (dB)
Theta (Deg)
60
50
40
30
20
10
0
-2.5
-2
-1.5
-1
-0.5
0
0.5
1
1.5
2
2.5

Manufactured Model

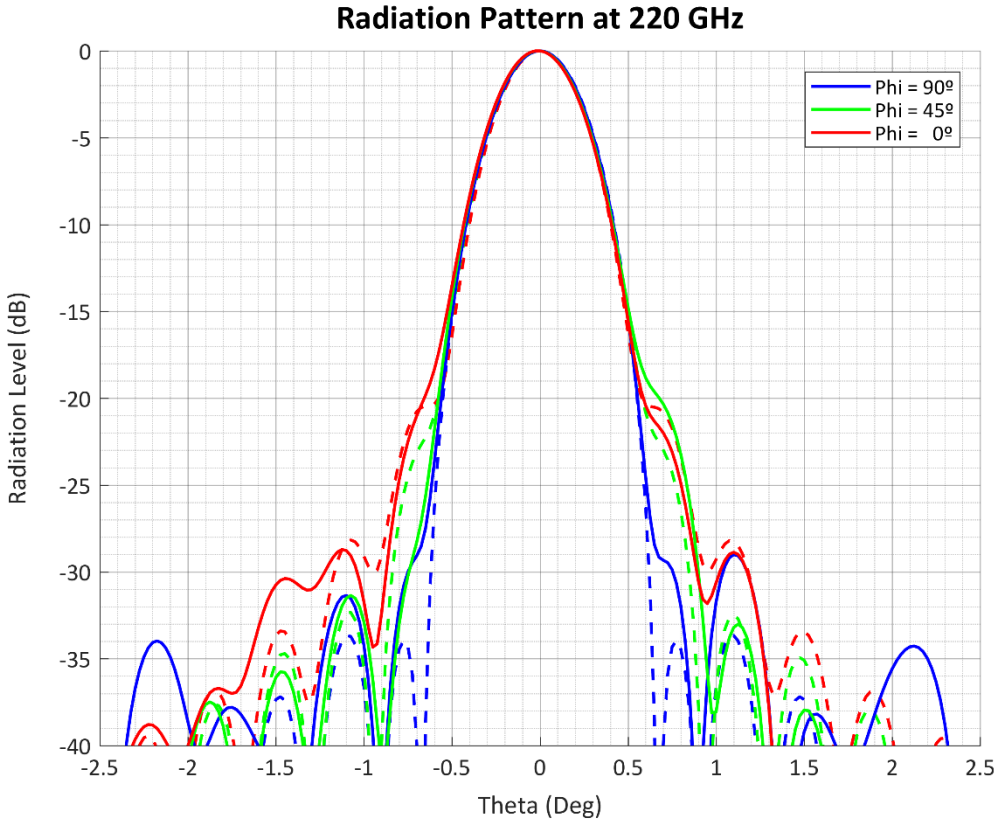

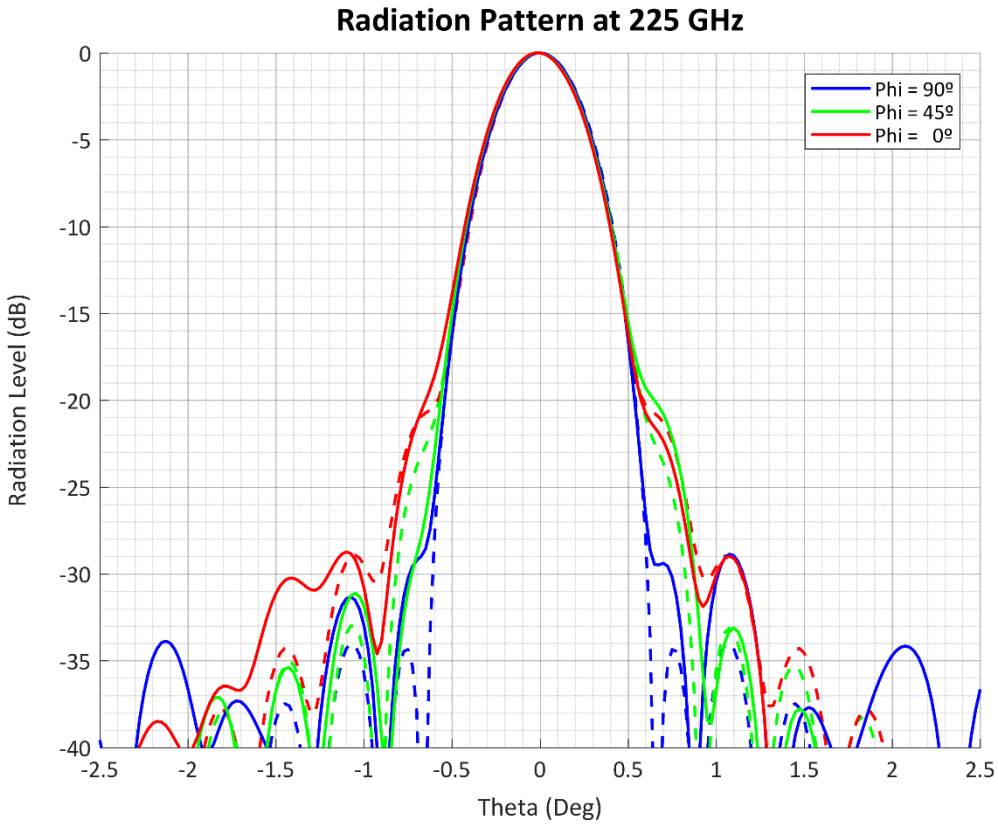

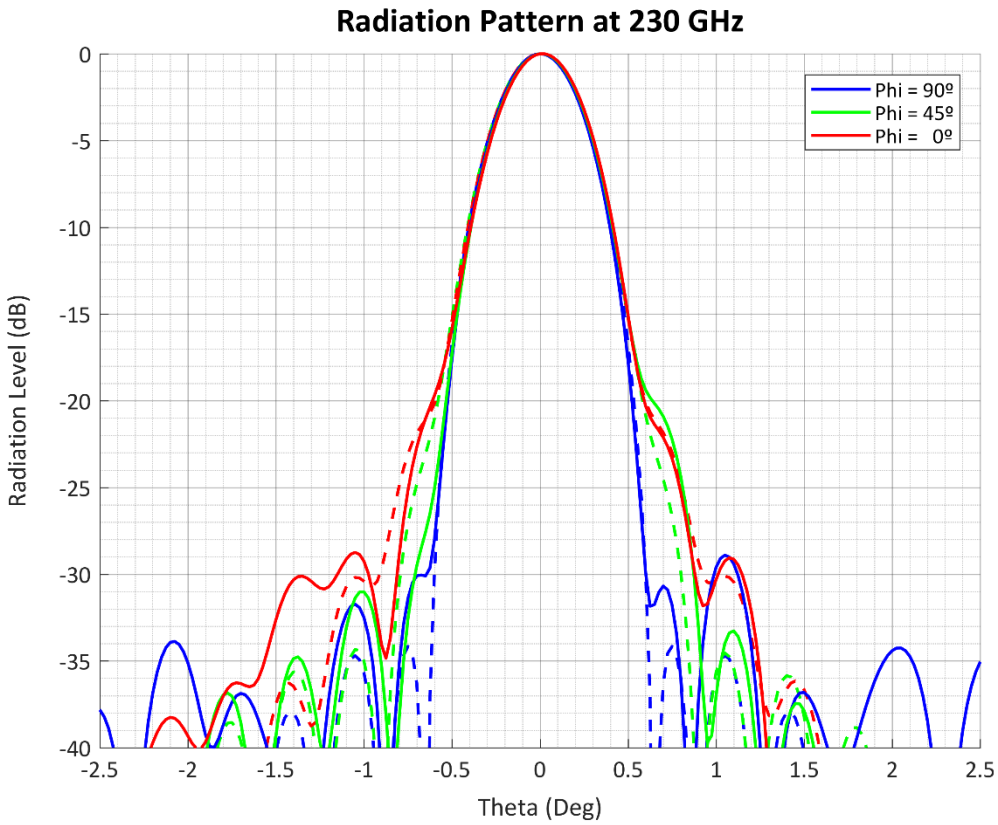
Radiation Pattern at 230 GHz
Phi = 90º
Phi = 45º
Phi = 0º
Radiation Level (dB)
Theta (Deg)
0
-5
-10
-15
-20
-25
-30
-35
-40
-2.5
-2
-1.5
-1
-0.5
0
0.5
1
1.5
2
2.5

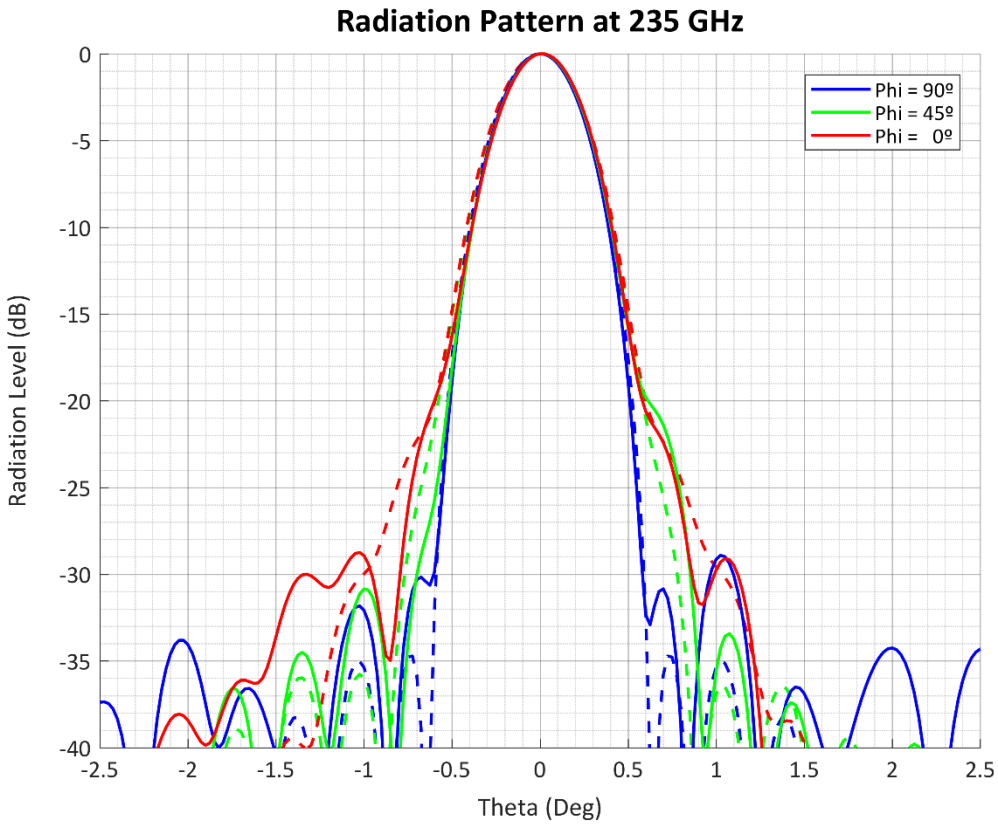
Radiation Pattern at 235 GHz
Phi = 90º
Phi = 45º
Phi = 0º
Radiation Level (dB)
Theta (Deg)
0
-5
-10
-15
-20
-25
-30
-35
-40
-2.5
-2
-1.5
-1
-0.5
0
0.5
1
1.5
2
2.5

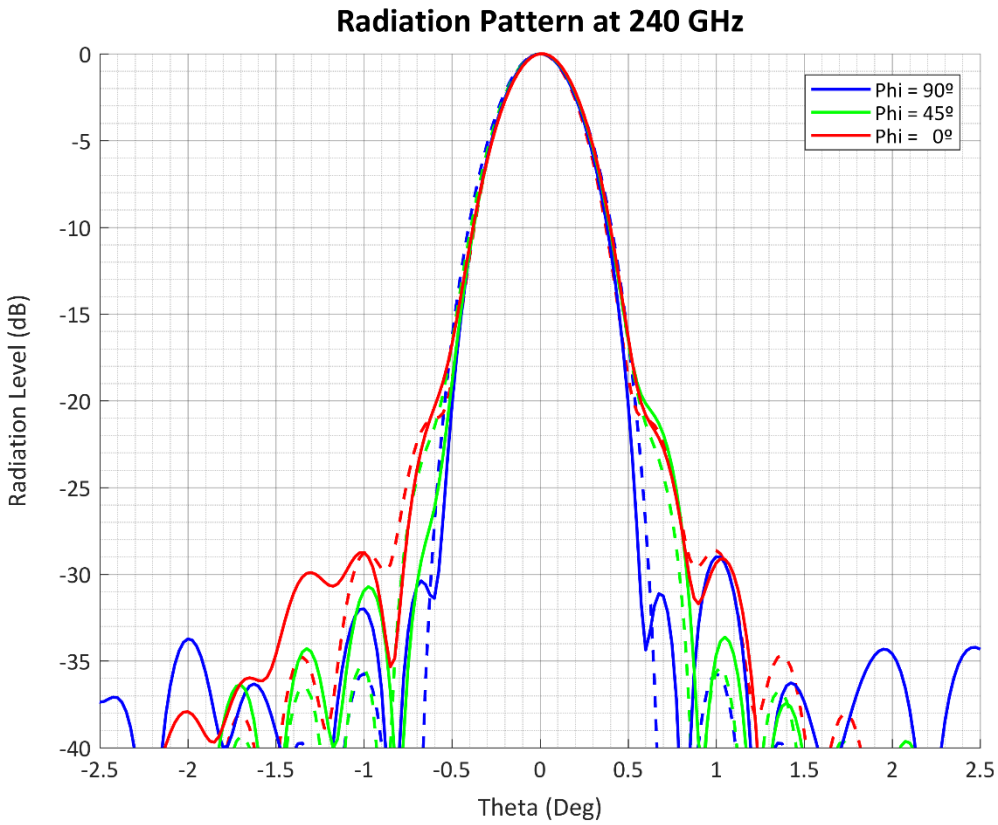
Radiation Pattern at 240 GHz
Phi = 90º
Phi = 45º
Phi = 0º
Radiation Level (dB)
Theta (Deg)
0
-5
-10
-15
-20
-25
-30
-35
-40
-2.5
-2
-1.5
-1
-0.5
0
0.5
1
1.5
2
2.5

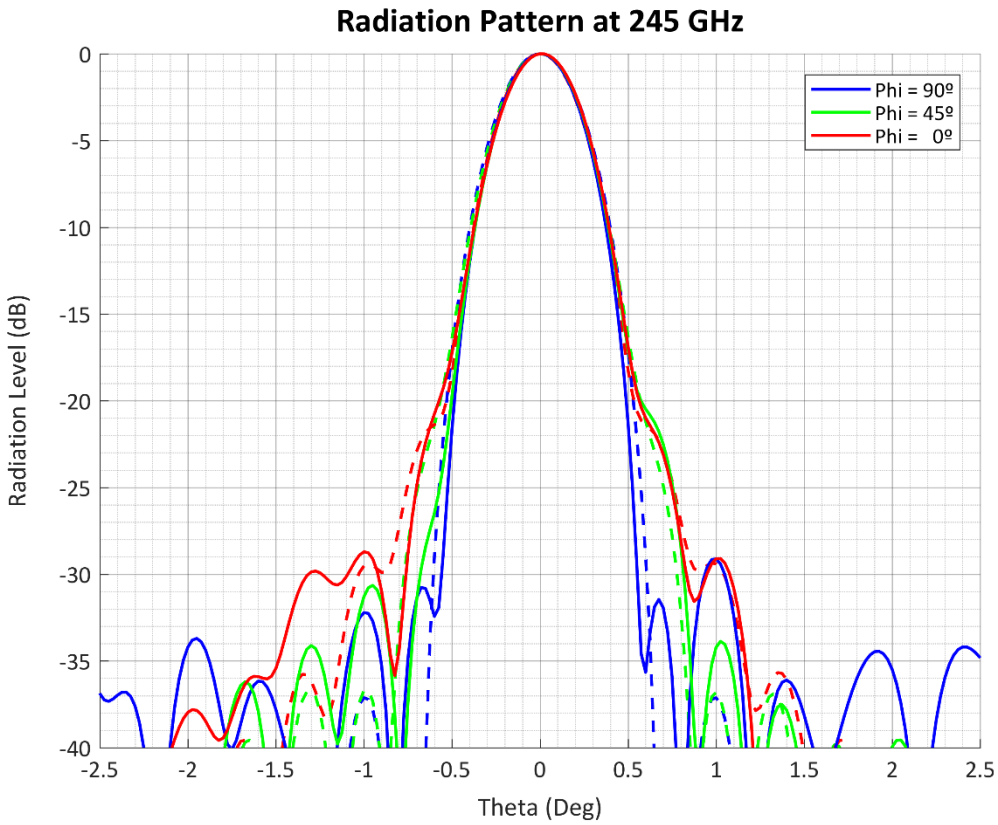
Radiation Pattern at 245 GHz
Phi = 90º
Phi = 45º
Phi = 0º
Radiation Level (dB)
Theta (Deg)
0
-5
-10
-15
-20
-25
-30
-35
-40
-2.5
-2
-1.5
-1
-0.5
0
0.5
1
1.5
2
2.5

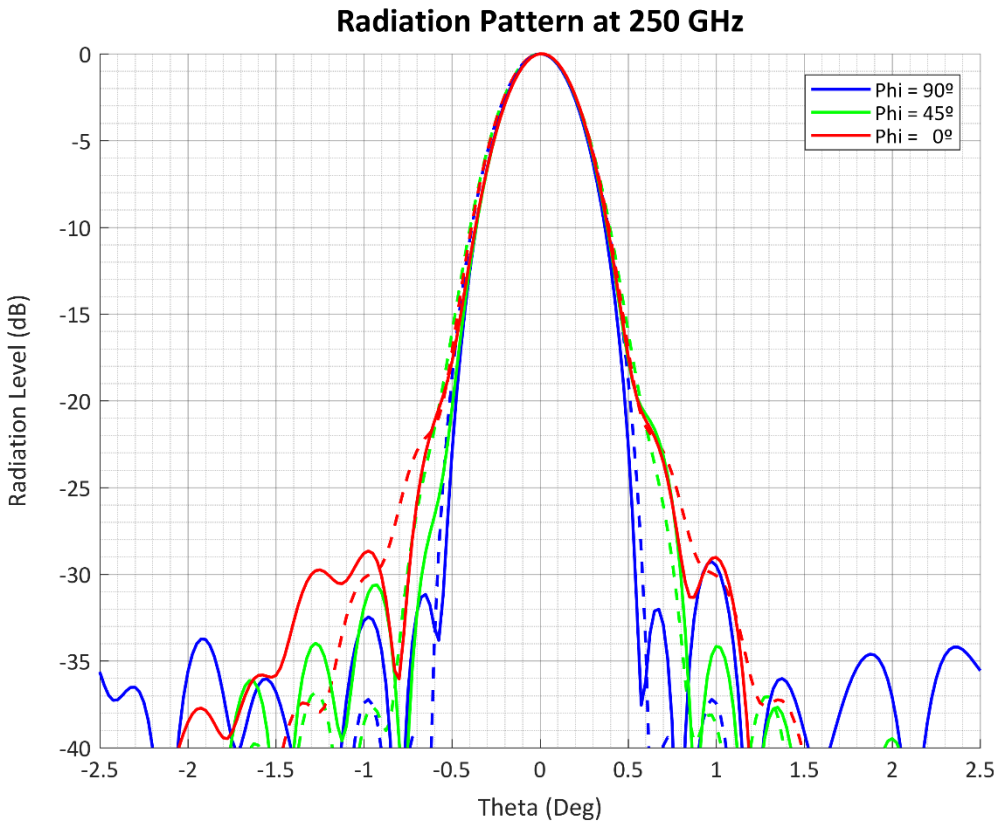
Radiation Pattern at 250 GHz
Phi = 90º
Phi = 45º
Phi = 0º
Radiation Level (dB)
Theta (Deg)
0
-5
-10
-15
-20
-25
-30
-35
-40
-2.5
-2
-1.5
-1
-0.5
0
0.5
1
1.5
2
2.5

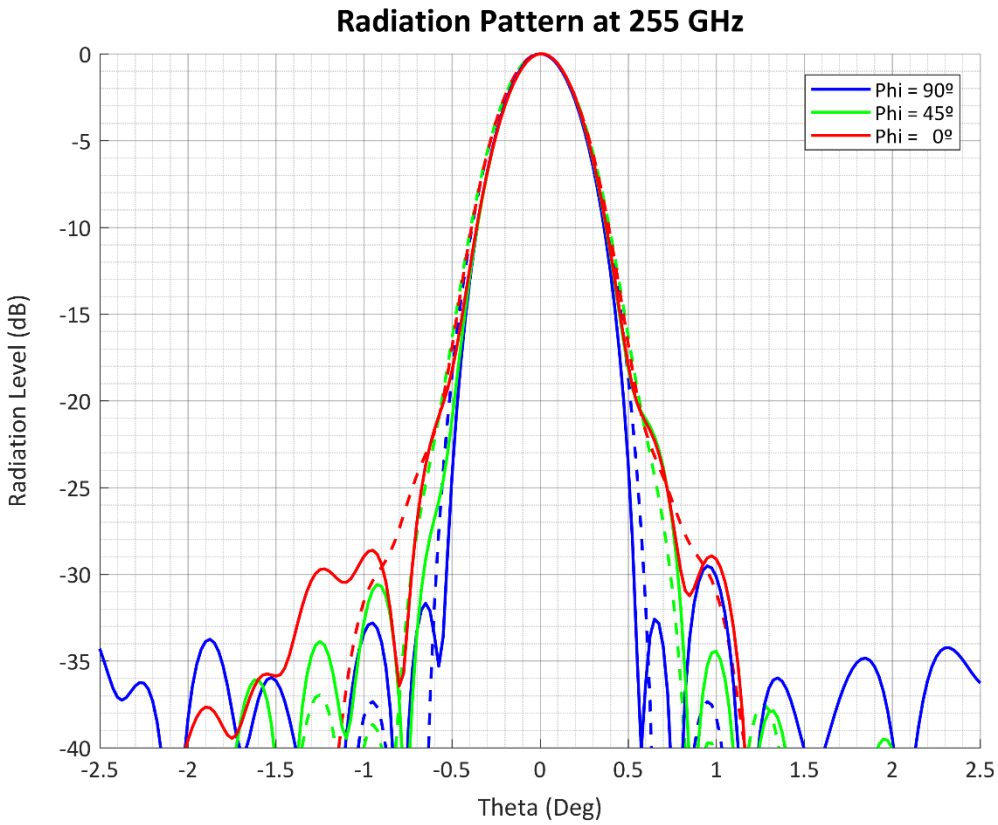
Radiation Pattern at 255 GHz
Phi = 90º
Phi = 45º
Phi = 0º
Radiation Level (dB)
Theta (Deg)
0
-5
-10
-15
-20
-25
-30
-35
-40
-2.5
-2
-1.5
-1
-0.5
0
0.5
1
1.5
2
2.5

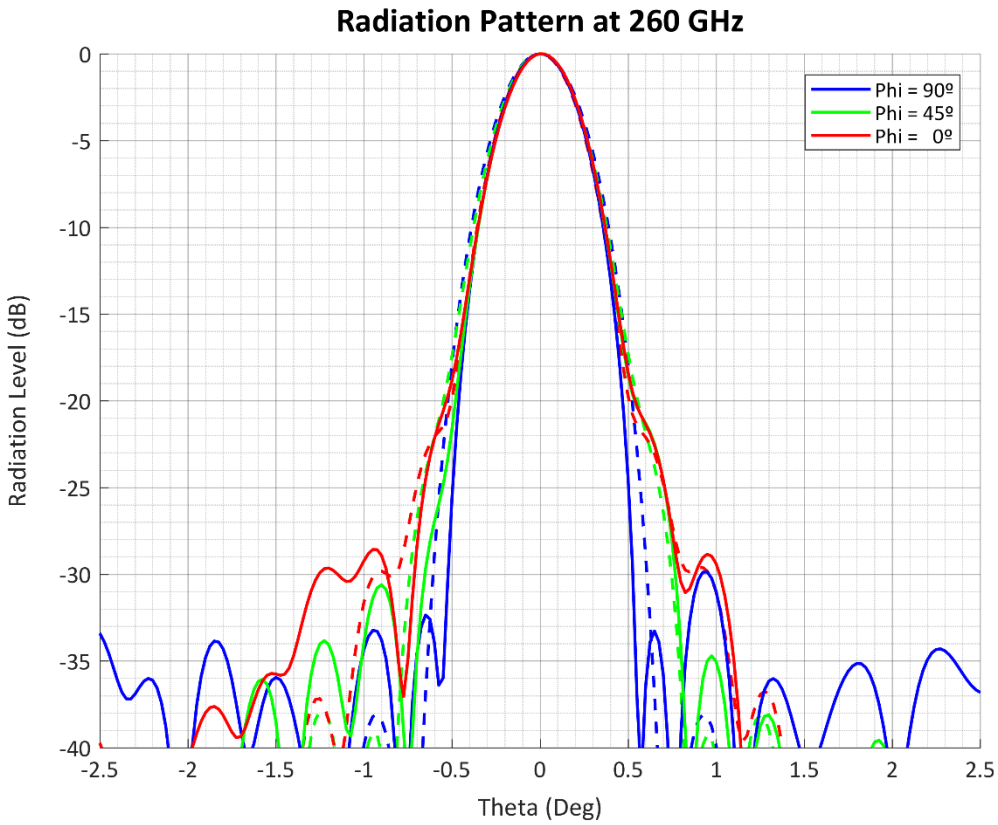
Radiation Pattern at 260 GHz
Phi = 90º
Phi = 45º
Phi = 0º
Radiation Level (dB)
Theta (Deg)
0
-5
-10
-15
-20
-25
-30
-35
-40
-2.5
-2
-1.5
-1
-0.5
0
0.5
1
1.5
2
2.5

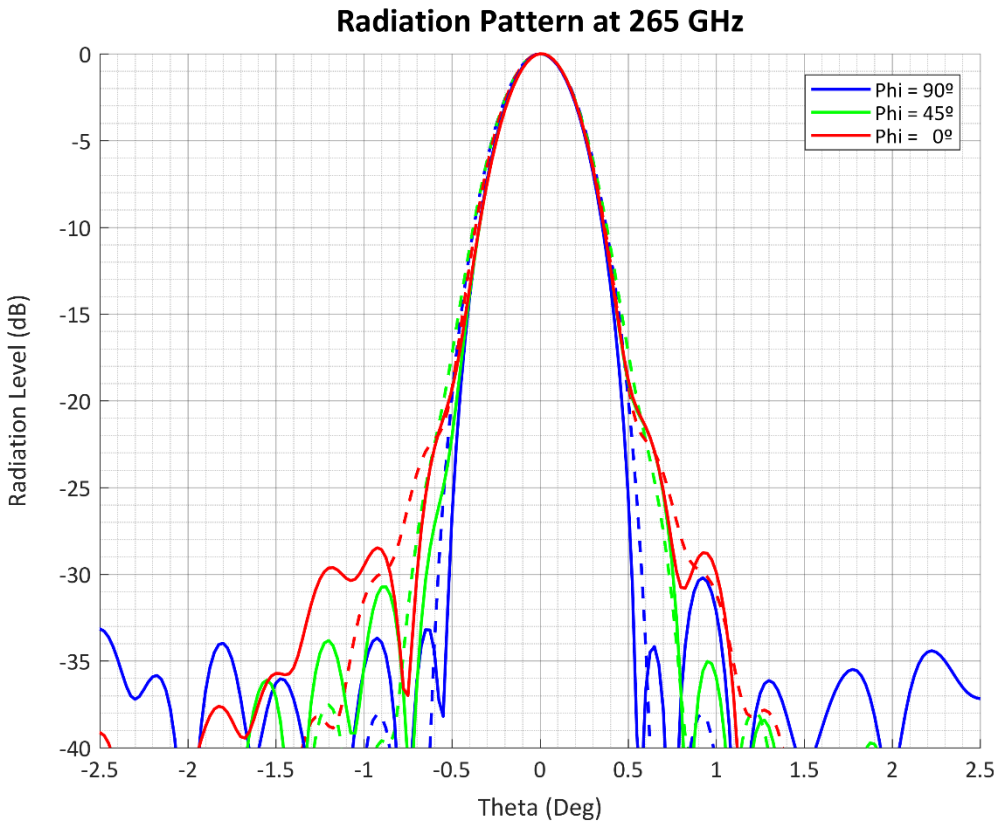
Radiation Pattern at 265 GHz
Phi = 90º
Phi = 45º
Phi = 0º
Radiation Level (dB)
Theta (Deg)
0
-5
-10
-15
-20
-25
-30
-35
-40
-2.5
-2
-1.5
-1
-0.5
0
0.5
1
1.5
2
2.5

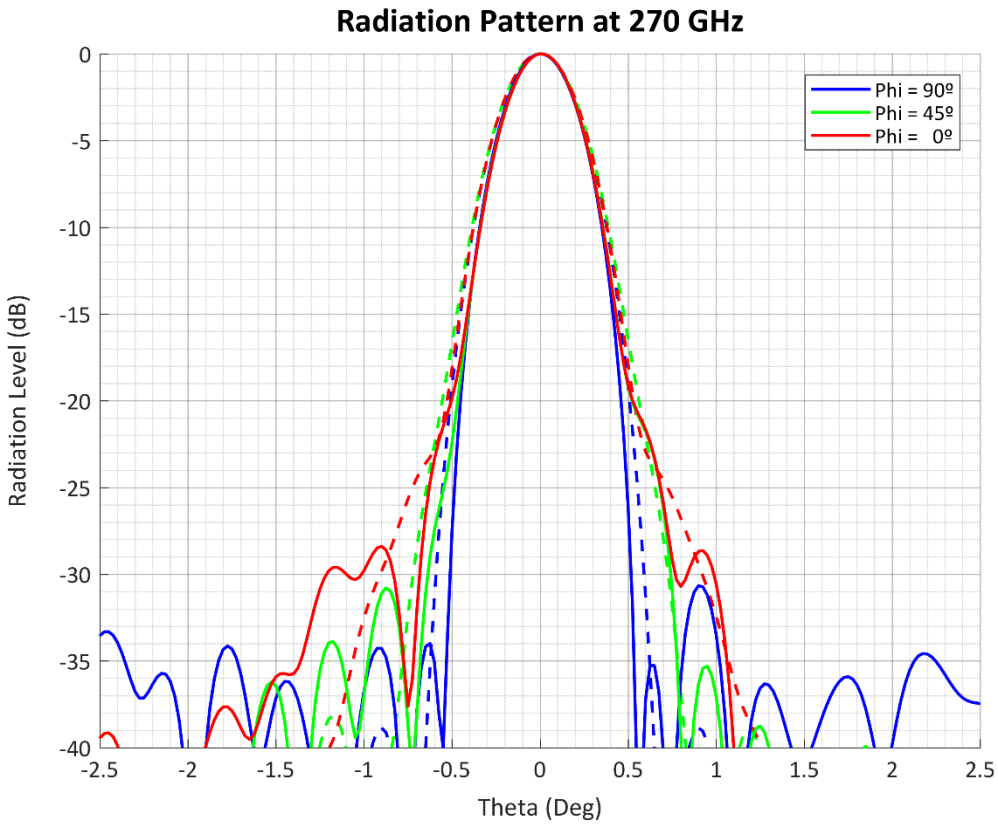
Radiation Pattern at 270 GHz
Phi = 90º
Phi = 45º
Phi = 0º
Radiation Level (dB)
Theta (Deg)
0
-5
-10
-15
-20
-25
-30
-35
-40
-2.5
-2
-1.5
-1
-0.5
0
0.5
1
1.5
2
2.5

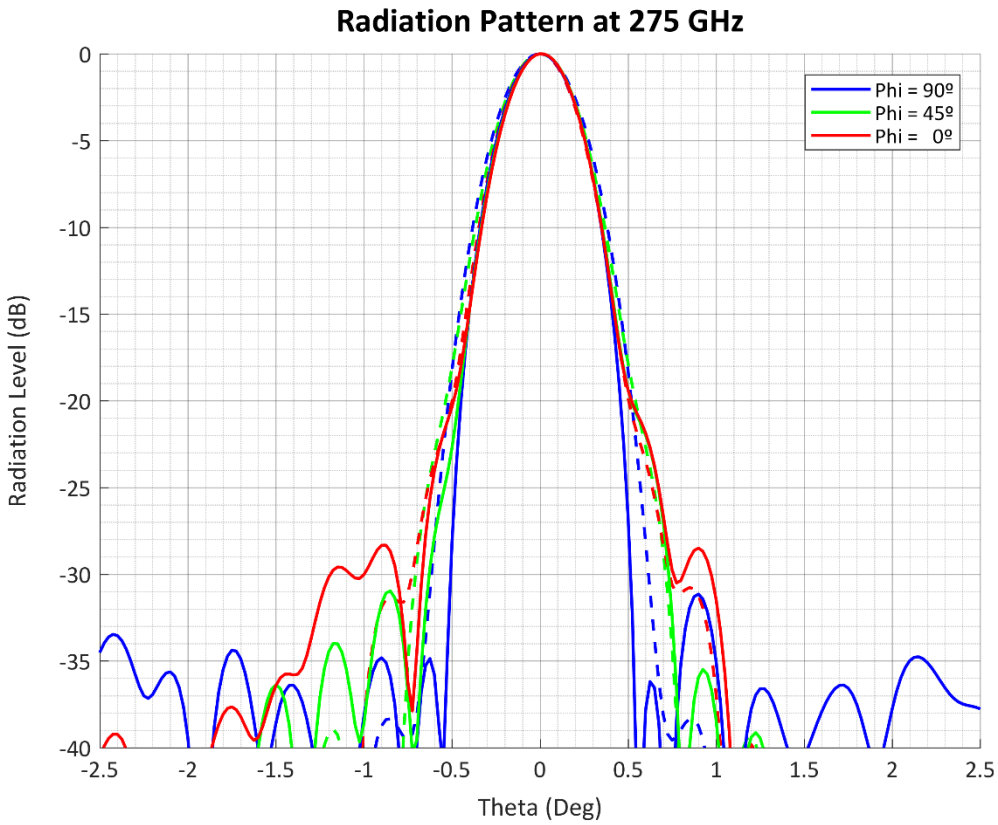
Radiation Pattern at 275 GHz
Phi = 90º
Phi = 45º
Phi = 0º
Radiation Level (dB)
Theta (Deg)
0
-5
-10
-15
-20
-25
-30
-35
-40
-2.5
-2
-1.5
-1
-0.5
0
0.5
1
1.5
2
2.5

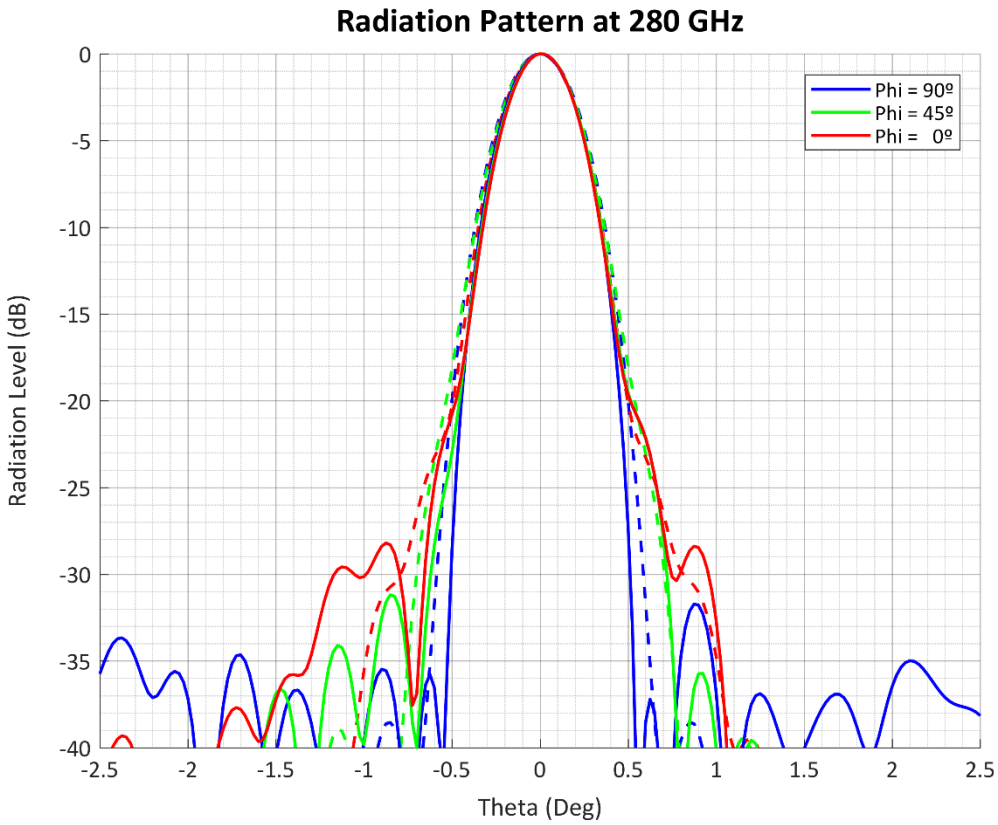
Radiation Pattern at 280 GHz
Phi = 90º
Phi = 45º
Phi = 0º
Radiation Level (dB)
Theta (Deg)
0
-5
-10
-15
-20
-25
-30
-35
-40
-2.5
-2
-1.5
-1
-0.5
0
0.5
1
1.5
2
2.5

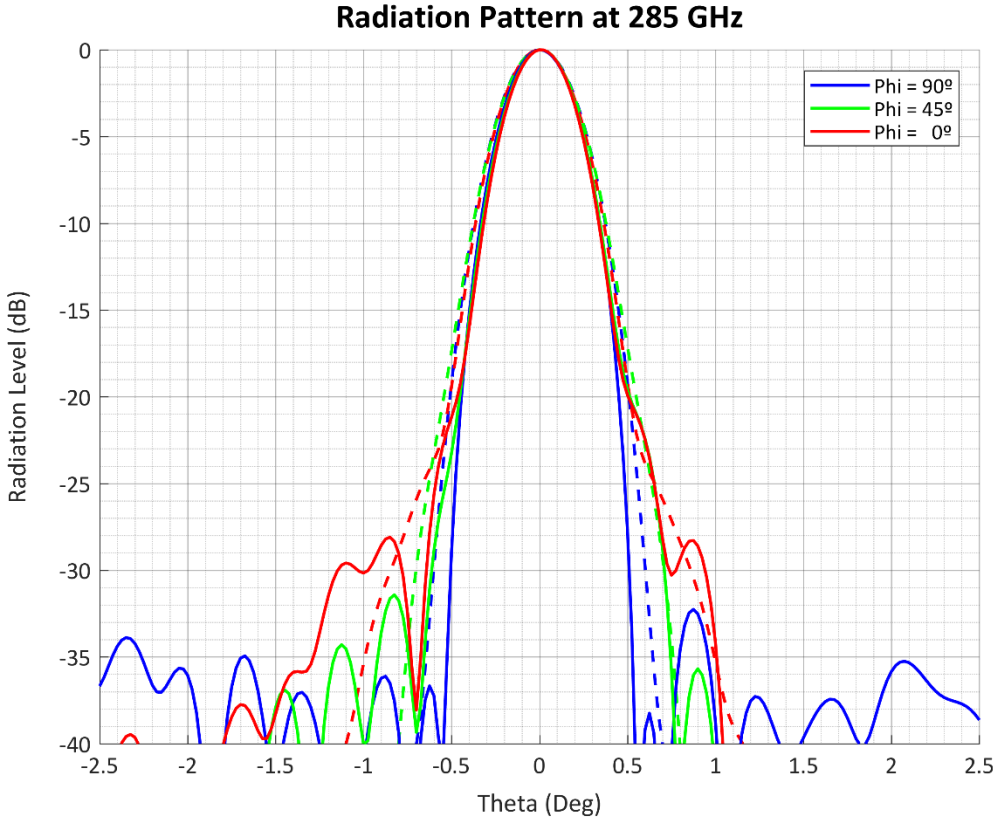
Radiation Pattern at 285 GHz
Phi = 90º
Phi = 45º
Phi = 0º
Radiation Level (dB)
Theta (Deg)
0
-5
-10
-15
-20
-25
-30
-35
-40
-2.5
-2
-1.5
-1
-0.5
0
0.5
1
1.5
2
2.5

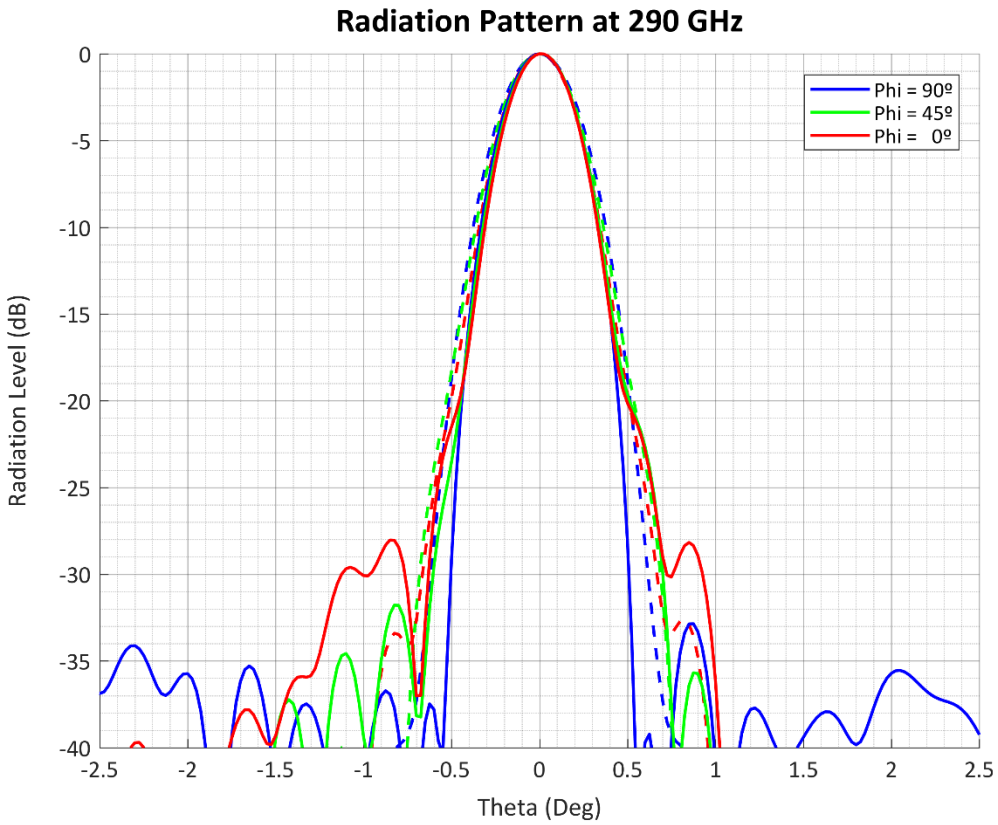
Radiation Pattern at 290 GHz
Phi = 90º
Phi = 45º
Phi = 0º
Radiation Level (dB)
Theta (Deg)
0
-5
-10
-15
-20
-25
-30
-35
-40
-2.5
-2
-1.5
-1
-0.5
0
0.5
1
1.5
2
2.5

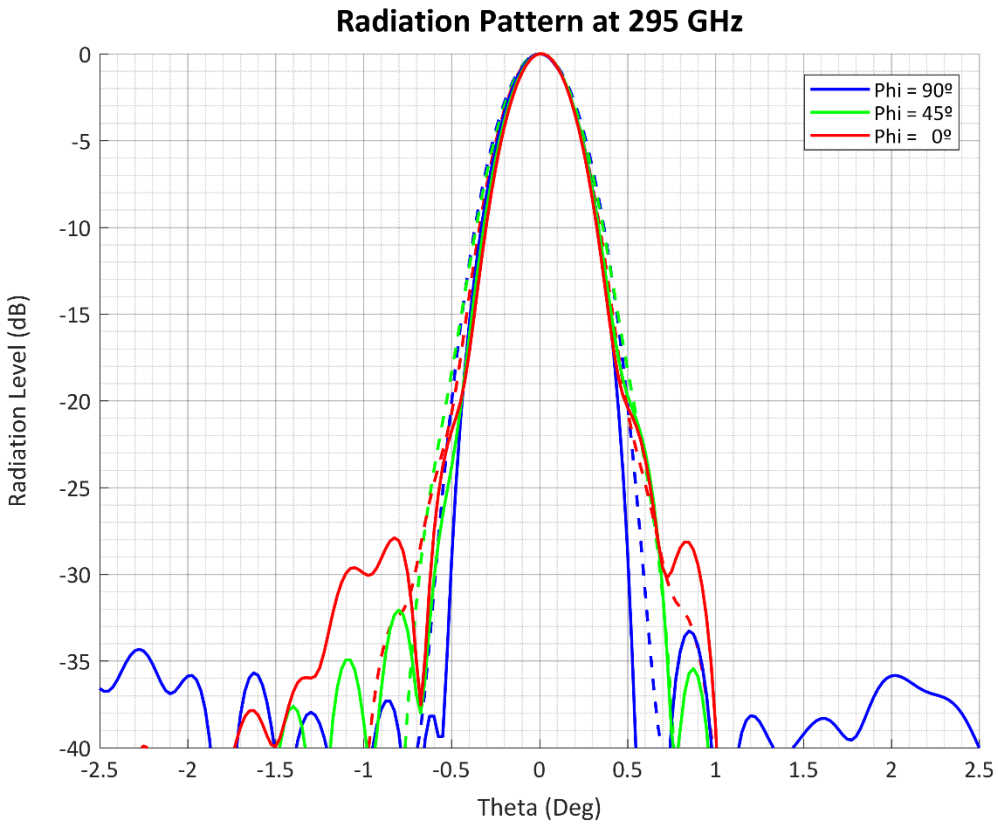
Radiation Pattern at 295 GHz
Phi = 90º
Phi = 45º
Phi = 0º
Radiation Level (dB)
Theta (Deg)
0
-5
-10
-15
-20
-25
-30
-35
-40
-2.5
-2
-1.5
-1
-0.5
0
0.5
1
1.5
2
2.5

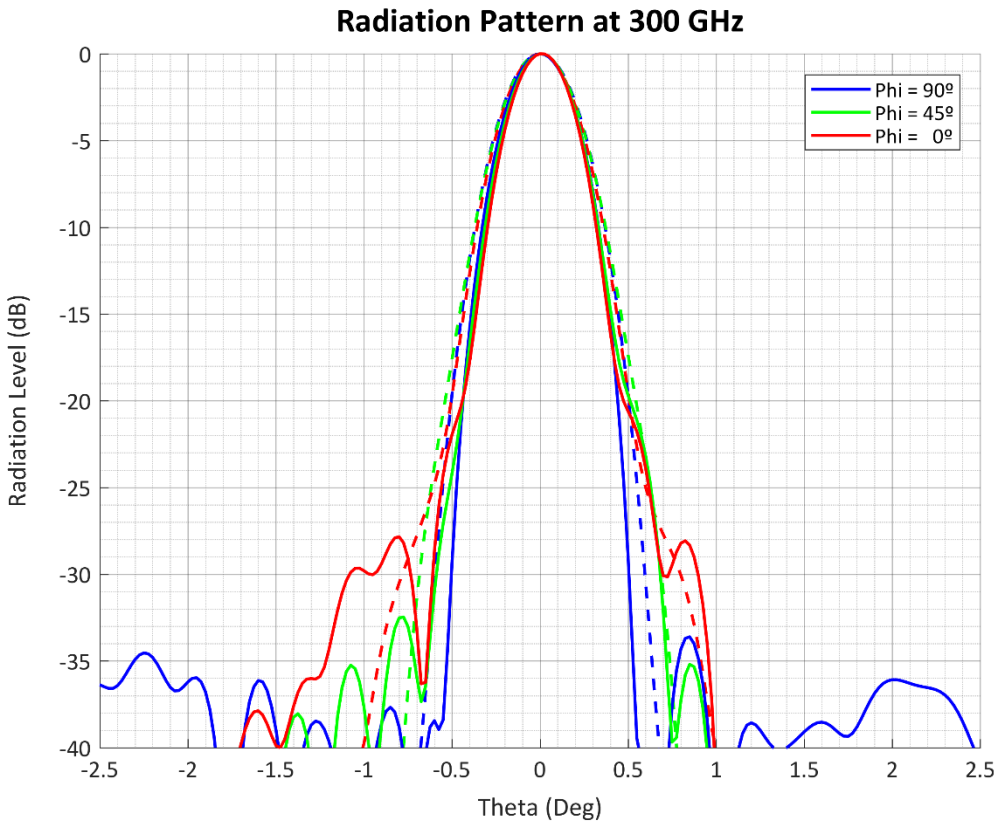
Radiation Pattern at 300 GHz
Phi = 90º
Phi = 45º
Phi = 0º
Radiation Level (dB)
Theta (Deg)
0
-5
-10
-15
-20
-25
-30
-35
-40
-2.5
-2
-1.5
-1
-0.5
0
0.5
1
1.5
2
2.5

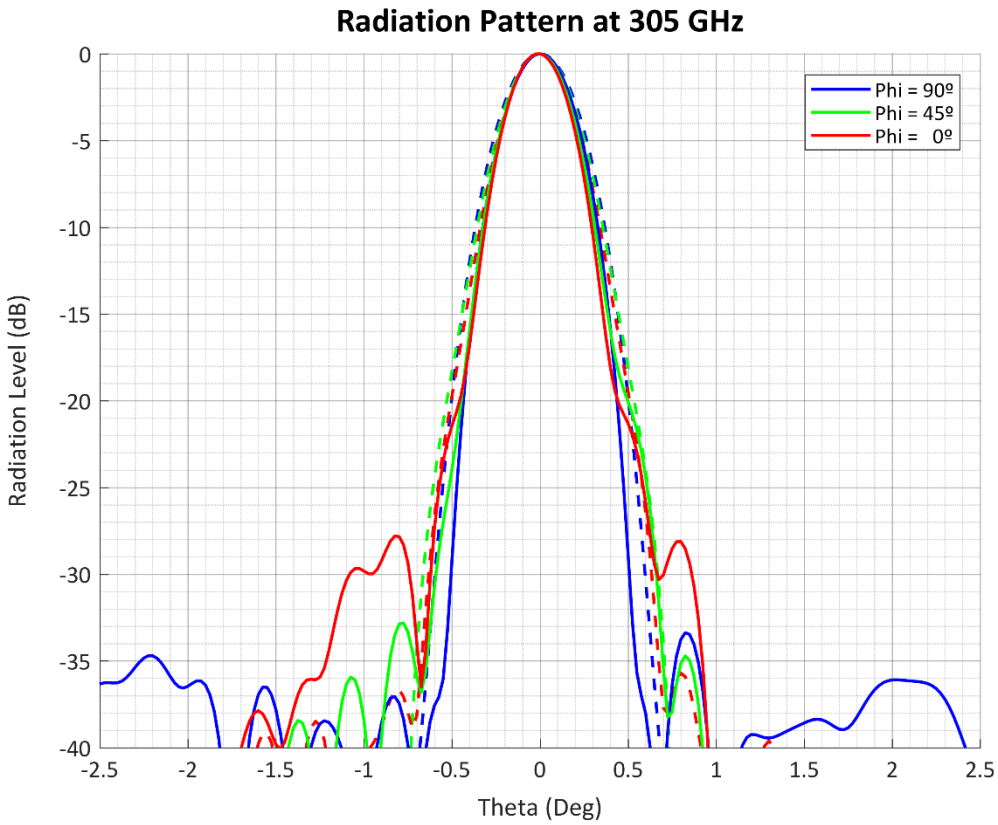
Radiation Pattern at 305 GHz
Phi = 90º
Phi = 45º
Phi = 0º
Radiation Level (dB)
Theta (Deg)
0
-5
-10
-15
-20
-25
-30
-35
-40
-2.5
-2
-1.5
-1
-0.5
0
0.5
1
1.5
2
2.5

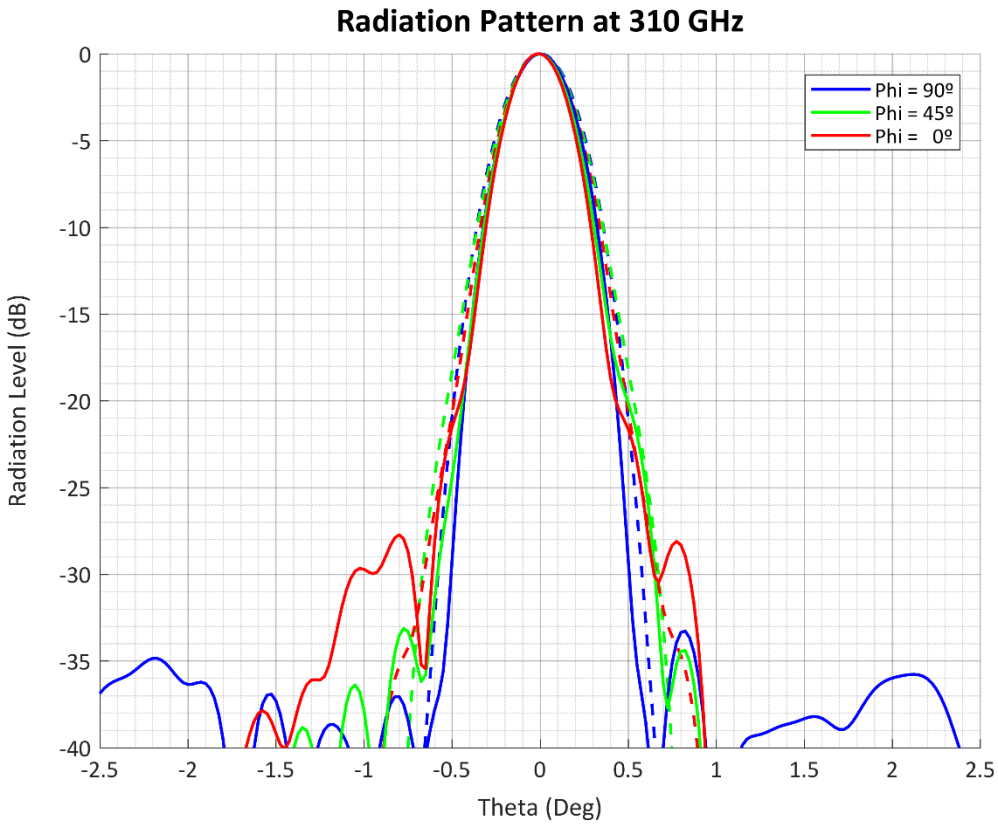
Radiation Pattern at 310 GHz
Phi = 90º
Phi = 45º
Phi = 0º
Radiation Level (dB)
Theta (Deg)
0
-5
-10
-15
-20
-25
-30
-35
-40
-2.5
-2
-1.5
-1
-0.5
0
0.5
1
1.5
2
2.5

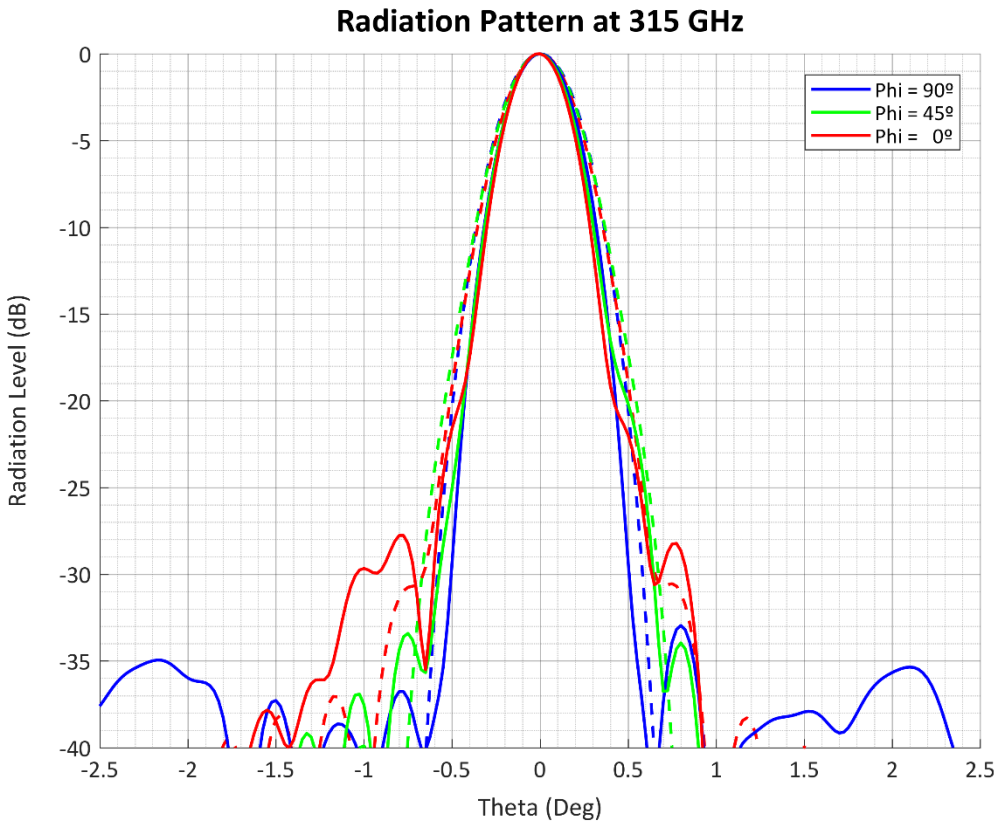
Radiation Pattern at 315 GHz
Phi = 90º
Phi = 45º
Phi = 0º
Radiation Level (dB)
Theta (Deg)
0
-5
-10
-15
-20
-25
-30
-35
-40
-2.5
-2
-1.5
-1
-0.5
0
0.5
1
1.5
2
2.5

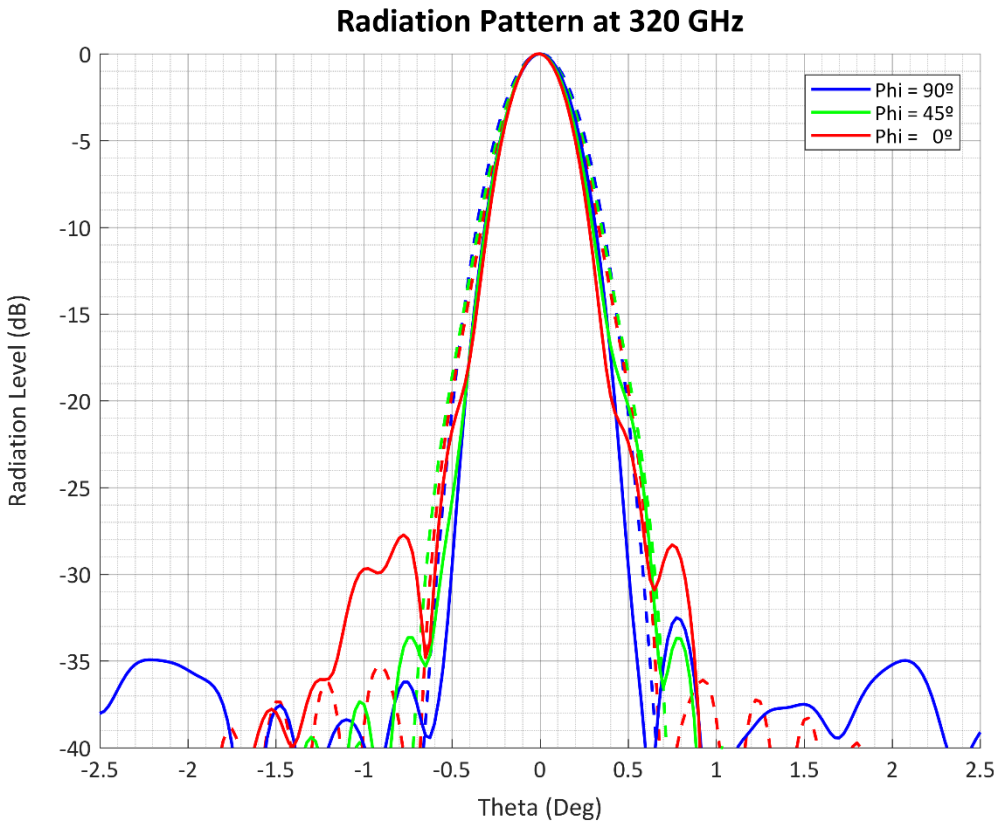
Radiation Pattern at 320 GHz
Phi = 90º
Phi = 45º
Phi = 0º
Radiation Level (dB)
Theta (Deg)
0
-5
-10
-15
-20
-25
-30
-35
-40
-2.5
-2
-1.5
-1
-0.5
0
0.5
1
1.5
2
2.5

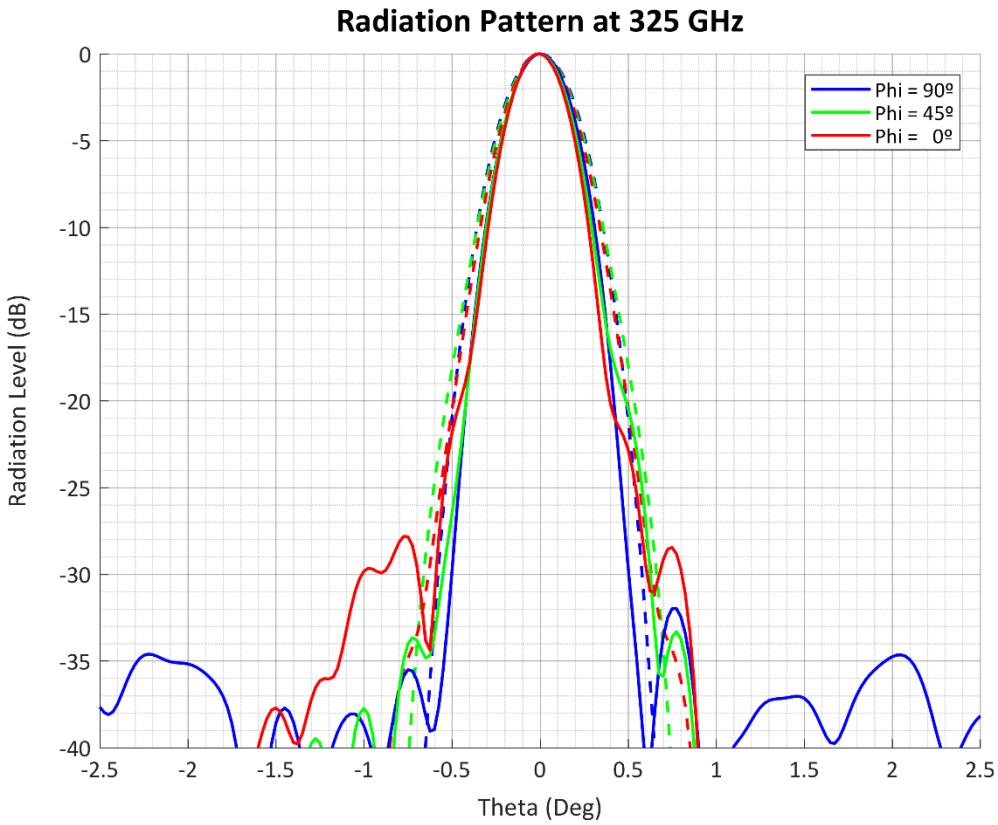
Radiation Pattern at 325 GHz
Phi = 90º
Phi = 45º
Phi = 0º
Radiation Level (dB)
Theta (Deg)
0
-5
-10
-15
-20
-25
-30
-35
-40
-2.5
-2
-1.5
-1
-0.5
0
0.5
1
1.5
2
2.5

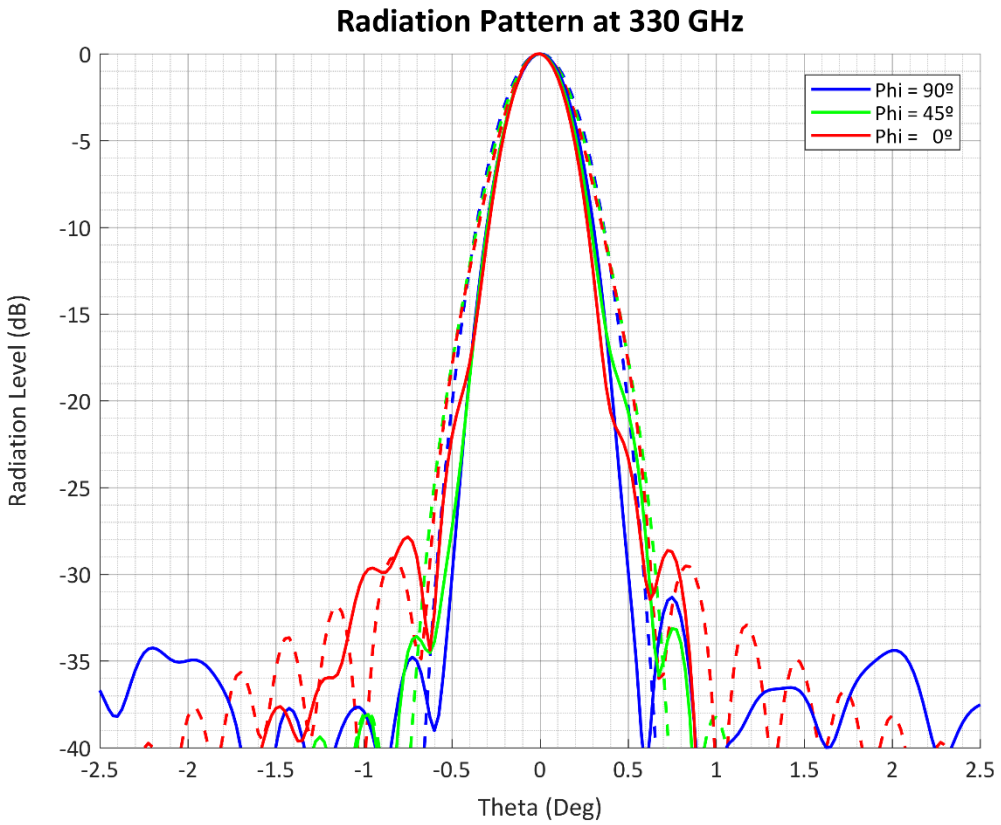
Radiation Pattern at 330 GHz
Phi = 90º
Phi = 45º
Phi = 0º
Radiation Level (dB)
Theta (Deg)
0
-5
-10
-15
-20
-25
-30
-35
-40
-2.5
-2
-1.5
-1
-0.5
0
0.5
1
1.5
2
2.5

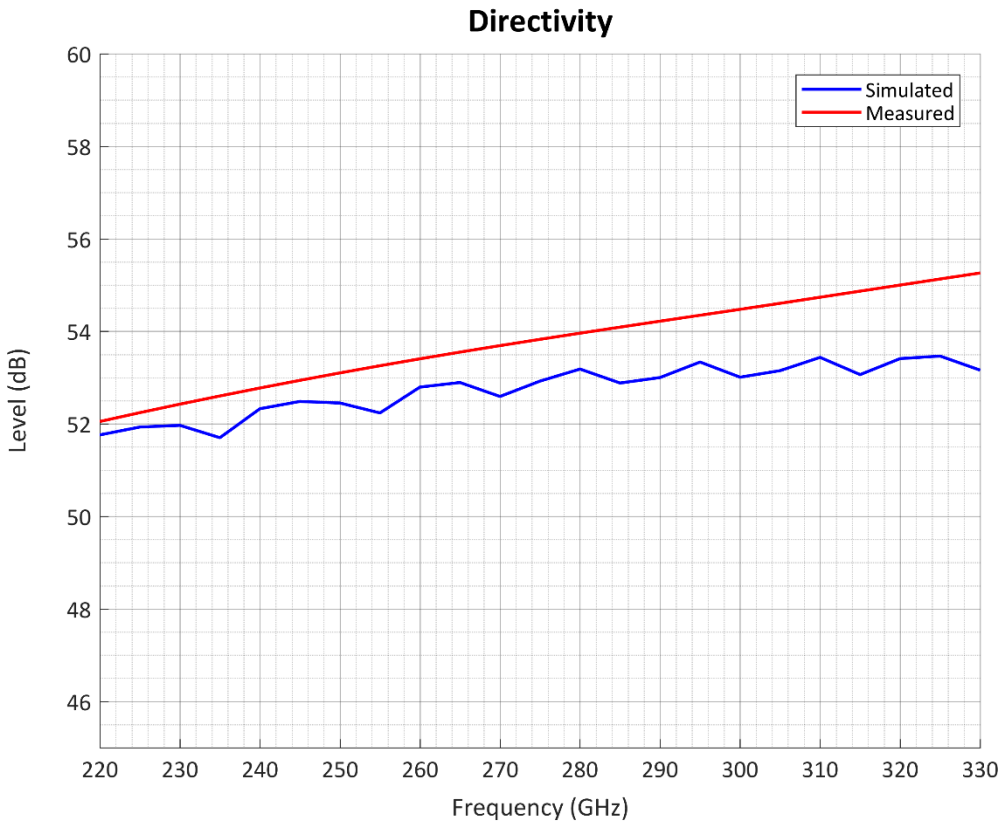
Directivity
Simulated
Measured
Level (dB)
Frequency (GHz)
60
58
56
54
52
50
48
46
220
230
240
250
260
270
280
290
300
310
320
330

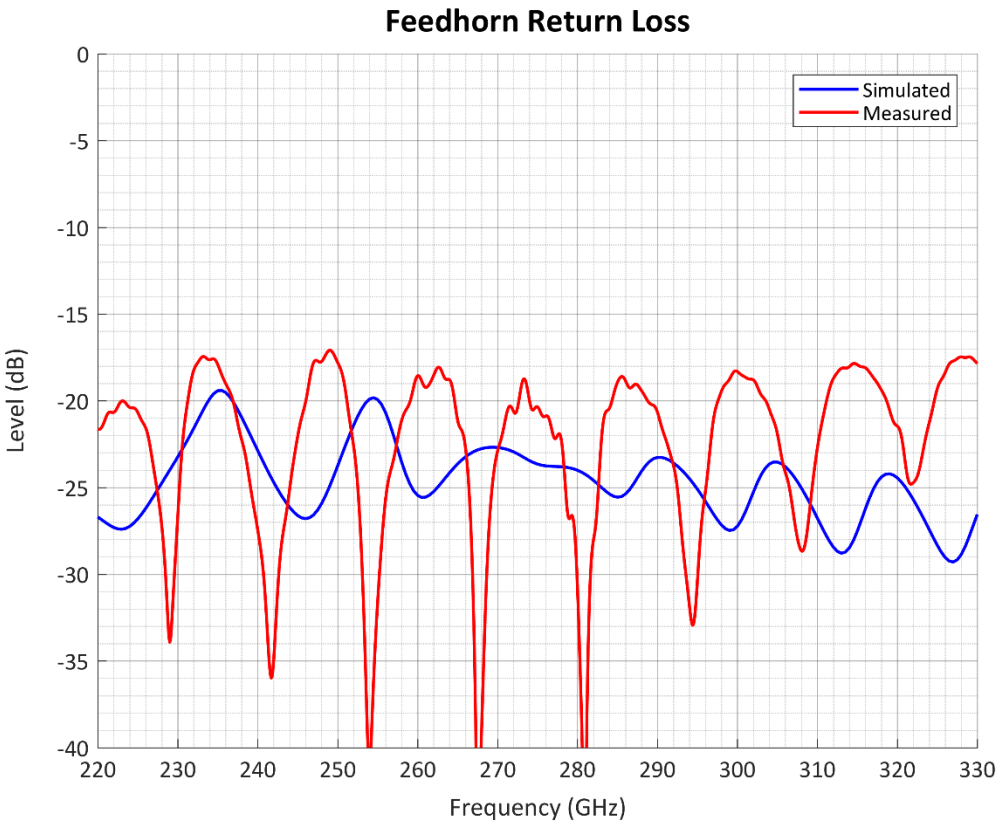
Feedhorn Return Loss
Simulated
Measured
Level (dB)
Frequency (GHz)
0
-5
-10
-15
-20
-25
-30
-35
-40
220
230
240
250
260
270
280
290
300
310
320
330

340 GHz Cassegrain Reflector System

Initial Model

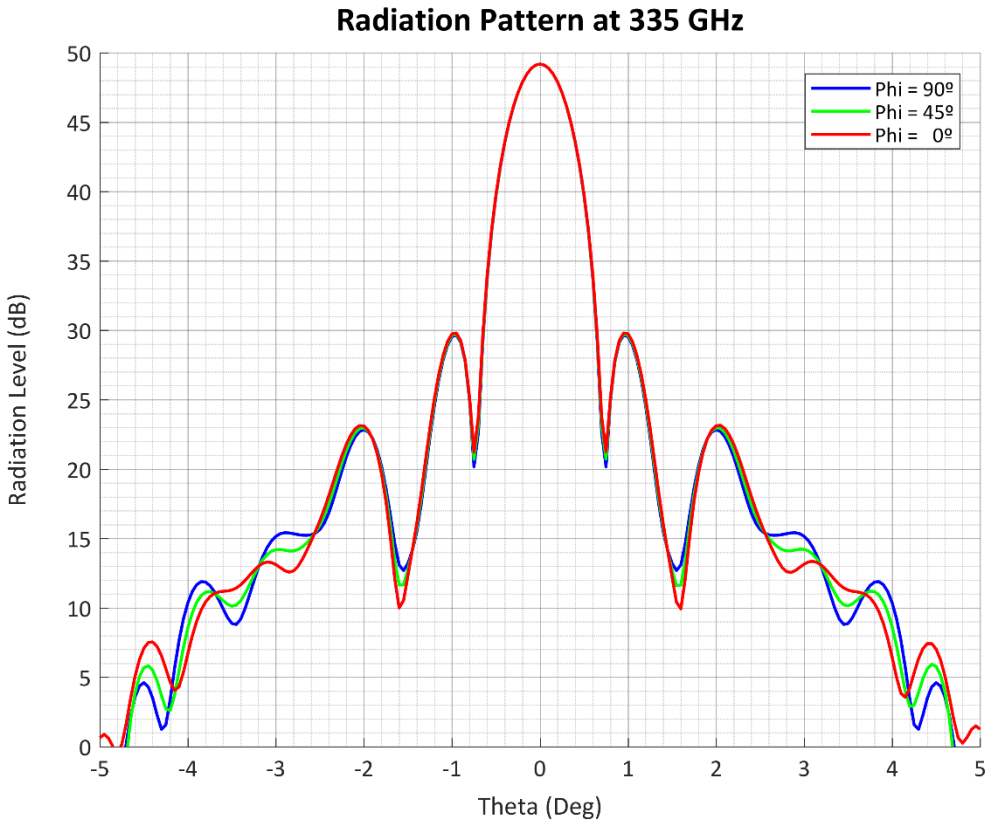

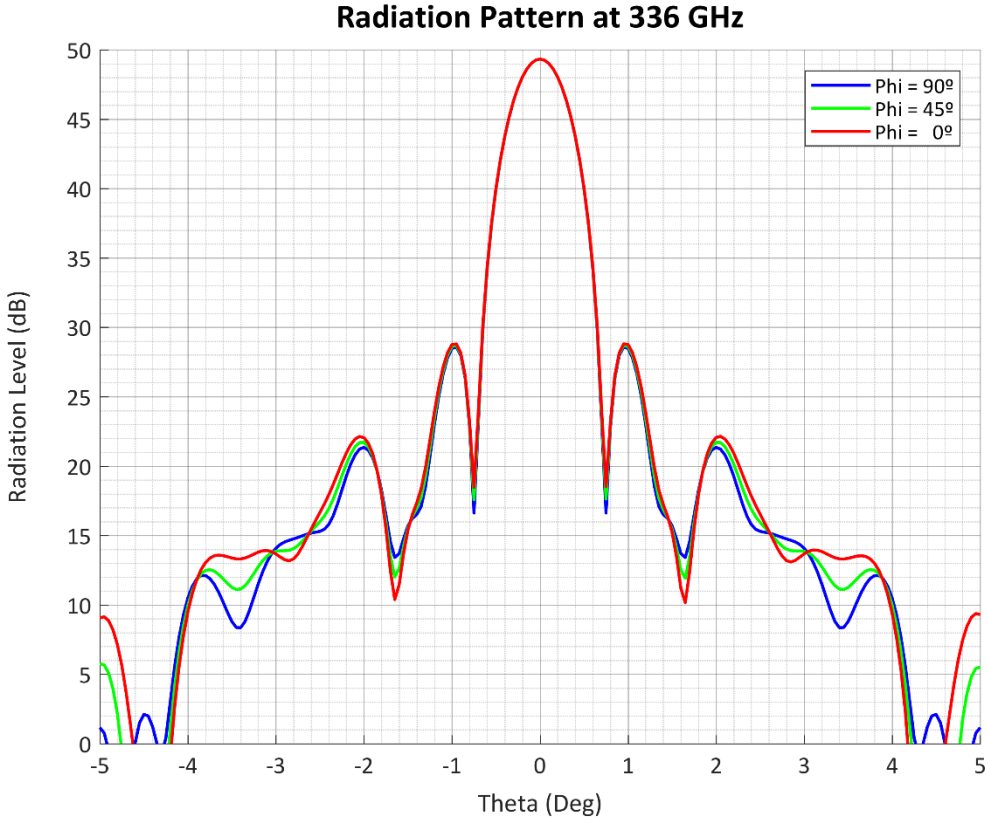

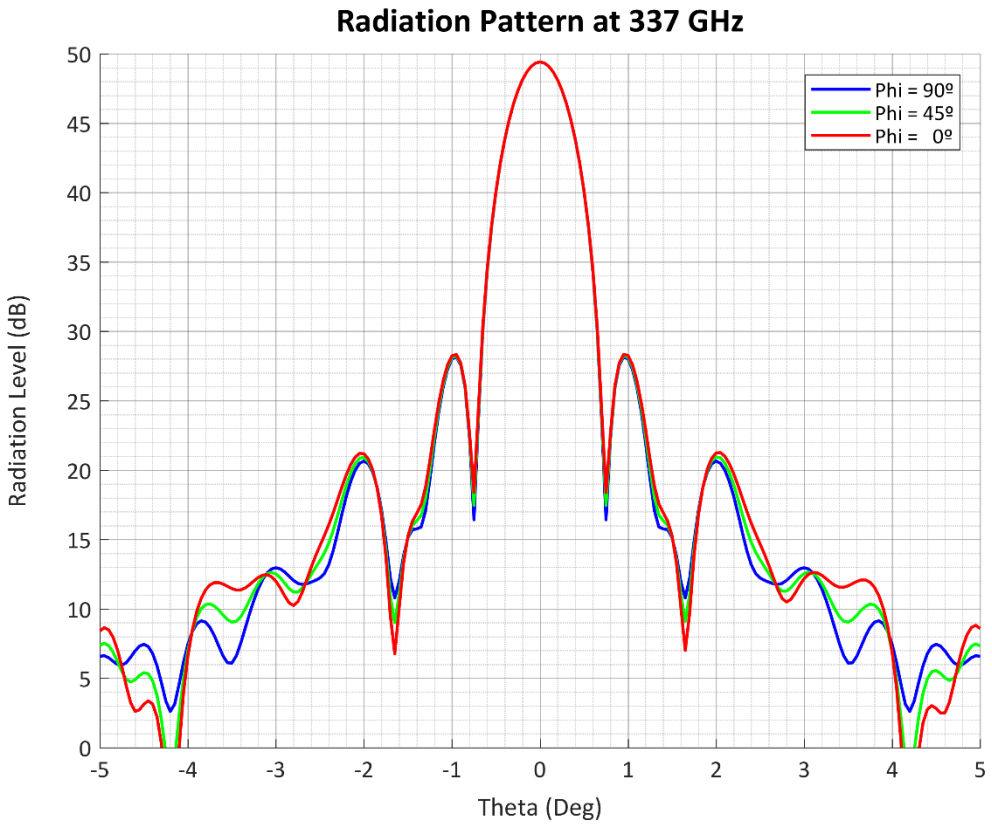
Radiation Pattern at 337 GHz
Phi = 90º
Phi = 45º
Phi = 0º
Radiation Level (dB)
Theta (Deg)
50
45
40
35
30
25
20
15
10
5
0
-5
-4
-3
-2
-1
0
1
2
3
4
5

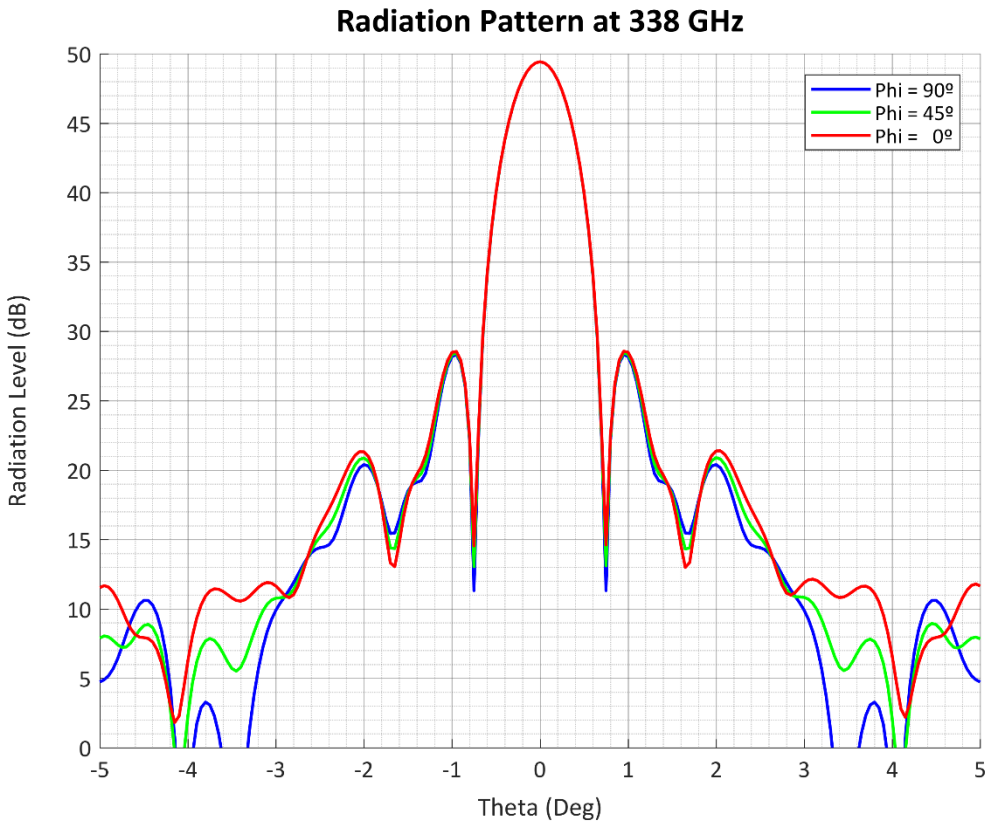
Radiation Pattern at 338 GHz
Phi = 90º
Phi = 45º
Phi = 0º
Radiation Level (dB)
Theta (Deg)
50
45
40
35
30
25
20
15
10
5
0
-5
-4
-3
-2
-1
0
1
2
3
4
5

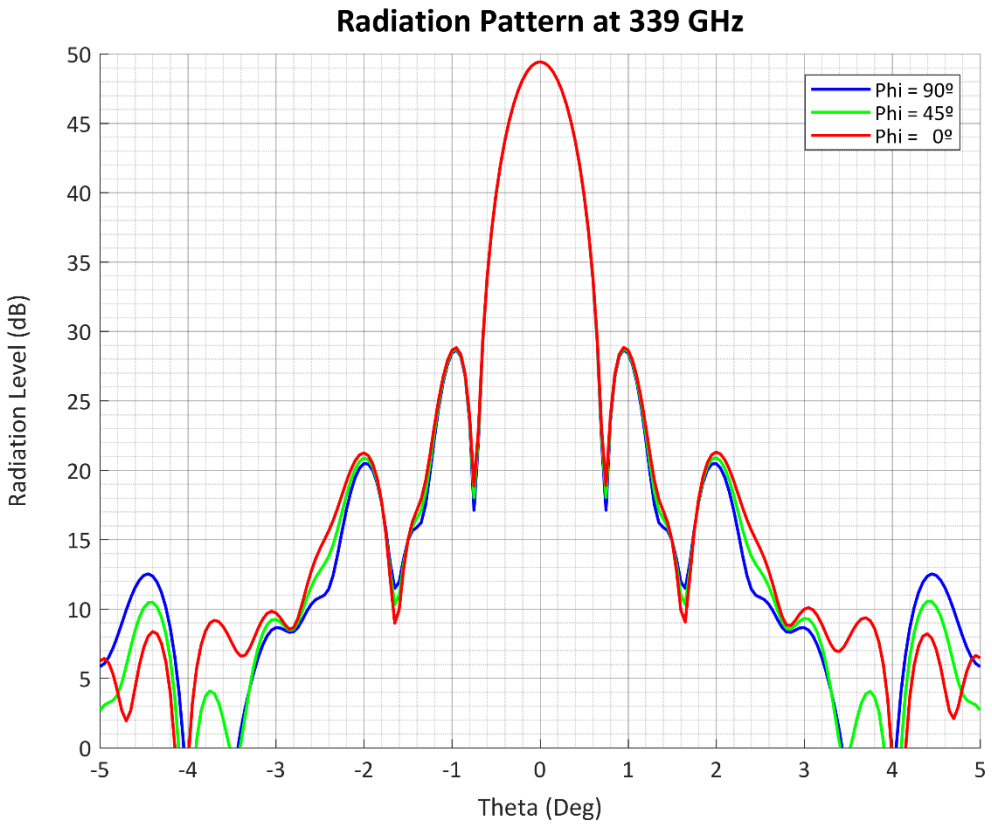
Radiation Pattern at 339 GHz
Phi = 90º
Phi = 45º
Phi = 0º
Radiation Level (dB)
Theta (Deg)
50
45
40
35
30
25
20
15
10
5
0
-5
-4
-3
-2
-1
0
1
2
3
4
5

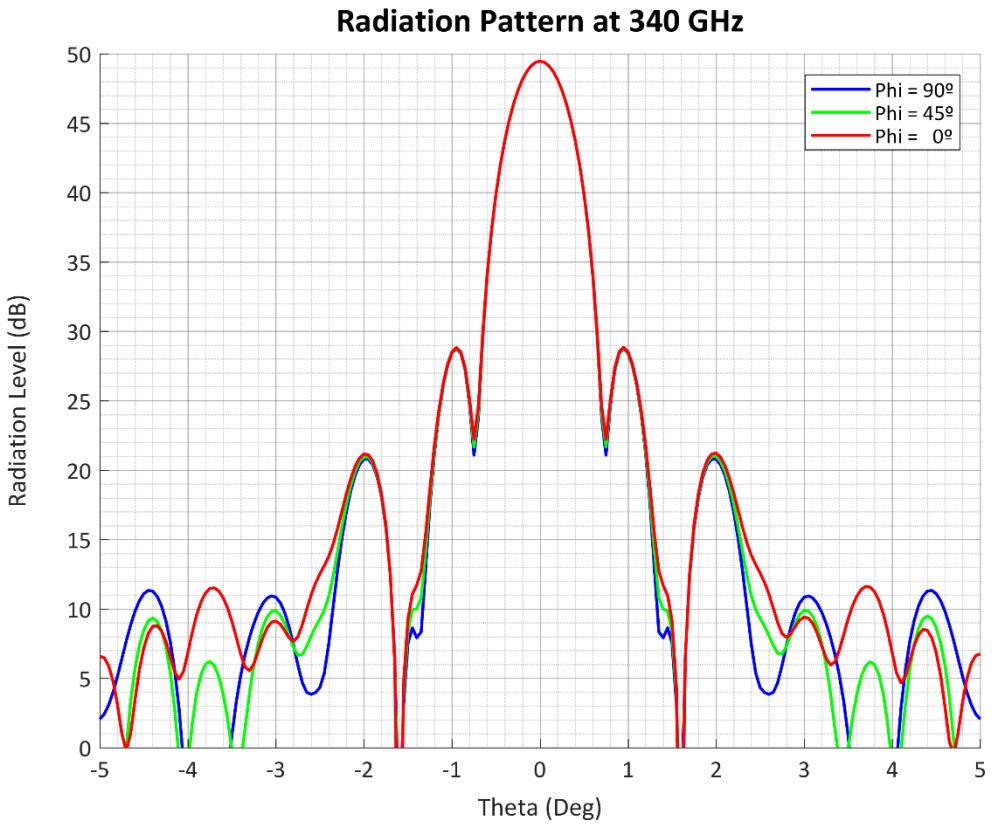
Radiation Pattern at 340 GHz
Phi = 90º
Phi = 45º
Phi = 0º
Radiation Level (dB)
Theta (Deg)
50
45
40
35
30
25
20
15
10
5
0
-5
-4
-3
-2
-1
0
1
2
3
4
5

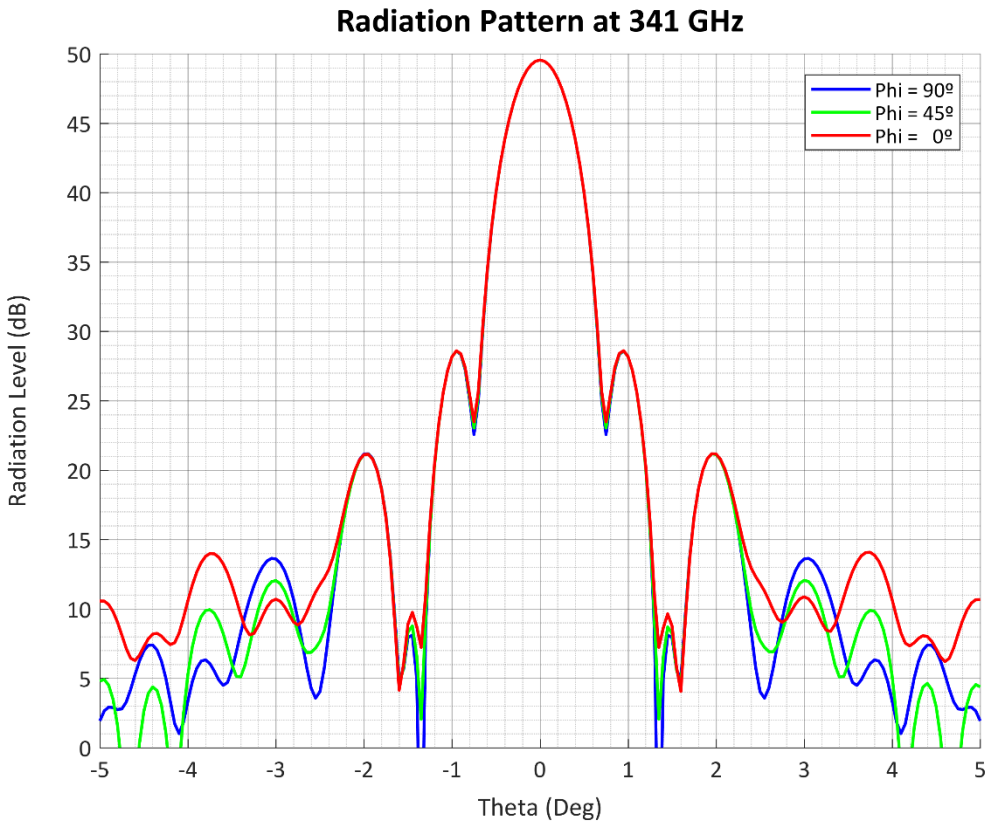
Radiation Pattern at 341 GHz
Phi = 90º
Phi = 45º
Phi = 0º
Radiation Level (dB)
Theta (Deg)
50
45
40
35
30
25
20
15
10
5
0
-5
-4
-3
-2
-1
0
1
2
3
4
5

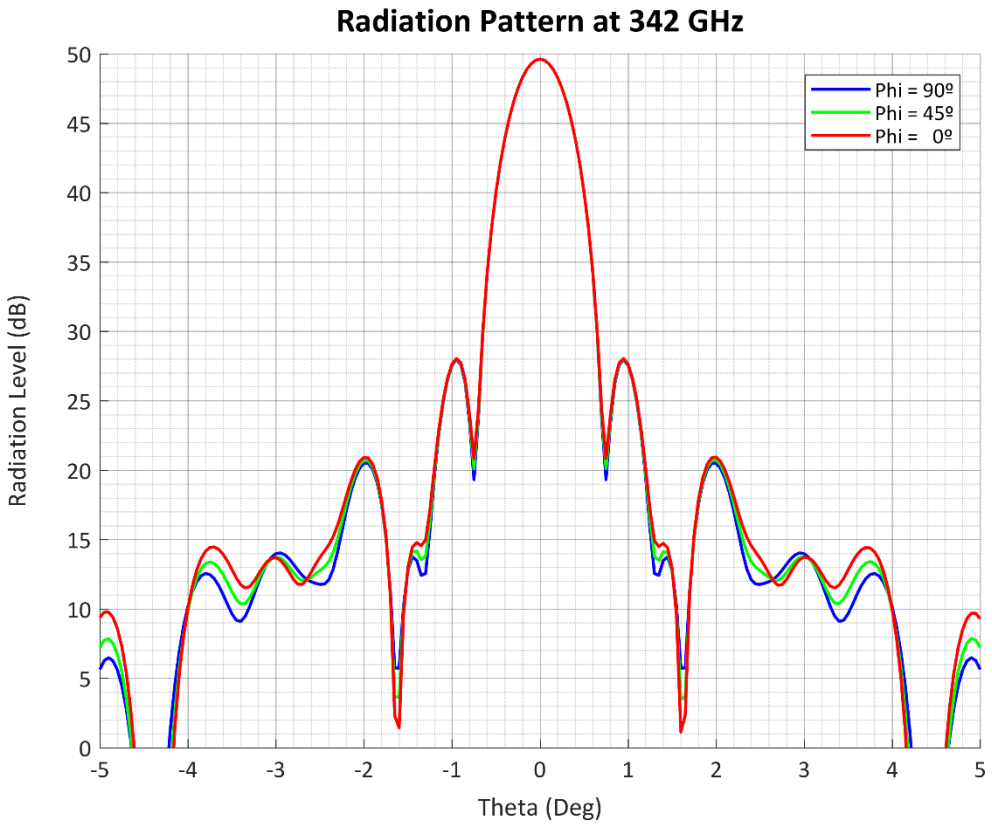
Radiation Pattern at 342 GHz
Phi = 90º
Phi = 45º
Phi = 0º
Radiation Level (dB)
Theta (Deg)
50
45
40
35
30
25
20
15
10
5
0
-5
-4
-3
-2
-1
0
1
2
3
4
5

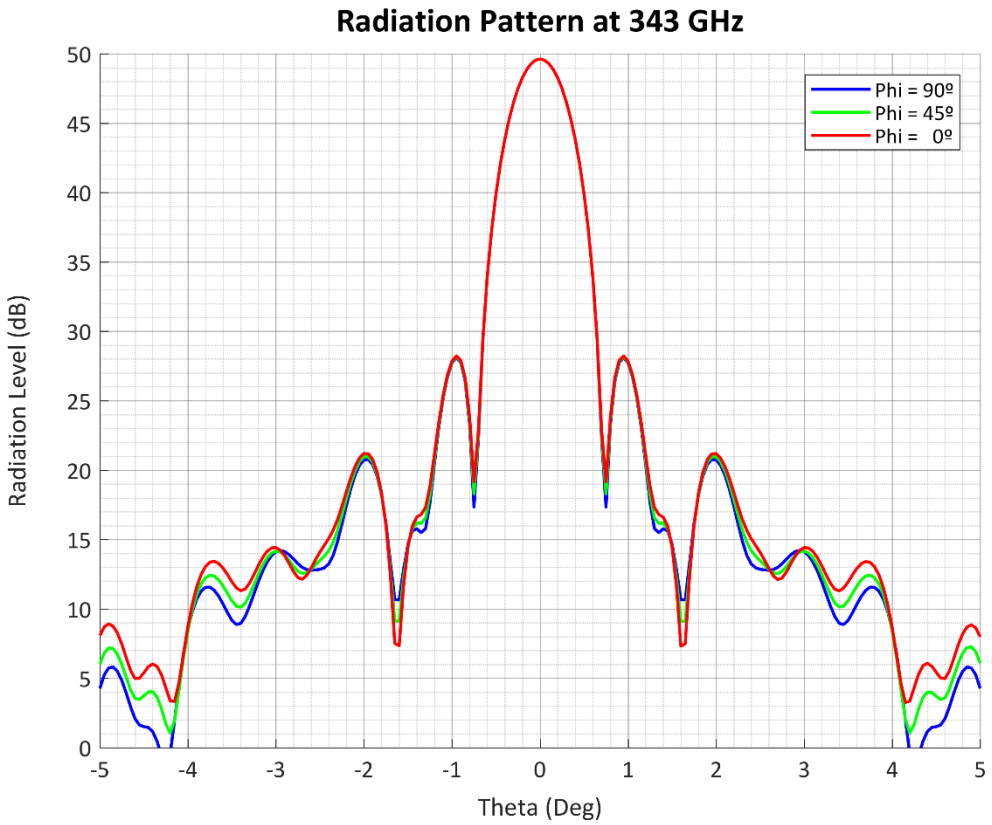
Radiation Pattern at 343 GHz
Phi = 90º
Phi = 45º
Phi = 0º
Radiation Level (dB)
Theta (Deg)
50
45
40
35
30
25
20
15
10
5
0
-5
-4
-3
-2
-1
0
1
2
3
4
5

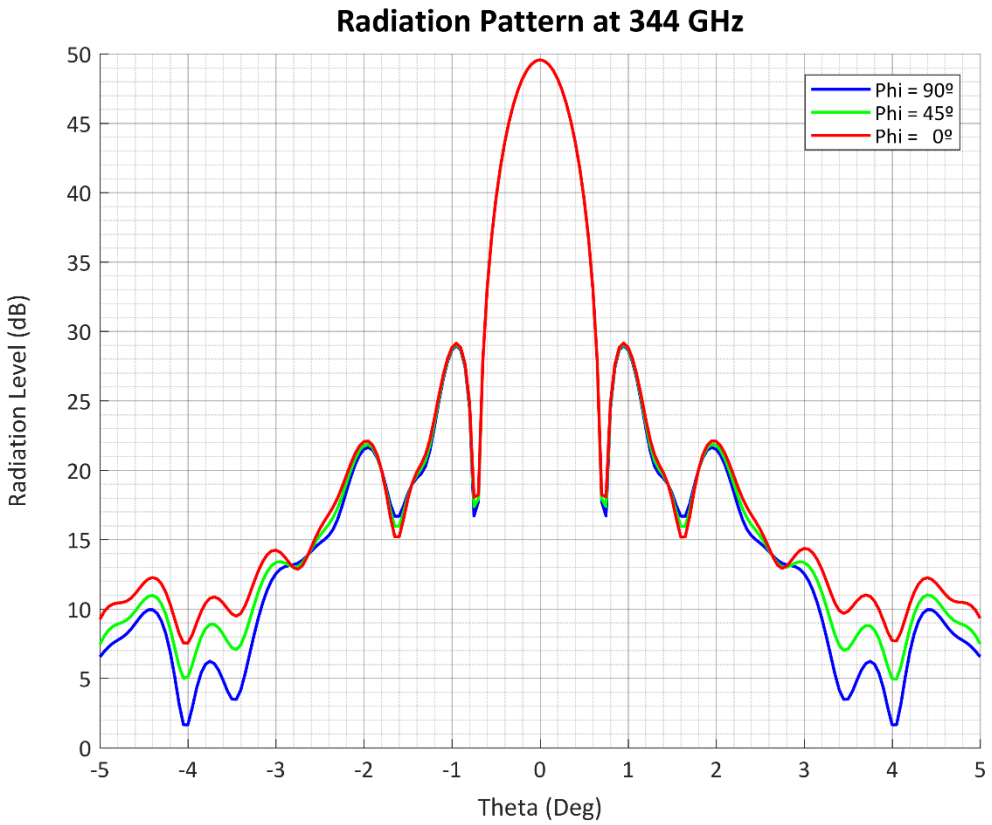
Radiation Pattern at 344 GHz
Phi = 90º
Phi = 45º
Phi = 0º
Radiation Level (dB)
Theta (Deg)
50
45
40
35
30
25
20
15
10
5
0
-5
-4
-3
-2
-1
0
1
2
3
4
5

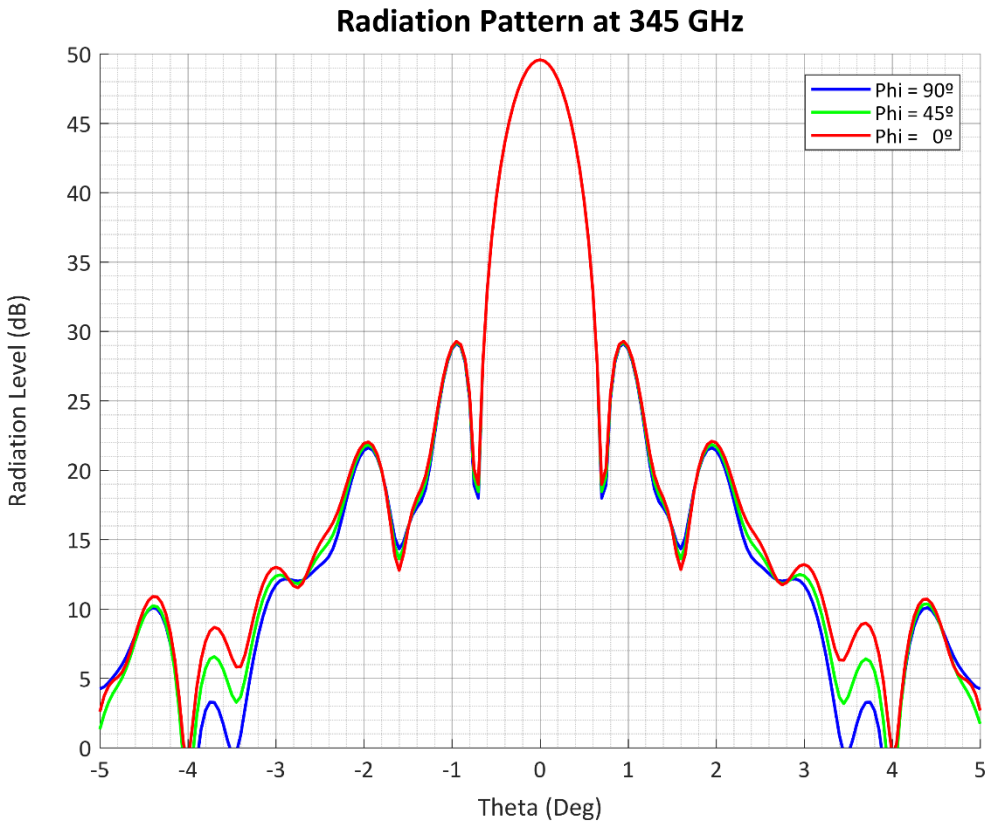
Radiation Pattern at 345 GHz
Phi = 90º
Phi = 45º
Phi = 0º
Radiation Level (dB)
Theta (Deg)
50
45
40
35
30
25
20
15
10
5
0
-5
-4
-3
-2
-1
0
1
2
3
4
5

Final Model

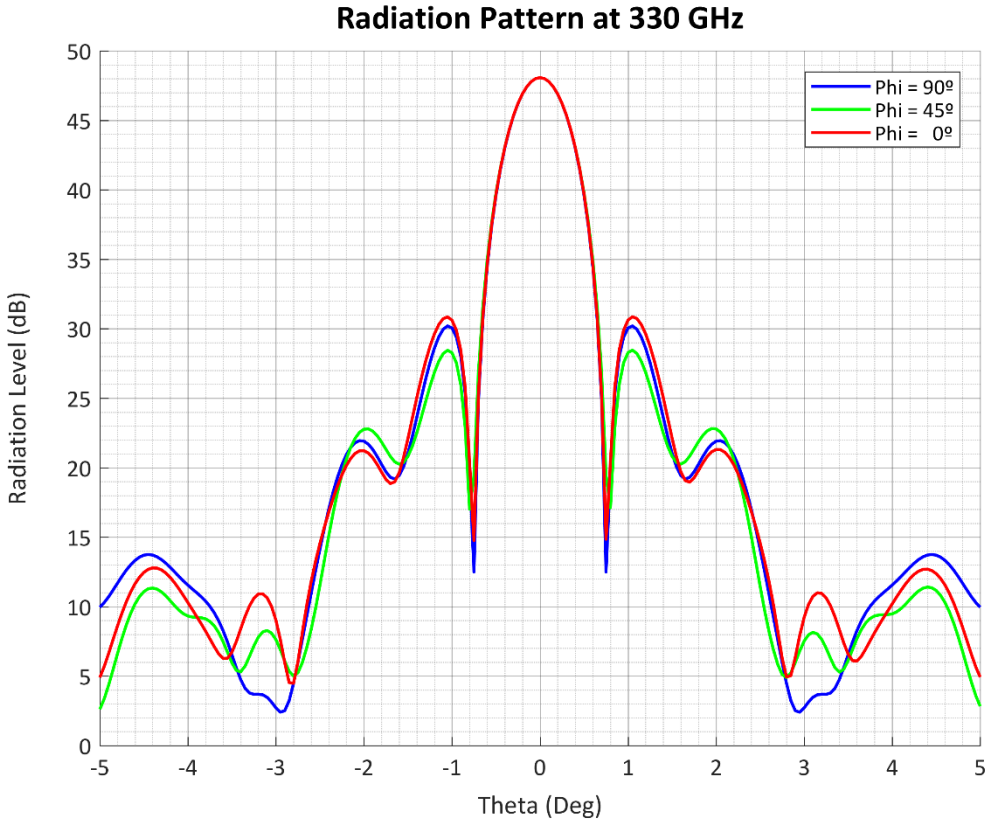
Radiation Pattern at 330 GHz
Phi = 90º
Phi = 45º
Phi = 0º
Radiation Level (dB)
Theta (Deg)

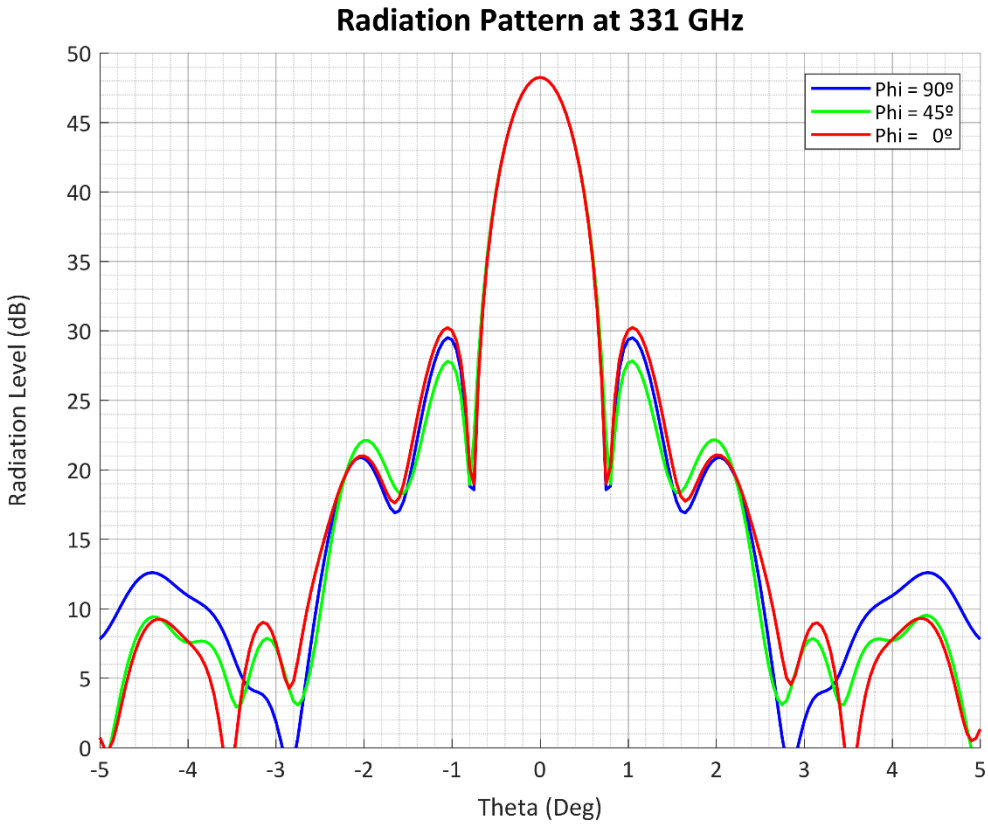
Radiation Pattern at 331 GHz
Phi = 90º
Phi = 45º
Phi = 0º
Radiation Level (dB)
Theta (Deg)

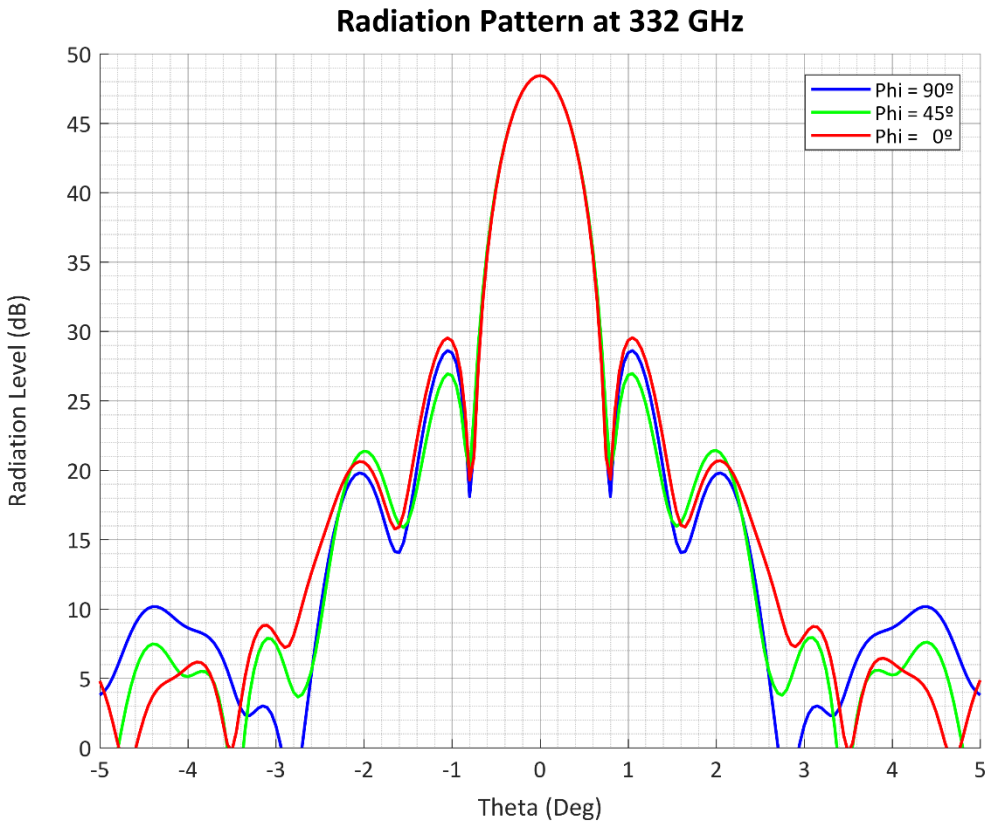
Radiation Pattern at 332 GHz
Phi = 90º
Phi = 45º
Phi = 0º
Radiation Level (dB)
Theta (Deg)
50
45
40
35
30
25
20
15
10
5
0
-5
-4
-3
-2
-1
0
1
2
3
4
5

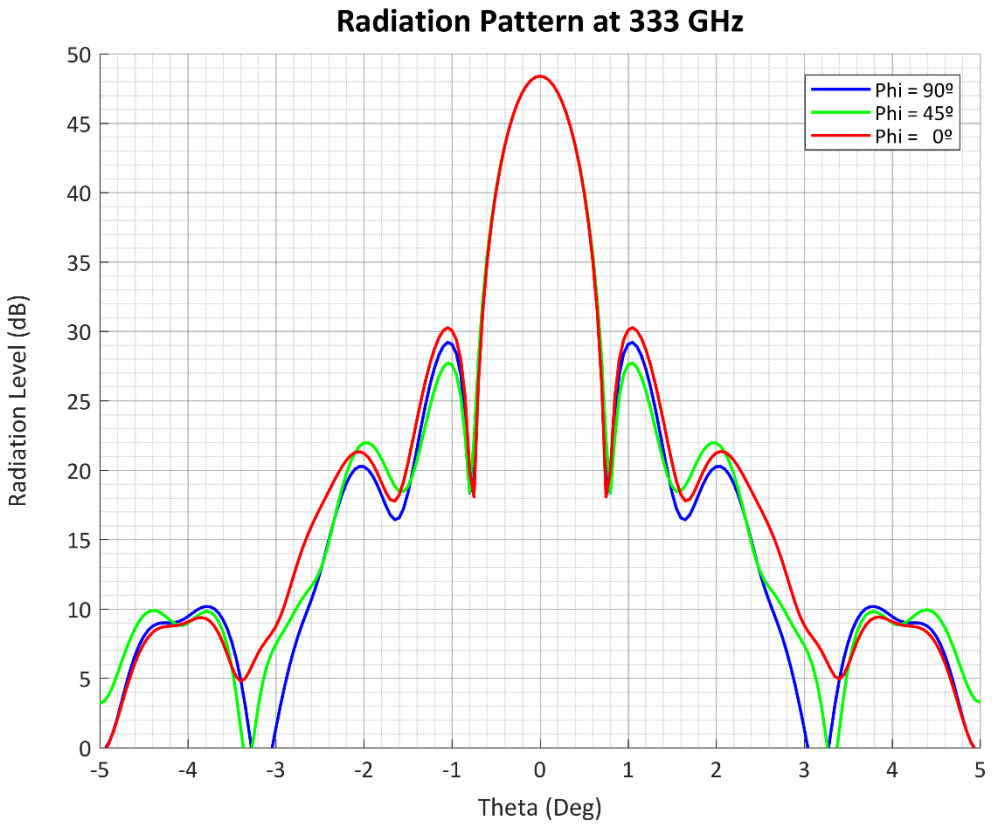
Radiation Pattern at 333 GHz
Phi = 90º
Phi = 45º
Phi = 0º
Radiation Level (dB)
Theta (Deg)
50
45
40
35
30
25
20
15
10
5
0
-5
-4
-3
-2
-1
0
1
2
3
4
5

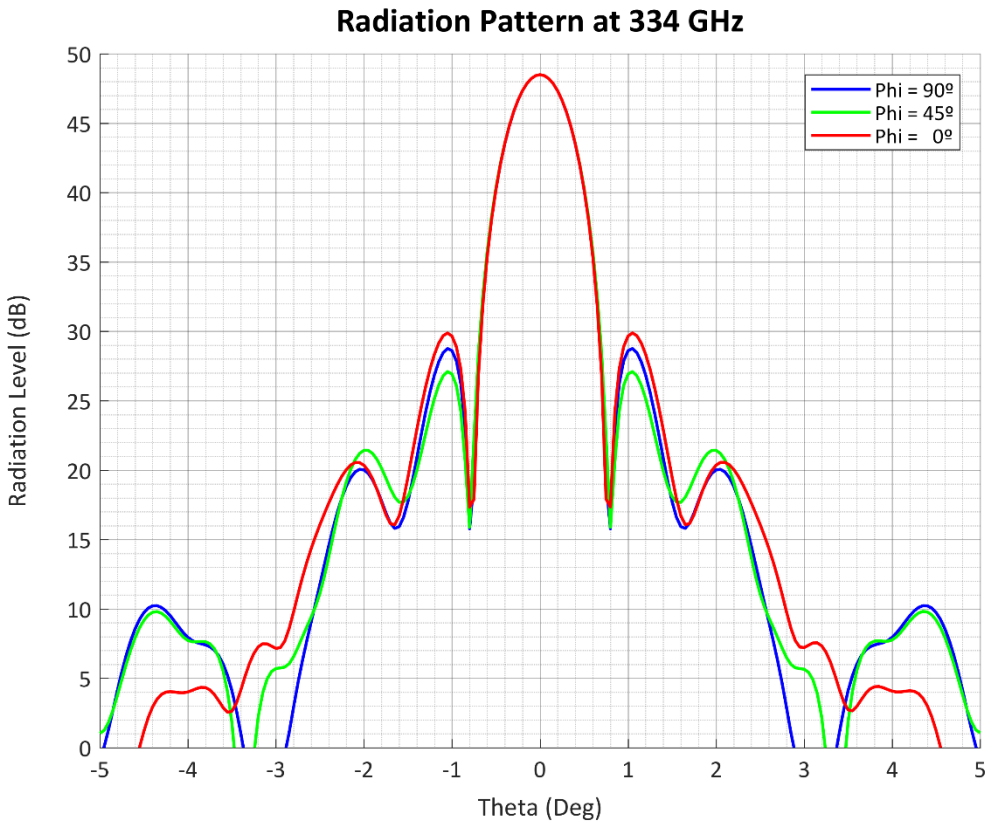
Radiation Pattern at 334 GHz
Phi = 90º
Phi = 45º
Phi = 0º
Radiation Level (dB)
Theta (Deg)
50
45
40
35
30
25
20
15
10
5
0
-5
-4
-3
-2
-1
0
1
2
3
4
5

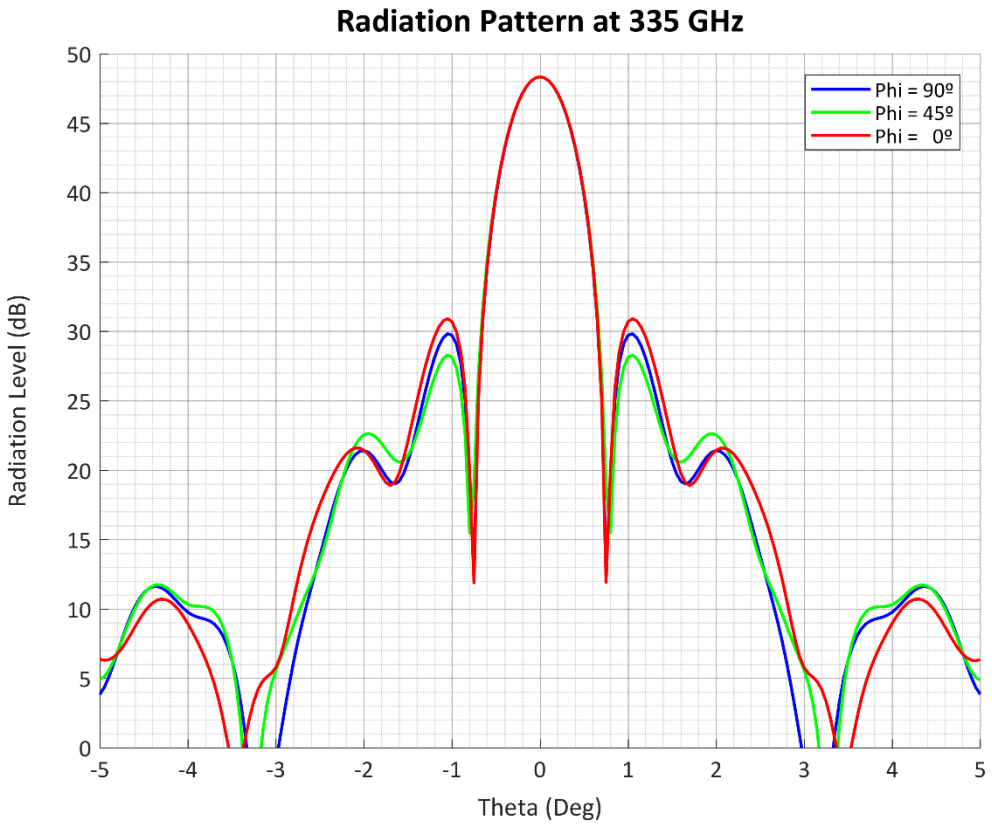
Radiation Pattern at 335 GHz
Phi = 90º
Phi = 45º
Phi = 0º
Radiation Level (dB)
Theta (Deg)
50
45
40
35
30
25
20
15
10
5
0
-5
-4
-3
-2
-1
0
1
2
3
4
5

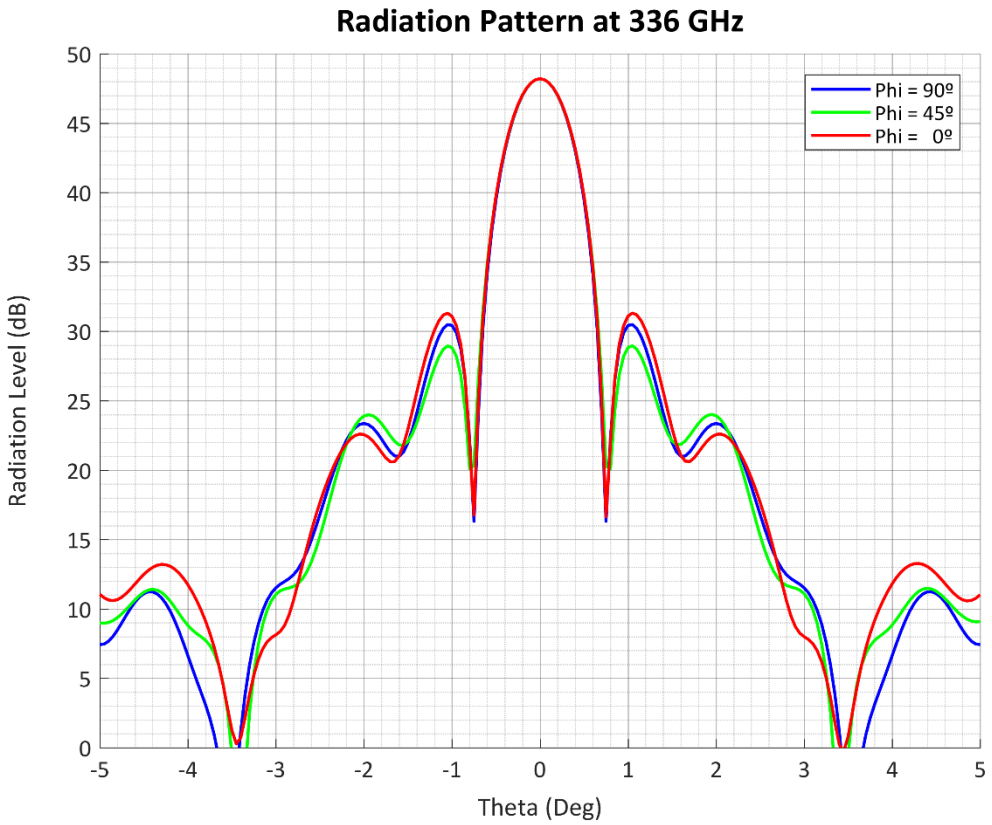
Radiation Pattern at 336 GHz
Phi = 90º
Phi = 45º
Phi = 0º
Radiation Level (dB)
Theta (Deg)
50
45
40
35
30
25
20
15
10
5
0
-5
-4
-3
-2
-1
0
1
2
3
4
5

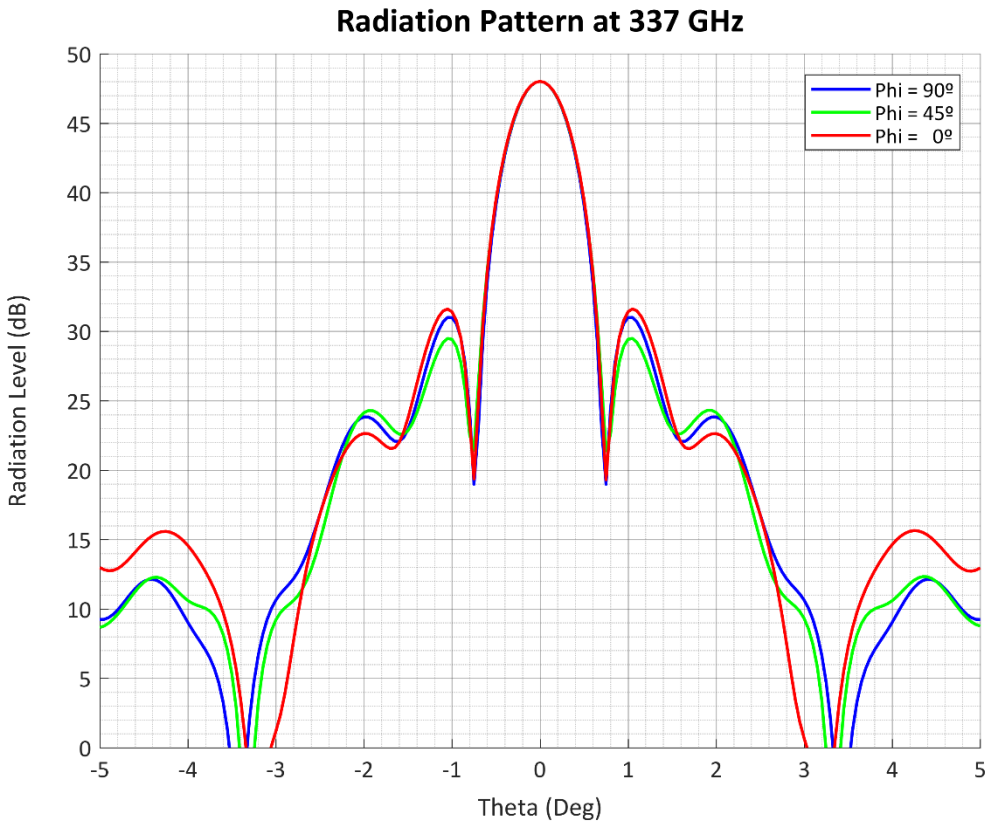
Radiation Pattern at 337 GHz
Phi = 90º
Phi = 45º
Phi = 0º
Radiation Level (dB)
Theta (Deg)
50
45
40
35
30
25
20
15
10
5
0
-5
-4
-3
-2
-1
0
1
2
3
4
5

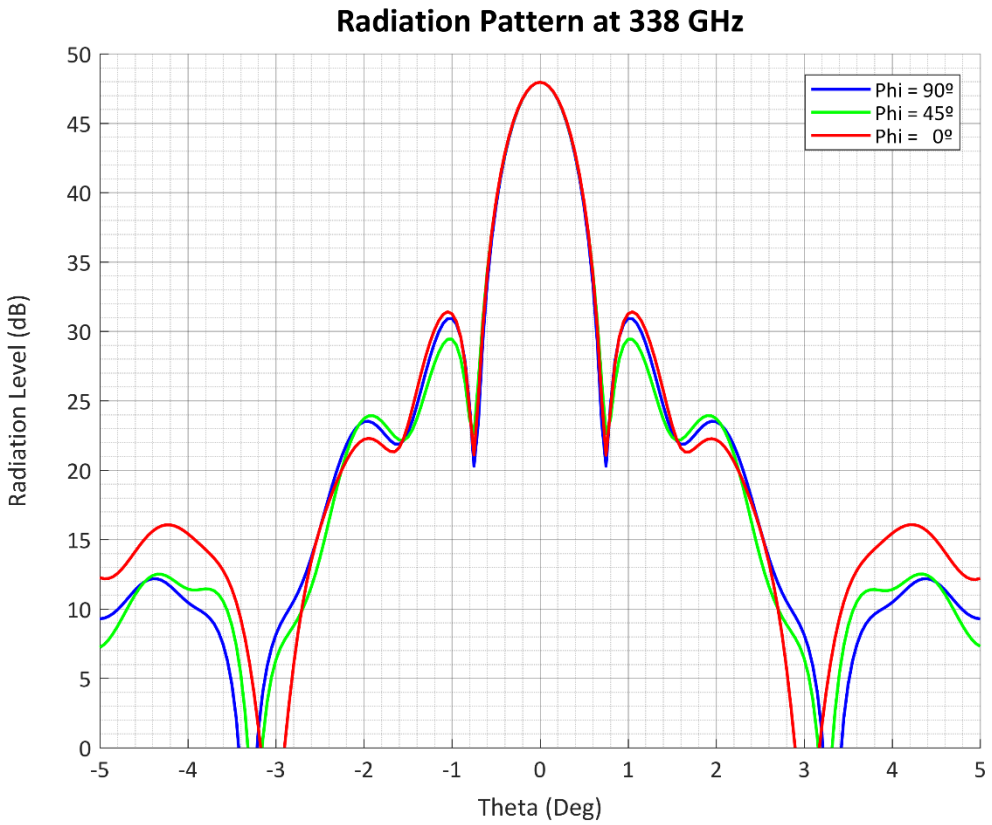
Radiation Pattern at 338 GHz
Phi = 90º
Phi = 45º
Phi = 0º
Radiation Level (dB)
Theta (Deg)
50
45
40
35
30
25
20
15
10
5
0
-5
-4
-3
-2
-1
0
1
2
3
4
5

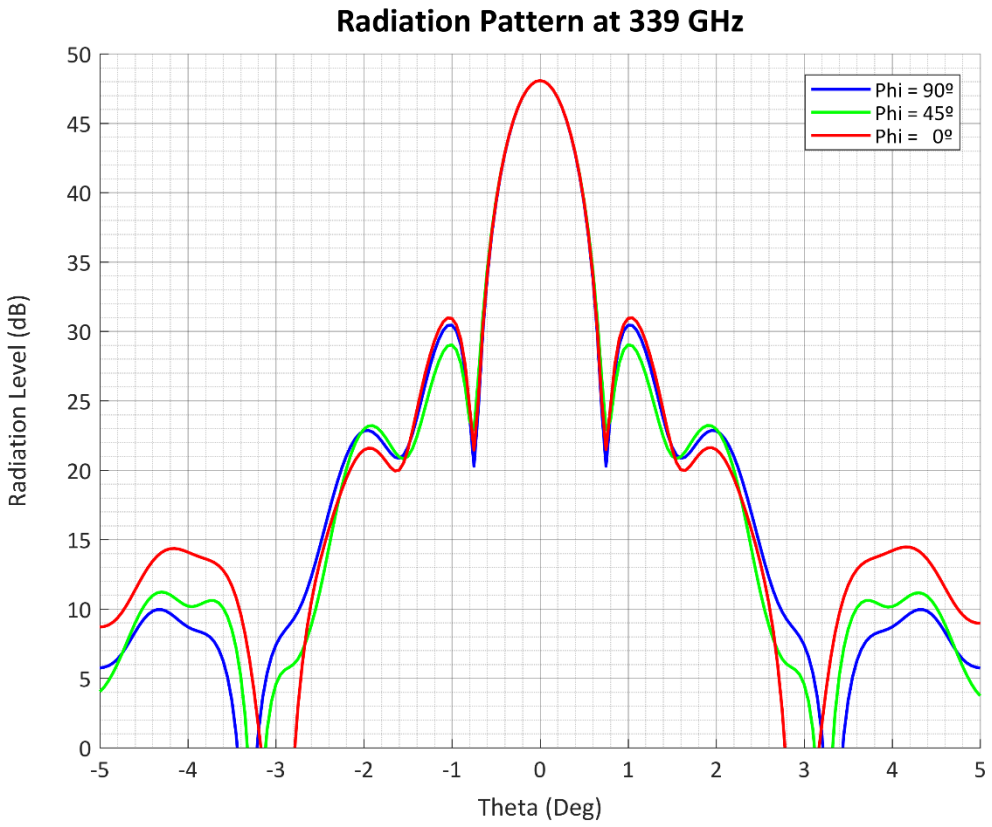
Radiation Pattern at 339 GHz
Phi = 90º
Phi = 45º
Phi = 0º
Radiation Level (dB)
Theta (Deg)
50
45
40
35
30
25
20
15
10
5
0
-5
-4
-3
-2
-1
0
1
2
3
4
5

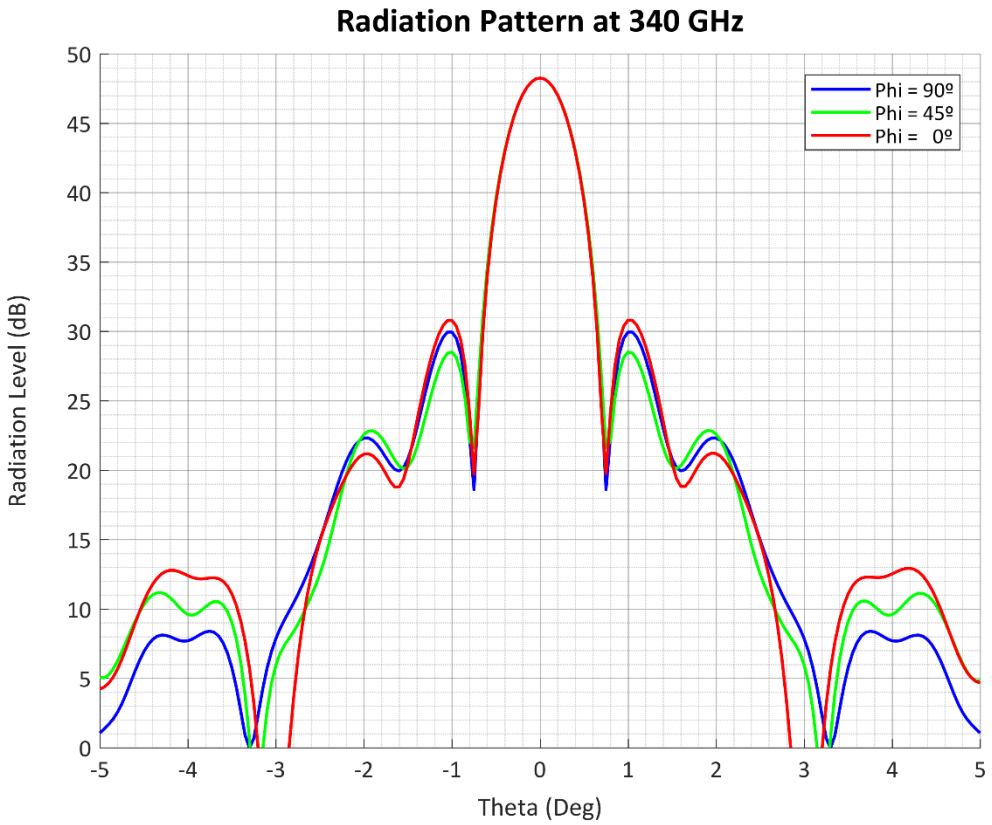
Radiation Pattern at 340 GHz
Phi = 90º
Phi = 45º
Phi = 0º
Radiation Level (dB)
Theta (Deg)
50
45
40
35
30
25
20
15
10
5
0
-5
-4
-3
-2
-1
0
1
2
3
4
5

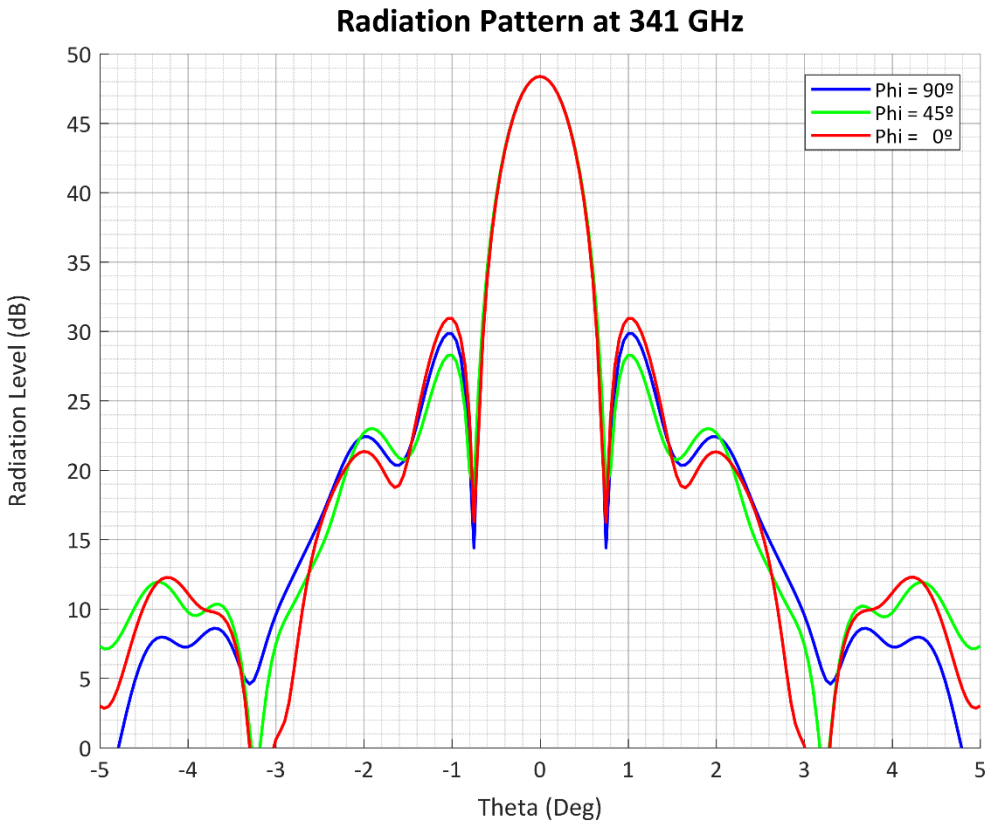
Radiation Pattern at 341 GHz
Phi = 90º
Phi = 45º
Phi = 0º
Radiation Level (dB)
Theta (Deg)
50
45
40
35
30
25
20
15
10
5
0
-5
-4
-3
-2
-1
0
1
2
3
4
5

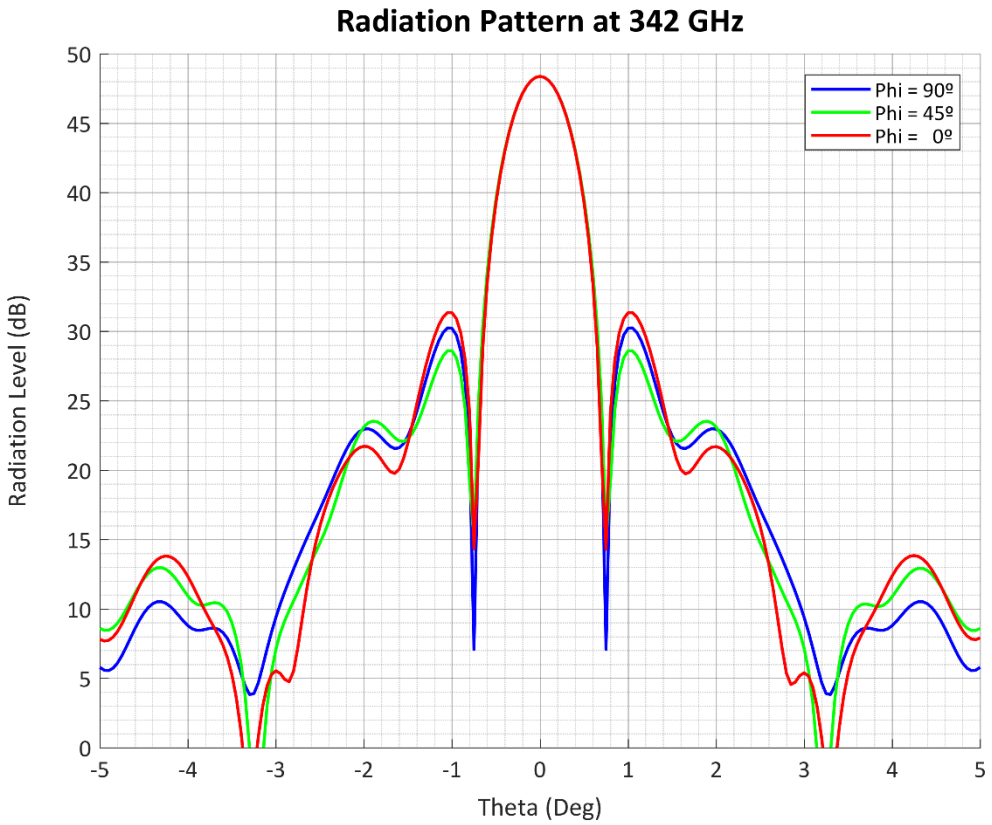
Radiation Pattern at 342 GHz
Phi = 90º
Phi = 45º
Phi = 0º
Radiation Level (dB)
Theta (Deg)
50
45
40
35
30
25
20
15
10
5
0
-5
-4
-3
-2
-1
0
1
2
3
4
5

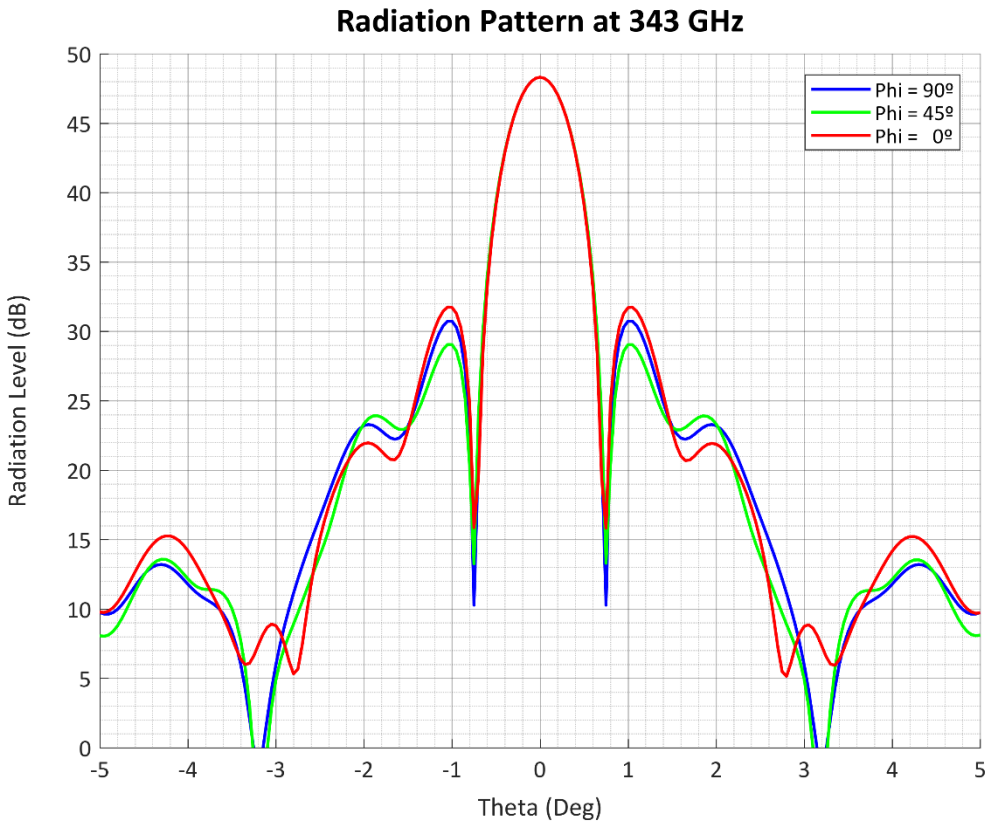
Radiation Pattern at 343 GHz
Phi = 90º
Phi = 45º
Phi = 0º
Radiation Level (dB)
Theta (Deg)
50
45
40
35
30
25
20
15
10
5
0
-5
-4
-3
-2
-1
0
1
2
3
4
5

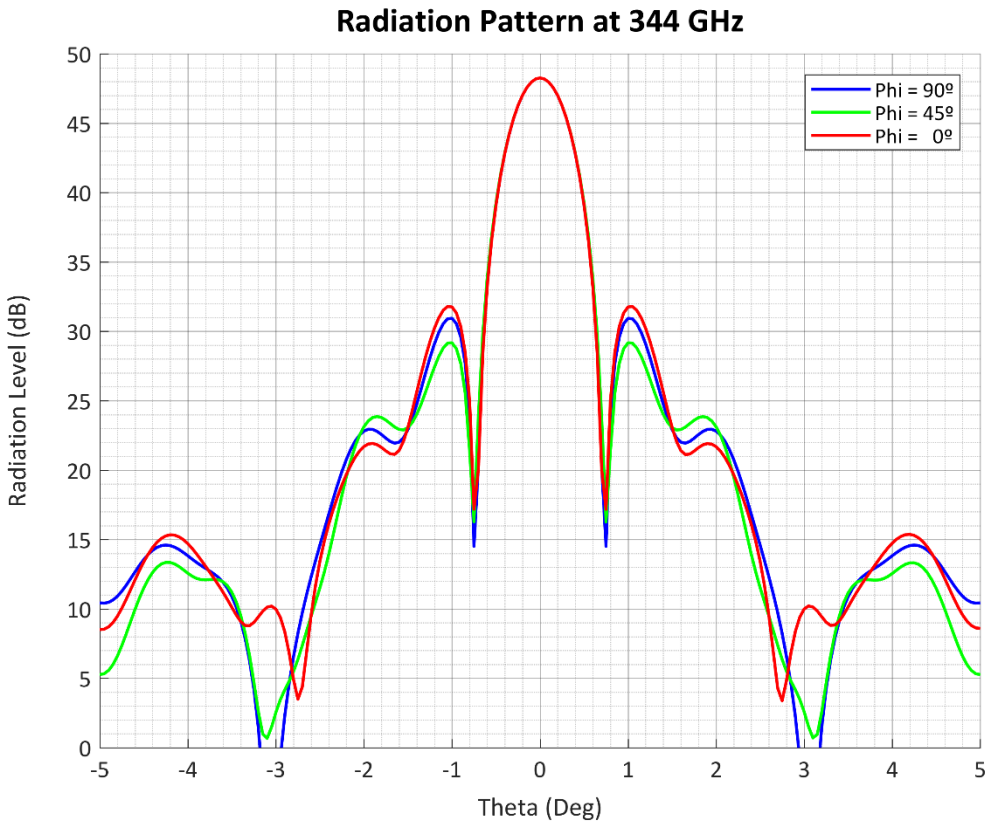
Radiation Pattern at 344 GHz
Phi = 90º
Phi = 45º
Phi = 0º
Radiation Level (dB)
Theta (Deg)
50
45
40
35
30
25
20
15
10
5
0
-5
-4
-3
-2
-1
0
1
2
3
4
5

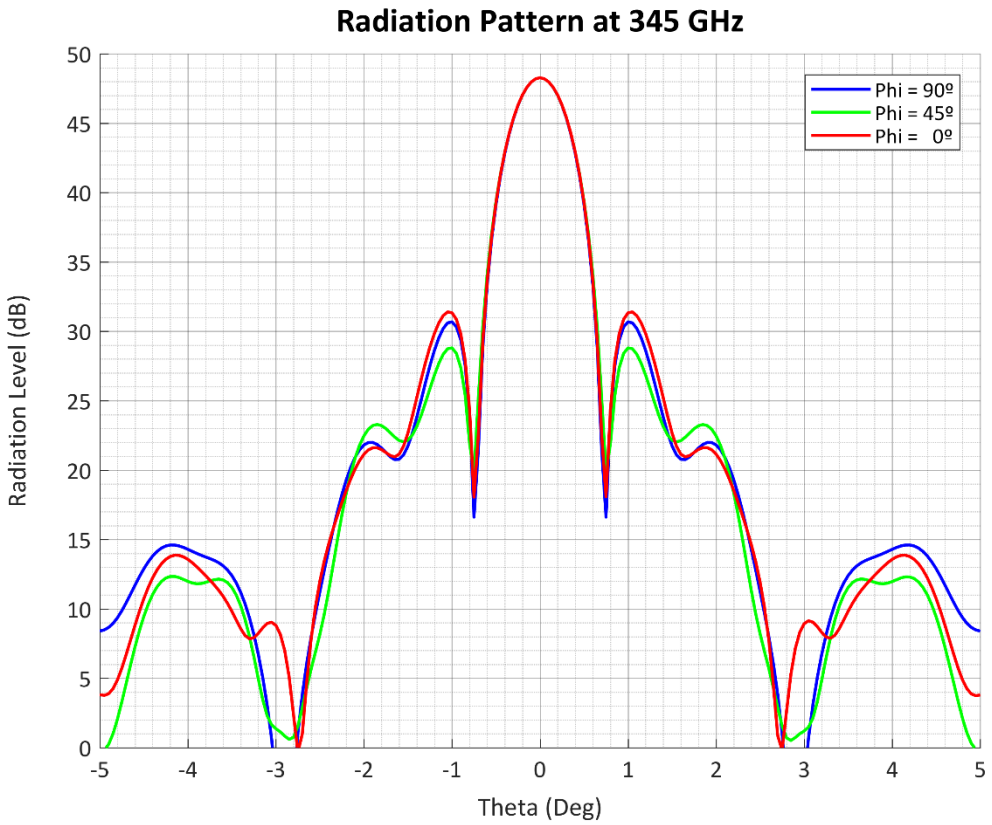
Radiation Pattern at 345 GHz
Phi = 90º
Phi = 45º
Phi = 0º
Radiation Level (dB)
Theta (Deg)
50
45
40
35
30
25
20
15
10
5
0
-5
-4
-3
-2
-1
0
1
2
3
4
5

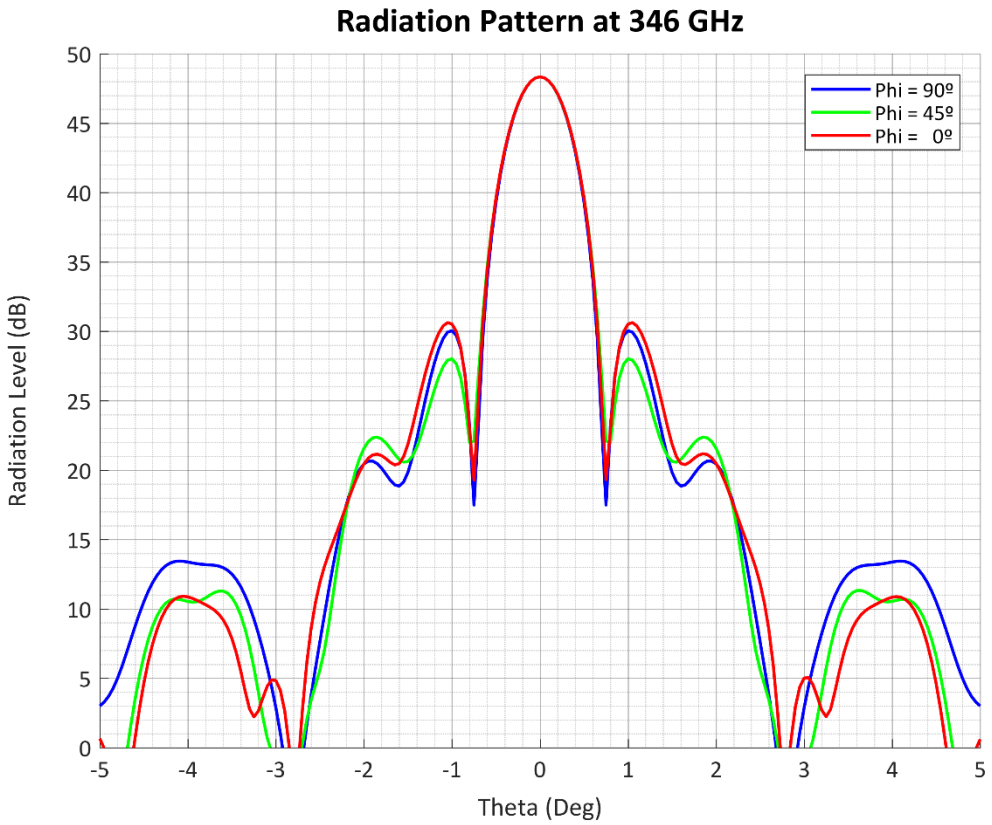
Radiation Pattern at 346 GHz
Phi = 90º
Phi = 45º
Phi = 0º
Radiation Level (dB)
Theta (Deg)
50
45
40
35
30
25
20
15
10
5
0
-5
-4
-3
-2
-1
0
1
2
3
4
5

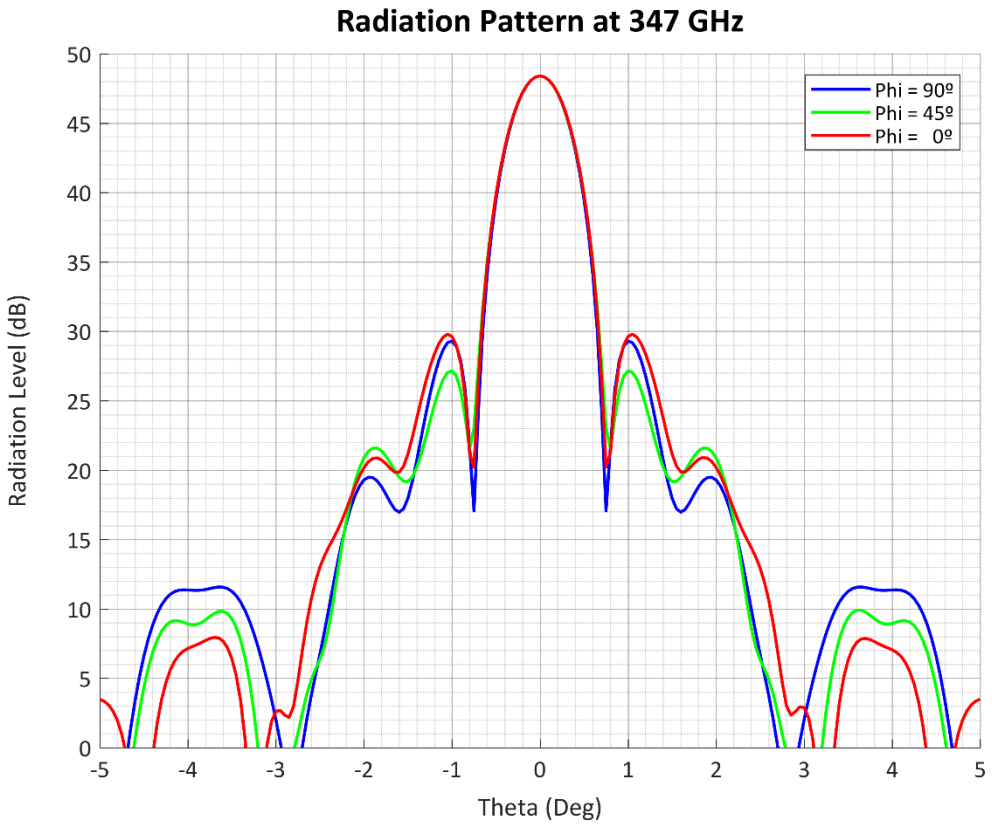
Radiation Pattern at 347 GHz
Phi = 90º
Phi = 45º
Phi = 0º
Radiation Level (dB)
Theta (Deg)
50
45
40
35
30
25
20
15
10
5
0
-5
-4
-3
-2
-1
0
1
2
3
4
5

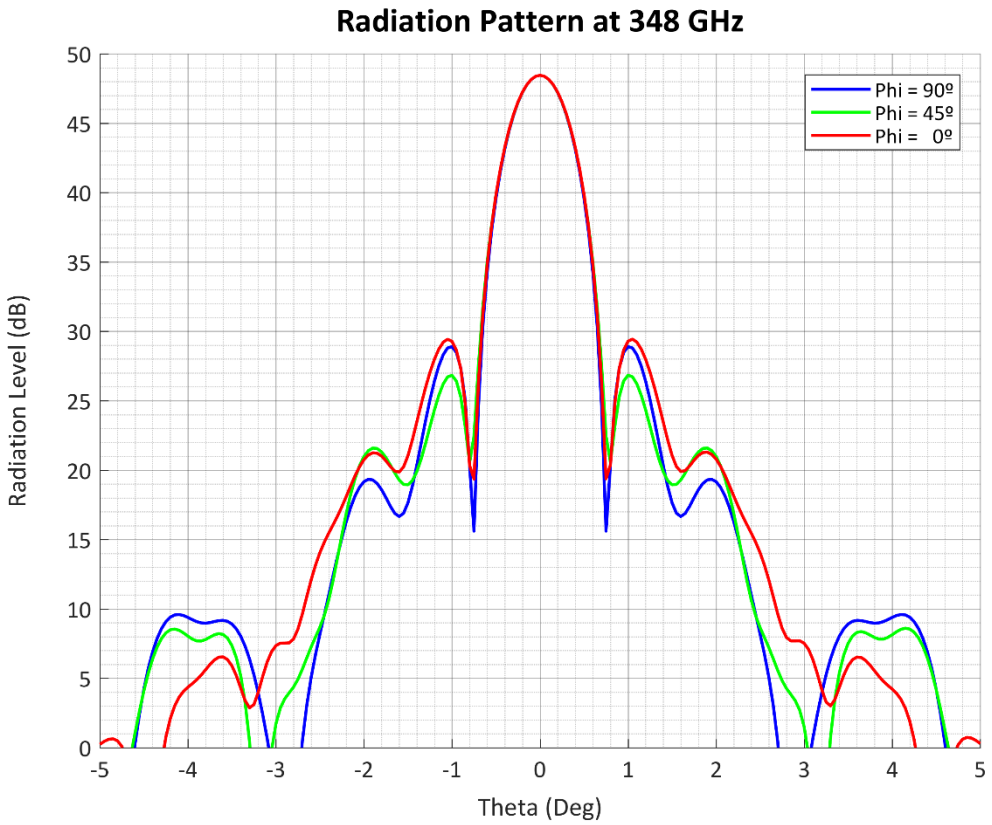
Radiation Pattern at 348 GHz
Phi = 90º
Phi = 45º
Phi = 0º
Radiation Level (dB)
Theta (Deg)
50
45
40
35
30
25
20
15
10
5
0
-5
-4
-3
-2
-1
0
1
2
3
4
5

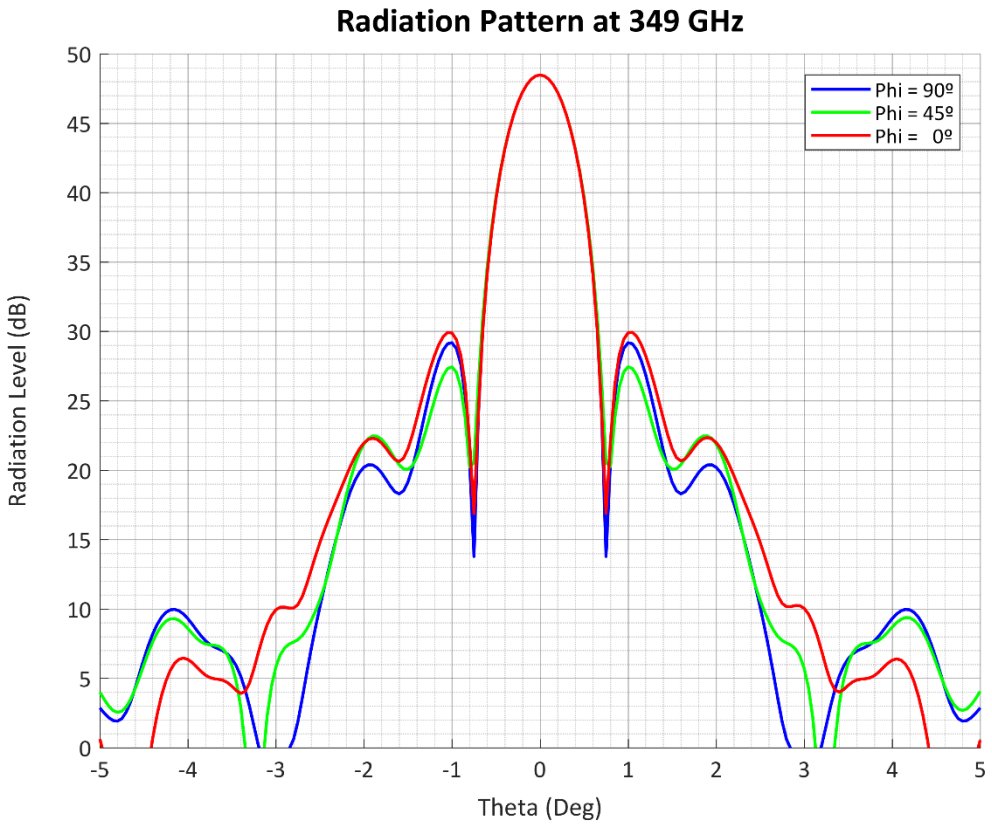
Radiation Pattern at 349 GHz
Phi = 90º
Phi = 45º
Phi = 0º
Radiation Level (dB)
Theta (Deg)
50
45
40
35
30
25
20
15
10
5
0
-5
-4
-3
-2
-1
0
1
2
3
4
5

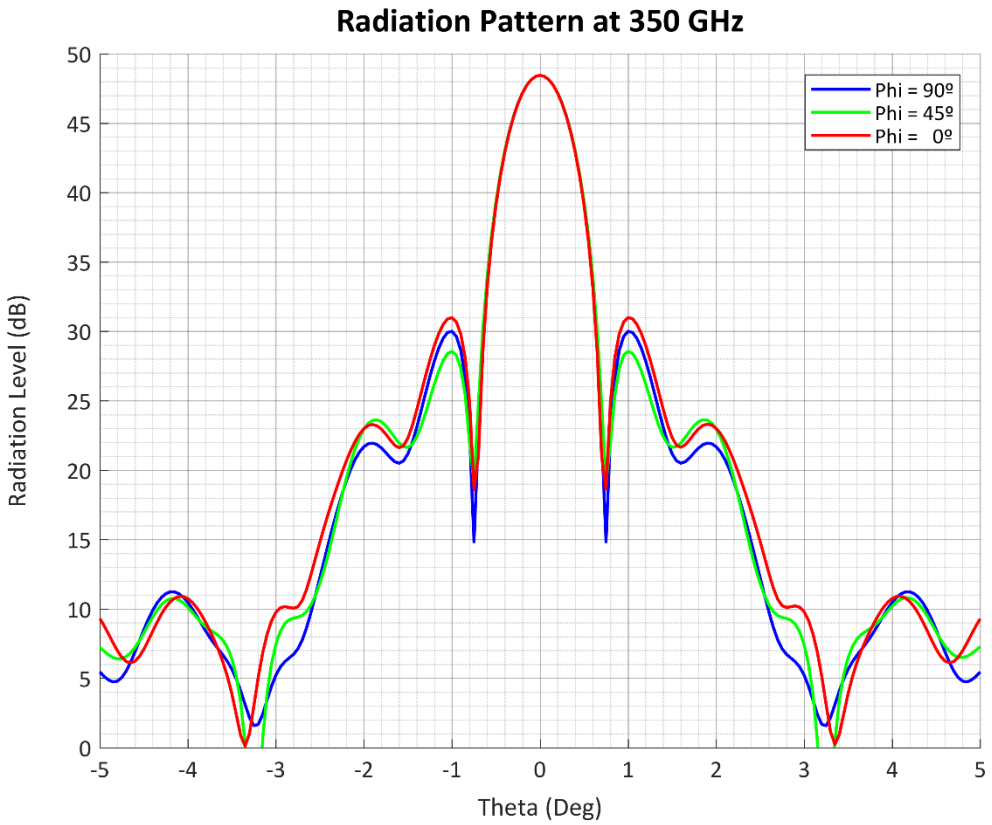
Radiation Pattern at 350 GHz
Phi = 90º
Phi = 45º
Phi = 0º
Radiation Level (dB)
Theta (Deg)
50
45
40
35
30
25
20
15
10
5
0
-5
-4
-3
-2
-1
0
1
2
3
4
5

Manufactured Model

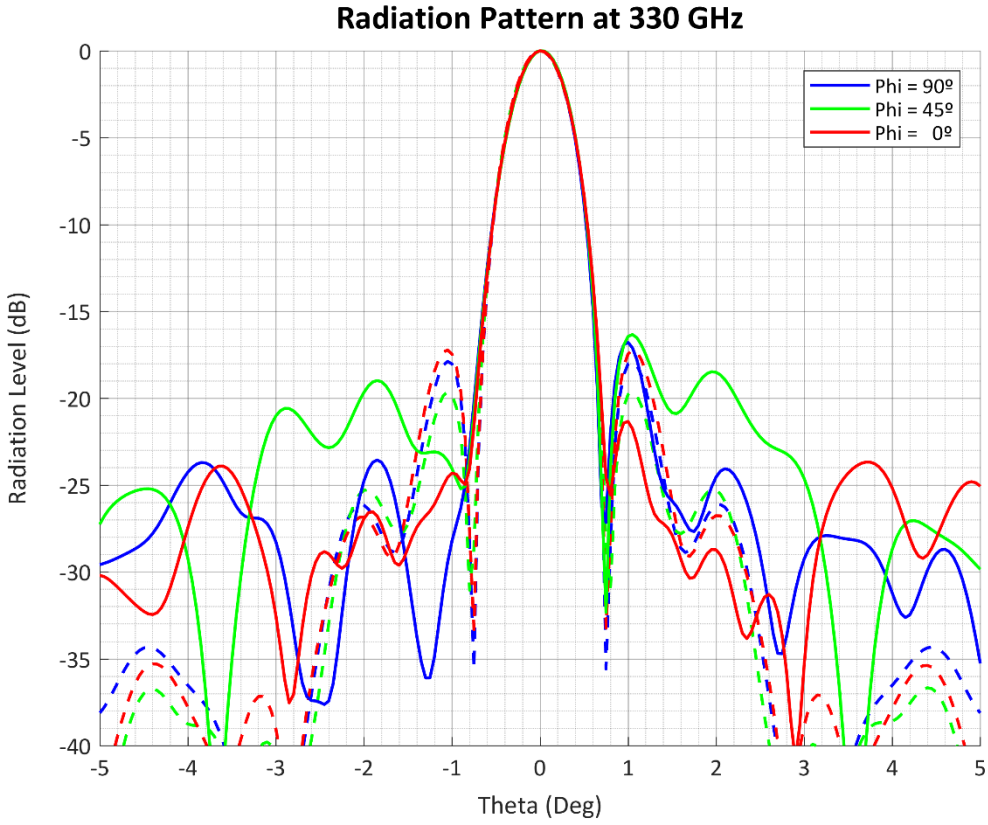

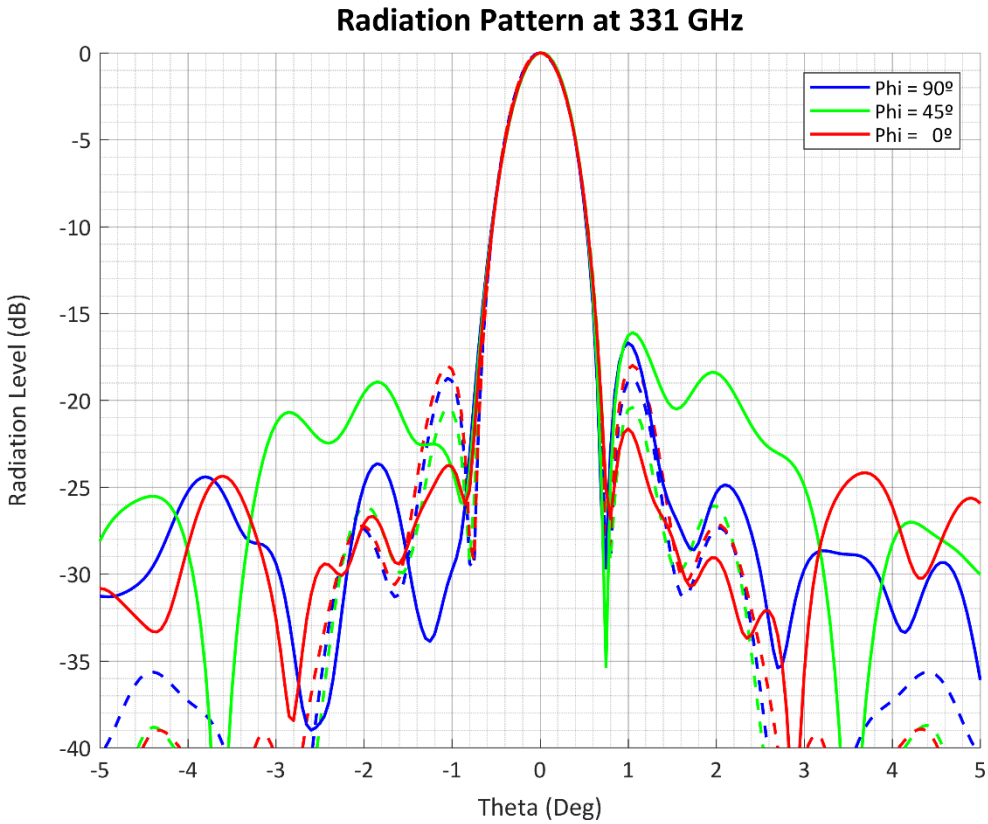

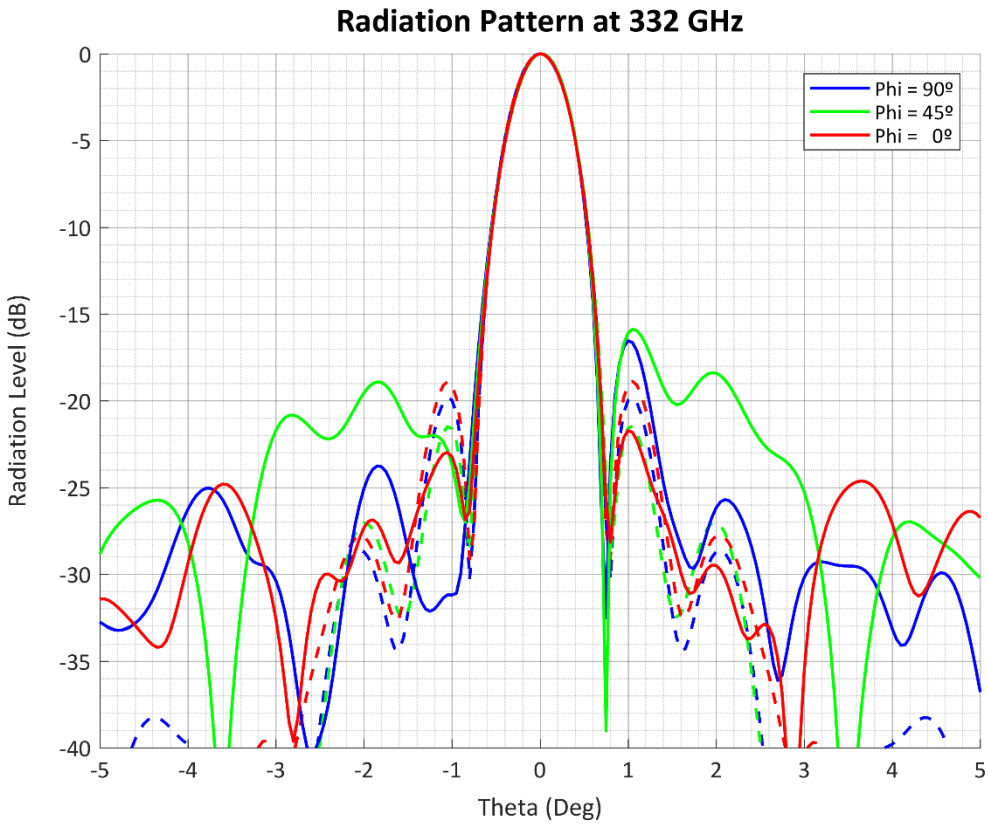
Radiation Pattern at 332 GHz
Phi = 90º
Phi = 45º
Phi = 0º
Radiation Level (dB)
Theta (Deg)
0
-5
-10
-15
-20
-25
-30
-35
-40
-5
-4
-3
-2
-1
0
1
2
3
4
5

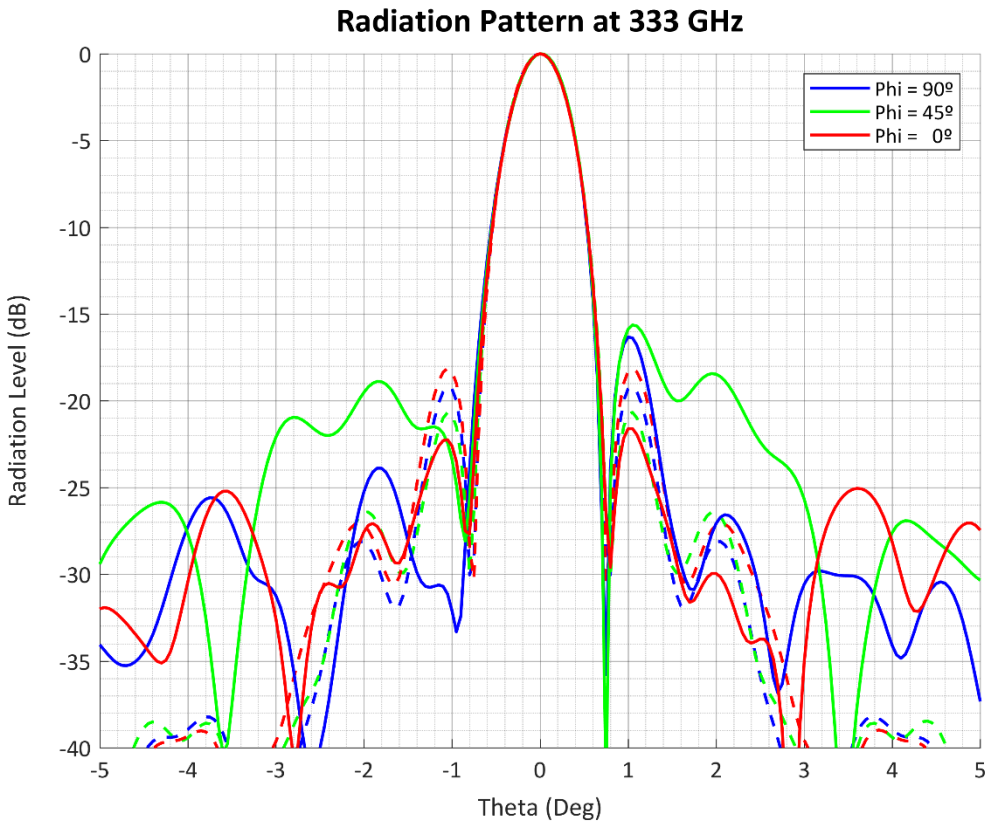
Radiation Pattern at 333 GHz
Phi = 90º
Phi = 45º
Phi = 0º
Radiation Level (dB)
Theta (Deg)
0
-5
-10
-15
-20
-25
-30
-35
-40
-5
-4
-3
-2
-1
0
1
2
3
4
5

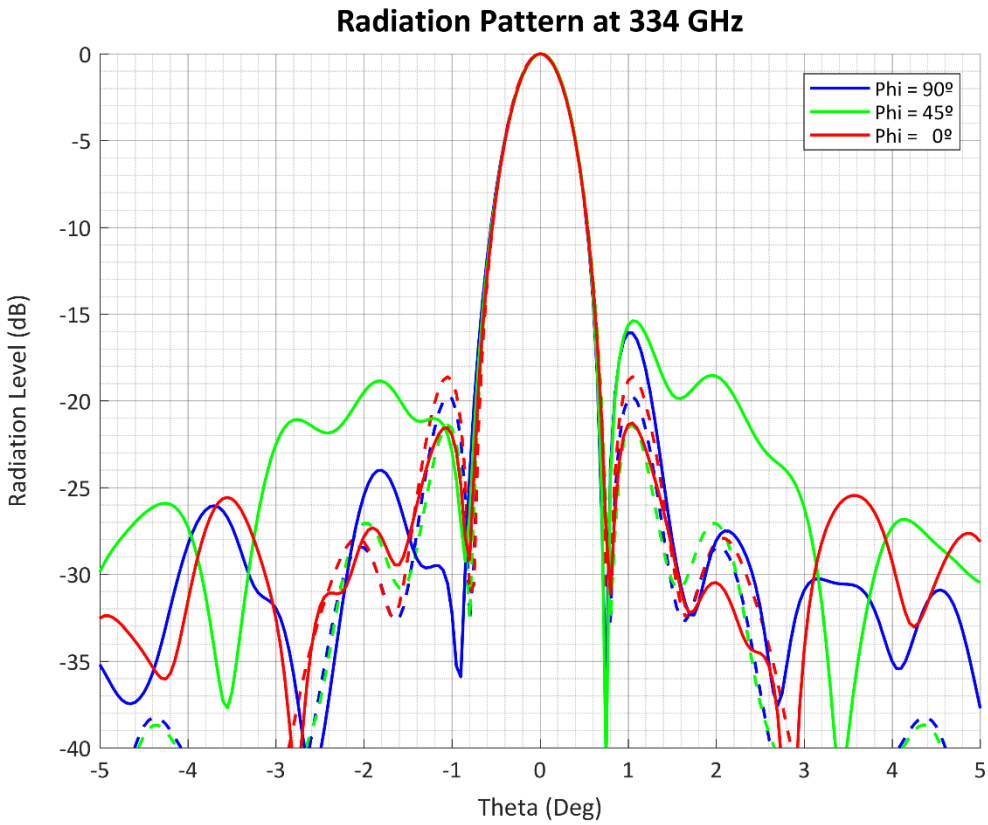
Radiation Pattern at 334 GHz
Phi = 90º
Phi = 45º
Phi = 0º
Radiation Level (dB)
Theta (Deg)
0
-5
-10
-15
-20
-25
-30
-35
-40
-5
-4
-3
-2
-1
0
1
2
3
4
5

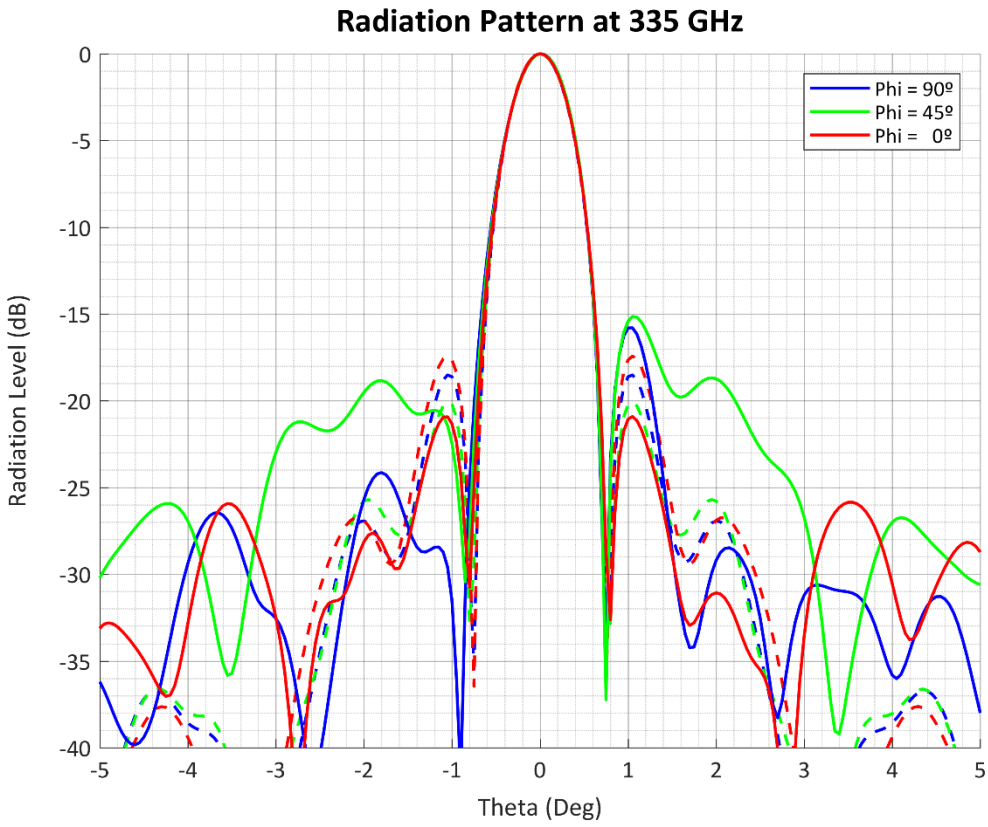
Radiation Pattern at 335 GHz
Phi = 90º
Phi = 45º
Phi = 0º
Radiation Level (dB)
Theta (Deg)
0
-5
-10
-15
-20
-25
-30
-35
-40
-5
-4
-3
-2
-1
0
1
2
3
4
5

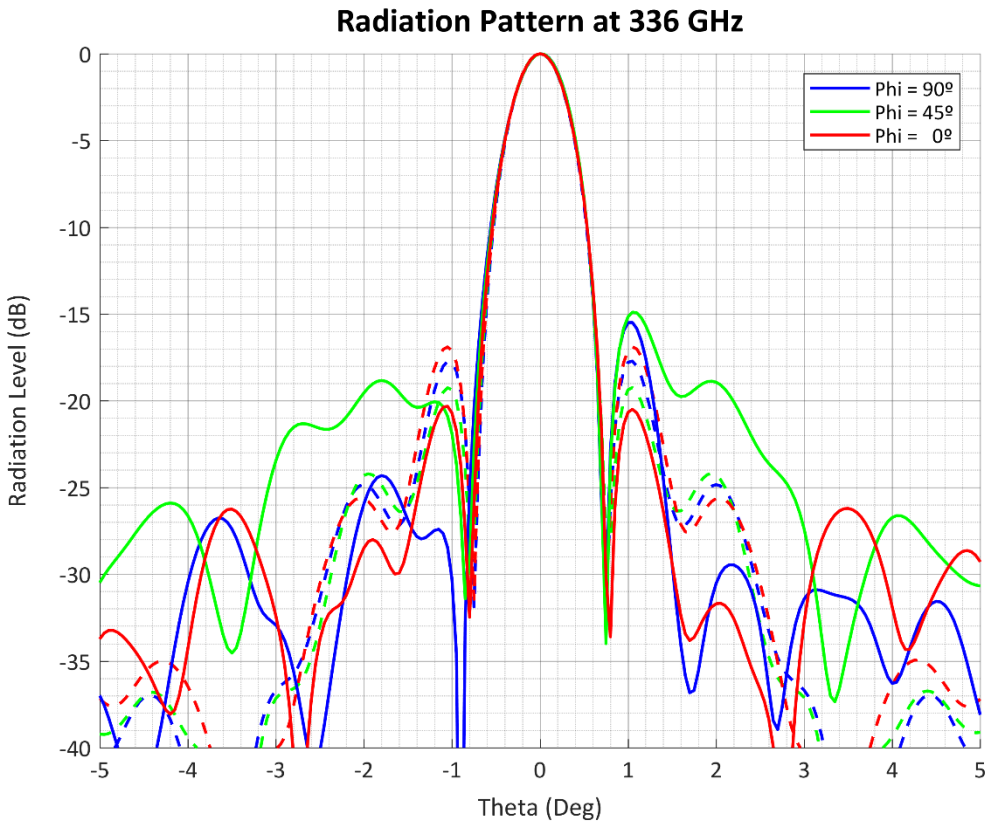
Radiation Pattern at 336 GHz
Phi = 90º
Phi = 45º
Phi = 0º
Radiation Level (dB)
Theta (Deg)
0
-5
-10
-15
-20
-25
-30
-35
-40
-5
-4
-3
-2
-1
0
1
2
3
4
5

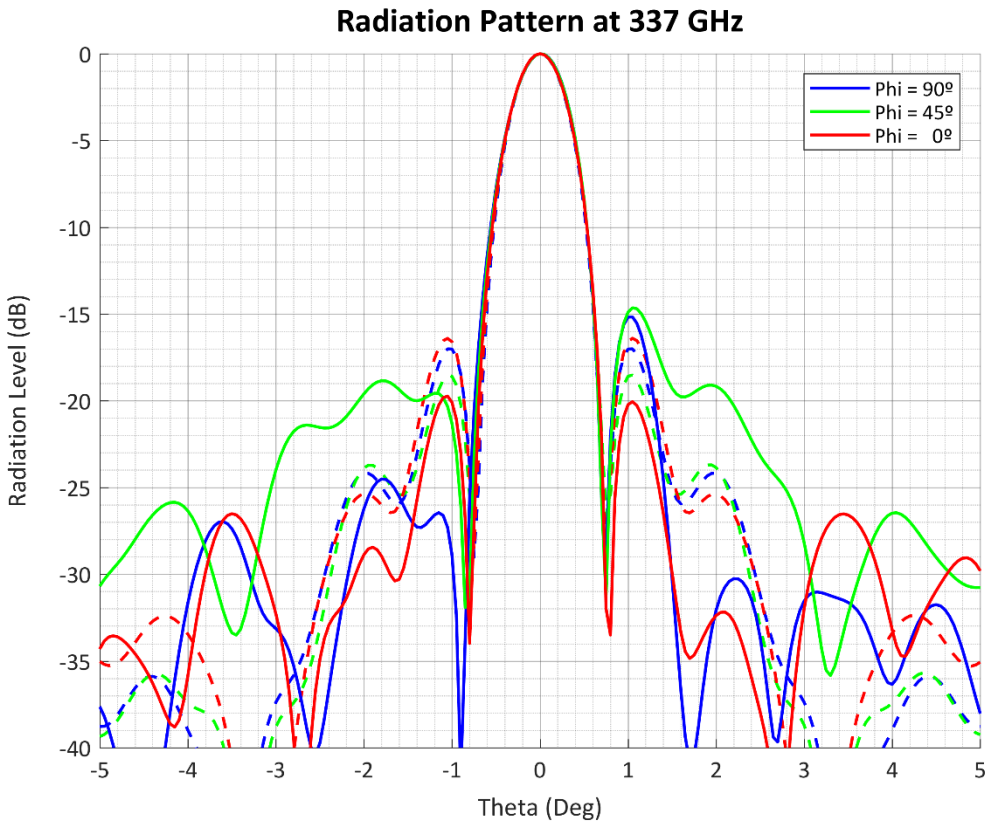
Radiation Pattern at 337 GHz
Phi = 90º
Phi = 45º
Phi = 0º
Radiation Level (dB)
Theta (Deg)
0
-5
-10
-15
-20
-25
-30
-35
-40
-5
-4
-3
-2
-1
0
1
2
3
4
5

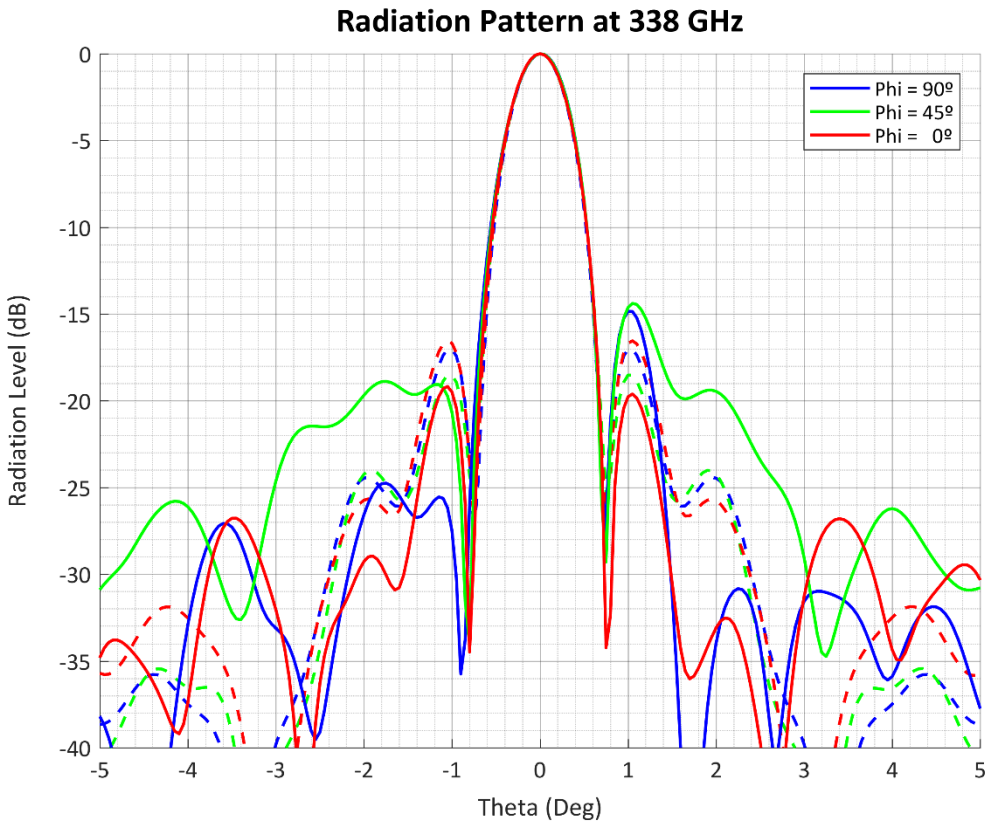
Radiation Pattern at 338 GHz
Phi = 90º
Phi = 45º
Phi = 0º
Radiation Level (dB)
Theta (Deg)
0
-5
-10
-15
-20
-25
-30
-35
-40
-5
-4
-3
-2
-1
0
1
2
3
4
5

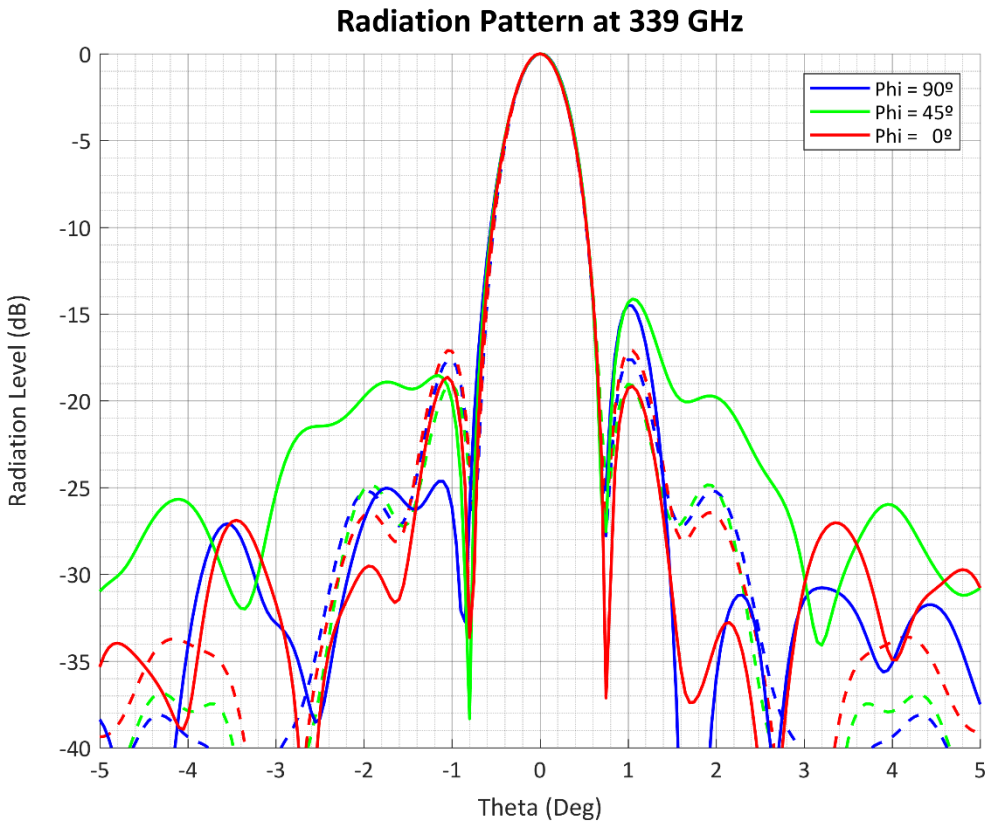
Radiation Pattern at 339 GHz
Phi = 90º
Phi = 45º
Phi = 0º
Radiation Level (dB)
Theta (Deg)
0
-5
-10
-15
-20
-25
-30
-35
-40
-5
-4
-3
-2
-1
0
1
2
3
4
5

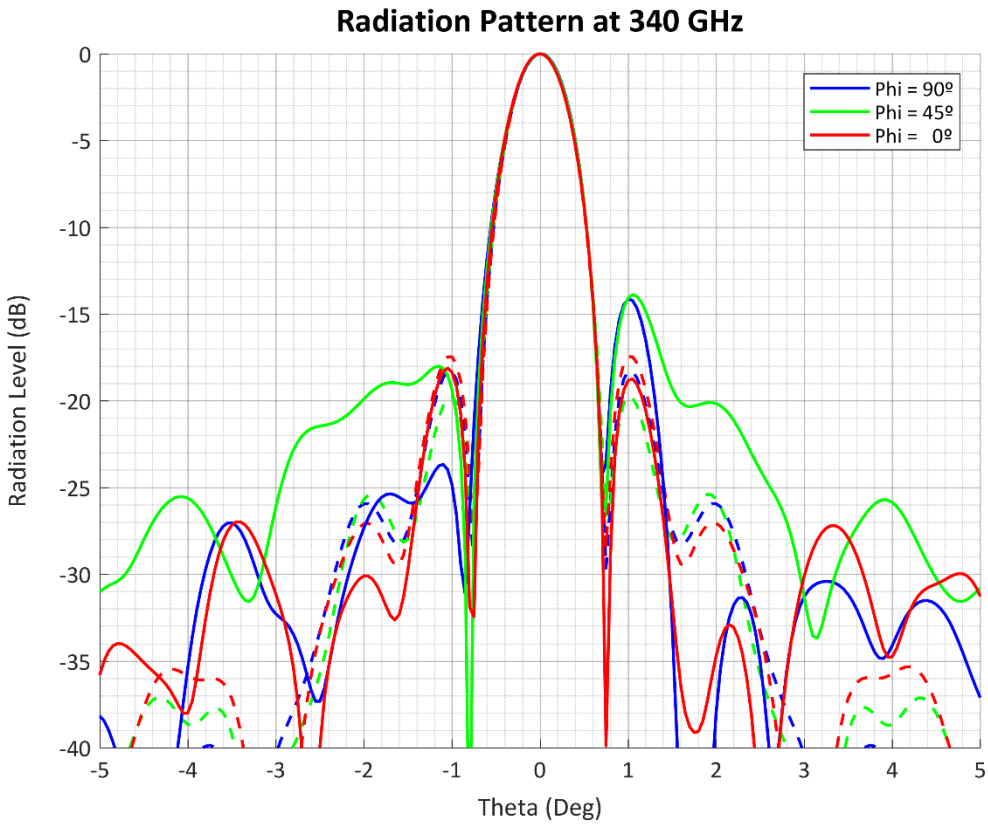
Radiation Pattern at 340 GHz
Phi = 90º
Phi = 45º
Phi = 0º
Radiation Level (dB)
Theta (Deg)
0
-5
-10
-15
-20
-25
-30
-35
-40
-5
-4
-3
-2
-1
0
1
2
3
4
5

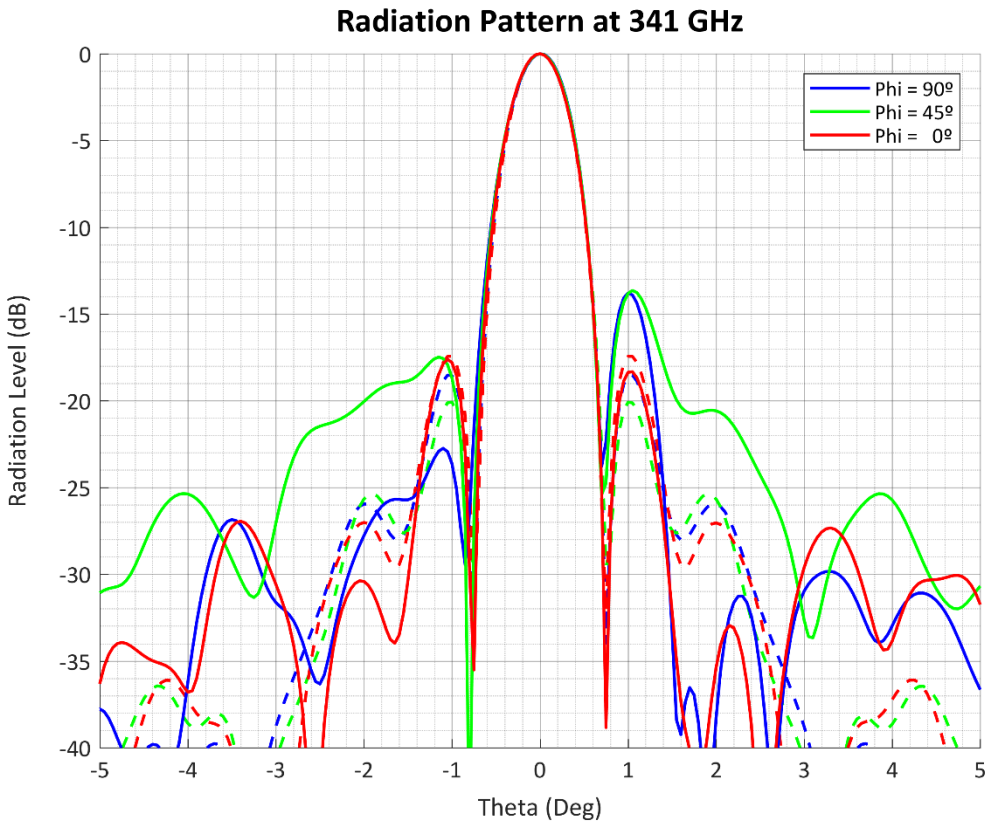
Radiation Pattern at 341 GHz
Phi = 90º
Phi = 45º
Phi = 0º
Radiation Level (dB)
Theta (Deg)
0
-5
-10
-15
-20
-25
-30
-35
-40
-5
-4
-3
-2
-1
0
1
2
3
4
5

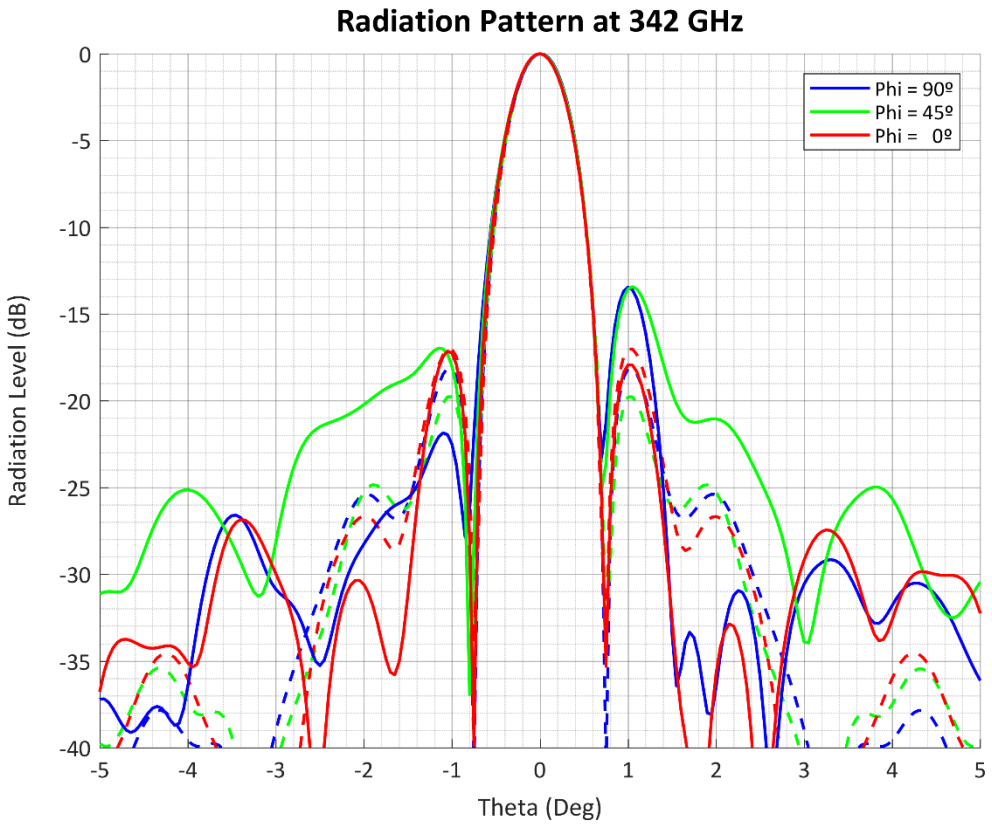
Radiation Pattern at 342 GHz
Phi = 90º
Phi = 45º
Phi = 0º
Radiation Level (dB)
Theta (Deg)
0
-5
-10
-15
-20
-25
-30
-35
-40
-5
-4
-3
-2
-1
0
1
2
3
4
5

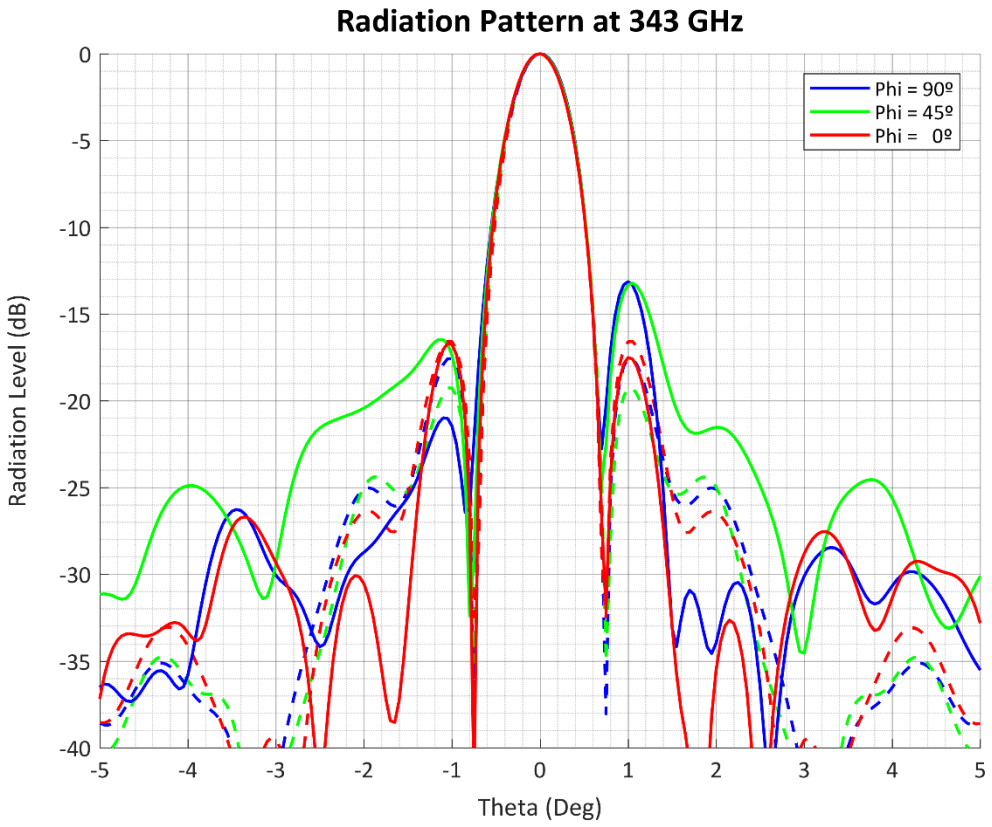
Radiation Pattern at 343 GHz
Phi = 90º
Phi = 45º
Phi = 0º
Radiation Level (dB)
Theta (Deg)
0
-5
-10
-15
-20
-25
-30
-35
-40
-5
-4
-3
-2
-1
0
1
2
3
4
5

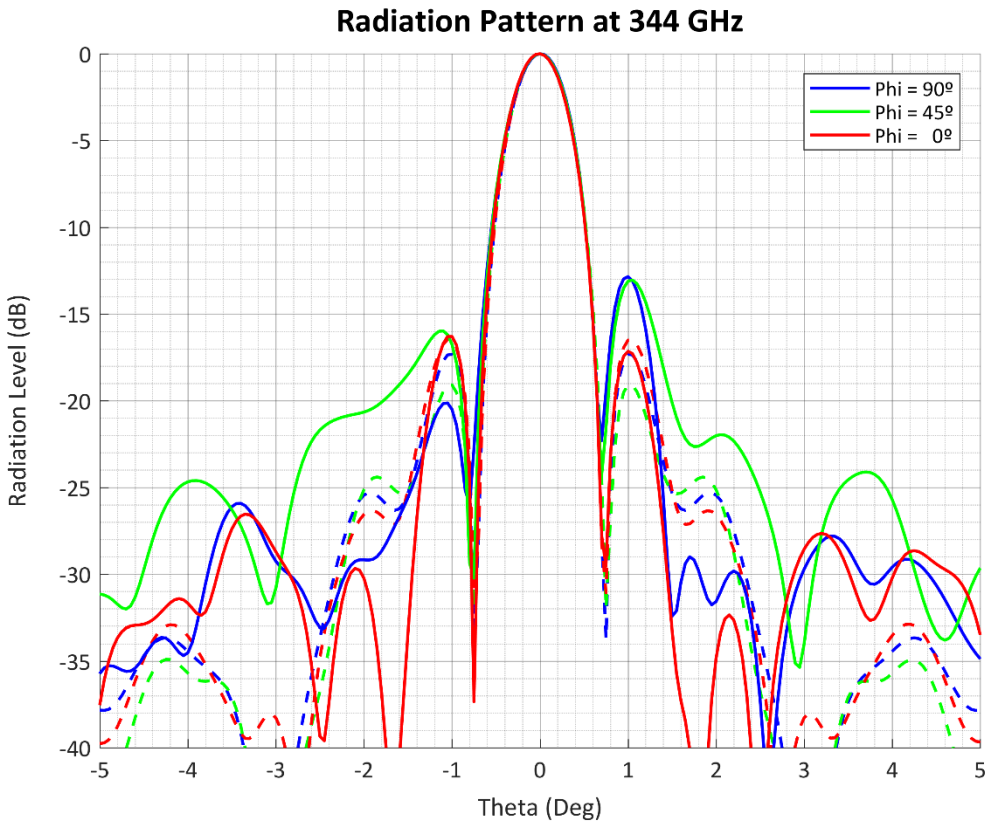
Radiation Pattern at 344 GHz
Phi = 90º
Phi = 45º
Phi = 0º
Radiation Level (dB)
Theta (Deg)
0
-5
-10
-15
-20
-25
-30
-35
-40
-5
-4
-3
-2
-1
0
1
2
3
4
5

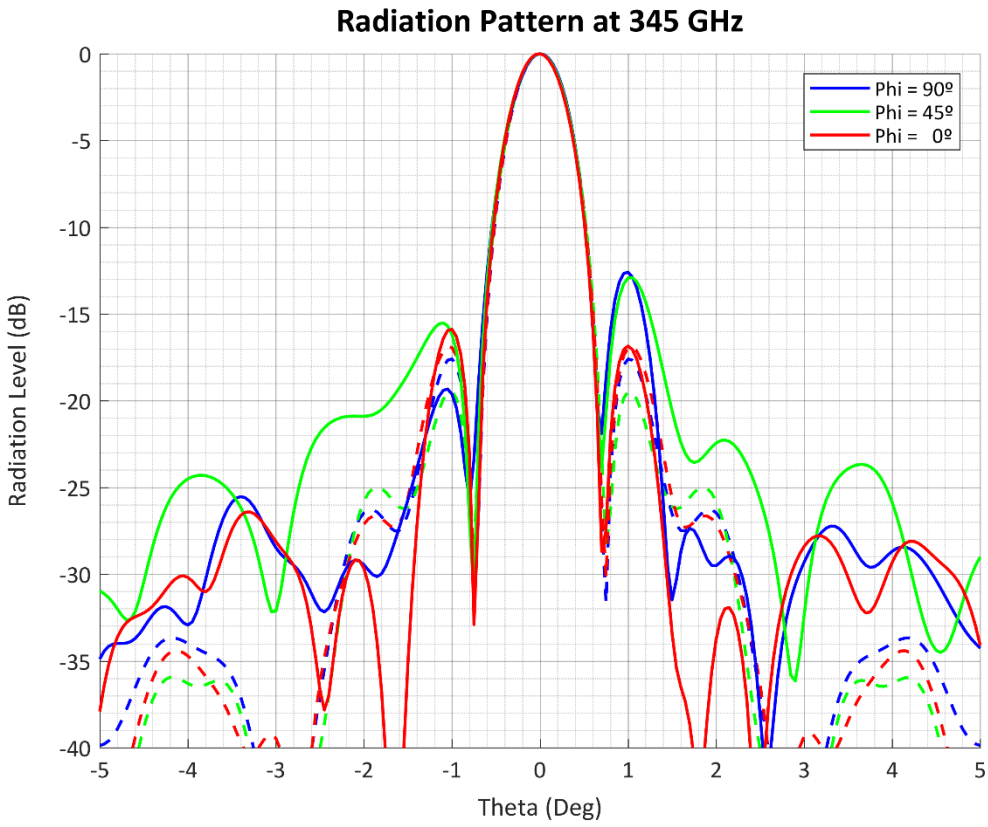
Radiation Pattern at 345 GHz
Phi = 90º
Phi = 45º
Phi = 0º
Radiation Level (dB)
Theta (Deg)
0
-5
-10
-15
-20
-25
-30
-35
-40
-5
-4
-3
-2
-1
0
1
2
3
4
5

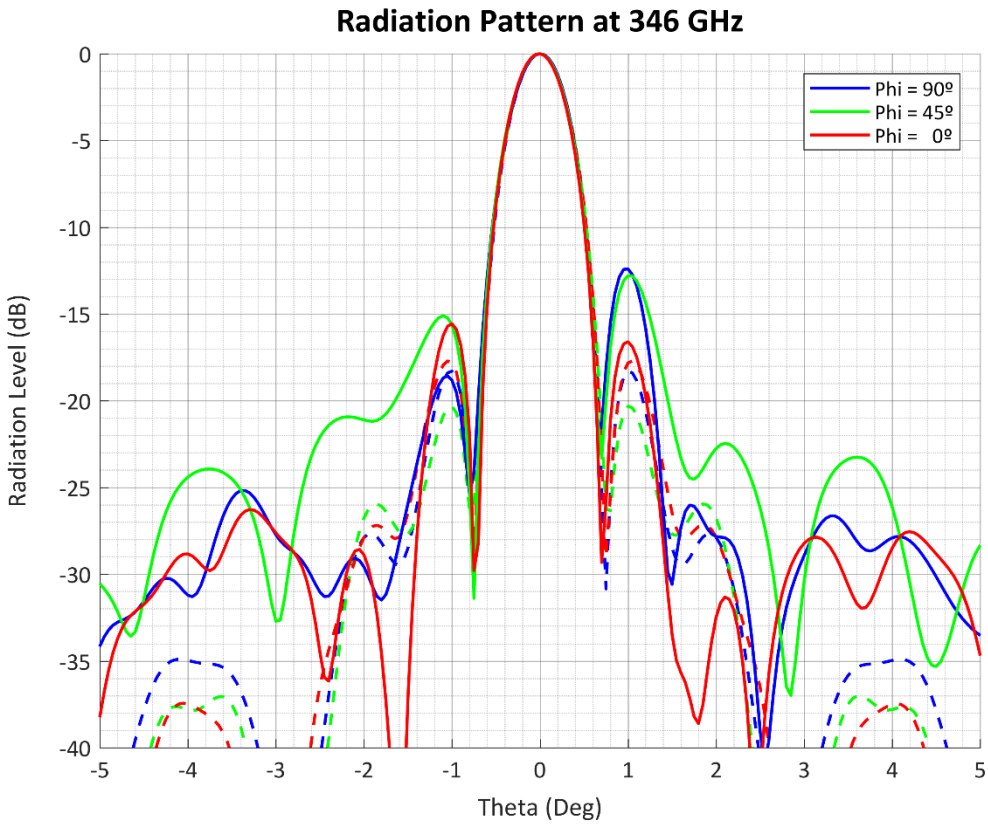
Radiation Pattern at 346 GHz
Phi = 90º
Phi = 45º
Phi = 0º
Radiation Level (dB)
Theta (Deg)
0
-5
-10
-15
-20
-25
-30
-35
-40
-5
-4
-3
-2
-1
0
1
2
3
4
5

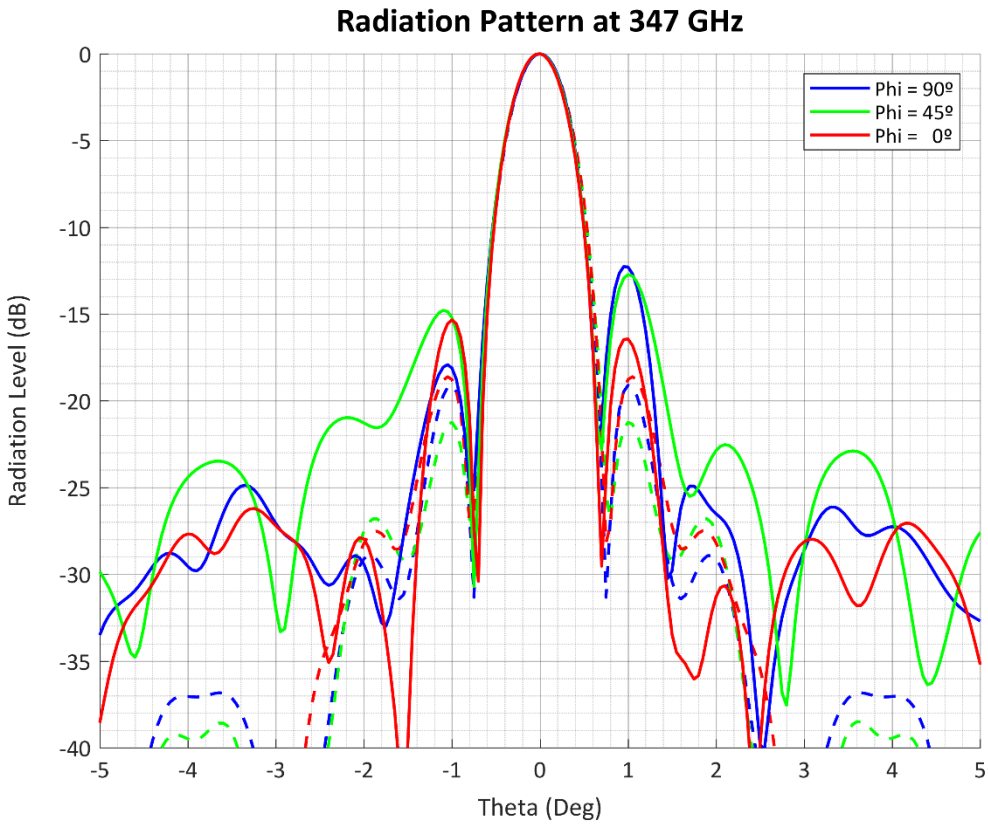
Radiation Pattern at 347 GHz
Phi = 90º
Phi = 45º
Phi = 0º
Radiation Level (dB)
Theta (Deg)
0
-5
-10
-15
-20
-25
-30
-35
-40
-5
-4
-3
-2
-1
0
1
2
3
4
5

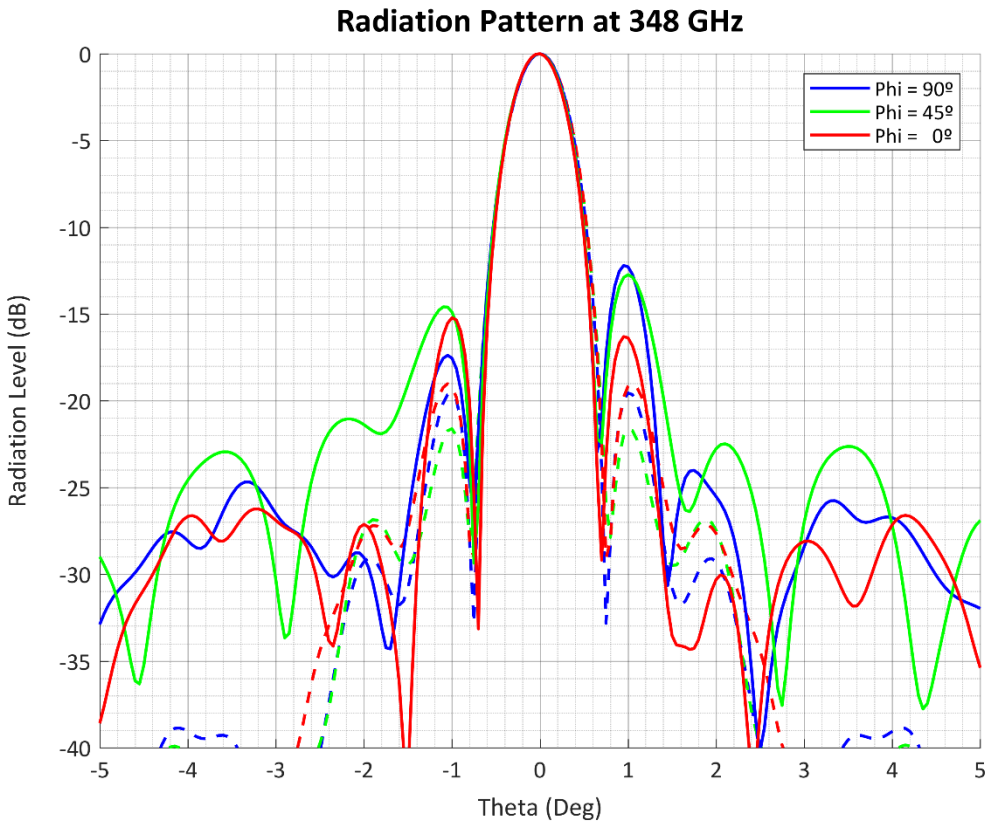
Radiation Pattern at 348 GHz
Phi = 90º
Phi = 45º
Phi = 0º
Radiation Level (dB)
Theta (Deg)
0
-5
-10
-15
-20
-25
-30
-35
-40
-5
-4
-3
-2
-1
0
1
2
3
4
5

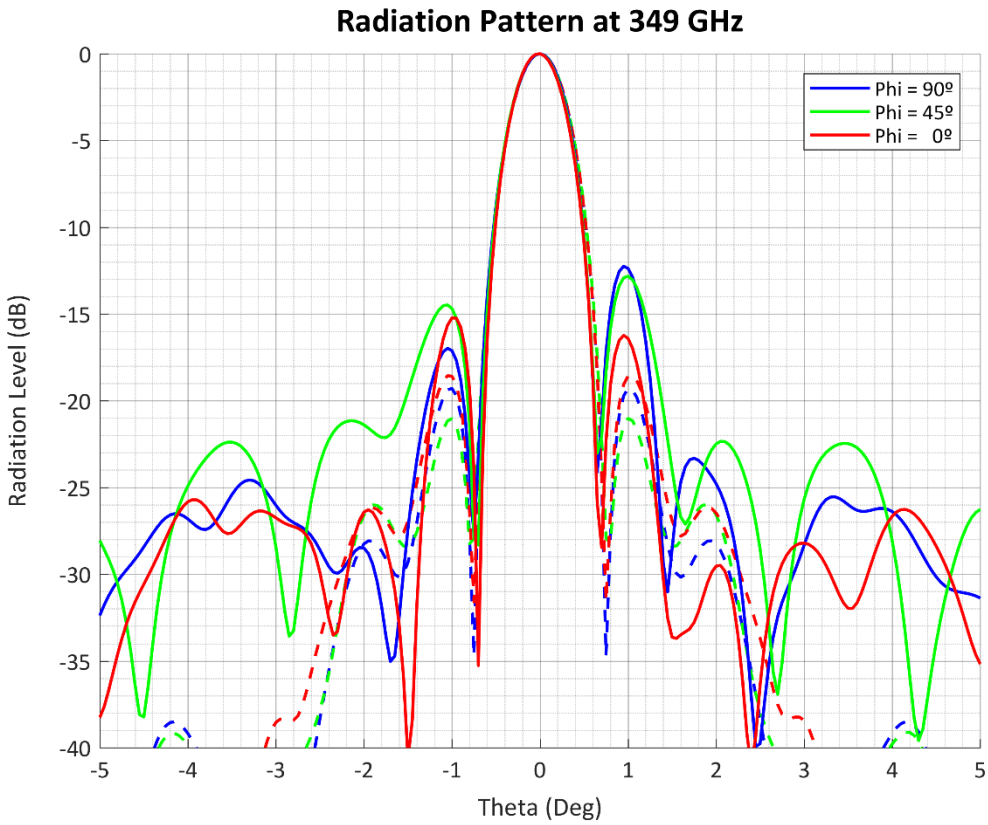
Radiation Pattern at 349 GHz
Phi = 90º
Phi = 45º
Phi = 0º
Radiation Level (dB)
Theta (Deg)
0
-5
-10
-15
-20
-25
-30
-35
-40
-5
-4
-3
-2
-1
0
1
2
3
4
5

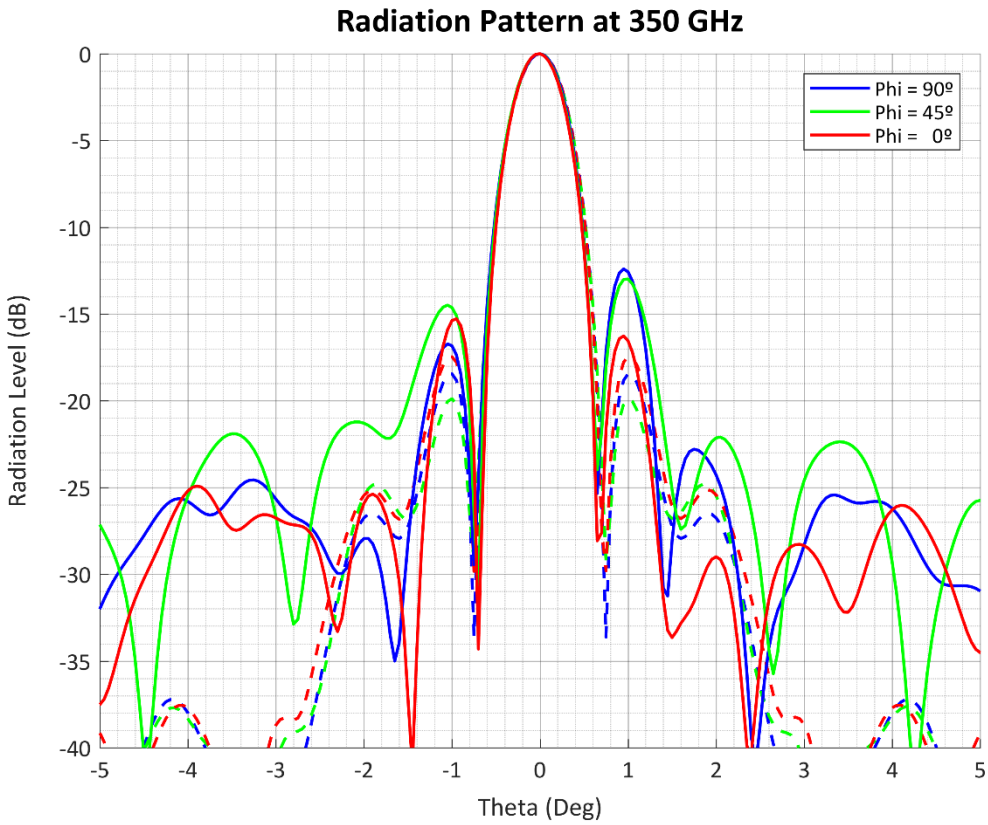
Radiation Pattern at 350 GHz
Phi = 90º
Phi = 45º
Phi = 0º
Radiation Level (dB)
Theta (Deg)
0
-5
-10
-15
-20
-25
-30
-35
-40
-5
-4
-3
-2
-1
0
1
2
3
4
5

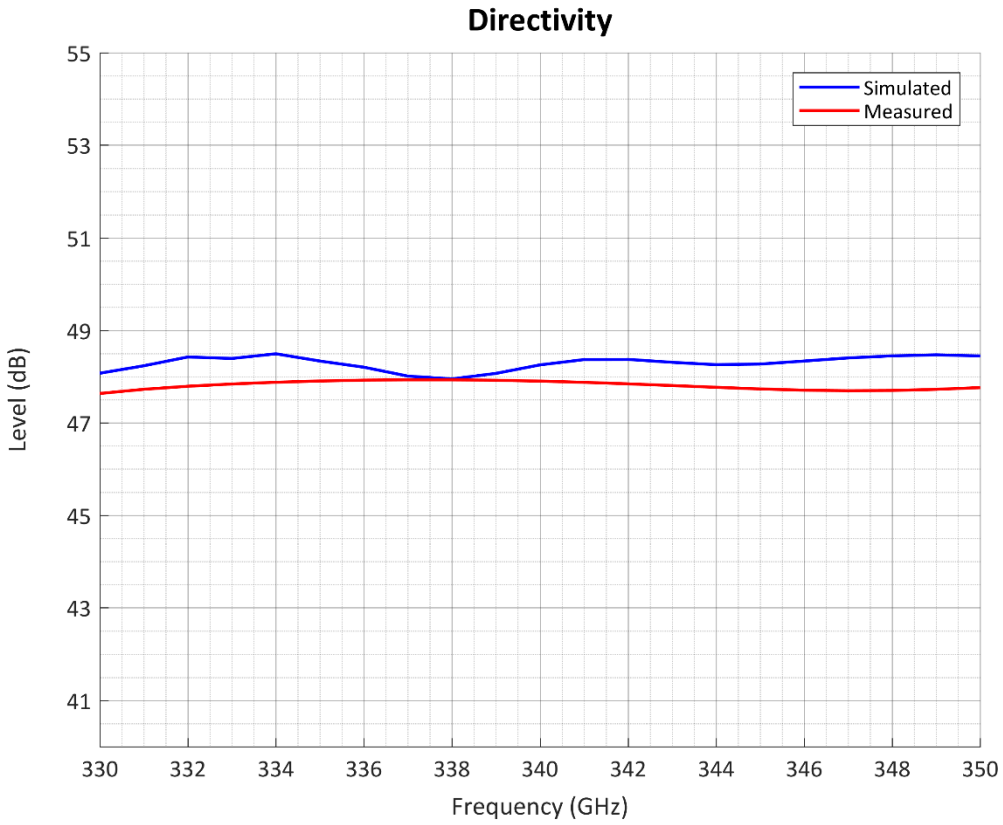
Directivity
Simulated
Measured
Level (dB)
Frequency (GHz)
55
53
51
49
47
45
43
41
330
332
334
336
338
340
342
344
346
348
350

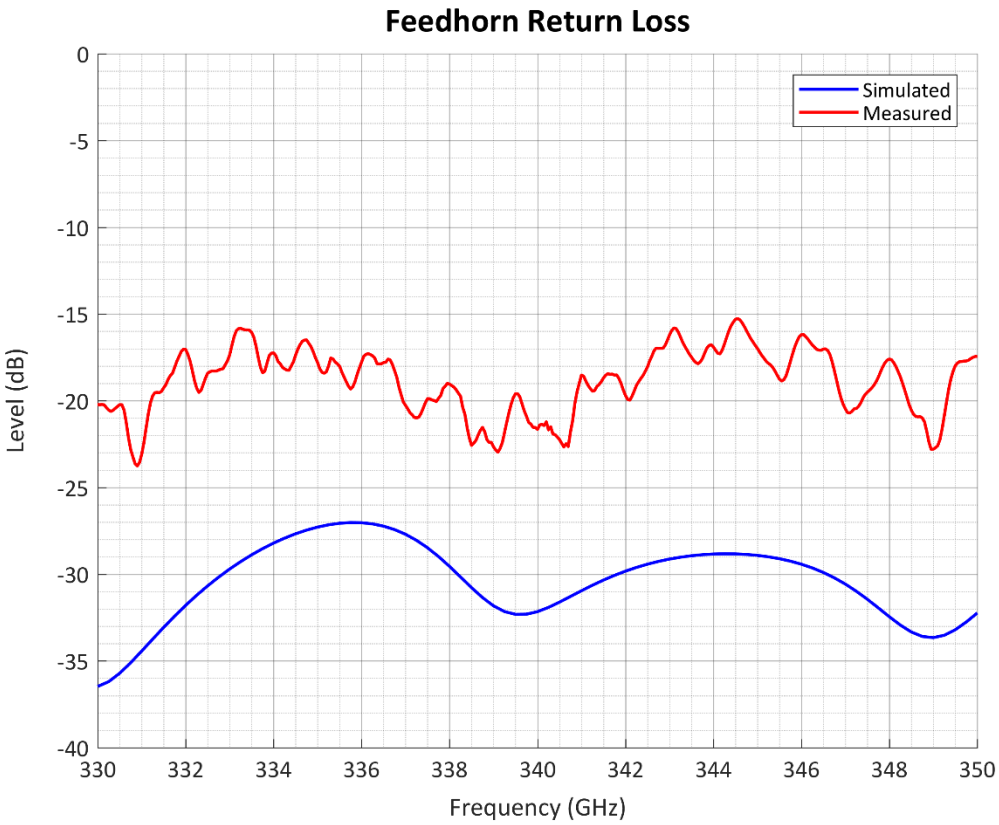
Feedhorn Return Loss
Simulated
Measured
Level (dB)
Frequency (GHz)
0
-5
-10
-15
-20
-25
-30
-35
-40
330
332
334
336
338
340
342
344
346
348
350